# CaII absorption in the circumstellar disk of Beta Pictoris and other A-type stars

—————————————————————————

A thesis

submitted in partial fulfilment

of the requirements for the Degree

of

Masters of Science in Astronomy

in the

University of Canterbury

by

Orlon K. L. Petterson

—————————————————

University of Canterbury

1996

Dedicated to my parents,

George and Chew Yoong,

who have always helped

me to achieve my best.

# Abstract

Presented here are the results of observations made at Mt John University Observatory (MJUO) during the spectroscopic campaigns to observe $\beta$ Pictoris in 1992, 1993, 1994 and observations conducted in 1995 to characterise the behaviour of the Ca II H and K lines and to test the Falling Evaporating Bodies scenario. Using the method of division by a reference spectrum both narrow and broad variable absorption features in both the redshifted and blueshifted sides of the Ca II H and K lines are clearly detected. The large data set obtained allows the determination of the evolution in terms of velocity, equivalent width, FWHM and timescales of variability of the variable absorption features. These are then compared with the results of Lagrange-Henri *et al.* (1996) in their paper on the 1992 observing campaign.

Lagrange-Henri *et al.* find that there are 2 velocity regimes and this is confirmed in the MJUO data. The higher the redshift, the smaller the variability timescales and the smaller the absorbing cloud. In contrast the low velocity features tend to be longer lived and to have the deepest absorptions. The correlation between the FWHM and velocity of the features found by Lagrange-Henri *et al.* is confirmed, but with the larger set of data the correlation is found to be somewhat weaker. Significant activity was seen in each set of observations with long-lived absorption features at low velocity almost always being present, and it has been found that 1/4 of all features observed are most likely due to more that one FEB.

The effect of stellar rotation is suggested in the data of some of the strong and more variable absorption features. However conclusive evidence of the changes in equivalent width are not forthcoming. Large numbers of high velocity features are also observed and are seen to vary in timescales no longer than the crossing time for an orbiting body to pass across the stellar disk. This lends further support to the FEB scenario as an explanation for the variable absorption features. The measurement of the filling factors of the clouds of ions indicate that these clouds do indeed cover large fractions of the stellar disk and some of the lines even exhibit pK/pH less than 1, as predicted.

The FEB scenario appears to explain many of the characteristics of the variable absorption features very well, simulations can reproduce many of the absorptions however there are some cases where the FEB scenario fails to adequately explain the observations. The ability for some of the long-lived features to last as long as they are observed to would require either large numbers of bodies on similar orbits crossing the line of sight for many weeks, or that there is some other explanation for the origin of the absorptions.

*The quest for knowledge eventually fills all Time and Space.*

# Contents

# Figures

# Tables

# Chapter 1

# Introduction

Stars are probably the most basic objects one can see in the sky at night. One of the most interesting and fundamental problems in modern astrophysics is understanding their origins. Of particular interest in this thesis is the formation and evolution of low mass ($\sim 1 M_\odot$) stars, which can form planetary systems capable of supporting life in a form as we know it. With the recent announcements of planetary bodies orbiting other solar-type stars, there is a need to understand the processes behind planet formation and the circumstellar disks they are believed to form from.

## 1.1   The history of models of the Solar System's formation

### Question : How did the Sun and planets come into being ?

This question was really only considered after the Copernican revolution. The theory that the Sun was at the centre of the Solar System with the planets and other bodies orbiting around it was first advanced by *Aristarchos of Samos*, but wasn't really accepted until the scientific work of *Kepler, Galileo and Newton* proved that Aristotle's view of the Solar System didn't accurately describe the workings of the Solar System. It was clear in the beginning that any theory advanced would have to take various factors into account:

1. the orbits of the planets are close to the plane of the Earth's orbit

2. the orbits are to a certain degree of approximation roughly circular

3. the planets all orbit in the same direction as the Sun's rotation.

At the beginning of the 20th century theorists had an added problem to solve in the formation of the Solar System, namely that even though 99.8% of the mass of the Solar System resides in the Sun, it only has 2% of the angular momentum possessed by all the planets (see Mouschovias 1991[50]). Late in the second half of the 20th century new theories of stellar formation and new data about the ages of various bodies have helped to advance our understanding of Solar System formation[22]. Finally observations by the *Hubble Space Telescope* are giving Astronomers unprecedented views of stars in various stages of formation. These observations are undoubtedly helping to constrain and advance theories of planetary formation about other stars as well as the formation of our own Solar System.

### 1.1.1   The nebular theory

The concept of a primitive nebula, from which both the Sun and its system of planets were born was first proposed by Kant (1724-1804) and Laplace (1749-1827). According to Laplace, the nebula contracts under gravitation and its rotational velocity increases until it collapses into a disk. Subsequently rings of material are shed, from which form planets and satellites.

This model had the merit of being able to explain all the observational phenomena known at the time with respect to the motions of the planets. However later two problems arose with this model, namely the difficulty with which planets formed from the rings of planetoids and then the distribution of angular momentum in the Solar System. Under this model the Sun should still have most of the angular momentum and hence be rotating at the rate of 1 rotation every 12 hours, as opposed to the 26 day period at present.

During the 20th century Laplace's model has been modified and expanded in various ways to answer the objections that have been raised. The role of the solar wind and magnetic field have taken on an increasing importance, as ways to brake the rotation of the Sun. A rotating star loses mass through the flow of particles along the lines of force of its magnetic field. This transports the particles to large distances far greater than the stellar radius and therefore leads to a large loss of angular momentum. This view is backed up by observation which shows that young stars tend to have intense magnetic activity and high rotation rates. As these stars age their magnetic activity declines and the rotation rate slows. This explanation involving magneto-hydrodynamic braking of a star removes the objection about angular momentum.

### 1.1.2   The tidal theories

The first catastrophic theory of the formation of the Solar System was proposed by the naturalist Buffon (1707-1788) who suggested that the Solar System was formed from the ejected material from the Sun resulting from the collision with a comet 70 000 years ago. This theory had no scientific justification, but with objections raised with the the nebular theory the catastrophic theories were re-examined. At the beginning of the 20th century the Buffon's comet was replaced by a star and the planets formed by the condensation of material lost from the Sun. The tidal force at the moment of closest approach between the two stars would then draw out a filament of material from one star and this would orbit the star with considerable angular momentum. However it was found that this model had problems with making large planetary masses. Another version proposed that the Sun was part of a binary system and the planets formed from this second star. It was later suggested that the Sun encountered a protostar from which the planets formed; this took advantage of the new determinations that the planets formed from a cold medium.

### 1.1.3   Accretion theories

This final class of models consider the possibility that the planets formed around the Sun from accreting interstellar material. In order to avoid the accreted matter from falling into the Sun, another nearby star is postulated which allows the material to condense into planets. Another version supposes that the Sun encountered two different nebulae, one consisting of non-volatile grains, from which the inner planets evolved, and another consisting of mainly hydrogen, from which the Jovian planets formed. However this hypothesis was rejected when it became apparent that the collision of particles would lead to dispersal rather than planet formation.

## 1.2   Modern theories of Solar System formation and evolution

Modern theories of Solar System formation tend to follow the nebular theory as proposed by Laplace, but modified to take advantage of new observations. There are two categories of models for the evolution of proto-planetary disks which explain planetary formation. They are:

1. *The massive nebula model*, which considers a viscous disk of about 1 $M_{\odot}$. A large fraction of this disk is removed by the action of the solar wind in a very short time, while the rest is accreted by the Sun. The planets are to form directly from the gaseous nebula by gravitational instabilities.

2. *The low-mass-nebula model*, where the mass of the circumstellar disk after collapse is about $10^{-2} M_{\odot}$. The disk later cools, the dust accumulates in the central plane and forms planetesimals which can combine to form planets.

The current view seems to suggest that the low-mass-nebula model is more likely and indeed does appear to be the case in the Beta Pictoris system. So this is the main model to be discussed in the rest of this chapter.

It should also be noted that the current thinking on the subject of circumstellar disk formation about stars, is that planets will only be produced if sufficient time is available for accretion of material. This constraint therefore rules out O and B stars as sites of any disk formation, as any disk will be blown away by the strong stellar winds of the young star before any accretion can occur [16]. Therefore planetary formation will be limited to low to mid mass stars ($\leq 3 \ M_{\odot}$).

### 1.2.1   Formation of a proto-star and circumstellar disk

At the most basic level the evolution of a low mass star from birth is driven by gravity, consequently the amount of mass a star has plays a fundamental role in its development.

Star formation occurs on widely varying scales, ranging from relatively isolated, low-mass ($\sim 1 M_\odot$) dark clouds to giant molecular cloud complexes containing as much as $\sim 10^6 M_\odot$ of gas and dust. Giant molecular cloud complexes are also the sites of high-mass star formation and therefore can influence their surroundings considerably. Since low-mass star formation is what interests us here, our attention is directed to the dark cloud complexes with masses of $10^3 - 10^4 M_\odot$. In these dark cloud complexes low-mass star formation occurs largely without high-mass stars. Dark cloud complexes contain clusters of localised mass concentrations, termed dense cloud cores, with masses in the range $0.3 - 10 M_\odot$, mean densities of $10^4 - 10^5 \mathrm{cm}^{-3}$, sizes on the order of 0.1 pc, and temperatures close to 10 K [12]. These dark cloud cores define the initial conditions for the formation of many low-mass stars (see Figs. 1.1, 1.2).
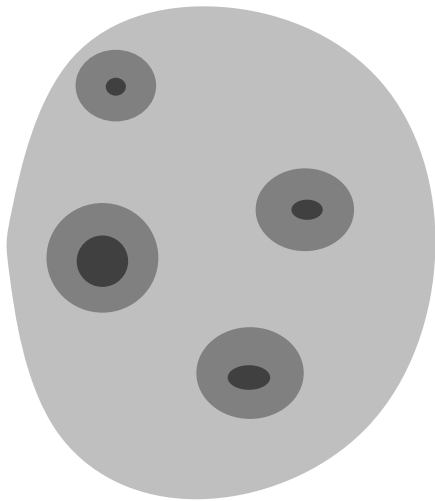


Figure 1.1: A schematic diagram showing the formation of cores of dense gas and dust that will serve as the seeds of new stars in a dark molecular cloud.
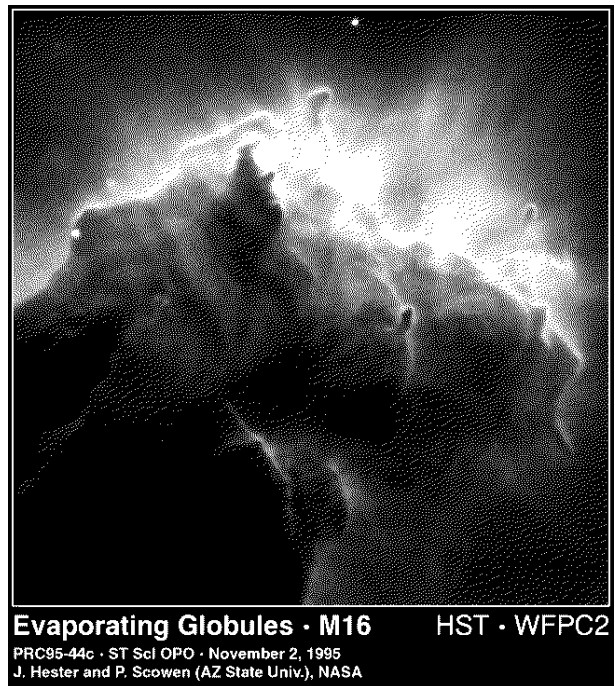


Figure 1.2: H$_\alpha$ image of M16 showing one site of star formation where a blob of gas and dust containing still forming stars is slowly being eroded away by ultraviolet light from nearly hot stars (courtesy of NASA).

## 1.2.2  Cloud collapse and fragmentation

The classical initial conditions for cloud collapse are an optically thin cloud in the infrared (IR), allowing dust grains in the cloud to radiate away compressional energy produced by the collapse. As a result, the initial collapse phase occurs isothermally (T $\sim$10 K). A pressure gradient develops in the envelope as the effects of the finite cloud size propagate inward, and this pressure gradient retards the collapse of the envelope. As the density

becomes higher at the centre of the cloud than in the surrounding envelope, this region of higher density collapses faster and the central density begins to increase in a run away fashion. The time taken for this to occur is the free-fall time:

$$t_{ff} = \sqrt{\frac{3\pi}{32G\rho}}$$

The run away process of increasing density in the core is halted when the centre of the cloud becomes optically thick in the IR. Then the compressional energy is trapped and the rising thermal pressure halts the collapse of the core. The result is the formation of a protostellar core surrounded by an infalling envelope. When the temperature rises sufficiently to dissociate molecular hydrogen in the "outer core", another collapse is initiated allowing the collapsing gas to reach stellar densities and the protostar begins fusion reactions in its core. The collapsing cloud also imparts rotation to the still forming protostar and forms a surrounding accretion disk. The time for the pre-hydrogen burning evolution is initially given by the Kelvin-Helmholtz time:

$$t_{KH} \approx \frac{GM_*^2}{R_* L_*}$$
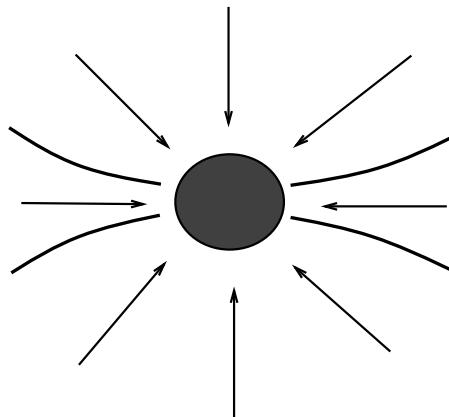


**Figure 1.3**: Accretion of material onto the rotating proto-star and surrounding accretion disk.

### 1.2.3 Protostellar objects and disks

At this point both the protostar and circumstellar disk are still gaining mass through accretion of infalling gas from the clouds envelope, also the protostellar object may be accreting material from the adjoining disk (see Fig. 1.3). The embedded protostellar object and its disk appear as a strong source of IR emission with an effective temperature of $\sim$200 K. At some time during this stage a bipolar outflow develops from the developing protostar which is seen as a highly collimated flow of material (see Section 2.2). The bipolar flows are generally aligned perpendicular to the major axis of the disk (see Figs. 1.4, 1.5), suggesting that the disk may in some way help to collimate the flow.
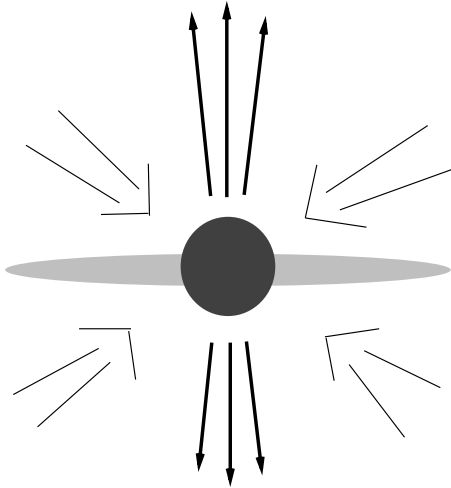
**Figure 1.4**: Schematic representation of the bipolar outflow from young stellar object as material continues to accrete.
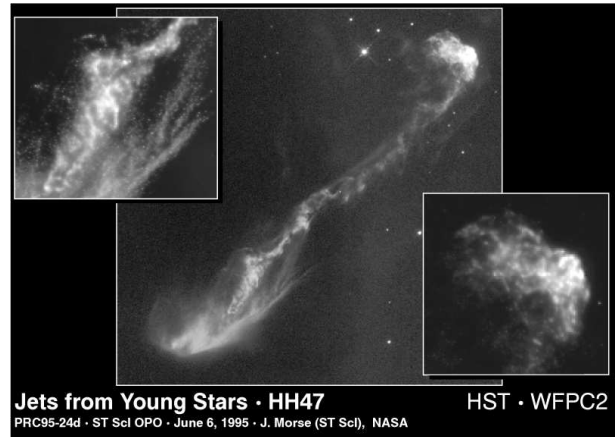


**Figure 1.5**: HST images of bipolar jets from young stars (courtesy NASA).

### 1.2.4   Planetary formation

In this stage of formation, grains of dust and ice form in the circumstellar disk, in Keplerian orbits, and the dust grains rapidly grow in size. This is believed to occur once turbulence in the disk ceases, so allowing dust grains to coagulate to sizes of the order of 1 cm, in timescales $\sim 10^3$yrs. Collisions of dust grains within the disk are believed to produce the 1 km sized planetesimals, the precursors to planets, due to differential motion caused by gas drag in as little as $\sim 10^4$yrs. Calculations of the subsequent phases of planet formation typically assume the existence of a swarm of about $10^{12}$ planetesimals in the terrestrial planet region alone. Subsequent planetesimal growth requires collisions of these 1 km sized bodies to produce $\sim 500$ km sized bodies in circular orbits. This is probably a run away process, with the largest bodies growing fastest as the gravitation of these bodies increases their effective cross-section. Formation of planets occurs from collisions of these more widely spaced bodies through perturbations of the orbits from close encounters resulting in increasing orbital eccentricity. So the terrestrial planets probably formed from the collisions of bodies of similar sizes; indeed the formation of the Moon around the Earth is believed to be the result of a glancing blow by a Mars-sized body.

### 1.2.5   Termination of formation

For the first time the centre of the disk is dominated by the presence of a hydrogen-burning star, arriving on the main-sequence (see Figs. 1.6, 1.7). The young star is observed to be rapidly rotating with a great deal of magnetic activity, and via its interaction with the circumstellar disk a form of magneto-hydrodynamic braking occurs. The bipolar outflow
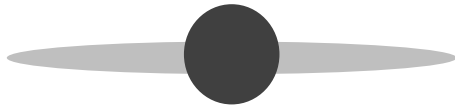
**Figure 1.6**: ZAMS star surrounded by a slowly eroding circumstellar disk



**Figure 1.7**: Edge on protoplanetary disks seen silhouetted against the bright background of the Orion Nebula (courtesy NASA).

previously found with the star fades away and a stellar wind begins to blow away the gas and dust in the inner disk. This represents the final stage of formation which is also known as the clearing out phase. The now main-sequence star blows away the left over material with a stellar wind that strips away the majority dust and gas leaving behind the planetary system of planets, asteroids and comets. Eventually the circumstellar disk will dissipate and fade from view, appear much as our Solar System does now.

# Chapter 2

# $\beta$ Pictoris

The circumstellar disk around $\beta$ Pictoris was first detected by the IRAS satellite in observations made in 1983, when the star was found to have a large infra-red excess. The disk was then imaged for the first time by Smith and Terrille in 1984 showing a disk of dust surrounding the star out to 25 arcsec in a nearly edge-on orientation. As a consequence of this observation $\beta$ Pictoris has been subject to a great deal of scrutiny from Astronomers around the world. The search for other objects similar to $\beta$ Pictoris also started at this time.

## 2.1 The evolutionary status of $\beta$ Pictoris

The evolutionary status of $\beta$ Pictoris poses some interesting problems when the number of unique characteristics this star are considered. It exhibits a prominent and in the IRAS observations a barely spatially resolved IR excess (Aumann *et al.* 1984[4]; Telesco *et al.* 1988[68]), a flattened nearly edge-on disk of visible and near IR scattering material extending out hundreds of AUs (Smith and Terrille, 1984[63]; Paresce and Burrows, 1987[54]) and a circumstellar gaseous shell detectable as a strong narrow absorption feature in the Ca II K & H and Na I D photospheric lines (Slettebak, 1975[60]; Slettebak and Carpenter, 1983[61]; Hobbs *et al.* 1985[36]; Vidal-Madjar *et al.* 1986[74]). In more recent times variable absorption features have been seen in the UV resonance lines of Al III, Mg II, Fe II as well as in the Ca II and Na I lines which are sporadic in appearance.

To truly understand this bizarre object, we need to have a proper physical characterisation of the prominent circumstellar disk. Are we observing a young planetary system in formation or is it the remnant of a dusty proto-stellar accretion disk in its clearing out phase? Or could it be a bipolar nebula emanating from an older, evolved post-main-sequence star as Herbig, 1989[33] has speculated on the optical appearance and an A5IV classification of the central star by Slettebak, 1975?[60] Using all available observational data and fully self-consistent models of the disk, the current view is that the disk is essentially a flattened swarm of orbiting particles viewed in a nearly edge-on disk and the inner region of the disk may have objects akin to star-grazing comets causing the variable absorption features seen.

As Smith and Terrille, 1984[63] first pointed out, the absolute brightness of $\beta$ Pictoris is about 0.8 magnitudes fainter than a typical A5V star and even 0.3 magnitudes fainter than

the ZAMS. The determination of spectral type came from Kondo and Bruhweiler 1995[40] who found that the IUE spectra of $\beta$ Pictoris matched perfectly the IUE archival spectrum of the unreddened A5V comparison star 80 U Ma. More specifically, the argument is as follows. $\beta$ Pictoris is near enough (parallax = 0.055 arcsec) for an $E(B - V) = 0.0$. Its observed $B - V = 0.17$ with $V = 3.85$ (Hoffleit and Jaschek, 1982)[37]. This colour corroborates Kondo and Bruhweiler's, 1985[40] result that its UV spectrum is that of an A5 star for which $T_e$ is in the range $8100 - 8200$ K for the V to III luminosity classes and for which the bolometric correction is $\sim -0.15$. These data translate directly into an absolute magnitude $M_V = 2.78$ and an absolute bolometric magnitude $M_{bol} = 2.63$. Since a normal galactic A5 dwarf has an $M_V$ in the range $1.9 - 2.4$ depending on how far it has evolved off the ZAMS (Allen, 1973[2]; Schmidt-Kaler, 1982[59]), its supposed underluminosity is indeed in the range 0.4 to 0.9 magnitudes. It should be noted that this discrepancy rises to 1.4 magnitudes for a typical subgiant of luminosity class IV. This result raises the question of whether circumstellar material might be absorbing some of the light from the star, hence its underluminosity. If this is due to gray extinction from the disk then the particles must be quite large, however this would then give a very small effective disk size in the near IR flatly contradicting the observed tens of arcsecond disk claimed by Telesco *et al.* 1989 and Backman and Gillett, 1990. Therefore large particles blocking light from $\beta$ Pictoris cannot account for its apparent underluminosity.

A thorough analysis of $\beta$ Pictoris' spectrum and the calibration of narrow band photometry to the main physical stellar parameters, allows the reasonably accurate determination of fundermental parameters. Because of the complete spectral coverage, - from IUE data (Kondo and Bruhweiler 1985[40]), visible and IR data from U,B,V,R,I,J,H,K and L band fluxes (Hoffleit and Jaschek, 1982[37] and Glass 1974[27]) and IRAS 12,25,60 and $100\mu$ fluxes (Gillett 1986[26]), - and its well known distance, the luminosity of $\beta$ Pictoris is $5.69L_\odot$ (Paresce 1991[53]). Thus, the observed bolometric luminosity is $M_{bol} = 2.80 \pm 0.05$. The Strömgren indices (Hauck and Mermilliod 1980[31], and Crawford *et al.* 1970[18]) are $H_\beta = 2.86, (b - y) = 0.094, m_1 = 0.196, c_1 = 0.891$ while the Geneva photometry (Ruferner 1988[57]) yields $d = 1.25, B2 - V1 = -0.02, m_2 = 0.484$. From the Strömgren photometry, one can see that $\beta$ Pictoris is unusual in that it has the $(b - y), c_1$ indices as expected for a A5V, but a lower than average metallicity as indicated by its position in the $[m_1]$ vs $[c_1]$ diagram (Strömgren 1966[67]).

The observed values of the Geneva indices can be placed on the $d$ vs $B2 - V1$ graphs for various $[M/H]$ values and iterated until the appropriate parameters converge. The resulting parameters are $\log g = 4.2, T_e = 8200K$, and $[M/H] = -0.6 \pm 0.3$dex[1]. This gives $\beta$ Pictoris' metallicity as appropriately 0.25 of the Solar abundance, which would explain why $\beta$ Pictoris appears underluminous for an A5V star (Paresce 1991[53]). Some other fundamental stellar parameters can now be extracted, such as, $R = 1.2R_\odot$ and

---

[1]Note that there are no metal lines from which a direct determination of metallicity can be made.

$M = 1.5 M_\odot$, both slightly lower than the typical A5 dwarf but still within a quite plausible range.

The kinematics of $\beta$ Pictoris, as measured by its U,V,W velocities which are all less than 10 kms$^{-1}$ (Woolley *et al.* 1970[80]), suggest a normal galactic disk star while its metallicity is characteristic of a more distant and older thick disk star. But its high rotational velocity of 139kms$^{-1}$ is typical for a A5V star (Uesugi and Fukuda 1982[72]). On closer inspection however, this seemingly inconsistent result with the standard picture of galactic evolution appears to be a peculiar and somewhat widespread phenomenon among A stars (Wolff 1983[79] Lance 1988[48]).

Using the Green, Demarque and King 1987[29], revised Yale isochrones for the $Z = 0.004, Y = 0.2, T_e = 8200K$ case, which is most appropriate for the above data, one obtains given the uncertainties in the data and the analysis an upper age of $2 \times 10^8$ yrs. Therefore $\beta$ Pictoris is most likely on the ZAMS and has an age of $\sim 10^8$ yrs and certainly not exceeding $2 \times 10^8$ yrs (Paresce 1991[53]).

## 2.2   The circumstellar disk

Although $\beta$ Pictoris had been known as a shell star for decades, the first detection of the circumstellar disk came when $\beta$ Pictoris was examined by the Infra Red Astronomical Satellite (IRAS) in 1983. The observations of $\beta$ Pictoris revealed it was among the Vega-like stars which all exhibit infra-red excesses in the IRAS bands of 25, 60, and 100$\mu$m. This was interpreted to mean that these stars had cool circumstellar material surrounding them resulting in the observed excesses (Aumann *et al.* 1984[4]).

In fact of all the Vega-like stars $\beta$ Pictoris has the largest overall IR excess seen by IRAS, and exhibits the only substantial excess at 12$\mu$m (Gillett 1986[26]). Quite soon after this detection the circumstellar material was imaged around $\beta$ Pictoris by Smith and Terrille in 1984 whose coronagraphic images revealed the dust to be distributed in a highly flattened circumstellar structure, suggestive of a disk seen nearly edge-on. The disk was traced out to 25$''$ from the star in the NE and SW directions (25$'' \simeq 400$ AU at 16.4pc). Smith and Terrille measured an $r^{-4.3}$ power law for the projected brightness of the disk. Smith and Terrille in later observations (Smith and Terrille 1987[64]), also traced the disk out to more than 1000 AU and also noted that at about 300 AU the disk appears to be 50 AU thick.

Broadband B, V, R, I$_c$ multicolour photometry by Paresce and Burrows 1987[54] and Smith and Terrille revealed no colour differences from their coronagraphic imaging. Therefore the particle sizes are likely to be $\geq$ 1$\mu$m in radius. When these multicolour measurements are combined with the IRAS data the disk is found to have an inner region nearly clear of dust or the extinction expected is greater than observed (Artymowicz *et al.* 1989[3]).

$10\mu$m and $20\mu$m ground-based imaging with 5 arcsec resolution by Telesco *et al.* 1988[68] was able to constrain the models by revealing an inner region relatively clear of dust, possibly out to 30AU from the star.

Further imaging using anti-blooming CCDs of the $\beta$ Pictoris disk by Lecavelier des Etangs *et al.* 1993[21] found the disk fits an $r^{-3.6}$ power law. Multicolour photometry reveals a flat albedo for the dust particles, demonstrating the probable large sizes of the grains in the outer disk as predicted by Paresce and Burrows 1987[54] and Backman *et al.* 1992[5]. However the decrease in brightness in B differs from that in longer wavelength filters. From $2.5''$, where measurements begin out to $7.3''$ the B signal is a factor of 4 less than would be expected from inward extrapolation of the brightness outside $7.3''$. This change in albedo indicates a change in the nature of the grains. This is expected because of ice sublimation in this region ($\sim$ 20-40AU from the star). A difference in the grains occurs due to their less icy nature which should reveal more about the dust composition of the circumstellar disk. The disk also shows some asymmetry in the images which could be the signature of planet formation.

Observations from $8\mu$m to $12\mu$m by Telesco and Knacke 1991[69] detect the spectral signature of silicates. This is only seen within 3 arcsec of $\beta$ Pictoris, but this silicate emission at $10.8\mu$m suggests small grains ($\leq 1\mu$m) present near the star. Aitken *et al.* 1993[1] from $8\mu$m $- 13\mu$m spectroscopy confirms the presence of silicate emission, probably from small ($\leq 2 - 3\mu$m) grains in the disk. The sizes are believed to be similar to cometary dust. They also note that large particle sizes are required for the dust particles for orbital stability against radiation-pressure blow out or Poynting-Robertson drag. However, thermal modelling by Backman *et al.* 1992[5] requires particles near $1\mu$m in size to reproduce the IR measurements. Therefore the small particles must be replenished from collisions by larger bodies. The Backman *et al.* 1992[5] model can be summarised by Fig. 2.1.

This model quite simply describes what is currently known about the $\beta$ Pictoris disk.

Polarisation observations of the $\beta$ Pictoris disk indicate it exhibits polarisation orientation characteristics similar to those of a simple reflection nebula with polarisation of $\sim 17 \pm 3\%$ (Gledhill *et al.* 1991[28]). These observations in conjunction with the known colours of the disk suggest large grains ($\geq 10\mu$m), typical of interplanetary grains, are present. Also Knacke *et al.* 1993[39] shows that the dust around $\beta$ Pictoris cannot be interstellar like, indeed a better match is found with cometary spectra (like Halley's) indicating that the dust about $\beta$ Pictoris has been processed in some way. This data is supported by Savoldini and Galletta 1994[58] whose CO measurements of $\beta$ Pictoris shows the circumstellar material is depleted in CO which indicates that the star is in quite an evolved state. This requires some active process of gas transformation by means of accretion of solid bodies or conversely evaporation.

Lagage and Pantin[41] in their 1994 paper note dust depletion in the inner disk and
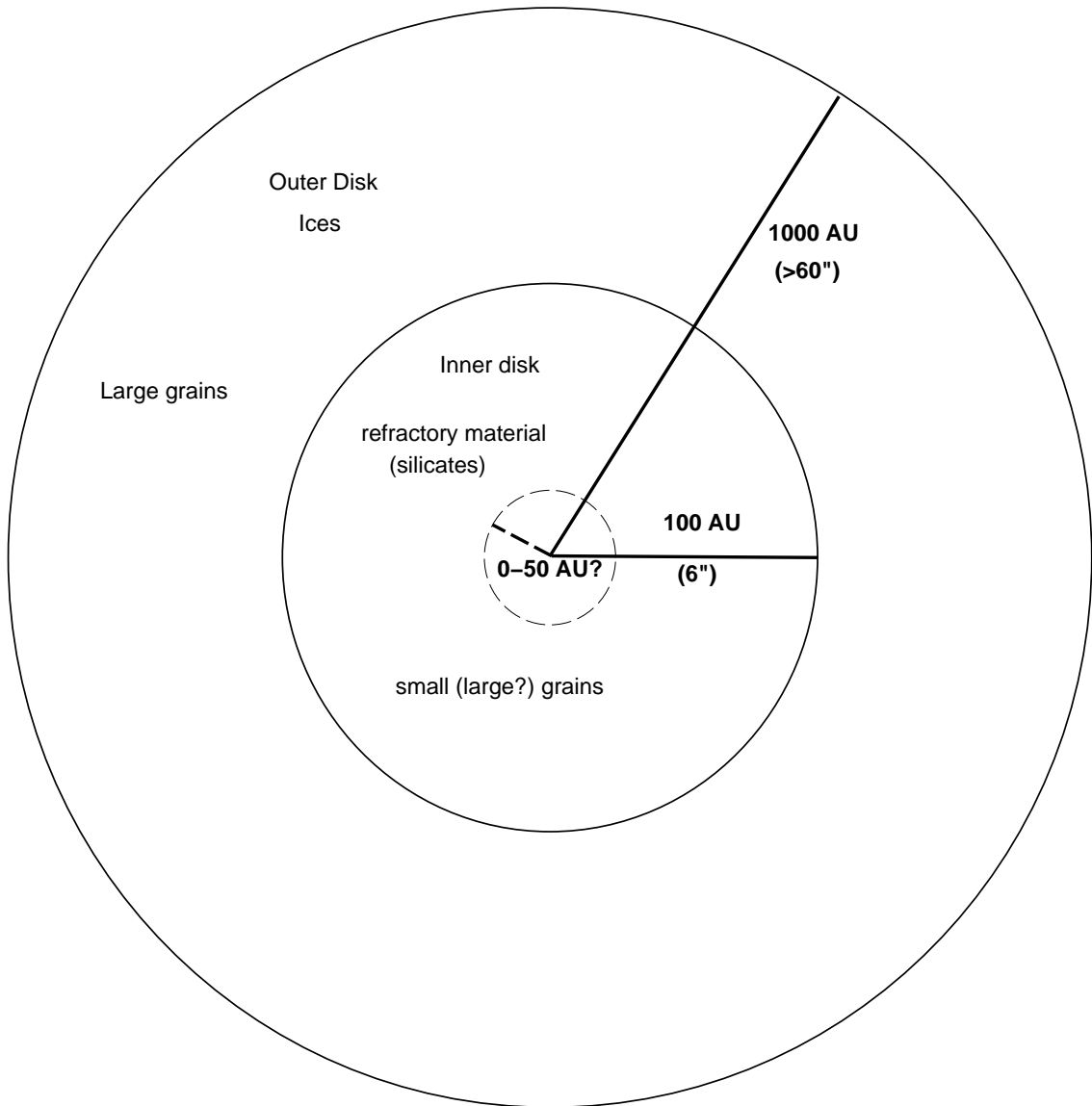
**Figure 2.1**: Backman *et al.* model for the circumstellar disk of $\beta$ Pictoris. (Not to scale).

also an asymmetry in the structure of the disk which hints at the existence of planets. These asymmetries in the circumstellar disk are confirmed in the paper by Kalas and Jewitt 1995[38] which demonstrate the existence of many asymmetries, such as:

- A size asymmetry where the NE extension of the disk can be measured out to $48''$ (790 AU) from the star, while the SW extension is seen only out to $40''$ (650 AU).

- A brightness asymmetry is also observed in the outer disk beyond $20''$ with the NE extension being observed to be brighter than the SW extension.

Other asymmetries are also mentioned in their paper, which could lend support to the idea of a Jovian-like planet causing perturbation in the dust disk.

One of the more interesting observations to come to light is the possible detection of a planet orbiting $\beta$ Pictoris in Lecavelier des Etangs *et al.* 1995[20] paper who show that Geneva Observatory photometry of $\beta$ Pictoris shows a gradual brightness and dimming in the visual magnitude which could be interpreted as the dust-free zone surrounding a planet coming into view and anti-occulting the star allow more of the star's light to be seen.

Of great interest in the future will be the result gleaned from observations of the refurbished Hubble Space Telescope like Fig. 2.2 which shows that the disk around $\beta$ Pictoris is a lot thinner than previously thought. This lends further support to the theory that planets have formed from the circumstellar disk, and also to the presence of large numbers of planetesimals which are believed to be observed spectroscopically (see Section 6.1).

In fig. 2.3 the disk appears slightly warped, had this been present when the star formed it should have flattened out by now. Therefore this has been taken to mean there is a planet or planets pulling at the disk and distorting it.

Future observations of the disk which can see closer into the star should help to prove one theory about the presence of arc-like structures in the disk in the planet-forming region. It is expected that if there are planets in orbit about $\beta$ Pictoris, they may reveal their presence by leaving regions clear of dust in their wake.

## 2.3  Variations in the spectroscopic lines - an overview

Because $\beta$ Pictoris is seen edge on it is well suited for absorption line studies of its circumstellar gas. High resolution observations of the spectrum of $\beta$ Pictoris reveal the presence of various anomalous features in some of its spectral lines. These features are sharp absorption features in the cores of some photospheric lines, as well as broad absorptions in the wings of those lines. The observed gas consists generally of low-ionization material somewhat similar to that in interstellar HI regions. Its temperature is $T_K \leq 4200K$ and a typical density is $n(H) \approx 10^5 cm^{-3}$ (Kondo and Bruhweiler 1985[40]; Hobbs *et al.* 1985[36];
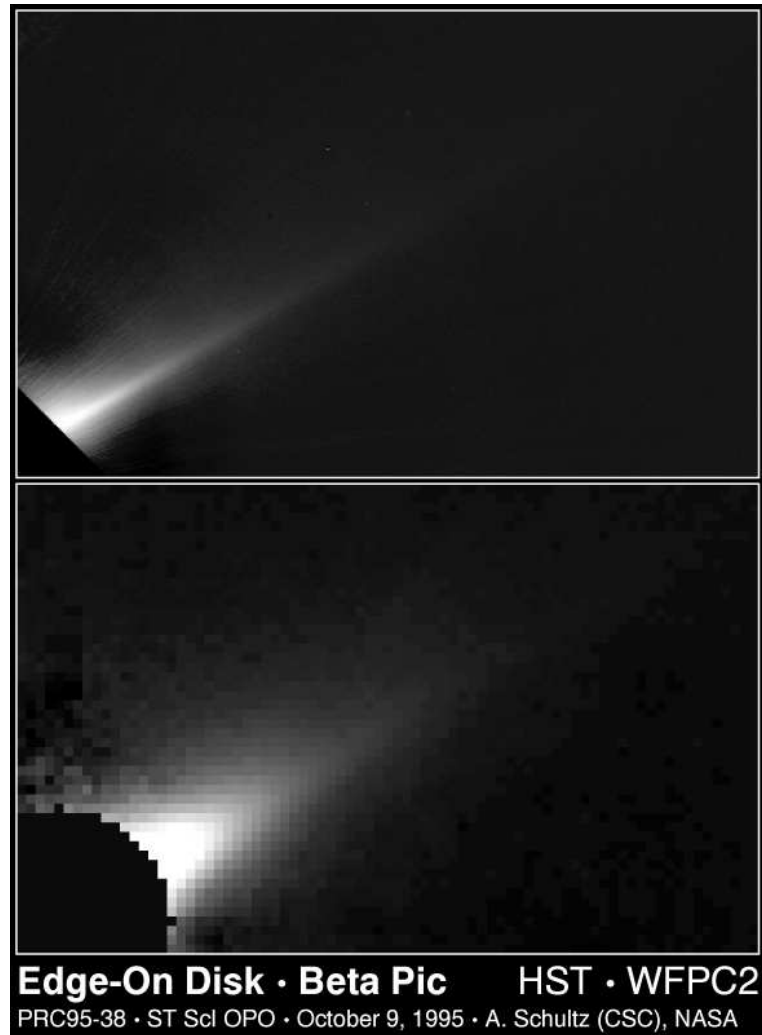
**Figure 2.2**: HST coronagraphic image of the circumstellar disk of $\beta$
Pictoris which reveals a thinner disk than previous ground based images
reveal.

Vidal-Madjar *et al.* 1986[74]). The circumstellar gas elements so far observed with these
features are Na I, Fe I, C I, Fe II, Mn II, Ca II, Zn II, Mg II, and Al III. The observed
features can be divided into 3 broad categories:

- A saturated circumstellar line centred at the radial velocity of $\beta$ Pictoris.

- Sharp absorption lines at low velocities, almost always redshifted.

- Broad absorption features found mainly at high velocities.

**The circumstellar line**
Is this line interstellar, or circumstellar in origin? Upon examination of the narrow absorption lines of Ca II and Na I seen in the spectrum of $\beta$ Pictoris, the interstellar origin
can be ruled out on several grounds;
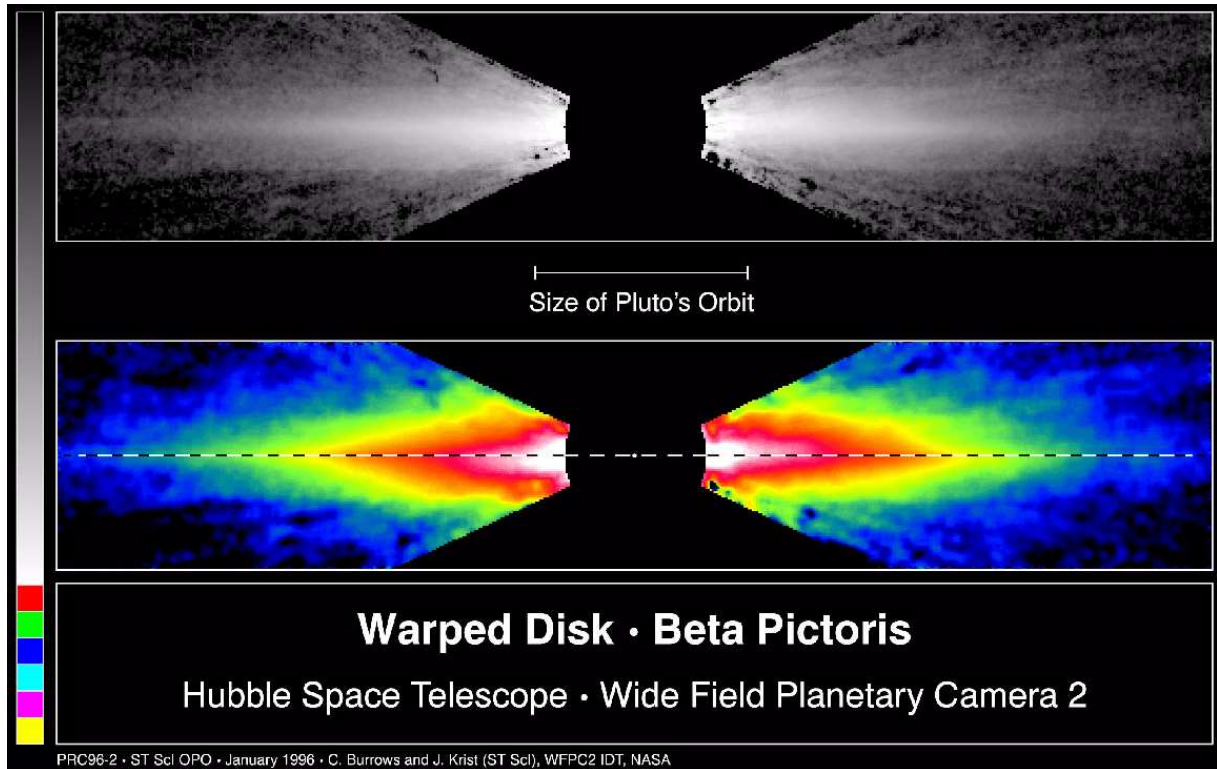
**Figure 2.3**: HST coronagraphic image of the circumstellar disk of $\beta$ Pictoris which shows an S shaped warp, which is interpreted as the signature of planets closer to the star.

1. For a star at $\sim$18 pc, the K line is much stronger than the interstellar K line seen towards any other comparably near star.

2. A ratio N(CaII)/N(NaI)$\gg$1 is found only in interstellar lines arising in high velocity gas, in contrast to the case for $\beta$ Pictoris.

3. Narrow absorption lines arising from excited, metastable, lower levels of Fe II, from which no interstellar absorption has been detected, have been extensively observed in the spectrum of $\beta$ Pictoris.

Having determined that the line cannot be of interstellar origin (Hobbs *et al.* 1985[36]), where does the gas come from to form this circumstellar absorption line given that an A5V star would quickly dissipate any Calcium around it.

There is considerable evidence the circumstellar Calcium K line component is fully saturated. Simultaneous observations of K and H allow the measurement of the doublet ratio. The equivalent widths of K and H were found to be 112$\pm$10 and 100$\pm$8 mÅ, respectively giving a doublet ratio of 1.12$\pm$0.13. The doublet ratio strongly implies that there is negligible flux in the core of the circumstellar lines. Ultra-high-resolution observations of the Ca K line by the Ultra High Resolution Facility at the Anglo-Australian

Telescope show that the circumstellar Calcium K line core is flat within the noise, which is characteristic of fully saturated absorption lines. It should be noted that if this line is truly saturated, it is unique in that no interstellar line has been observed to be fully saturated (Crawford *et al.* 1994[17]).

The source of the Ca II ions for the stable circumstellar line is probably from grains in the circumstellar disk evaporating near the star at a distance of about 0.5 AU. As the grains spiral towards the star due to Poynting-Robertson effect the intense starlight causes the grains to evaporate releasing the Calcium back into the gas phase and produce the bulk of the apparent stable part of the absorption (Lagrange *et al.* 1987[42]). This process insures that there is a constant supply of material to maintain a saturated absorption line. This has been termed the grain-evaporation hypothesis by Vidal-Madjar *et al.* 1986[74]. Hobbs *et al.* 1988[35], concluded that most of the Ca II absorption occurs at a distance of order 1 AU. This is consistent with the grain-evaporation hypothesis.

When other lines are examined it appears that the source of the stable absorptions are located in different regions. Na I and Ca II are located in two different regions of the circumstellar disk, the Na I in an outer region which contains nearly all of the mass of the disk. Also in this region Calcium is underabundant by a factor of perhaps $10^4$ (Vidal-Madjar *et al.* 1986[74]). Finally Vidal-Madjar *et al.* 1994[75] have determined that Ca II ions are blocked from leaving the $\beta$ Pictoris systems by collisions within the stable gaseous cloud that forms the torus around the star producing the circumstellar feature. Hence why we observe the stationary ions.

**The variable features**

Observations of the Calcium K line at different epochs shows drastic changes on timescales of months, weeks, days and hours. In the wings of the photospheric lines these absorptions can appear and disappear at will and tend to be broad in appearance at high velocities and at lower velocities narrow and deep. These changes could be related either to a "classical" shell close to the star or to the much more extended circumstellar dust disk around $\beta$ Pictoris. These variations could be due to a number of causes:

**A stellar photospheric phenomenon.**

This can be excluded. Such a mechanism occurring in the stellar atmosphere should affect all the main photospheric lines. The variable features however are only observed in the strongest resonance lines and some metastable lines of Fe II (Lagrange-Henri *et al.* 1988[47]).

**A shell phenomena close to the stellar surface**

Having previously been classified as a shell star by Slettebak in 1975, $\beta$ Pictoris shows a Ca II K line profile similar to those of other A-type stars. Since the velocity extent of the Ca II perturbations seen in $\beta$ Pictoris is $\sim$40 kms$^{-1}$ (for the easily detected absorption cores), significantly below the stellar escape velocity ($\sim$650 kms$^{-1}$) the corresponding gas was not able to escape from the star. It should thus fall back on the star and this could

explain the observed redshift. If at other epochs permanently blue-shifted material is detected, it will strengthen this possibility.

IUE spectra from late 1986 to early 1988 show:

1. minimal shell column densities

2. spectra showing outflowing plasma

3. broadened but "stationary" absorption

4. spectra showing infall

Ejection of a circumstellar envelope can be expected to produce all 4 phases that have been observed (Bruhweiler *et al.* 1991[13]). These effects would be observed as mass gets blown off the star - producing the blueshifted features - and falls back in to the star having not achieved escape velocity - hence producing the observed infall - some of this gas maybe for a time left in orbit about the star before falling back in - hence the broadened but "stationary" absorption.

**A phenomenon related to the dust shell present at larger distances from the star**

The circumstellar component of the K line is due to the gas associated with the inner disk at about 0.5 AU and enriched in Calcium because of dust grain evaporation. One therefore expects a relatively stable central core shape, as observed. If the variable absorptions are due to inhomogeneities in the continuously infalling dusty material, and these inhomogeneities are stable, their orbital period should then produce periodic perturbations of the line.

**Discrete events of freely falling material**

However one can interpret the observed variations as being due to discrete events of freely falling material. Large bodies like cometary nuclei could plausibly account for such observations (Ferlet *et al.* 1987[24]). The clumpy structure of the infalling material is confirmed by Lagrange-Henri *et al.* 1989[43] which lends further support to some form of discrete phenomenon.

The observed variability in the infalling plasma would imply, under a cometary inflow model $\approx$10-100 star grazing comets per year (Lagrange-Henri *et al.* 1988[47]). This rate is currently higher than is observed in the Solar System, but is compatible with the rate inferred for the initial phase of the Solar System (Beust *et al.* 1989[6], Telesco *et al.* 1988[68], Lagrange *et al.* 1987[42]). This scenario, which requires a large star-grazing comet bombardment rate, can account for the infalling plasma and potentially for intermittently enhanced "stationary" plasma (in Keplerian orbits).

The presence of Al III variable absorption features in the spectrum of $\beta$ Pictoris presents something of a mystery. Photoionization by an A5V star like $\beta$ Pictoris is unable to produce such a highly ionized species, implying that an additional mechanism

is required to explain the observed ionization (Deleuil *et al.* 1993[19]). The presence of infalling bodies may be one of the few possibilities that can adequately explain the presence of a highly ionized species such as Al III.

## 2.4   The Falling Evaporating Bodies scenario

The Falling Evaporating Bodies (FEB) scenario was formed to explain the observed variations in some of the metallic lines of the spectrum of $\beta$ Pictoris. These variations were observed to be predominantly red-shifted, i.e. falling towards the star at relatively low velocities.

The suggestion that the observed variations could be caused by comet-like bodies passing close to the star is quite appealing given the age of the $\beta$ Pictoris system. From our own Solar System we know that the early Solar System under went intense bombardment in the first 700 million years; evidence of this can be clearly seen in our own Moon. So one expects for the $\beta$ Pictoris system, with its clearly detectable circumstellar disk, that cometary bodies will have been formed in vast numbers. Given the edge-on orientation of the disk the possibility of a cometary body crossing the line of sight is greatly increased if, as we expect, most of the material orbiting the star is confined to the plane of the disk.

A model for these events has been developed by Beust *et al.* 1989[6] to explain the observed variations. The model assumes that the variations seen are due to evaporating material from a cometary body. As a first approximation they assumed a spherical distribution of the cometary gas for 2 reasons:

1. the radiation pressure is not very efficient on hydrogen atoms (at least not the EUV flux from an A5 star).

2. there is no appreciable stellar wind in normal A5 stars. Therefore hydrogen atoms are not efficiently repelled.

One can then consider the density of the gas as a function of 4 parameters

- the distance $r$ between the comet and the star.

- the distance $x$ between the considered point and the nucleus.

- the outflow velocity of hydrogen from the nucleus $v_e$

- the hydrogen production rate of the comet.

The infalling bodies, treated as points, are assumed to come from the circumstellar disk itself, i.e. quite far from the star, so the orbits can be taken to be parabolic ones (Beust *et al.* 1990[7]).

Each redshifted absorption is then interpreted as the signature of an infalling solid body, which evaporates in the vicinity of the star (Ferlet *et al.* 1987[24] and Beust *et al.* 1991[9]). The grains evaporated from the comet are assumed to produce the evaporated ion. These ions are then subjected to gravity, radiation pressure and collisions with the surrounding gas and grains. Simulations are able to reproduce some of the observed absorption features very well, once appropriate values for the orbital parameters are added (Lagrange-Henri *et al.* 1992[45]).



$$z \text{ at } 1 \text{ A.U.} = 15.0 \ 10^{33} \ s^{-1}$$
$$dm/dt = \ \ \ 0.010 \ 10^{10} \ kg \ s^{-1}$$
$$\text{outflow velocity} = 10.0 \ km \ s^{-1}$$
$$s_0 = \ \ \ \ 1. \ \mu m$$
$$q = 23.5 \ R_*$$
$$\Phi = -170.0^{\circ}$$
$$\text{proportion } H_2O : 80.0\%$$

Ion : CaII

$$t = \ 28^H \ 0 \ min. \ \ 0 \ s.$$
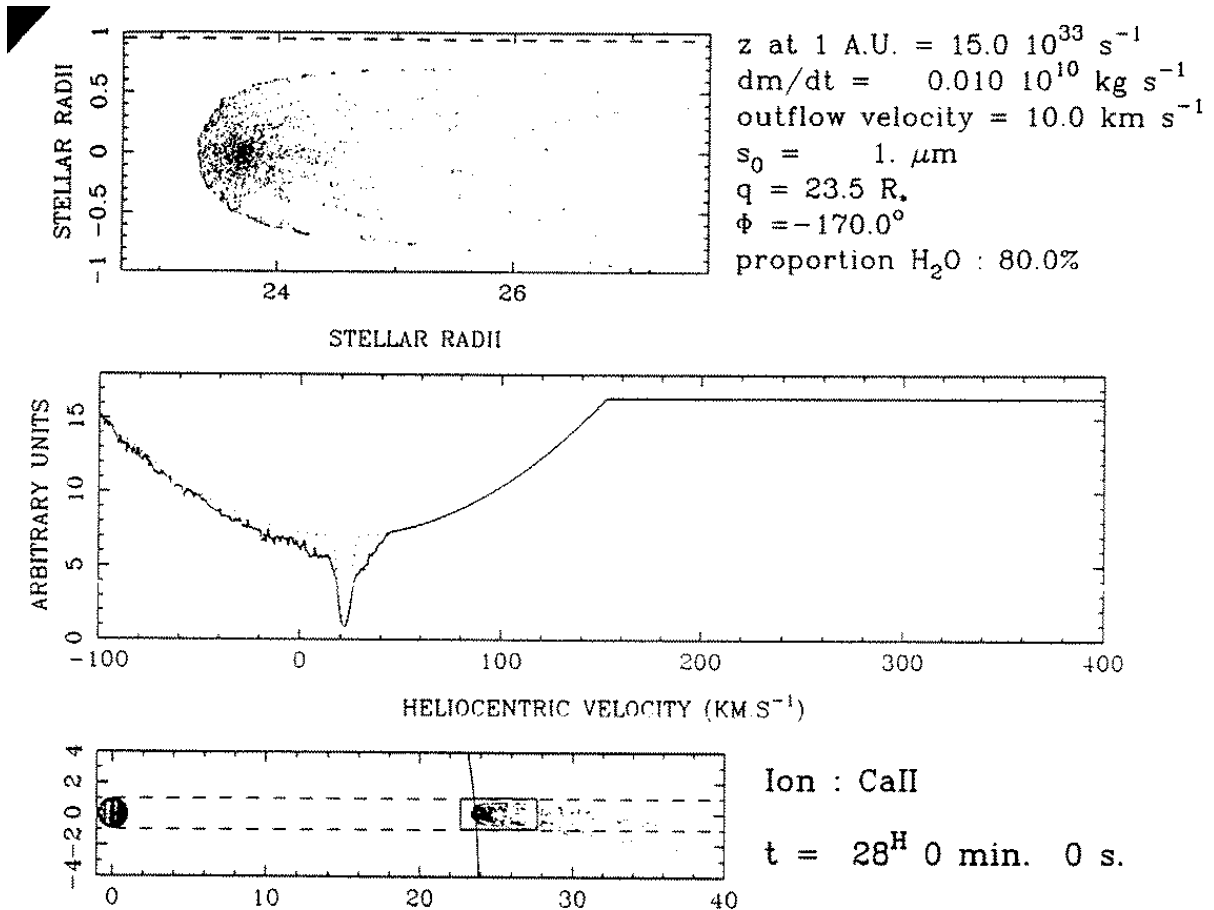
**Figure 2.4**: Plots of the simulations of an FEB in an orbit close to simple infall and passing close to the star. The first plot shows a 2-dimensional view of the Ca II cloud around the nucleus with each dot representing a Ca II ion which is numerically followed. The second plot is the synthetic spectrum. The third plot is a schematic representation of the situation (see Beust *et al.* 1990)

From these simulations it appears that the preponderance of redshifted absorption in the LVFs are due to bodies falling from a precise direction in the circumstellar disk (Beust *et al.* 1991[11]). For these bodies to be perturbed from a particular direction in the disk Beust *et al.* proposed a planet in an elliptical orbit ($e \sim 0.6$) as the perturber to make the star-grazing comets detectable by spectroscopic means. Levison *et al.* 1994[49] propose
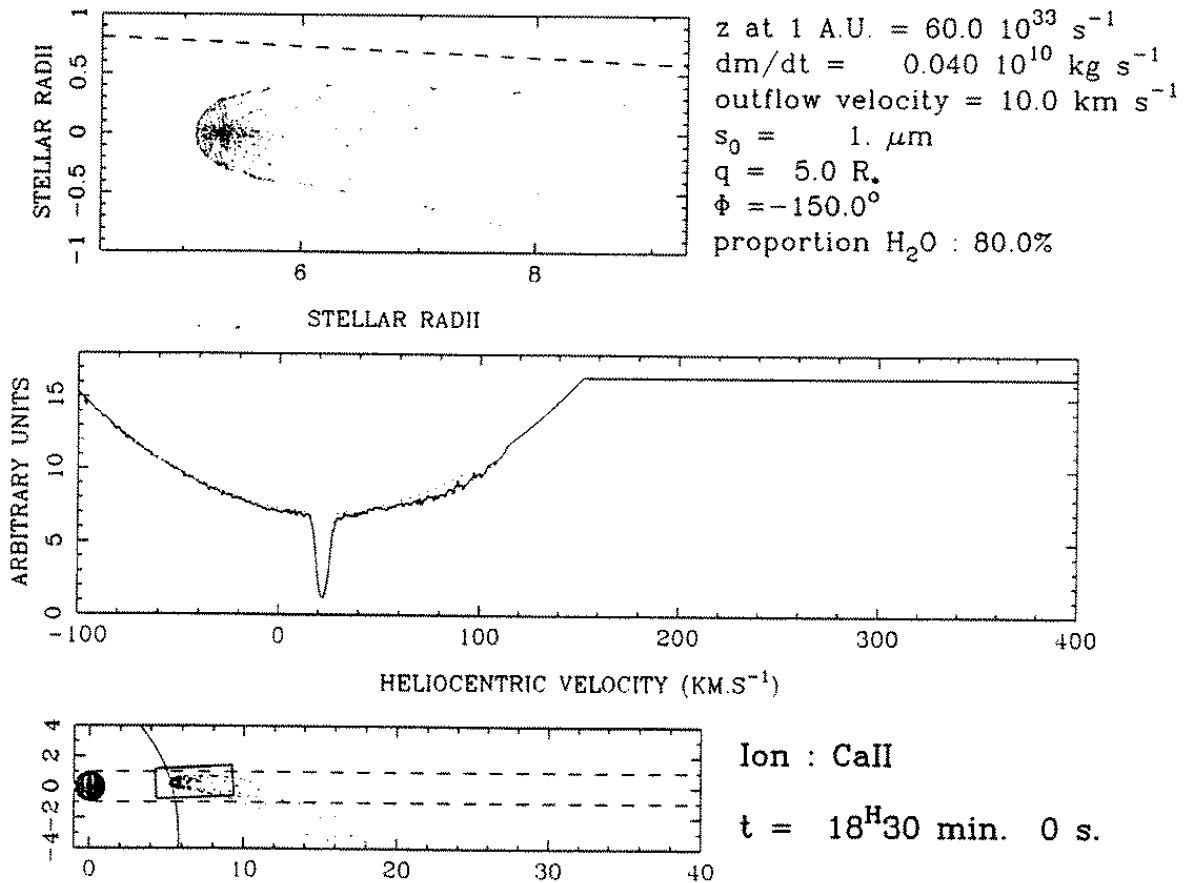
**Figure 2.5**: The plots here are similar to Fig. 2.4 but the body approaches the star much closer.

that secular resonances from a planetary system of at least 2 planets, a prerequisite for the existence of secular resonances, can align the orbits of some bodies in such a way one can reproduce the general features seen in $\beta$ Pictoris. Further simulations have reproduced the features seen at $\sim$20kms$^{-1}$ as being due to bodies arriving with an inclination of $-150\pm10°$ (Lagrange-Henri et al. 1992[45]).

The time taken by a body to cross the stellar disk is estimated to be of the order of $\sim$4 hrs, however many of the observed features are much longer lived (>4hrs). Since a single infalling body cannot explain this observation, these events must be due to several individual bodies crossing the line of sight at roughly the same moment, but with spread out periastrons. This also explains the multiple structure seen in some features. These bodies do not need to fall in as a simple queue, the only constraint is in the inclination to the line of sight (Lagrange-Henri et al. 1992). A very interesting and plausible consequence coming from the observations of several bodies falling in at once, is that from time to time a disk of gas might possibly form around the star which is fed by the evaporating "shower" of bodies (Ferlet et al. 1993[25]).

Ca II ions will be observed when they are ∼1 AU from the star, in to about 10 stellar radii. This is the region where most of the observed features occur, but should Ca II ions be closer than ∼10 stellar radii then one should observe blueshifted features and, or broad shallow redshifted features (Beust *et al.* 1991). High redshifted features due to bodies getting much closer to the star should evolve quicker as the body crosses the line of sight. These events are expected, as they should also be the bodies which produce the observed UV features (Beust *et al.* 1989[6] and Lagrange-Henri *et al.* 1992[45]).

Finally in 1989 blueshifted features were observed in the spectra of $\beta$ Pictoris: a narrow feature at low velocity and also a broad feature at high velocity. The narrow feature with the small blueshift can be reproduced with a larger inclination angle between the axis of the orbit and the line of sight. The broad feature is easier to interpret as being due to the cometary tail being observed, as the ions are blown away from the star via radiation pressure (Lagrange-Henri *et al.* 1992[45]).

A new theoretical development is the ability to derive information on the size of the cloud of ions from simultaneous observations of Ca II H & K depending on the level of saturation of the lines. For saturated lines $\alpha$ (the fraction of the stellar disk occulted by the cloud) can be determined easily, but for weak and unsaturated lines $\alpha$ cannot be so well determined. Unsaturated lines can only give a lower limit for the absorbing $\alpha$ (see Fig. 2.6).
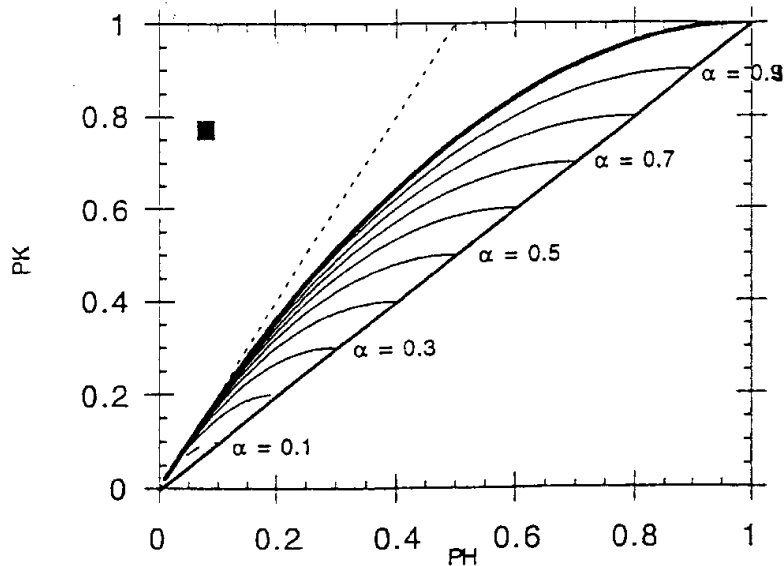


**Figure 2.6**: Theoretical diagram of the depths of the H & K lines. The curves are for different values of $\alpha$, the filling factor of the absorbing cloud for a non-rotating stellar disk. The values of $\alpha$ can infer the amount of the stellar disk being occulted. PK and PH are the central depths of the absorption features (see Lagrange-Henri *et al.* 1992).

A test of the FEB scenario by Beust and Lissauer, 1994[30] relies on the details of the absorption line spectra and their temporal variation and the effect on the absorption lines of the rotation of $\beta$ Pictoris itself. The ratio of the equivalent widths of certain observed absorption doublets imply that the absorber is often locally optically thick, but only covers a small portion of the stars disk. Stellar rotation implies that the portion of $\beta$ Pictoris' photosphere being occulted has a well-defined velocity which may be different from the star as a whole. The depth of the feature will depend on the portion of the disk being occulted. Comets crossing from the redshifted side to the blueshifted side or vice versa will give different patterns for the evolution of the equivalent widths. See Figs. 2.7 and 2.8. The effect is most striking in the K line.
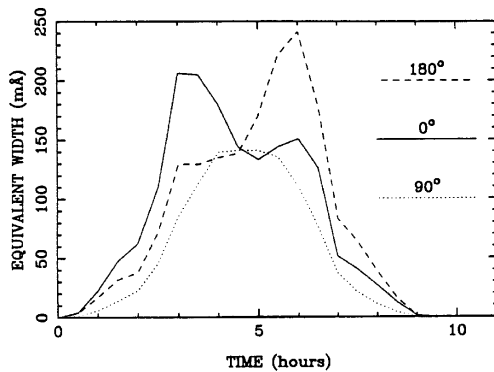


Figure 2.7: The expected evolution of the equivalent width of the K line for an FEB crossing the line of sight from different directions when the rotation of $\beta$ Pic is taken into account.
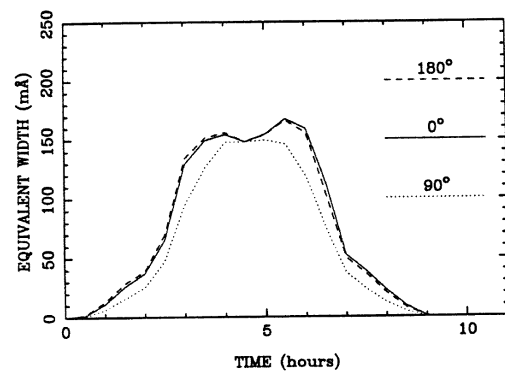
Figure 2.8: The expected evolution of the equivalent width of the H line for an FEB crossing the line of sight from different directions when the rotation of $\beta$ Pic is taken into account.

The presence of Al III in the spectra of $\beta$ Pictoris came as a great surprise given that the EUV flux of an A5V star is not able to produce such a highly ionized species by photoionization (Lagrange-Henri *et al.* 1988[47]). The FEB scenario suggest a natural process that can do this, namely collisional ionization in the shock region of a coma surrounding an evaporating body. A hydrodynamic model by Beust and Tagger 1993[8] studied the comas surrounding evaporating bodies in which shock surfaces form where high temperatures can occur allowing the ionization of exotic species such as Al II, Mg II and Al III to occur. Vidal-Madjar *et al.* 1994[75] note in this situation temperatures as high as T = $10^5$K are easily achieved. The conditions under which Al III can be formed is restricted to the immediate vicinity of the star d$\leq$5R$_*$ (Beust and Tagger 1993, and Beust *et al.* 1994[10]).

Observations of Al III show that the redshifted line is saturated while the blue part of it is the normal doublet ratio showing that the blue part is produced by a larger (possibly covering the whole stellar disk) and more dilute plasma (Vidal-Madjar *et al.* 1994[75]).

From the measurements of Al III it is possible to calculate the total mass of gas involved in the variable features. The Al III column densities, multiplied by the cross-section of the star provide a lower limit on the amount of variable aluminium. The aluminium can also be in other states (eg. Al II) but once normalised to Solar abundances and to meteoritic abundances one can determine the mass of the evaporated body. This gives the objects having sizes in the kilometre range (Lagrange-Henri *et al.* 1988[47]. These same calculations can be carried out for the other ions, and do indeed give similar sized objects as a result.

One can note that the terminal velocity for Al III is compatible to the free fall velocity at a few stellar radii from the star, while for Ca II the corresponding terminal velocities for the LVFs are typical of the free fall velocities at $\sim$2.2 AU (Beust *et al.* 1989[6]). The velocities that these lines are observed at do agree with theory as the variations have yet to be observed at velocities that exceed the free-fall velocities of objects near a star.

Supporting this FEB scenario is the completely different argument based on the theory of cometary dynamics in the Solar System which lead Weissman 1985[78] to the conclusion that the $\beta$ Pictoris disk of matter might be very similar to the wide cometary reservoir needed in the Solar System (Lagrange-Henri *et al.* 1988[47]).

## 2.5   Protoplanetary disks around other stars

With the reports from the IRAS satellite of certain nearby stars having infra red excesses in some of the infra red bands being used, it was believed that these could be the first detection of dust disks around other stars and indeed the first detection of circumstellar material that could be the precursor to planets. The visual detection of the circumstellar disk around $\beta$ Pictoris by Smith and Terrile confirmed that the IRAS detection was indeed of circumstellar material from which planets could form. $\beta$ Pictoris has since then been the best candidate for a nearby planetary system that could be studied from Earth, and indeed given its evolutionary status, provides a good test of theories on planetary formation.

Of course, the detections in the IRAS bands only indicate that there is some material around the stars reradiating in the infra red light; the radiation could be from the stellar wind or dust surrounding the star. However any detection in the 60 and $100\mu$m bands in the ratio expected for cool dust around the star, would rule out the other possibilities as the nature of the sources. Given this the strong excesses around the stars Vega, $\alpha$ PsA, $\epsilon$ Eri, and $\beta$ Pic were considered the best indicators of the possible presence of protoplanetary dust disks (Aumann *et al.* 1984[4]).

With that first detection of a disk of material around $\beta$ Pictoris, other stars in the IRAS point source catalogue were examined for further evidence of the existence of circumstellar material. Re-examination of the IRAS data and further observations of stars in the Point

Source Catalogue by Walker and Wolstencroft 1988[76], Cheng *et al.* 1992[14], and Chini *et al.* 1991[15] have determined that a number of the other sources identified as likely protoplanetary disks indeed have dust around them. In particular several of the stars such as Vega and $\alpha$ PsA appear to have disks seen face on or nearly so.

Spectroscopic observations have been made to detect any possible disks in a near edge on orientation like $\beta$ Pic. They too might exhibit a circumstellar line in the core of some of the photospheric features. These searchs have been made by Hobbs 1986[34], Lagrange-Henri *et al.* 1990[44], and Grady *et al.* 1991 who have been looking in the Na I, Ca II lines and IUE spectra for evidence of a circumstellar disk or infalling plasma. 3 more stars are now known to exhibit behaviour similar to $\beta$ Pic with the spectral signature of infalling plasma; they are HD 93563, $\sigma$ Her, and 51 Oph.

Smith and Terrile have continued their work in searching for further stars with circumstellar disks and imaging them coronagraphically. They report in their 1992 paper[62] that a survey of more than 100 stars within 100 pc looking for disks in an edge-on orientation or moderate inclination found no other examples other than $\beta$ Pic. Once again the stars selected were from among the IRAS Point Source Catalogue with additional stars added to give a better spread in spectral type.

In 1991 68 Ophiuchus, a spectroscopic binary, was imaged with a disk around it by Vidal-Madjar *et al.* 1993[73]. However the discovery of the disk has not been confirmed by other observers, infact it is now believed to be the result of imperfect removal of the scattered light from the telescopes secondary spider (see Waters *et al.* 1995[77]).

In 1994 it was reported that millimetre wave mapping observations of Fomalhaut revealed the presence of extended 1.3-mm emission around the star (see IAUC #5732[66]) in observations made in early 1993. Subsequent observations in 1994 failed to detect any evidence of this emission and it is now believed to be the result of some artifact in the earlier data (see Stern *et al.* 1994[65]).

The *Hubble Space Telescope* has imaged many proto-planetary disks around still forming stars in the Orion star forming region as well as other regions of star formation. The Orion images in question show the protoplanetary disks being silhouetted against the bright background of the Orion nebula. Other observations made of star forming regions reveal all the expected phases of star formation that theory has predicted. As a result of these observations by the Hubble Space Telescope it would appear that protoplanetary disks about forming stars are quite common (indeed many of the stages of star and circumstellar disk formation are seen) and that as a consequence planetary formation is also fairly common.
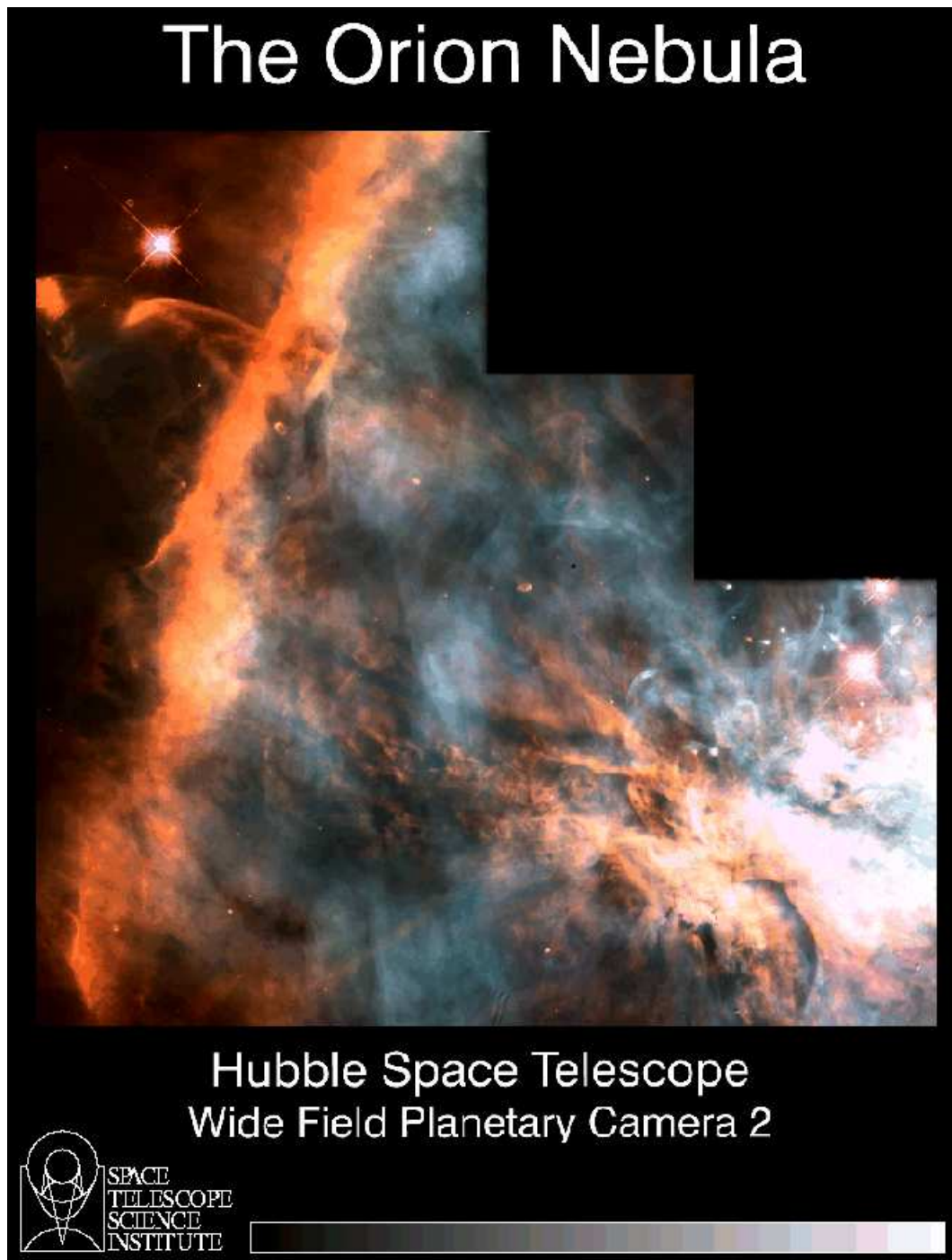
**Figure 2.9**: HST images of protoplanetary systems in the Orion nebula (courtesy of NASA).

# Chapter 3

# Aims of this Thesis

This thesis will look into any variations of the Calcium II H & K lines in the spectra of 3 stars which show promise as either proto-planetary systems or as stars surrounded by the remains of a circumstellar disk from which planets may have formed. The Ca II lines of $\beta$ Pictoris will be examined to study the variations and evolution of these variations and compare them with the predictions of the Falling Evaporating Bodies scenario.

## 3.1   Selection of targets

Selection criteria for the stars to be observed were that they exhibit some evidence of circumstellar material and be observable with the equipment available at MJUO. To be considered for selection the stars had to have an IRAS excess, which is considered as a good indicator of possible circumstellar material. Of these stars the following criteria were applied to narrow the selection to just a few objects. The stars had to be brighter than 7th magnitude in order for adequate spectra to be obtained. An additional but optional criterion was that the star had been coronagraphically imaged, and showed some indication of circumstellar material. Two stars in addition to $\beta$ Pictoris were found that satisfied the above criteria, namely $\alpha$ Piscis Australis and 68 Ophiuchus which were reported to have had images taken that revealed the presence of circumstellar material (see the IAUC #5732[66] and #5795[73]). Hopefully if these stars exhibit any of the activity seen in $\beta$ Pictoris, it would be observed and recorded. After analysis, it was hoped something would be able to be said about the activity around all these stars.

The data in the following tables were obtained from The Bright Star Catalogue [37] and the Hipparcos Input Catalogue [23]. See Table 3.1 for the data on $\beta$ Pictoris, Table 3.2 for the data on 68 Ophiuchus, and Table 3.3 for the data on $\alpha$ Piscis Australis.

## 3.2   Evaluation of the Falling Evaporating Bodies scenario

Previous spectroscopic observations of certain spectral lines at high resolution in the spectrum of $\beta$ Pictoris, reveal a changing structure in the cores of those photospheric lines affected. They have been divided into 3 types:

- a circumstellar feature at the radial velocity of the star.

| Name | $\beta$ PIC |
|------|-------------|
| HR | 2020 |
| HD | 39060 |
| RA(2000) h m s | 5 47 17.1 |
| Dec(2000) $^\circ$ $'$ $''$ | $-51$ 3 59.4 |
| $V$ | 3.85 |
| $B - V$ | $+0.17$ |
| $U - B$ | $+0.10$ |
| $R - I$ | $+0.16$ |
| Spectral class | A5V |
| PM($\alpha$) $''$yr$^{-1}$ | $+0.012$ |
| PM($\delta$) $''$yr$^{-1}$ | $+0.079$ |
| Parallax $''$ | 0.055 $\pm$0.008 |
| Distance | 18.1pc (59.3ly) |
| RV (kms$^{-1}$) | $+20$V? |
| $v \sin i$ (kms$^{-1}$) | 139 |

**Table 3.1**: Stellar parameters of $\beta$ Pictoris

- LVFs which are often quite deep and narrow, and appear to last for several days or even weeks.

- HVFs which vary rapidly in timescales of only hours and which are generally broader and less deep.

To understand these varying absorption features in the Calcium II H & K lines, one needs to derive the various parameters of interest:

- the velocities of the features.

- the widths of the features.

- the equivalent widths.

To do this one must distinguish between the photospheric and circumstellar features, and properly identify the variable ones. One must then either fit the photospheric "continuum" in the velocity range of interest, or divide the spectra by another reference spectrum assumed to be free of variable absorption features. Previously the parameters of the LVFs were measured directly on the spectrum, after fitting the "continuum" locally. The HVFs have only been observed in spectra that have been divided by a reference one.

These general observations of the variable absorption lines in the cores of the spectral lines of $\beta$ Pictoris are all features naturally associated with the predictions of the FEB

| Name | 68 OPH |
|---|---|
| HR | 6723 |
| HD | 164577 |
| RA(2000) h m s | 18 1 45.1 |
| Dec(2000) $^{\circ}\ '\ ''$ | +1 18 17.9 |
| $V$ | 4.42 |
| $B - V$ | +0.046 |
| $U - B$ | +0.00 |
| $R - I$ | +0.01 |
| Spectral class | A2Vn |
| PM($\alpha$) $''\mathrm{yr}^{-1}$ | +0.006 |
| PM($\delta$) $''\mathrm{yr}^{-1}$ | −0.025 |
| Parallax $''$ | 0.015 ±0.006 |
| Distance | 66.6pc (217 ly) |
| RV (kms$^{-1}$) | +6SB |
| $v \sin i$ (kms$^{-1}$) | 252 |
| $\Delta m$ | 4.8 |
| Separation $''$ | 0.6 |

**Table 3.2**: Stellar parameters of 68 Ophuchius

scenario. The FEB scenario has been able to explain many of the observed features seen in the Calcium lines and other species, but still many observations need explaining. To test the FEB scenario further, more information is required on:

1. the occurrence of variable absorption features. Particularly, do the deep and shallow absorptions differ significantly in their frequency of occurrence.

2. the velocities, duration and the small time scale variations of the variable components. This will help in determining the orbital parameters necessary to reproduce the observations in simulations from theoretical models.

3. the geometry and physical conditions in the absorbing cloud; namely how large the clouds of ions are with respect to the stellar disk.

4. the prediction by Beust and Lissauer[30] about the differences in the absolute and relative equivalent width of the Calcium H & K features, which varies depending on what part of the stellar disk is being occulted (see Fig 3.1).

5. single and group events. Are we seeing single events of ∼4 hrs duration, or longer lived events most likely due to groups of evaporating bodies?

| Name | $\alpha$ PsA |
|---|---|
| HR | 8728 |
| HD | 216956 |
| RA(2000) h m s | 22 57 39.0 |
| Dec(2000) $^\circ$ $'$ $''$ | $-29$ 37 20.1 |
| $V$ | 1.16 |
| $B - V$ | $+0.09$ |
| $U - B$ | $+0.08$ |
| $R - I$ | $+0.02$ |
| Spectral class | A3V |
| PM($\alpha$) $''$yr$^{-1}$ | $+0.333$ |
| PM($\delta$) $''$yr$^{-1}$ | $-0.165$ |
| Parallax $''$ | 0.144 $\pm$0.007 |
| Distance | 6.9pc (22.6ly) |
| RV (kms$^{-1}$) | $+6.1$ |
| $v \sin i$ (kms$^{-1}$) | 100 |

**Table 3.3**: Stellar parameters of $\alpha$ Pisces Australus

Another important aim of this thesis is to compare the results of the 1992 international observing campaign with the more extensive data set contained in this thesis, from MJUO. The results of the 1992 campaign which observed $\beta$ Pictoris over several days with near complete coverage, has revealed some interesting results. The variable features appear to be stronger and more numerous than ever before observed. The equivalent widths of the LVFs described in the paper by Lagrange-Henri *et al.* 1992[45] when present, were typically 30mÅ, whereas the Dec 1992 LVFs are always present and with equivalent widths larger than 100mÅ. HVFs are also observed much more often. For the first time, both the appearance and disappearance of these highly redshifted events were observed. The HVFs also vary both in central velocity and strength on very short timescales of a few hours. When they disappear it has been noted that they get broader. In fact the higher the redshift, the smaller the variability timescales, the smaller the filling factors of the clouds and the wider the lines.

High resolution studies reveal a clumpy structure to the infall of the Ca II clouds, and the estimate on the rate of infalling events is $\geq$200 events per year under the FEB scenario.
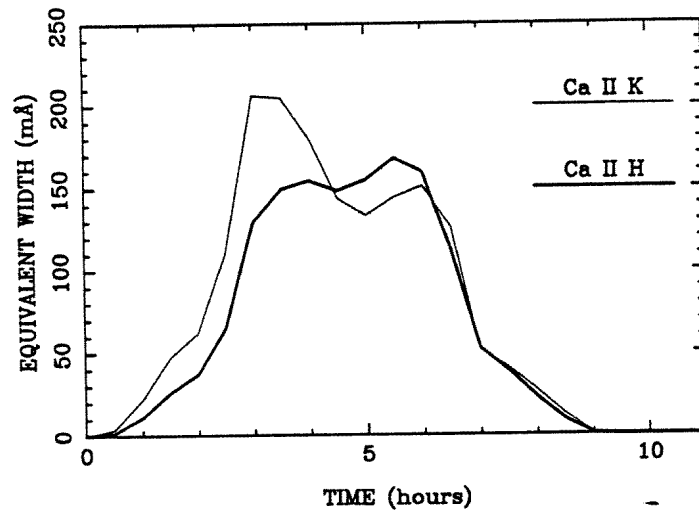
**Figure 3.1**: The expected evolution of an FEB crossing the line of sight.

# Chapter 4

# Observations

Observations were made of Beta Pictoris and the two other stars of interest (Fomalhaut and 68 Ophuchius) at the University of Canterbury's, Mt John University Observatory. The instruments used were the 1-metre McLellan Telescope which had mounted on it the Observatory's high-resolution échelle spectrograph and the PM 3000 CCD system as detector.

## 4.1 Observing log

Observation runs allocated on the telescope were of approximately one week and two weeks duration per observing quarter. Observing time was allocated from April till November 1995 to obtain the recent data contained in this thesis. Data from earlier observational runs as part of an international collaboration on Beta Pictoris were also available. Table 4.1 contains a list of the 1995 observations for this thesis.

Table 4.1: **Table of observations made at MJUO in 1995**
The table above shows the UT date, star, and number of spectra taken in each of the Calcium II lines observed.

| Date of observation | Star | # of spectra |
|---|---|---|
| 8 December 1992 | $\beta$ Pictoris | 12 CaII K |
| 9 December 1992 | $\beta$ Pictoris | 2 CaII K |
| 10 December 1992 | $\beta$ Pictoris | 12 CaII K |
| 11 December 1992 | $\beta$ Pictoris | 12 CaII K |
| 12 December 1992 | $\beta$ Pictoris | 6 CaII K |
| 13 December 1992 | $\beta$ Pictoris | 7 CaII K |
| 14 December 1992 | $\beta$ Pictoris | 8 CaII K |
| 15 December 1992 | $\beta$ Pictoris | 2 CaII K |
| 16 December 1992 | $\beta$ Pictoris | 7 CaII K |
| 9 January 1993 | $\beta$ Pictoris | 1 CaII K |
| 6 April 1993 | $\beta$ Pictoris | 2 CaII K |
| 24 October 1993 | $\beta$ Pictoris | 4 CaII K |
|  |  | 1 CaII H |
| 25 October 1993 | $\beta$ Pictoris | 4 CaII K |

**Table 4.1 cont.:** Table of observations made at MJUO in 1995

| Date of observation | Star | # of spectra |
|---|---|---|
| | | 5 CaII H |
| 27 November 1993 | $\beta$ Pictoris | 4 CaII K |
| | | 1 CaII H |
| 28 November 1993 | $\beta$ Pictoris | 5 CaII K |
| | | 1 CaII H |
| 29 November 1993 | $\beta$ Pictoris | 1 CaII K |
| | | 1 CaII H |
| 2 December 1993 | $\beta$ Pictoris | 3 CaII K |
| 3 December 1993 | $\beta$ Pictoris | 4 CaII K |
| | | 3 CaII H |
| 19 November 1994 | $\beta$ Pictoris | 2 CaII K |
| | | 2 CaII H |
| 21 November 1994 | $\beta$ Pictoris | 1 CaII K |
| | | 1 CaII H |
| 22 November 1994 | $\beta$ Pictoris | 4 CaII K |
| | | 2 CaII H |
| 23 November 1994 | $\beta$ Pictoris | 9 CaII K |
| 24 November 1994 | $\beta$ Pictoris | 6 CaII K |
| | | 2 CaII H |
| 26 November 1994 | $\beta$ Pictoris | 4 CaII K |
| | | 2 CaII H |
| 27 November 1994 | $\beta$ Pictoris | 1 CaII K |
| 19 April 1995 | $\beta$ Pictoris | 2 CaII K |
| | | 1 CaII H |
| 24 May | $\beta$ Pictoris | 4 CaII K |
| | | 2 CaII H |
| | 68 Ophiuchus | 3 CaII K |
| | | 2 CaII H |
| | $\alpha$ Pisces Australus | 3 CaII K |
| 25 May | $\beta$ Pictoris | 3 CaII K |
| | | 3 CaII H |
| | 68 Ophiuchus | 4 CaII K |
| | | 2 CaII H |
| | $\alpha$ Pisces Australus | 3 CaII K |
| | | 2 CaII H |
| 9 June | $\beta$ Pictoris | 2 CaII K |

**Table 4.1 cont.:** Table of observations made at MJUO in 1995

| Date of observation | Star | # of spectra |
|---|---|---|
| | | 2 CaII H |
| | 68 Ophiuchus | 2 CaII K |
| 10 June | $\beta$ Pictoris | 1 CaII K |
| 11 June | $\beta$ Pictoris | 2 CaII K |
| | | 1 CaII H |
| 16 June | 68 Ophiuchus | 2 CaII K |
| | $\alpha$ Pisces Australus | 2 CaII K |
| | $\beta$ Pictoris | 1 CaII K |
| 17 June | $\beta$ Pictoris | 1 CaII K |
| 19 June | $\alpha$ Pisces Australus | 2 CaII K |
| | | 2 CaII H |
| | $\beta$ Pictoris | 2 CaII K |
| 20 June | $\beta$ Pictoris | 6 CaII K |
| | | 2 CaII H |
| | 68 Ophiuchus | 3 CaII K |
| | | 2 CaII H |
| | $\alpha$ Pisces Australus | 2 CaII K |
| 27 July | 68 Ophiuchus | 2 CaII K |
| | $\beta$ Pictoris | 4 CaII K |
| | | 2 CaII H |
| 28 July | 68 Ophiuchus | 6 CaII K |
| | $\alpha$ Pisces Australus | 3 CaII K |
| | $\beta$ Pictoris | 4 CaII K |
| | | 3 CaII H |
| 29 July | 68 Ophiuchus | 5 CaII K |
| | $\alpha$ Pisces Australus | 2 CaII K |
| | $\beta$ Pictoris | 4 CaII K |
| | | 3 CaII H |
| 30 July | 68 Ophiuchus | 5 CaII K |
| | $\alpha$ Pisces Australus | 5 CaII K |
| | $\beta$ Pictoris | 4 CaII K |
| | | 4 CaII H |
| 31 July | 68 Ophiuchus | 5 CaII K |
| | $\alpha$ Pisces Australus | 4 CaII K |
| | $\beta$ Pictoris | 4 CaII K |
| | | 3 CaII H |

**Table 4.1 cont.:**Table of observations made at MJUO in 1995

| Date of observation | Star | # of spectra |
|---|---|---|
| 1 August | 68 Ophiuchus | 6 CaII K |
| | $\alpha$ Pisces Australus | 3 CaII K |
| | $\beta$ Pictoris | 4 CaII K |
| | | 3 CaII H |
| 7 September | 68 Ophiuchus | 2 CaII K |
| | $\alpha$ Pisces Australus | 4 CaII K |
| | $\beta$ Pictoris | 3 CaII K |
| | | 3 CaII H |
| 8 September | 68 Ophiuchus | 3 CaII K |
| | $\alpha$ Pisces Australus | 3 CaII K |
| | $\beta$ Pictoris | 4 CaII K |
| | | 4 CaII H |
| 9 September | 68 Ophiuchus | 3 CaII K |
| | $\alpha$ Pisces Australus | 3 CaII K |
| | $\beta$ Pictoris | 4 CaII K |
| | | 4 CaII H |
| 10 September | 68 Ophiuchus | 4 CaII K |
| | $\alpha$ Pisces Australus | 3 CaII K |
| | $\beta$ Pictoris | 5 CaII K |
| | | 4 CaII H |
| 11 September | 68 Ophiuchus | 4 CaII K |
| | $\alpha$ Pisces Australus | 2 CaII K |
| | $\beta$ Pictoris | 3 CaII K |
| | | 2 CaII H |
| 12 September | 68 Ophiuchus | 2 CaII K |
| | $\alpha$ Pisces Australus | 3 CaII K |
| 13 September | $\beta$ Pictoris | 2 CaII K |
| | | 2 CaII H |
| 6 October | $\alpha$ Pisces Australus | 2 CaII K |
| | $\beta$ Pictoris | 5 CaII K |
| | | 4 CaII H |
| 8 October | 68 Ophiuchus | 2 CaII K |
| | $\alpha$ Pisces Australus | 2 CaII K |
| | $\beta$ Pictoris | 2 CaII K |
| | | 1 CaII H |
| 10 October | 68 Ophiuchus | 2 CaII K |

**Table 4.1 cont.:**Table of observations made at MJUO in 1995

| Date of observation | Star | # of spectra |
|---|---|---|
|  | $\alpha$ Pisces Australus | 3 CaII K |
|  | $\beta$ Pictoris | 5 CaII K |
|  |  | 5 CaII H |
| 3 November | $\beta$ Pictoris | 1 CaII K |
| 4 November | $\alpha$ Pisces Australus | 1 CaII K |
| 6 November | $\alpha$ Pisces Australus | 1 CaII K |
|  | $\beta$ Pictoris | 5 CaII K |
|  |  | 5 CaII H |
| 7 November | $\alpha$ Pisces Australus | 1 CaII K |
|  | $\beta$ Pictoris | 6 CaII K |
|  |  | 6 CaII H |
| 9 November | $\beta$ Pictoris | 3 CaII K |
|  |  | 2 CaII H |
| 11 November | $\beta$ Pictoris | 2 CaII K |
|  |  | 1 CaII H |
| 12 November | $\beta$ Pictoris | 5 CaII K |
|  |  | 6 CaII H |
| 13 November | $\beta$ Pictoris | 6 CaII K |
|  |  | 6 CaII H |
| 14 November | $\beta$ Pictoris | 5 CaII K |
|  |  | 5 CaII H |

## 4.2   The telescope and échelle spectrograph

Observations were made using the high-resolution échelle spectrograph with a CCD detector to record the observations of the stars' Calcium H and K lines at 3965 and 3935 angstroms respectively. The échelle spectrograph was mounted on the 1-metre McLellan telescope at the cassegrain focus. The telescope is a Dall-Kirkham type optical system [51] and has interchangeable secondary mirrors which allow the telescope to be used in either a f/8 or f/13.5 cassegrain configuration. In this case the f/13.5 secondary was used for the échelle spectrograph.

The échelle spectrograph makes use of a 79 groove mm$^{-1}$ échelle grating with a blaze angle of $\theta_B = \tan^{-1} 2 = 63°26'$. The echelle has a resolving power in the visual part of the spectrum of R = 5.4x10$^4$ (see Hearnshaw[32]). This gives dispersion = 1.7Å mm$^{-1}$ at 5000Å, though in the ultra-violet at the Calcium II lines the dispersion = 1.31Å mm$^{-1}$. When using the échelle, the blue cross-grating was installed which is used to maximise

efficiency in the transmission of blue light through the spectrograph. The slit size was set
to a micrometer setting of $438\mu$m irrespective of seeing corresponding to 2.0 arcsec. This
allowed most of the light to pass down the slit opening in typical observing conditions at
Mt John. The tilt settings of the échelle and cross-grating were set using the thorium-
argon wavelength reference lamp to show the various lines that correspond to the spectral
regions of the Calcium H and K lines. Later the camera was focussed to give the maximum
sharpness corresponding to as high a signal as possible in the thorium lines.  When
the observing was begun on the first night of a run, the telescope was focussed on a
bright star (usually $\alpha$ Car or $\alpha$ PsA) at first visually with the eyepiece mounted on the
spectrograph and then using the CCD to get the maximum signal possible, in the orders
which corresponds to the sharpest focussed image of the star on the slit. When observing
the Calcium H & K lines with this spectrograph it is not possible to observe both lines
simultaneously on the same CCD image due to their position on the échellogram and
size of the chip. It was therefore necessary to change the échelle tilt which is altered
by a micrometer on the side of the spectrograph. Every effort was made during the
alternating between the two settings to have the échelle tilt return to a position that kept
the same spectral wavelengths on the CCD to a precision of a few pixels. This was done
by rotating the micrometers in one direction only when moving to a particular setting to
avoid backlash in the micrometer (see Table 4.2 for échelle parameters).

| Inside | Filter | BG39[1] |
|---|---|---|
|  | Cross-grating | Blue |
|  | Collimator | 635 |
| Outside | Slit width | 438 |
|  | Slit position | 250 |
|  | Slit Height | 280 |
|  | Cross-grating | 15.218† |
|  | Echelle tilt | 372†K |
|  |  | 470†H |
|  | Camera focus | 915† |

Table 4.2: **Settings on the MJUO échelle spectrograph.** Above
are given the various micrometer and other settings for the observations
of the CaII lines.
† These represent typical initial settings

For the smooth-fielding of the CCD (also known as spectral flat fields) a blue filter was
used to block out some of the significant amount of scattered red light from the tungsten

---

[1]The filter was only used for the smooth-fields.

lamp[2] used for smooth-fielding. This is important because it is known that the response of the pixels is wavelength dependent (see fig. 4.1 for an example of the flatness of the CCD).

## 4.3   MJUO CCD system

The MJUO CCD system is based around the Photometrics 3000 CCD camera system purchased in December 1988 from Photometrics Ltd of Tucson. The system is run by a Photometrics PM3000 computer, which operates the Thomson CSF TH7882 CDA CCD chip (see Tobin 1990[70] for a fuller description). All commands for operating the camera are in the FORTH command language which has been tailored for the operations of the system at MJUO (see Tobin 1991[71] and Photometrics 3000 Users Manual for Forth Programming System[55]). The CCD chip is overcoated with a fluorescent dye, Metachrome II, for enhanced ultraviolet and blue response. The chip is 384x576 pixels in dimension with a pixel size of $23\mu$m square and is contained within a cooled dewar with liquid nitrogen. The chip is maintained at a temperature of about $-110°$ Celsius which is the optimum operating temperature for the chip for observations in all parts of the sky [56]. At  400 nm the CCD chip has a quantum efficiency of  20% though the individual pixels may vary by as much as $\sim$ 1 part in 20 from the average. An example of this can be seen in the smooth-field (see Fig. 4.1).

## 4.4   Observation procedure

At the beginning of each run the échelle spectrograph was set up for observations in the near ultra-violet. This required the installation of the blue cross-grating which is most efficient from the UV atmospheric limit to $H_\beta$. The tilts of the gratings were then adjusted to appropriate regions for observations of the wavelengths corresponding to Ca II. The slit size was set as used in the observation runs conducted in previous years. The slit size used was approximately 2.0 arcsec. The camera focus in the spectrograph was adjusted as required on examination of several thorium reference spectra, exposed at slightly different camera settings. The camera focus position that gave the best result was then used[3]. Then final adjustments were made to the gratings in the spectrograph to match the thorium spectra used to calibrate the wavelength scales of the orders pertaining to the Calcium II lines to a copy of an image of a previous thorium spectra to consistently observe the same wavelength region. For ease of reduction, a copy of a CCD image of

---

[2]The tungsten lamp blew during the last observation run and was replaced by a new bulb which appears to be stronger than the old one in the UV part of the spectrum, improving also the ratio of the UV light in the spectral orders compared to the background of scattered red and near-infrared light.

[3]It should be noted that the camera focus did not change to any significant degree during individual runs. But a seasonal (ie. presumably temperature) dependence was observed.
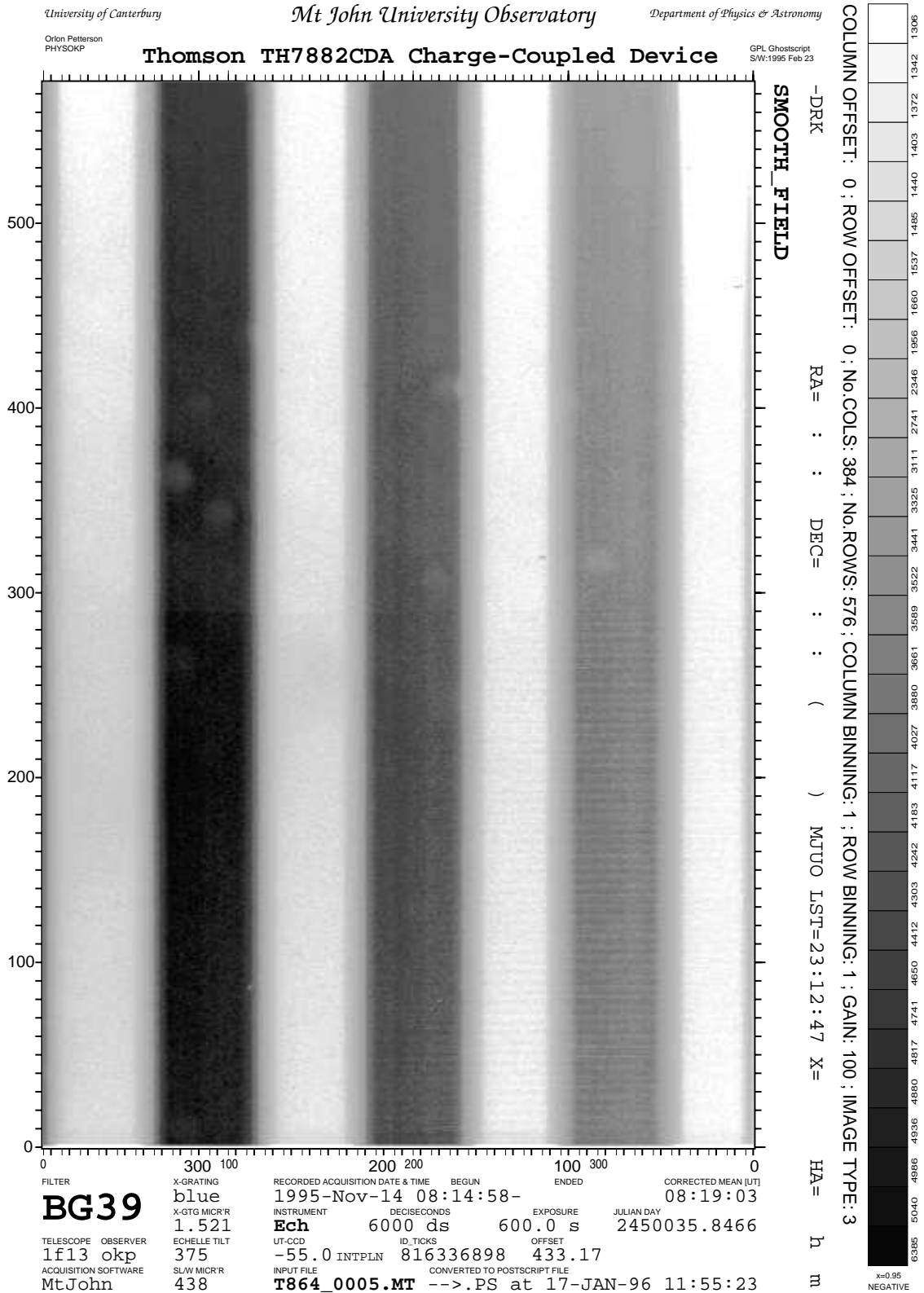
**Figure 4.1**: K line region smooth-field showing the flatness of the CCD

the thorium lines in question, taken at an earlier time, were used as the reference for the setting of the spectrograph (see Fig. 4.2 for the K line region and Fig. 4.3 for the H line region).

The observing procedure followed each night was to top up the dewar at least 1 hour before any use was made of the CCD so as to allow the CCD time to adjust to the addition of liquid to the dewar. Immediately after liquid nitrogen was added to the dewar, it was observed that the bias level changed quite significantly for some minutes. Some bias readouts were made to see if there were any major changes in the bias level of the CCD that indicated the chip had not reached equilibrium. Then 3 dark frames of 10 seconds duration, that were selected to be free of cosmic ray strikes, were acquired and used to make a median dark frame for subtraction from all subsequent CCD images taken. If there was a change in the level of dark current during the night, as indicated by a warning from the acquisition software, a new median dark was made. Next the spectral flat-fields or smooth-fields were made by exposing a tungsten light source through the slit of the spectrograph. A blue filter was placed behind the slit to reduce the amount of scattered red light in the spectrograph and a 10 minute exposure was made with the CCD. Typically 3 smooth-fields were made at each of the two spectrograph settings which were then added together in the reduction in order to reduce the magnitude of the systematic error in the response of the pixels hit by cosmic-rays. Median clipping of cosmic-ray strikes was not possible because spectral output of the tungsten lamp may change with time, altering the spectral shape of the 3 smooth-fields which cannot be scaled to identical mean signal levels at all points, as required for median clipping. Shortly after sunset the dome shutter was opened to allow the dome and telescope to reach the ambient outside temperature, at this time also the covers were rolled back from the primary mirror and the baffles. Once the smooth-fielding was completed the telescope drives were activated and the telescope pointed at the first object. After every exposure of a star a thorium-argon wavelength calibration image was made to calibrate the wavelength scale for that image. Once this was done another stellar spectrum could be taken or the telescope moved on to the next star. After each image was taken it was then saved on to tape. Each H or K line spectrum was also recorded on paper for immediate examination.

## 4.5   Observations of Beta Pictoris

Being a circumpolar star at the MJUO latitude, Beta Pictoris could be followed all night. However in order to obtain good spectra with high S/N in a reasonable time, observations were made whenever the star was below the preselected limit of 3 airmasses of extinction. This would keep observations to the proposed 30-minute exposure length required for appropriate temporal sampling. It was found in practice, that Beta Pictoris was best observed once it was above 2 airmasses to keep to the 30 minute exposure duration. It

**Figure 4.2**: Thorium-argon lines for CaII K line region
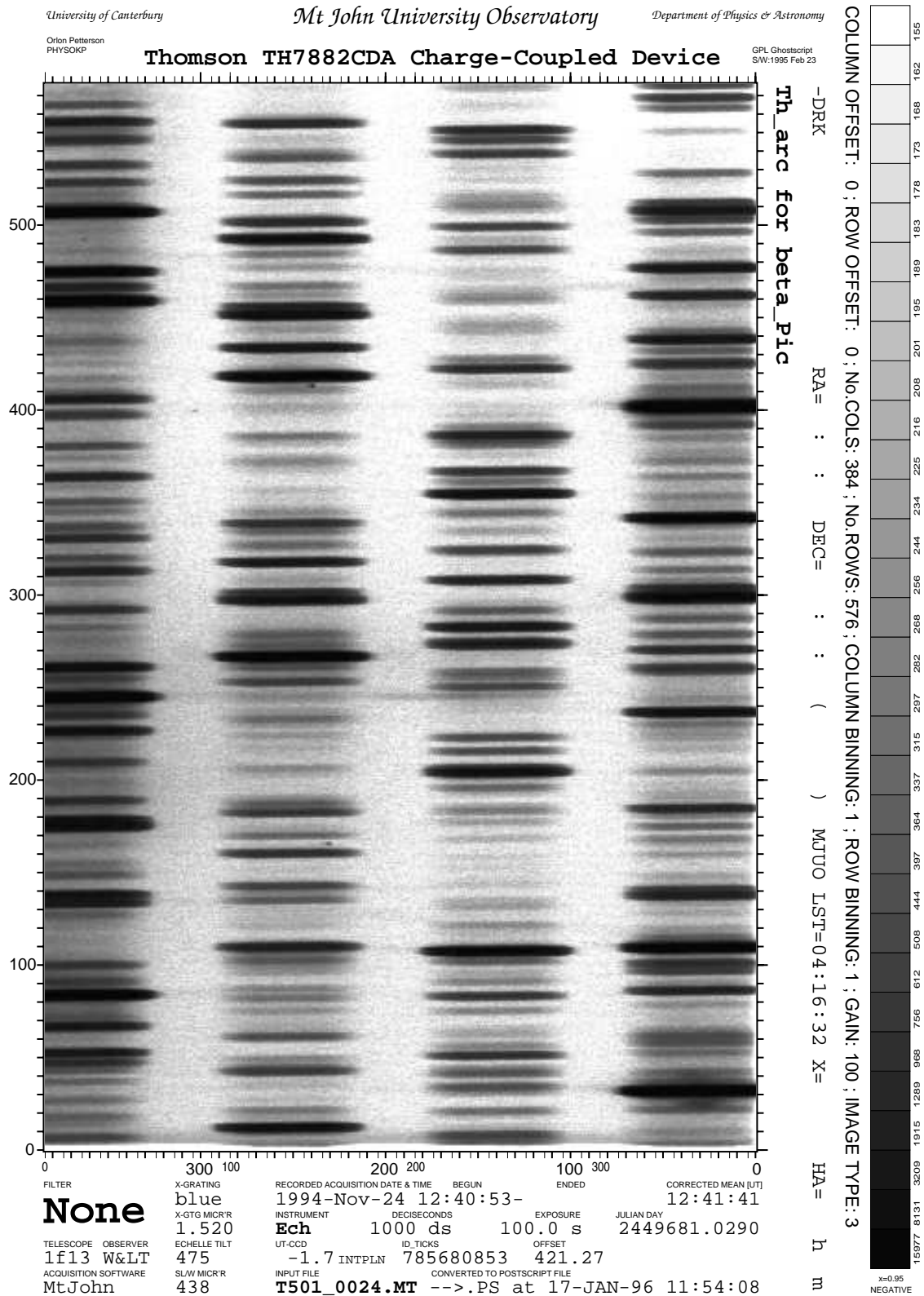
**Figure 4.3**: Thorium-argon lines for CaII H line region

was not always possible to keep to those constraints, so when the seeing was bad or observing was conducted through cloud, good signals were deemed more important than time resolution. Spectra were taken of both the Calcium II H & K lines, usually alternating between the two eg. K H K H K.... In order to determine the best times to observe the programme stars, a small procedure was written for MIDAS to calculate the airmass for a star at Mt John Observatory for any time of the year and night (see Fig. 4.4). The plots were only used as a guide to observing times at the observatory. The plots in themselves are not meant to be very accurate and have points plotted that represent at what times of night the stars are at certain airmasses. Airmasses were calculated for every 15 minutes of the year and the times that were within certain limits (ie. $\pm 0.05$ airmasses) were plotted as representing the airmasses, which explains why there are sometimes more than one line of symbols corresponding to a particular airmass.
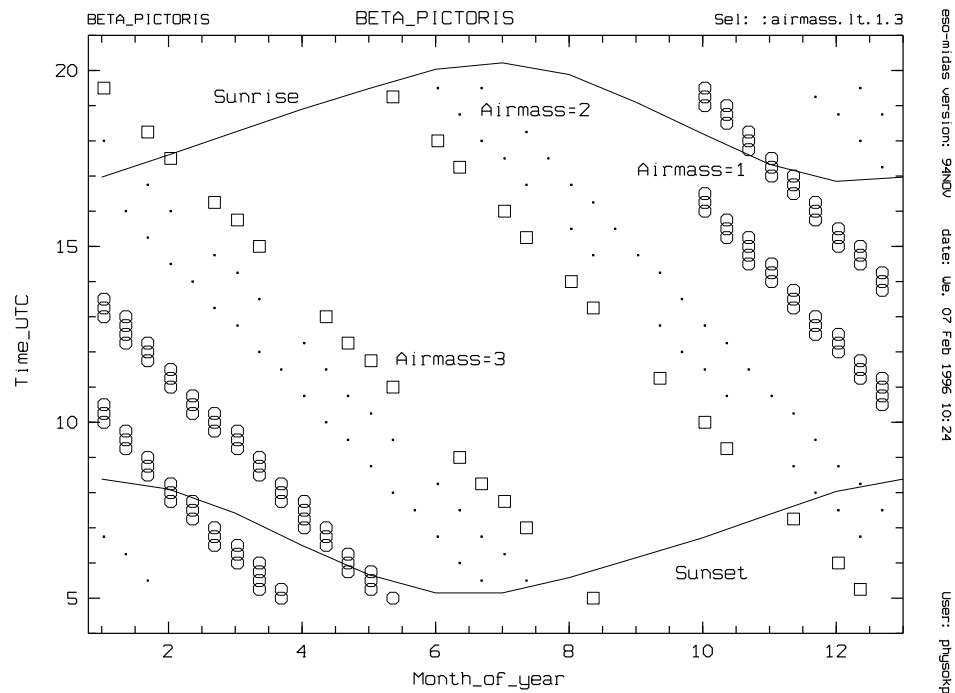


Figure 4.4: **Plot of airmass vs time of year and time of night for Beta Pictoris.** The above plot shows the time of night for a given time of the year and time of night when Beta Pictoris is at 3 airmasses of extinction or less. Observations were planned from this plot in order to make observations that record sufficient signal for a reasonable exposure time. This plot was used to plan observations that would record sufficient signal for a reasonable exposure time.

It should be noted that the best time for observing Beta Pictoris is during the southern summer from about October to April when it is at low airmass through most of the night.

## 4.6   Observations of 68 Ophiuchus

68 Ophiuchus was the only binary system observed, and because of its position near the celestial equator was observed whenever it was below $\sim 3$ airmasses. Because of its position in the northern sky at MJUO and though it is only half a magnitude fainter than Beta Pictoris, the typical exposure times were of the order of an hour. The absorption features in the K line spectra are only very slight, so it was necessary to get high signal spectra so that the noise was very much smaller than the absorption features being observed. Observations were made mainly of the K line, as it was decided early on that unless something significant was happening in the K line, the H line would not be observed. It should be noted that the H line spectrum of 68 Ophiuchus shows none of the circumstellar absorption features visible in the K line.
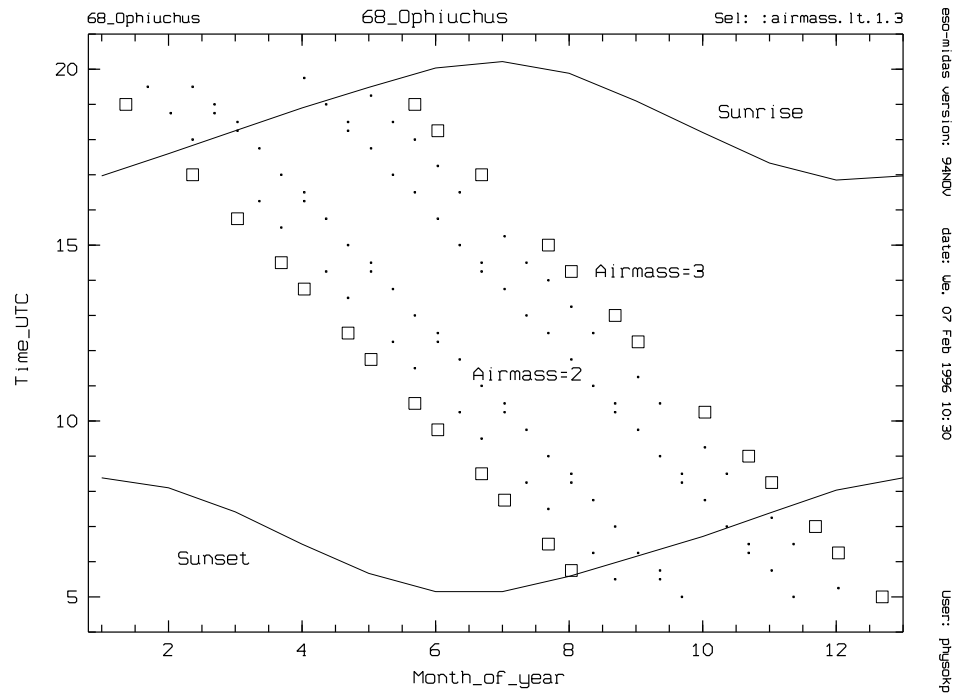


**Figure 4.5**: **Plot of airmass vs time of year and time of night for 68 Ophiuchus.** The above plot shows the time of night for a given time of the year and time of night when 68 Ophiuchus is at 3 airmasses of extinction or less. Observations were planned from this plot in order to make observations that record sufficient signal for a reasonable exposure time. This plot was used to plan observations that would record sufficient signal for a reasonable exposure time.

The best time to observe 68 Ophiuchus is during the months of May to September when it is highest in the northern sky (see Fig. 4.5).

## 4.7   Observations of Alpha Pisces Australus

Formulhaut (or $\alpha$ PsA) is the brightest of the 3 stars at $V = 1.12$ and is well placed in the sky, where it passes near the zenith at MJUO. $\alpha$ PsA was also observed when it was below the 3 airmass limit, usually between observations of 68 Oph and $\beta$ Pic (see Fig. 4.6. As a result of when it was observed, most observations were at low airmasses $\leq 1.5$. Observations were again almost all of the K line after being decided that the H line could be ignored unless something happened in the K line spectra that warranted further investigation at H.
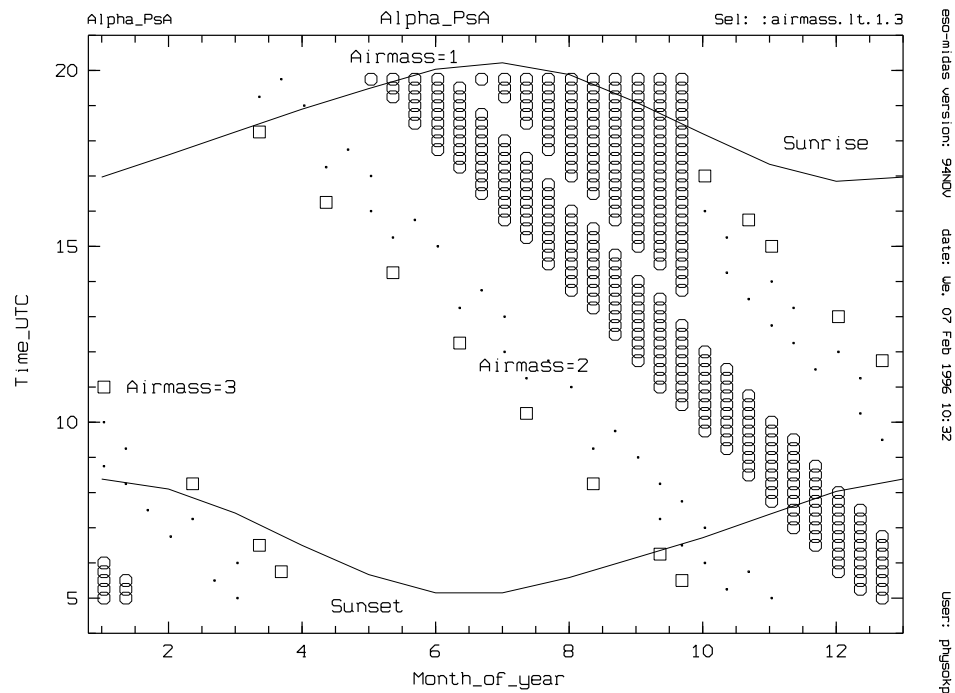


**Figure 4.6**: **Plot of airmass vs time of year and time of night for Alpha Pisces Australus.** The above plot shows the time of night for a given time of the year when Formulhaut is at 3 airmasses of extinction or less.  Observations were planned from this plot in order to make observations that record sufficient signal for a reasonable exposure time. This plot was used to plan observations that would record sufficient signal for a reasonable exposure time.

Due to its brightness, $\alpha$ PsA is ideal for focusing the telescope on the slit and maximising the throughput to the CCD. Also note that in Fig. 4.6 an error occurred in the routine causing the triangular region of circles in the plot.

# Chapter 5

# Data reduction and analysis procedures

The tapes containing the data taken at MJUO with the CCD, were read onto disk in Christchurch where the data could then be reduced using the reduction program of choice. The European Southern Observatory - Munich Image Data Analysis System (ESO-MIDAS or simply MIDAS) is the computing package used in the reduction and analysis of all the data contained in this thesis.

## 5.1 Munich Image Data Analysis System

MIDAS is essentially a set of general purpose programs for the reduction and analysis of astronomical data which has been obtained from various detectors or sources. The MIDAS system can be run both in interactive and batch modes. MIDAS is available in both UNIX and VAX/VMS versions. It can be adapted to suit the requirements for all sorts of image processing and data reduction. It is also designed to allow the integration of future application modules. This is achieved by the use of procedure files which can be created by the user to perform a simple or complex sequence of MIDAS commands. The procedure files are programmed in the MIDAS command language, which consists of a control language and set of commands. In addition context-specific commands can be added from the various MIDAS application modules. MIDAS is run on the University of Canterbury's, Computer Services Centre Sparc Centre 2000 (known as "cantua"). The earlier versions of MIDAS were run on the University's VAX 7610 computer.

Data reduction was undertaken using ESO-MIDAS 91NOV and later 94NOV versions of this package for the reductions of observations of Beta Pictoris acquired in earlier years and only the 94NOV version for the rest of the observations made for this thesis.

## 5.2 The MIDAS échelle reduction package

The reduction of the raw CCD data begins with the starting up of a MIDAS session. The data on disk is converted from the FITS format to the idiosyncratic format used by MIDAS. Due to the orientation in which the CCD is mounted on the échelle spectrograph, it is necessary to rotate the images clockwise by 90° into the orientation required by MIDAS for spectral reductions: that is, orders increasing from top to bottom, and wavelength increasing from left to right.

Next the échelle application package is enabled allowing the use of échelle specific commands. The reduction procedure was as follows:

The orders are located from the smooth-field image and also their orientation as recorded on the CCD. The orders were found using either the DEFINE/ECHELLE command for the Calcium K line region, or the HOUGH/ECHELLE command for the Calcium H line.

The offset between the centres of the smooth-field orders and the stellar orders are then found. A gaussian is fitted to one of the stellar orders and the difference between the centre of the stellar order and the corresponding smooth-field order is recorded. The full width of the stellar order is also recorded. This is important for determining where on the image the different types of filtering are applied.

Next the thorium-argon spectrum for the stellar image being reduced is fitted by a polynomial that bests fits the wavelengths of lines stored in a reference table to the lines detected in the image. The wavelengths reference table is a subset of one of the MIDAS tables augmented with lines from the Atlas of the Thorium Spectrum[52]. The resulting polynomial fit is applied to the extracted orders of the stellar spectrum to obtain spectra plotted on a wavelength scale.

Probably the most difficult and sensitive part of the reduction process is the filtering applied to the stellar spectral image. In the removal of the cosmic-ray strikes on the image, two different types of filtering are necessary. A median filter is applied to the background between the orders to remove cosmic-ray strikes and smooth the background. A cosmic-ray filter is applied in the orders which shouldn't affect the spectrum which uses CCD information such as the read-out-noise (in $e^-$), inverse gain factor ($e^-$/ADU), and threshold value for evaluating spikes for cosmic-ray removal in the spectral orders. It works by fitting a one-dimensional point spread function (PSF) perpendicular to the dispersion direction and replacing pixels that have large deviations from the PSF.

Finally the filtered image is divided through by the smooth-field to remove pixel-to-pixel sensitivity variations across the image and then recorded as 1-dimensional spectra. Before this division is done, the smooth-field image is scaled so that the signal levels in the orders are close to unity. The signal levels in the final reduced spectra are then still reasonably indicative of the total number of ADU in the original raw images. The process followed is described more fully in Appendix A, which describes the general procedure for reducing spectra recorded on the PM3000 CCD system[1].

The resulting spectra were then plotted out and overplotted with the background subtracted order which should contain all the cosmic rays. The plots are examined to identify absorption features that are real and those that might be due to over-correction for the removal of a cosmic ray strike in the order, see Fig. 5.1.

---

[1]The above reduction procedure was then written in the MIDAS command language to semi-automate the process for speed and ease of use. The program is named "echorlon" and is found in Appendix B.2.
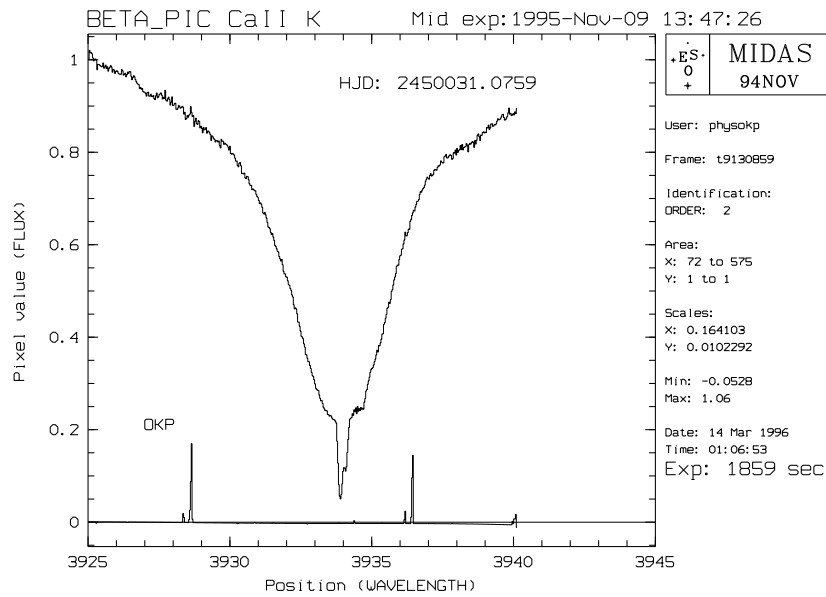
**Figure 5.1**: A reduced K line spectrum with its corresponding cosmic ray "spectrum" which is used for confirming the reality of any variable absorption features.

### 5.2.1 Modification to MIDAS

Due to the unique combination of the échelle spectrograph and CCD found at MJUO, it is necessary to modify the MIDAS software. The échelle orders are quite wide, some 20 pixels, due to the original design of the spectrograph being for photographic spectroscopy. Also the small size of the CCD chip means that less than 8 orders are usually recorded, less than MIDAS was programmed for. In the UV only a maximum of 4 orders can be recorded on the chip.

Because of the wide orders it is necessary to modify the cosmic-ray filtering routines to remove cosmic-rays more efficiently. The wavelength calibration routine needed to be modified to work with as little as 3 orders.

## 5.3 Determination of resolving power

The determination of the resolving power of the spectra from the échelle spectrograph is an important step in the reduction process. The resolving power at the two settings of the échelle grating tilt is important to know as observations of the Ca II lines of H & K occur in different orders of the échellogram. One would expect the difference in the FWHM to be :

$$\frac{order_{\mathrm{K}}}{order_{\mathrm{H}}} = \frac{59}{58} = 1.017$$

When the thorium calibration frames were examined, and then gaussians fitted to the emission lines, it was found that the best fits occurred for emission lines of intermediate strength. From these fits, the average for those lines FWHM measured in the spectra were taken and then an average of all the averages of the spectra to give the overall average of the FWHM for the regions of the Calcium II H & K lines. The result of those measurements are :

The FWHM for the region of the K line $= 0.1047$ Å

which gives a resolving power of

$$\frac{1}{W_\lambda}.\lambda = R = 37600$$

or about $8.0\text{kms}^{-1}$ for the clear separation of 2 features in the K line.

The FWHM for the region of the H line $= 0.1088$ Å

which gives a resolving power of

$$\frac{1}{W_\lambda}.\lambda = R = 36500$$

or about $8.2\text{kms}^{-1}$ for the clear separation of 2 features in the H line.

The differences in the resolving powers at H & K (about 2%) are most likely due to the small change in focus between the 2 regions in the échellogram.

# Chapter 6

# Presentation of Spectra

In this chapter the Calcium II H & K spectra for all the stars are presented as a series of graphical plots in which the spectra are stacked on top of one another in time order. Any changes in the spectra should be readily apparent if the additional absorption is strong enough to be seen.

## 6.1 The Beta Pictoris H & K lines

The spectra of $\beta$ Pictoris are presented here in order of time with both H & K spectra plotted next to each other where available. The time of observation can be estimated by finding the time from the point of the circumstellar line in each spectrum. The reference spectrum for the H and K lines (see Chapter 7) are included for comparison and to aid in identifying additional absorption features in the spectra.

### 6.1.1 The 1992 observing campaign

Presented in this section are the stacked plots for the $\beta$ Pictoris International Observing Campaign 1992. For the analysis of these spectra see Section 8.1.
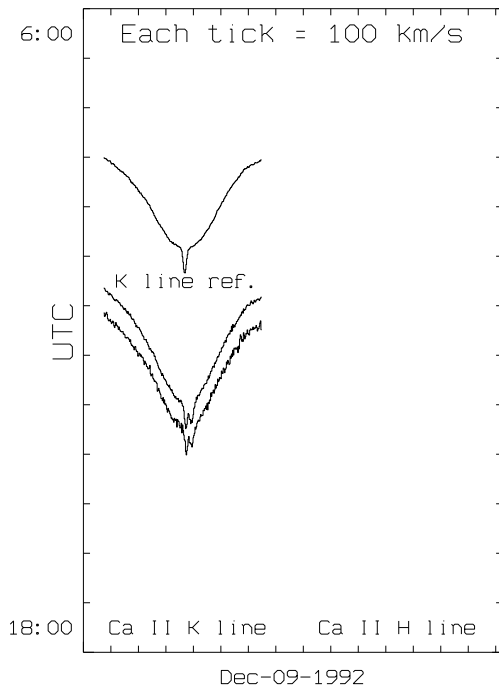
**Figure 6.1**: Spectra taken on 9 Dec 1992.
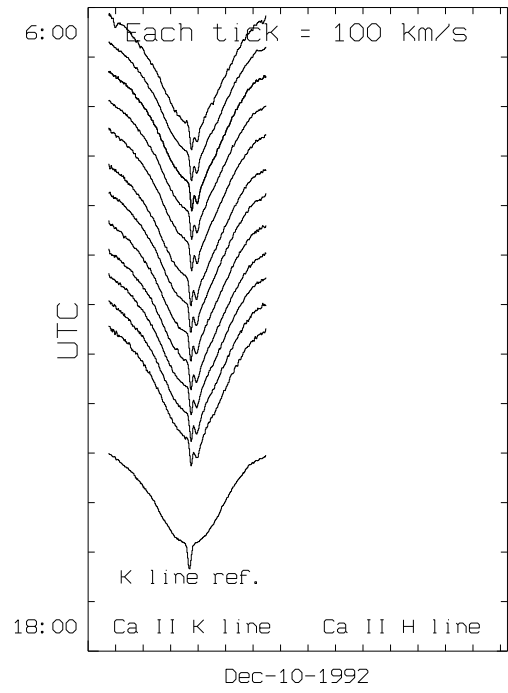


**Figure 6.2**: Spectra taken on 10 Dec 1992.
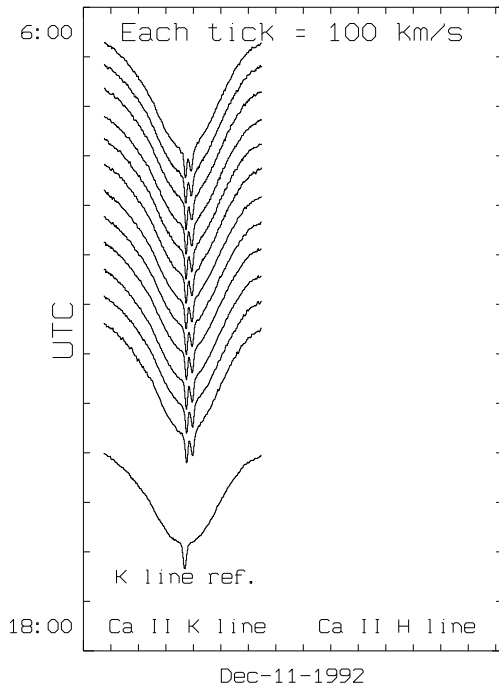


**Figure 6.3**: Spectra taken on 11 Dec 1992.
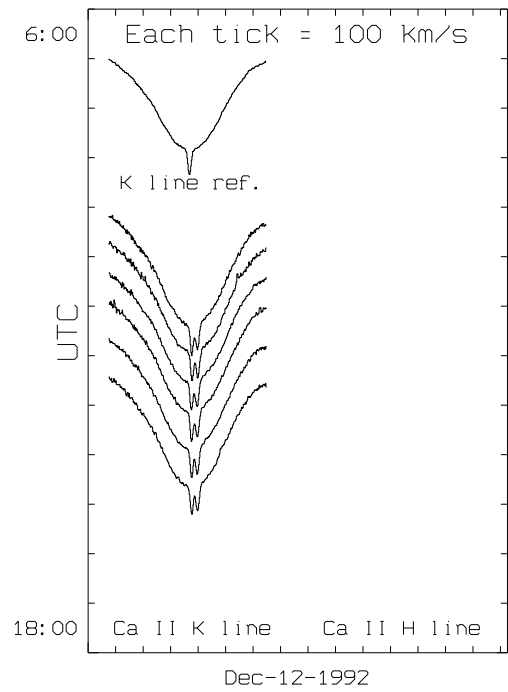


**Figure 6.4**: Spectra taken on 12 Dec 1992.
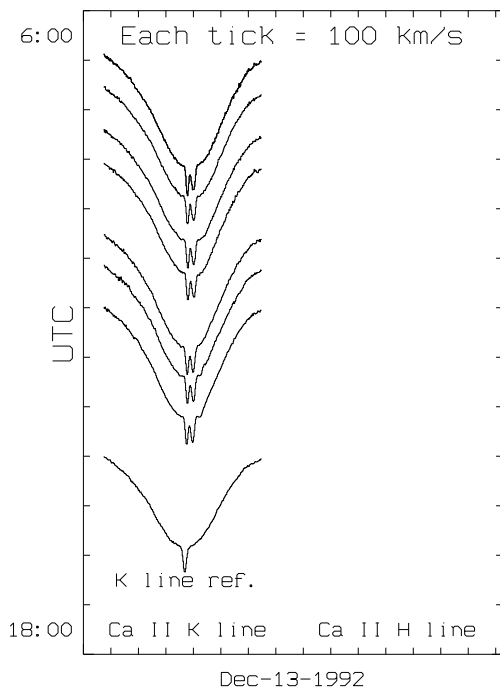
**Figure 6.5**: Spectra taken on 13 Dec 1992.
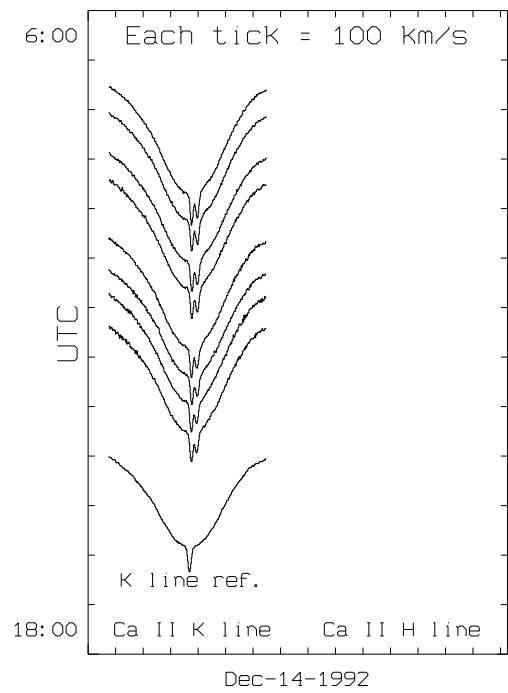


**Figure 6.6**: Spectra taken on 14 Dec 1992.
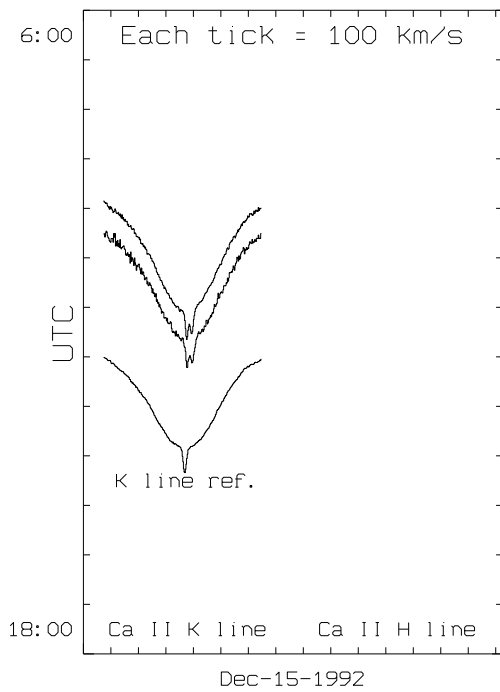


**Figure 6.7**: Spectra taken on 15 Dec 1992.
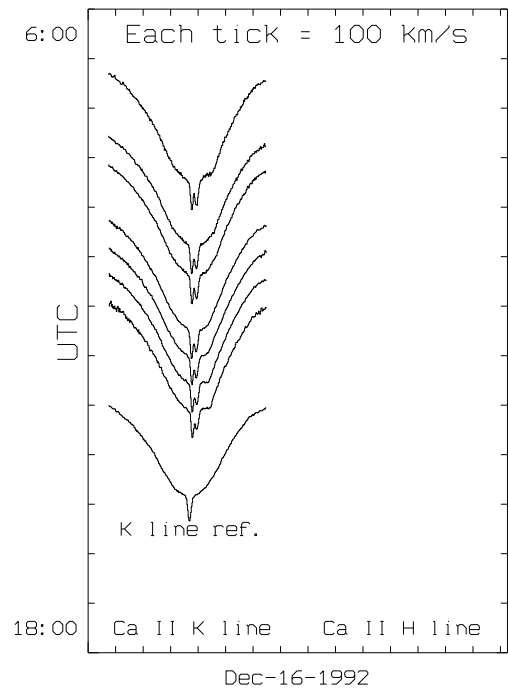


**Figure 6.8**: Spectra taken on 16 Dec 1992.

### 6.1.2   The 1993 observing campaign

Presented in this section are the stacked plots for the $\beta$ Pictoris International Observing Campaign 1993. Also included are the follow up observation to the 1992 campaign on January 9 1993, and also the spectra collected during the runs used for gaining experience in observing $\beta$ Pictoris in both H and K. For the analysis of these spectra see Section 8.2.
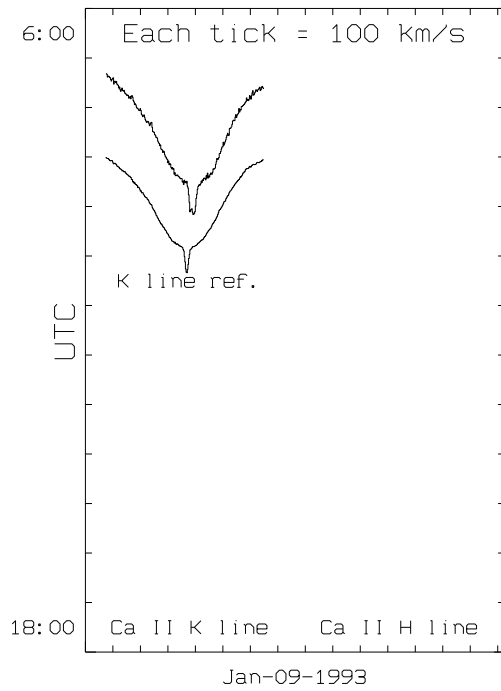


**Figure 6.9**: Spectra taken on 1 Jan 1993.
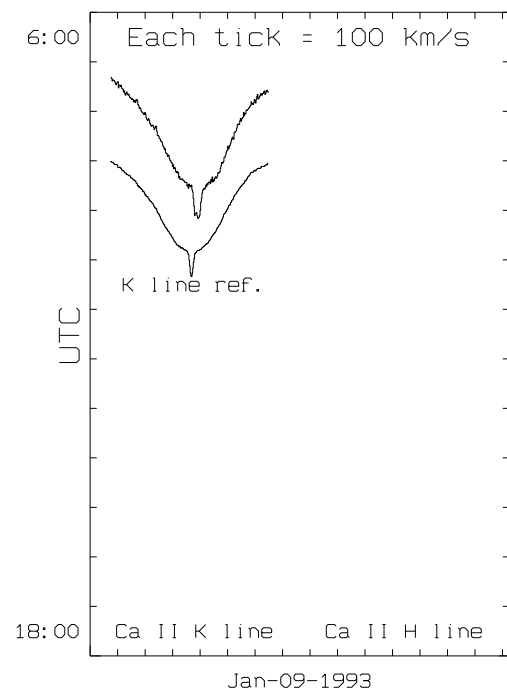


**Figure 6.10**: Spectra taken on 9 Jan 1993.
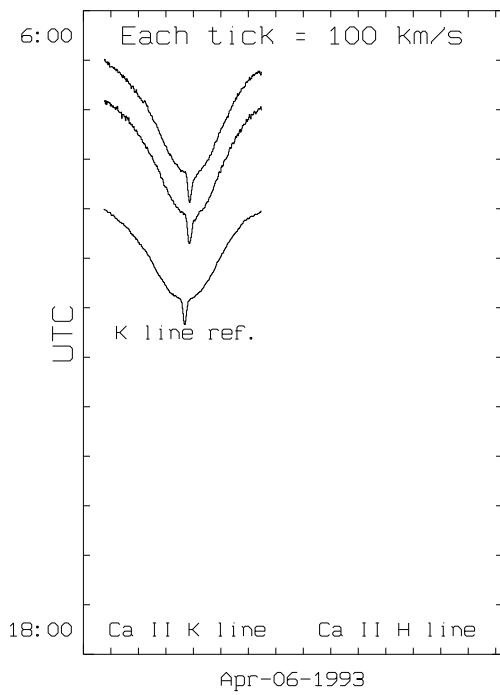
**Figure 6.11**: Spectra taken on 6 Apr 1993.
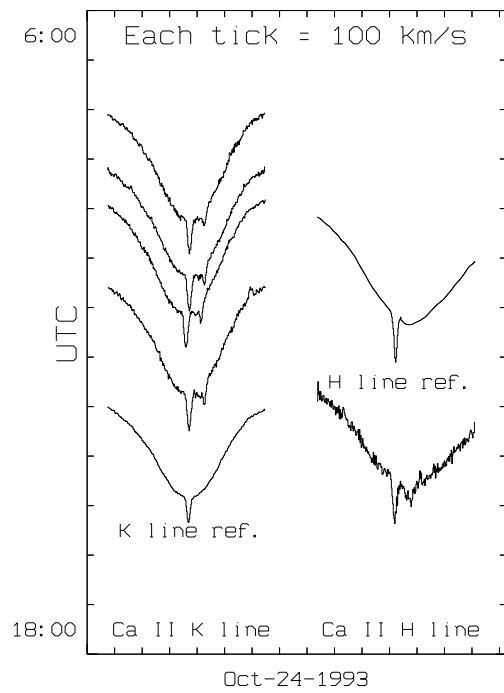


**Figure 6.12**: Spectra taken on 24 Oct 1993.
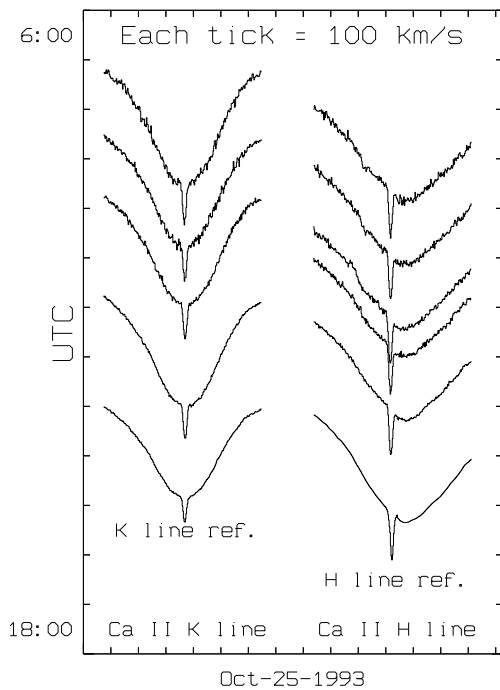


**Figure 6.13**: Spectra taken on 25 Oct 1993.
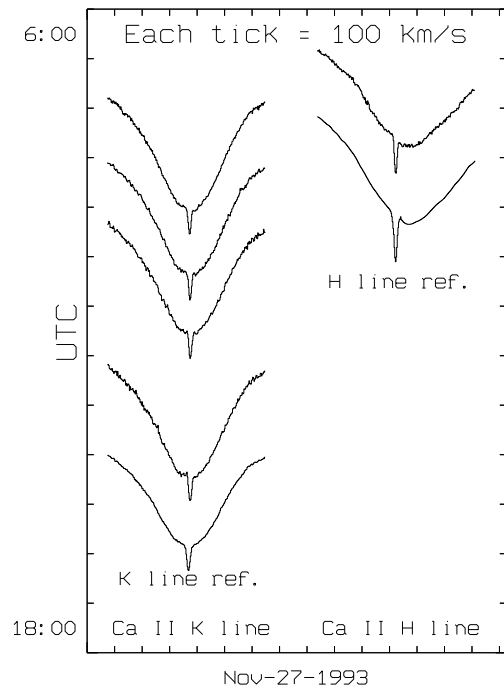


**Figure 6.14**: Spectra taken on 27 Nov 1993.
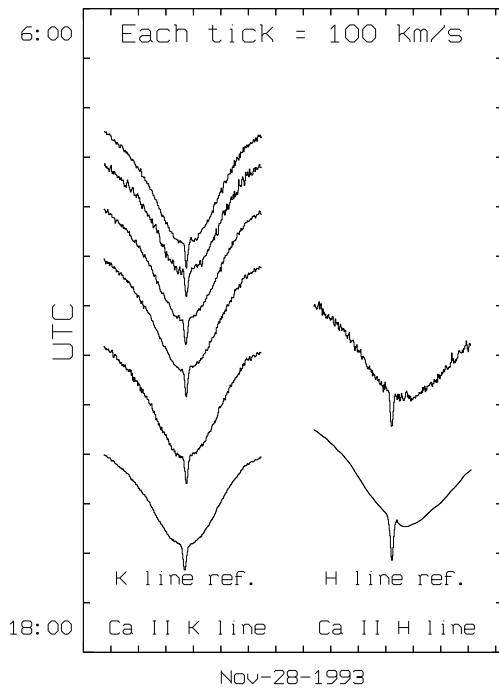
**Figure 6.15**: Spectra taken on 28 Nov 1993.
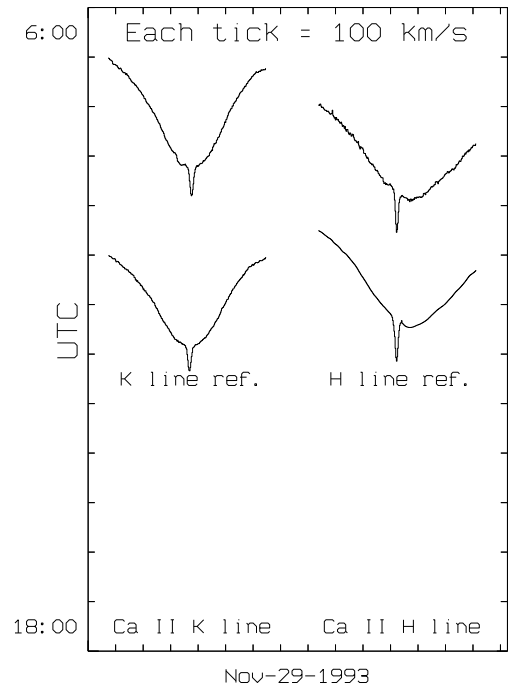


**Figure 6.16**: Spectra taken on 29 Nov 1993.
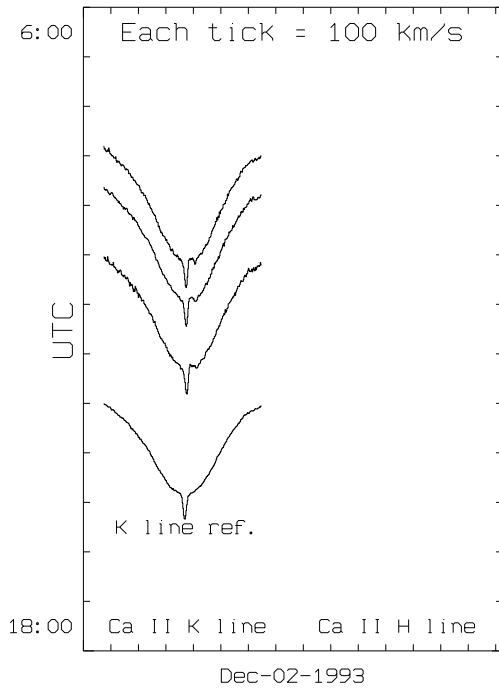


**Figure 6.17**: Spectra taken on 2 Dec 1993.
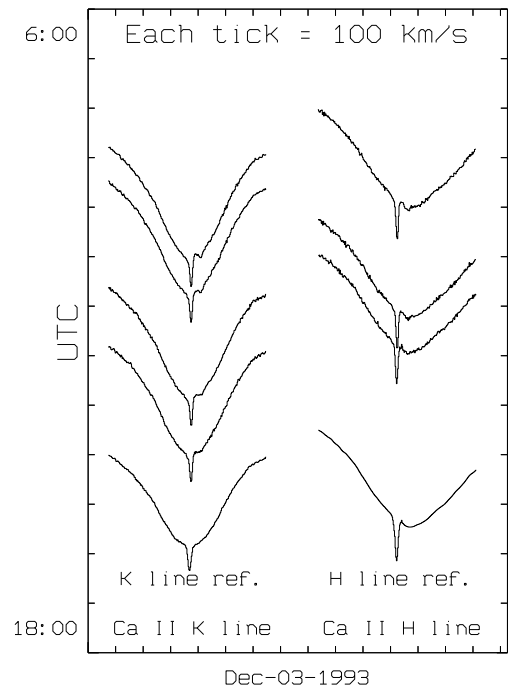


**Figure 6.18**: Spectra taken on 3 Dec 1993.

### 6.1.3   The 1994 observing campaign

Presented in this section are the stacked plots for the $\beta$ Pictoris International Observing Campaign 1994. For the analysis of these spectra see Section 8.3.
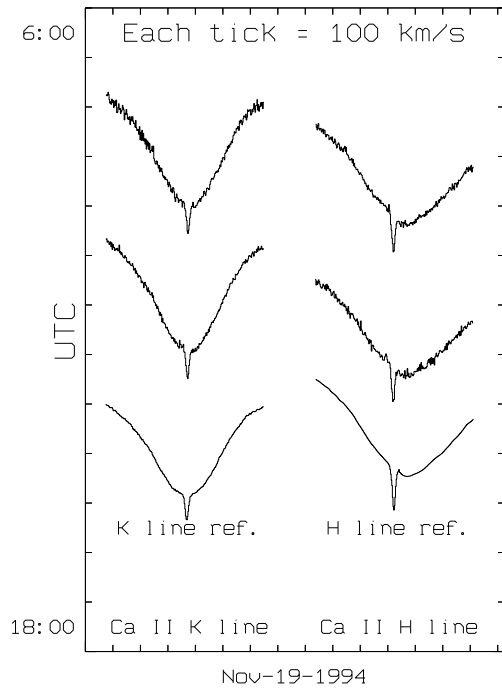


**Figure 6.19**: Spectra taken on 19 Nov 1994.
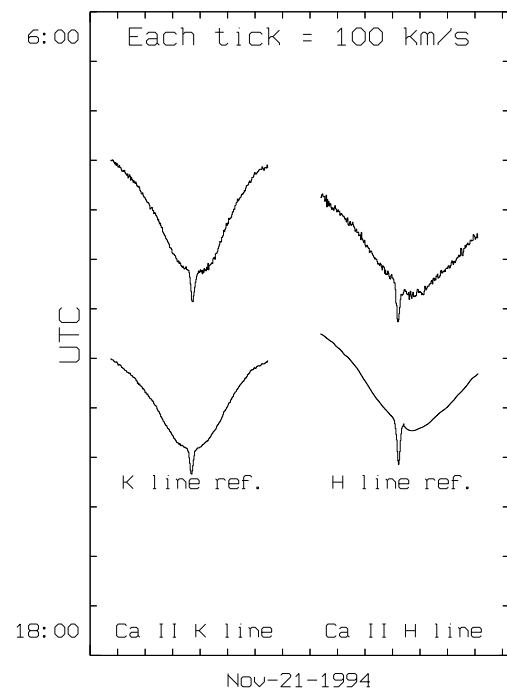


**Figure 6.20**: Spectra taken on 21 Nov 1994.
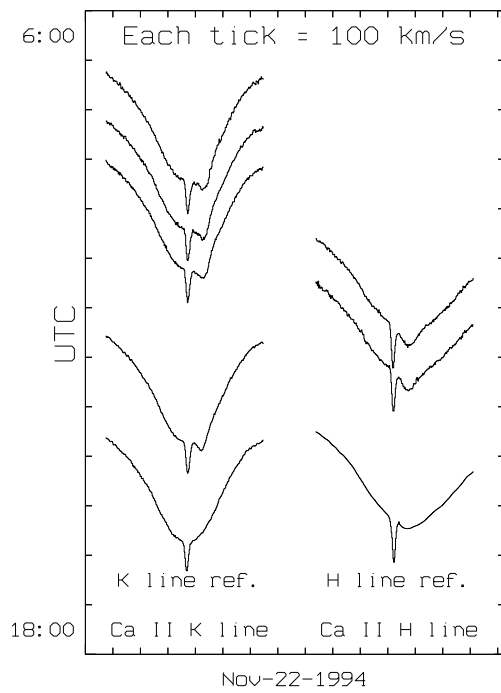
**Figure 6.21**: Spectra taken on 22 Nov 1994.
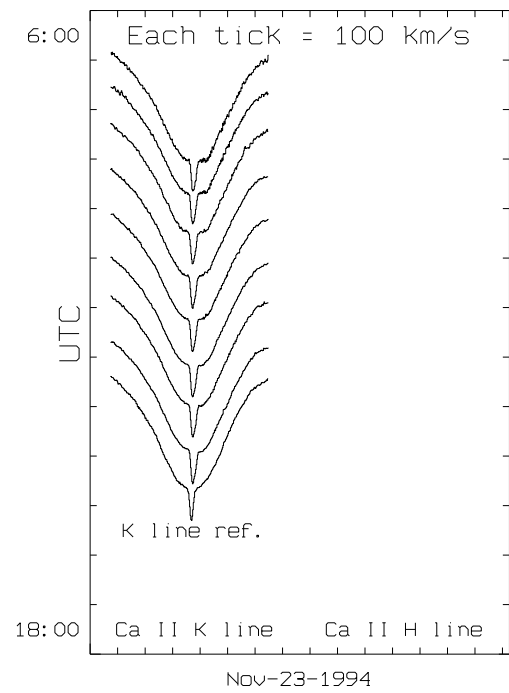


**Figure 6.22**: Spectra taken on 23 Nov 1994.
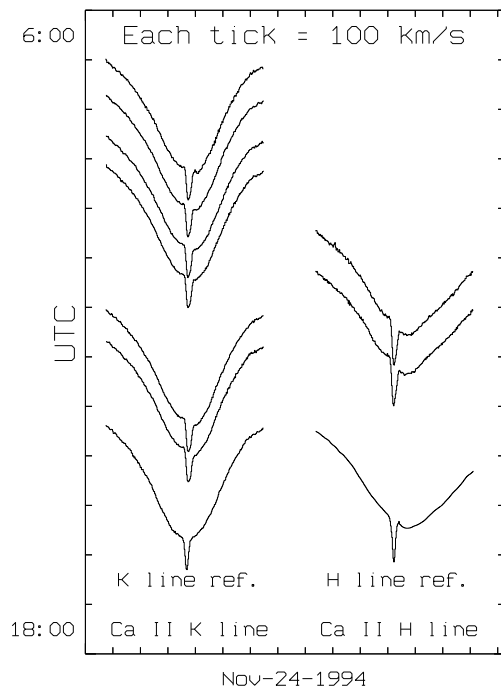


**Figure 6.23**: Spectra taken on 24 Nov 1994.
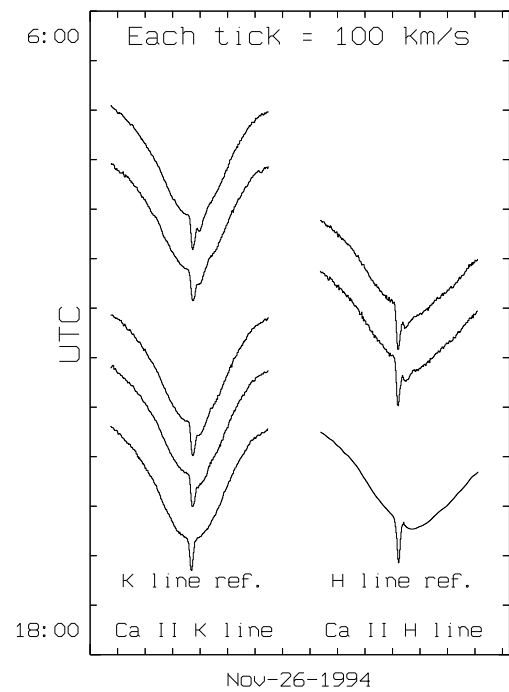


**Figure 6.24**: Spectra taken on 26 Dec 1994.
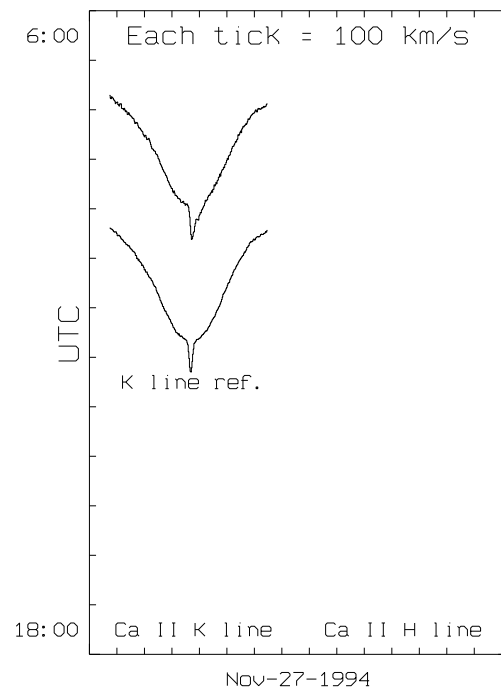
**Figure 6.25**: Spectra taken on 27 Nov 1994.

### 6.1.4 The 1995 observations

Presented in this section are the stacked plots for $\beta$ Pictoris taken during 1995 for this thesis by the author. For the analysis of these spectra see Section 8.4.
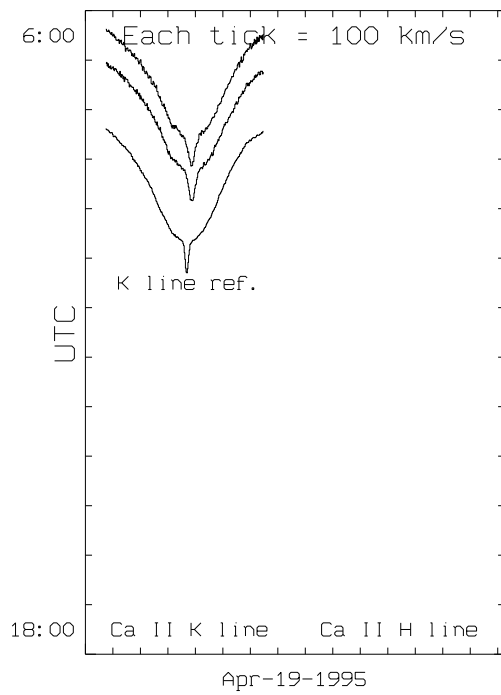
**Figure 6.26**: Spectra taken on 19 Apr 1995.
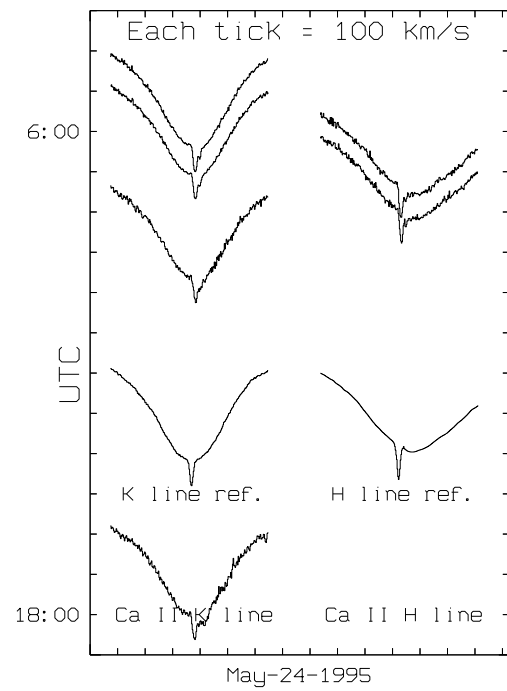


**Figure 6.27**: Spectra taken on 24 May 1995.
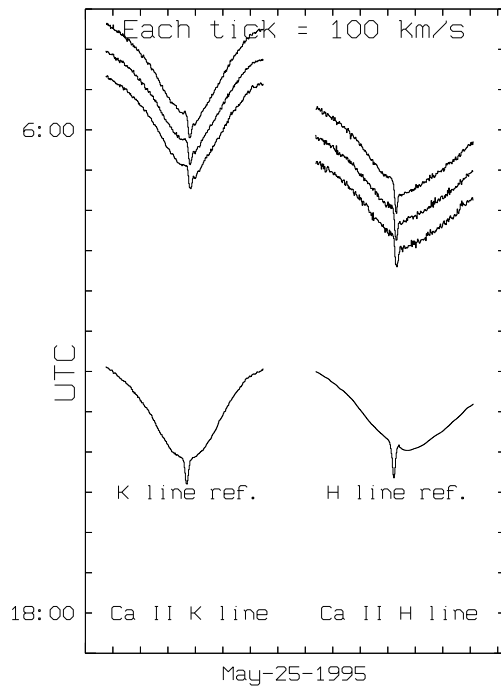


**Figure 6.28**: Spectra taken on 25 May 1995.
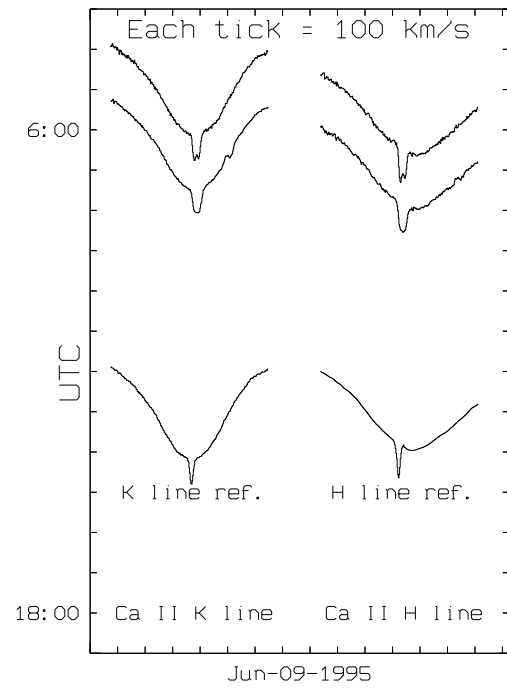


**Figure 6.29**: Spectra taken on 9 Jun 1995.
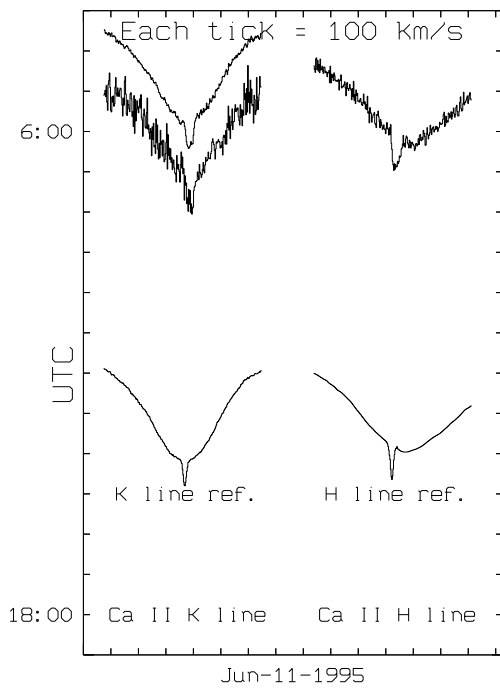
**Figure 6.30**: Spectra taken on 11 Jun 1995.
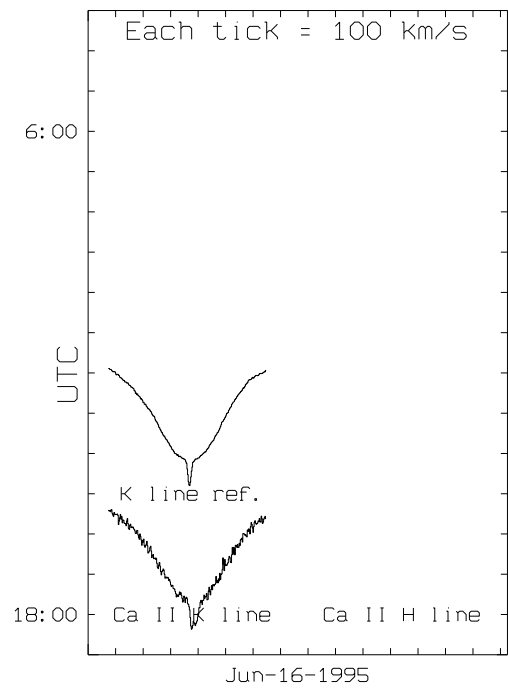


**Figure 6.31**: Spectra taken on 16 Jun 1995.
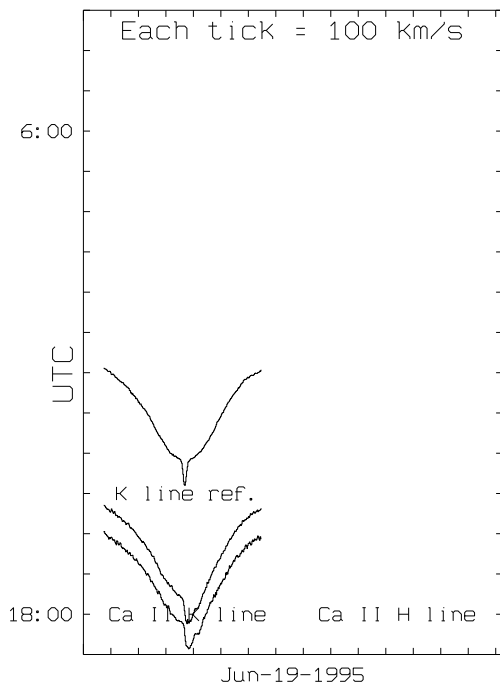


**Figure 6.32**: Spectra taken on 19 Jun 1995.
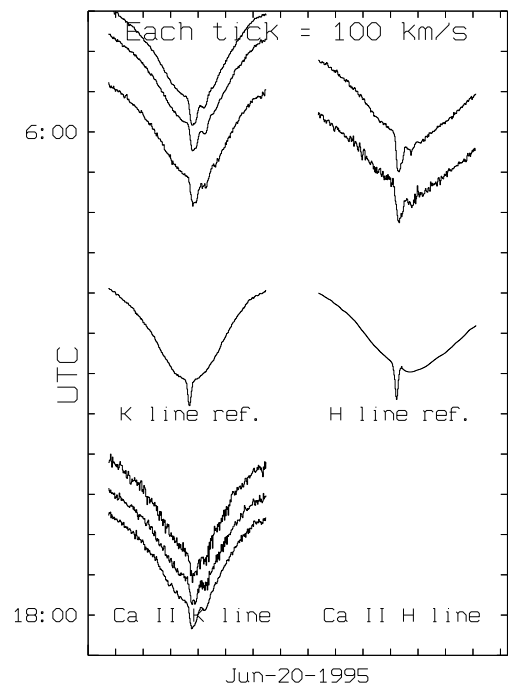


**Figure 6.33**: Spectra taken on 20 Jun 1995.
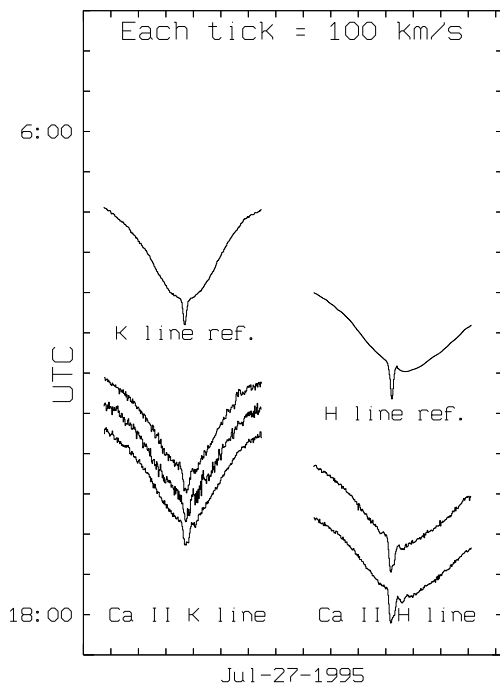
**Figure 6.34**: Spectra taken on 27 Jul 1995.
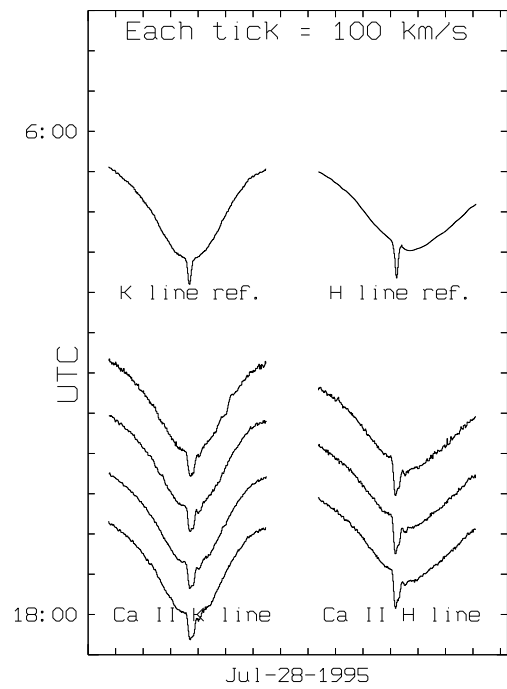


**Figure 6.35**: Spectra taken on 28 Jul 1995.
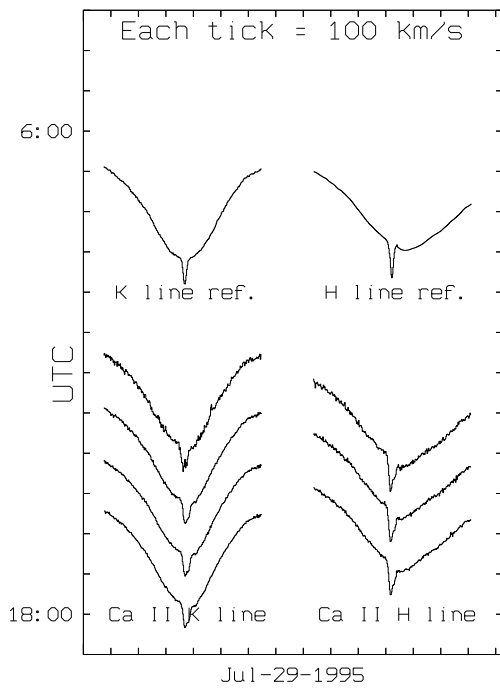


**Figure 6.36**: Spectra taken on 29 Jul 1995.
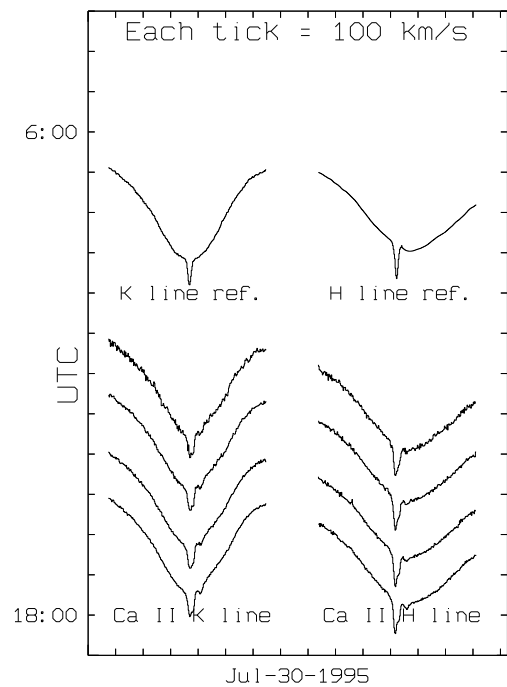


**Figure 6.37**: Spectra taken on 30 Jul 1995.
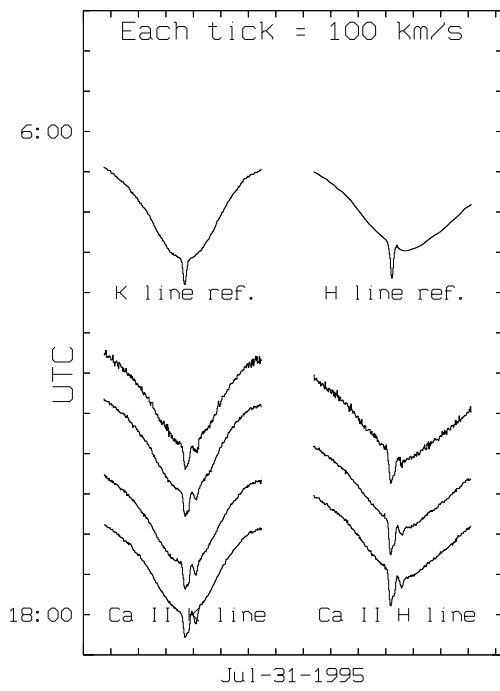
**Figure 6.38**: Spectra taken on 31 Jul 1995.
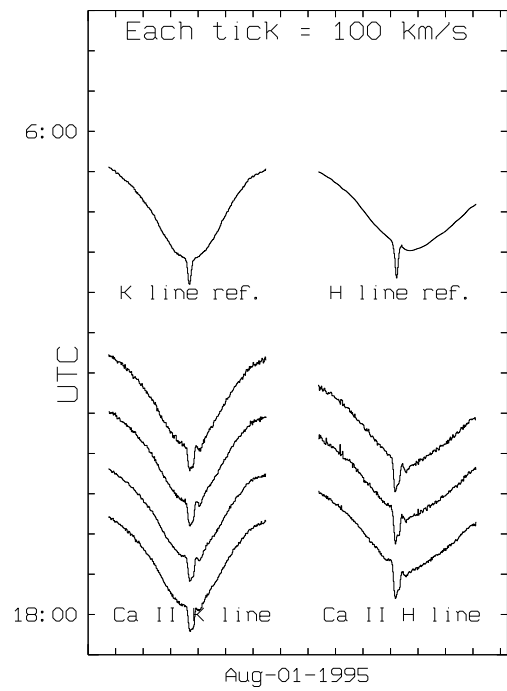


**Figure 6.39**: Spectra taken on 1 Aug 1995.
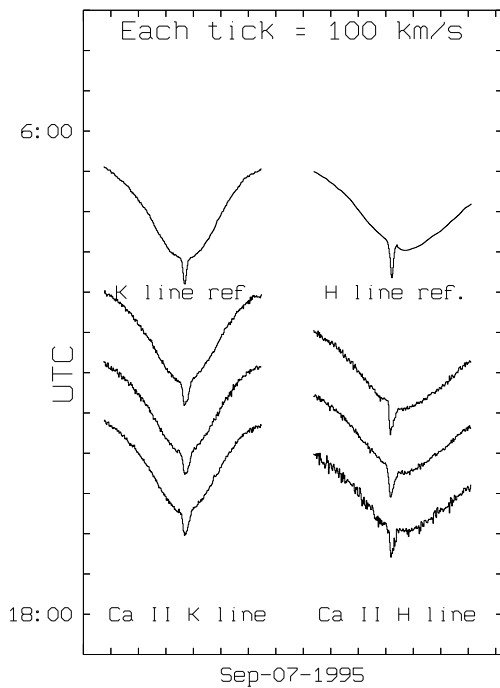


**Figure 6.40**: Spectra taken on 7 Sep 1995.
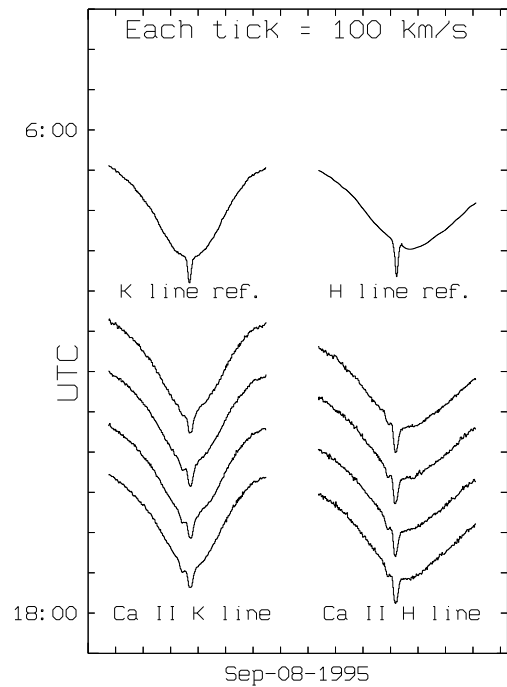


**Figure 6.41**: Spectra taken on 8 Sep 1995.
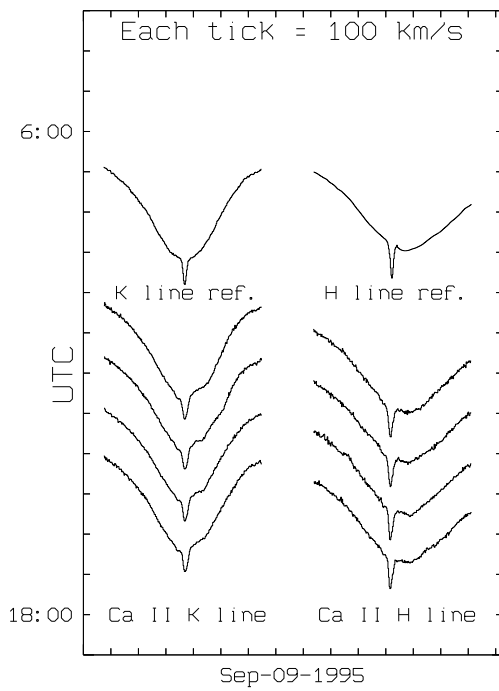
**Figure 6.42**: Spectra taken on 9 Sep 1995.
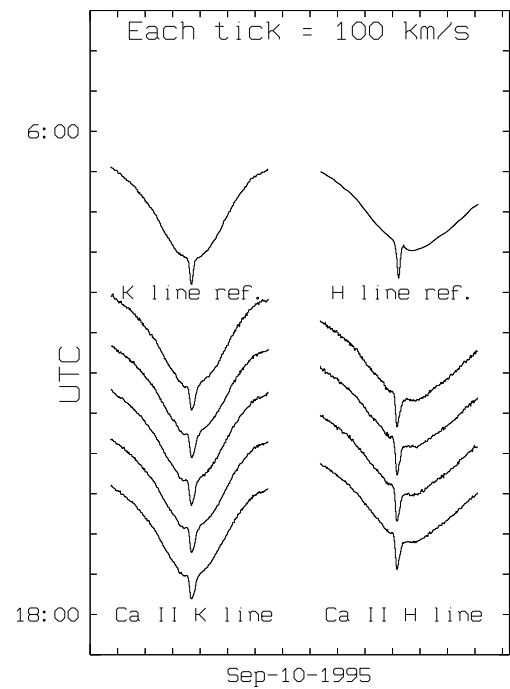


**Figure 6.43**: Spectra taken on 10 Sep 1995.
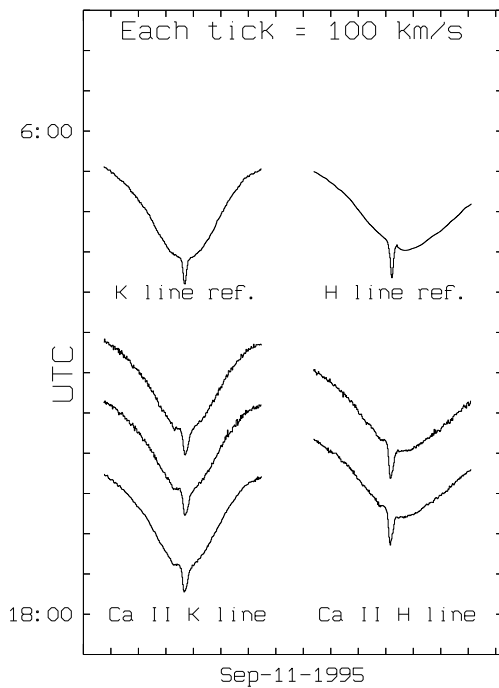


**Figure 6.44**: Spectra taken on 11 Sep 1995.
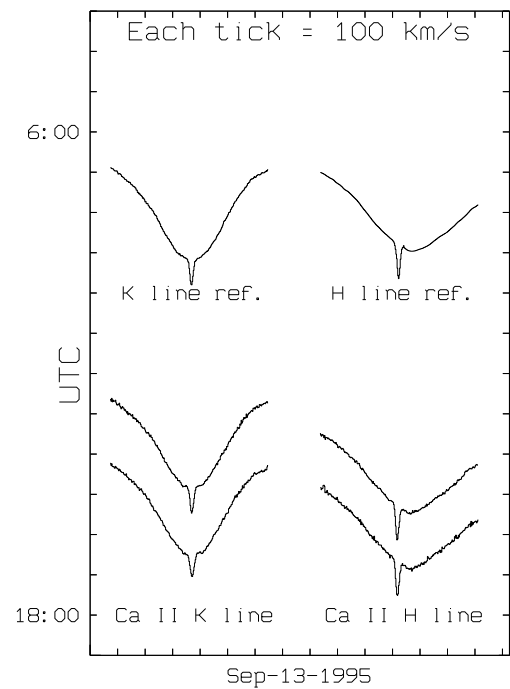


**Figure 6.45**: Spectra taken on 13 Sep 1995.
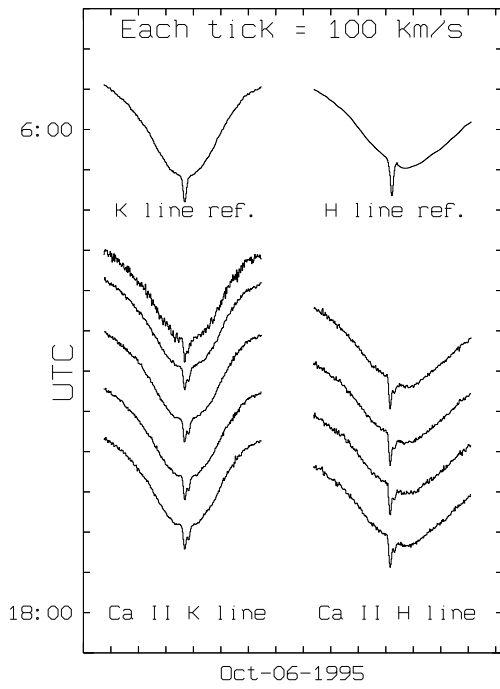
**Figure 6.46**: Spectra taken on 6 Oct 1995.
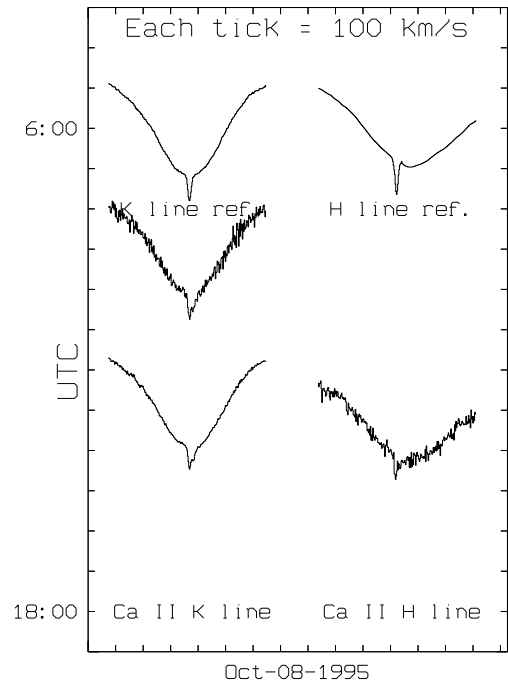


**Figure 6.47**: Spectra taken on 8 Oct 1995.
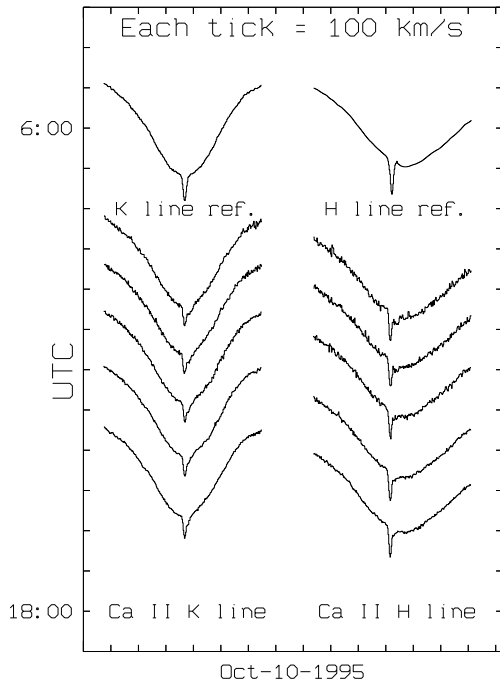


**Figure 6.48**: Spectra taken on 10 Oct 1995.
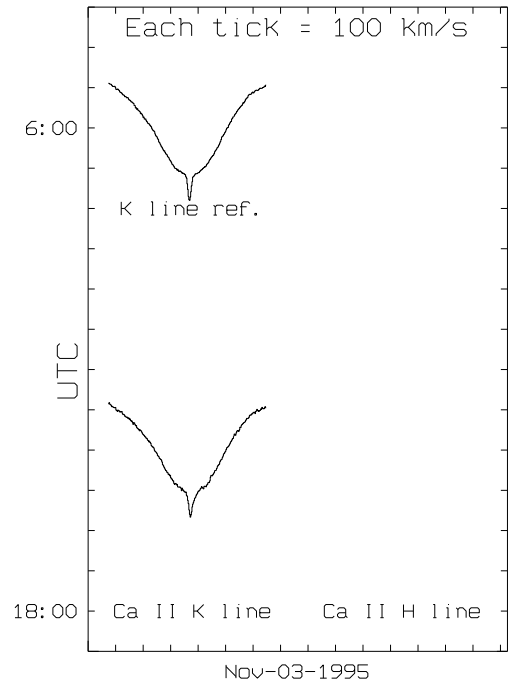


**Figure 6.49**: Spectra taken on 3 Nov 1995.
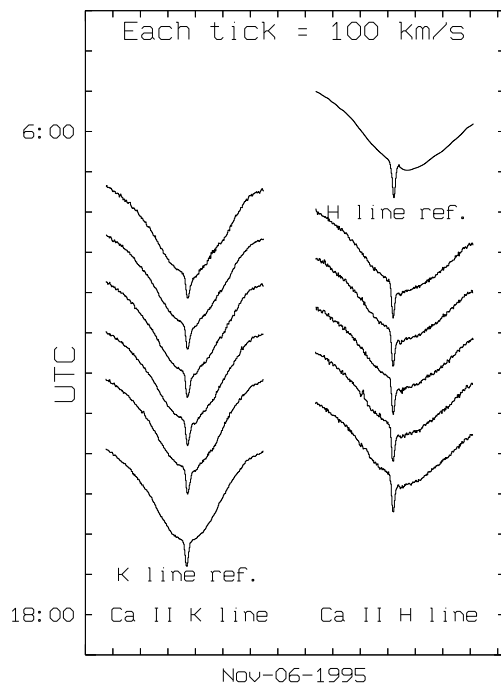
**Figure 6.50**: Spectra taken on 6 Nov 1995.
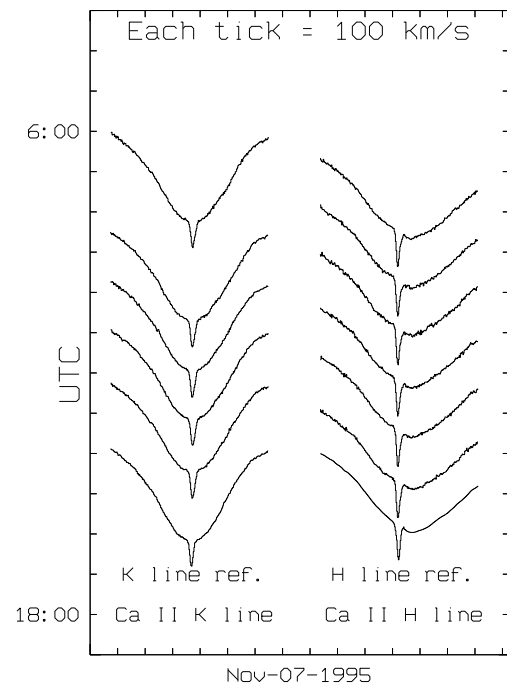


**Figure 6.51**: Spectra taken on 7 Nov 1995.
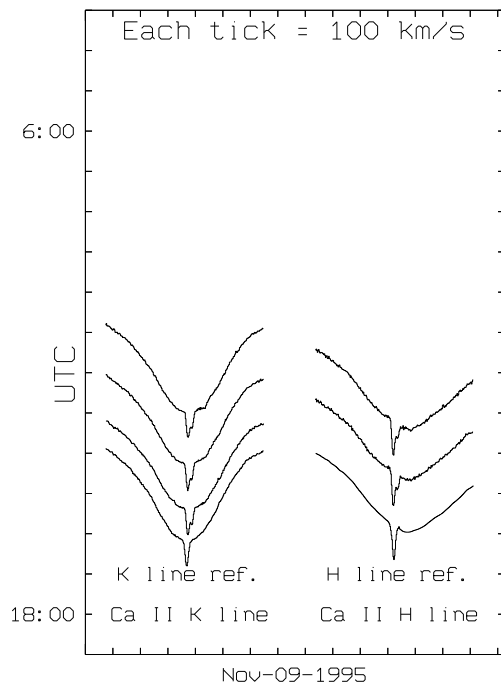


**Figure 6.52**: Spectra taken on 9 Nov 1995.
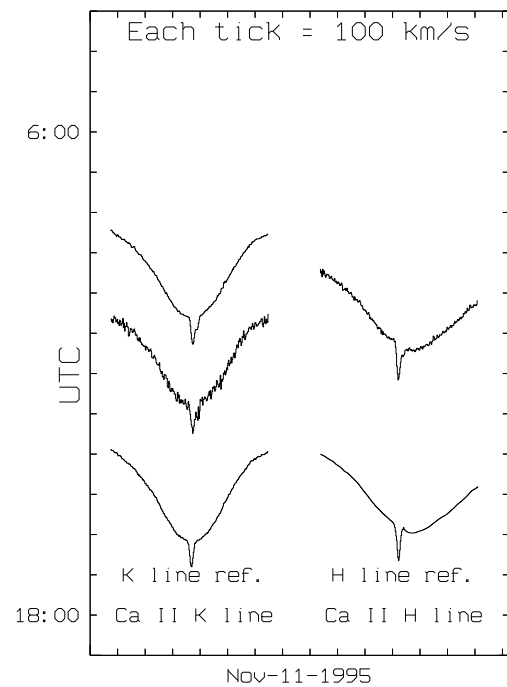


**Figure 6.53**: Spectra taken on 11 Nov 1995.
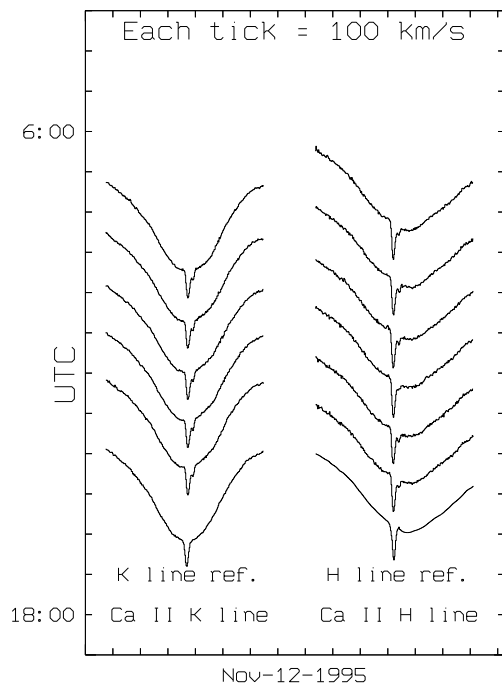
**Figure 6.54**: Spectra taken on 12 Nov 1995.
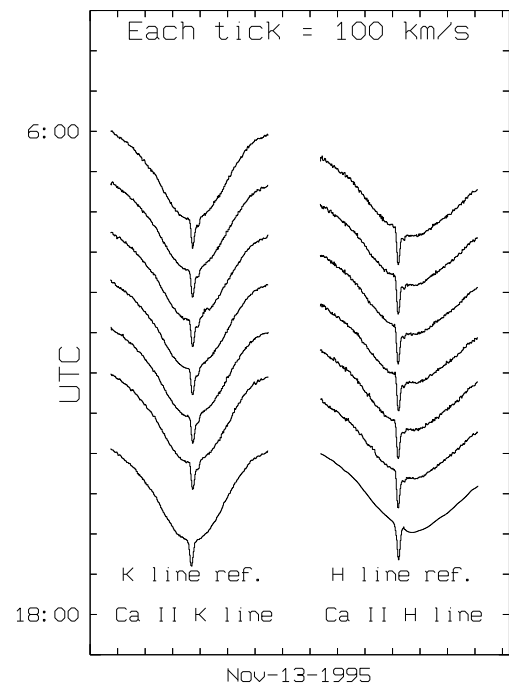
**Figure 6.55**: Spectra taken on 13 Nov 1995.
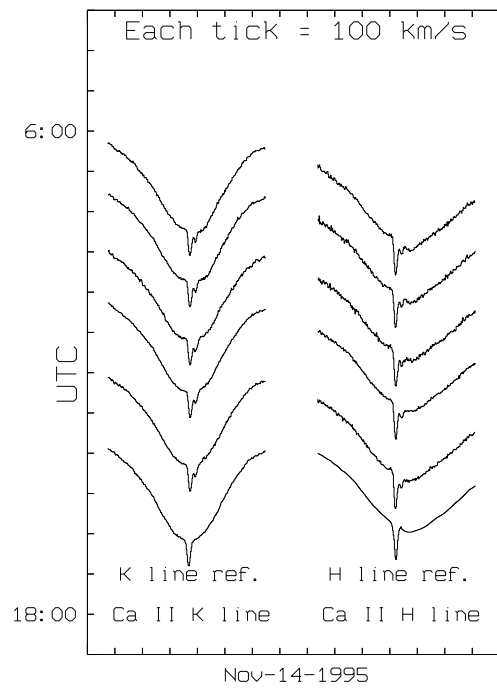


**Figure 6.56**: Spectra taken on 14 Nov 1995.

## 6.2   The 68 Ophiuchus K line

In this section the spectra taken of 68 Ophiuchus are presented for examination. Note that the spectra without the 2 small absorption features are H line spectra.

The K line spectra of 68 Ophiuchus is dominated by the smooth photospheric profile onto which are superimposed 2 narrow absorption lines due to interstellar clouds containing Calcium II at 40 and 18kms$^{-1}$ Heliocentric velocity. The H line spectra show no sign of these absorption features so any additional features strong enough to be detected in H should correspond to infalling matter in the star system.

At the available noise levels there are no clearly-apparent circumstellar absorption features. The two additional absorptions seen in the K line spectra obtained on October 8 and 10 are due to dust on the window in front of the CCD detector and are not evidence of variable absorption features (see Fig. 6.61).
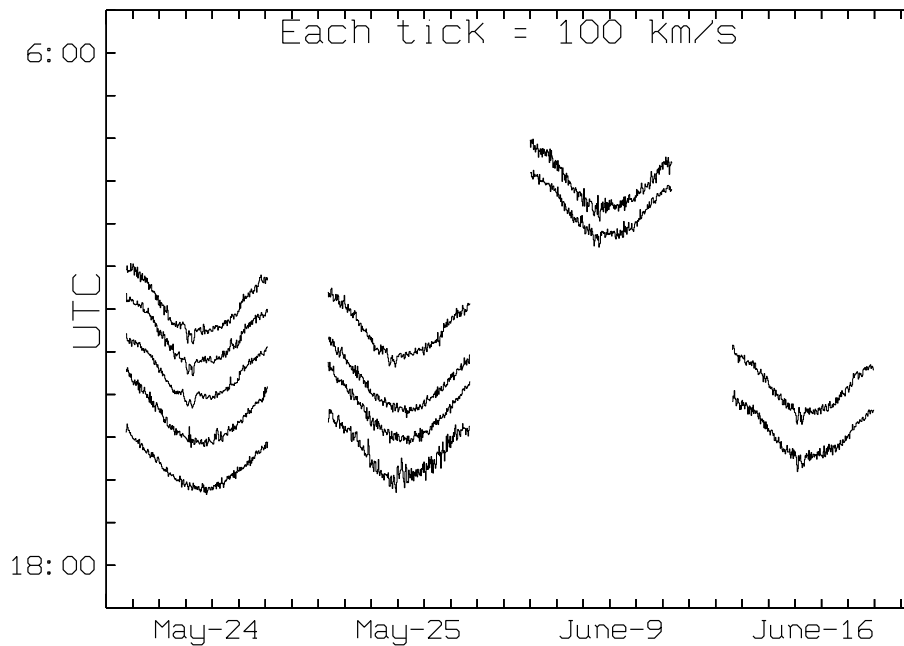


**Figure 6.57**: H & K line spectra of 68 Ophiuchus taken from MJUO in May and June.
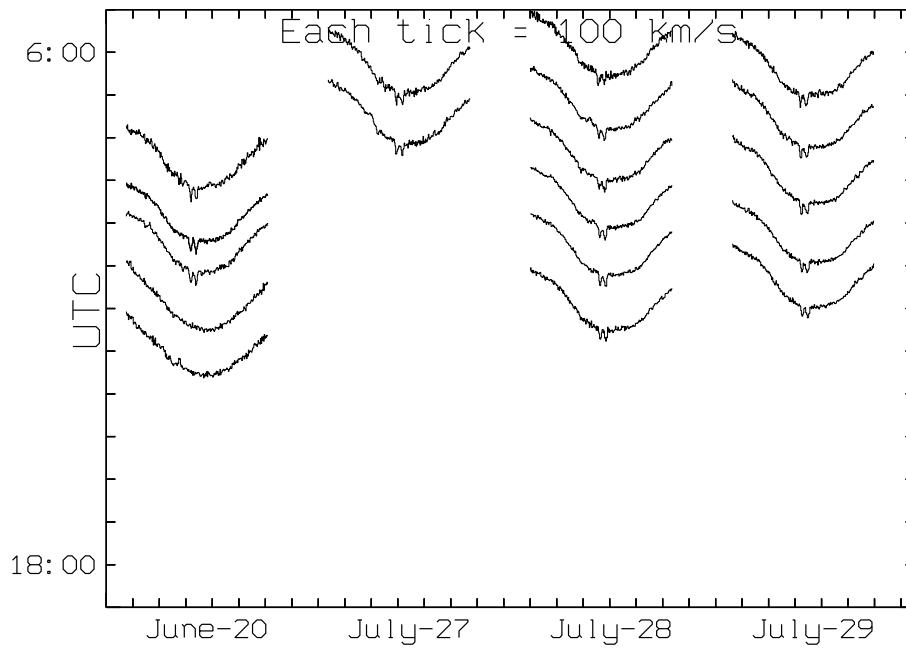
**Figure 6.58**: H & K line spectra of 68 Ophiuchus taken from MJUO in June and July.
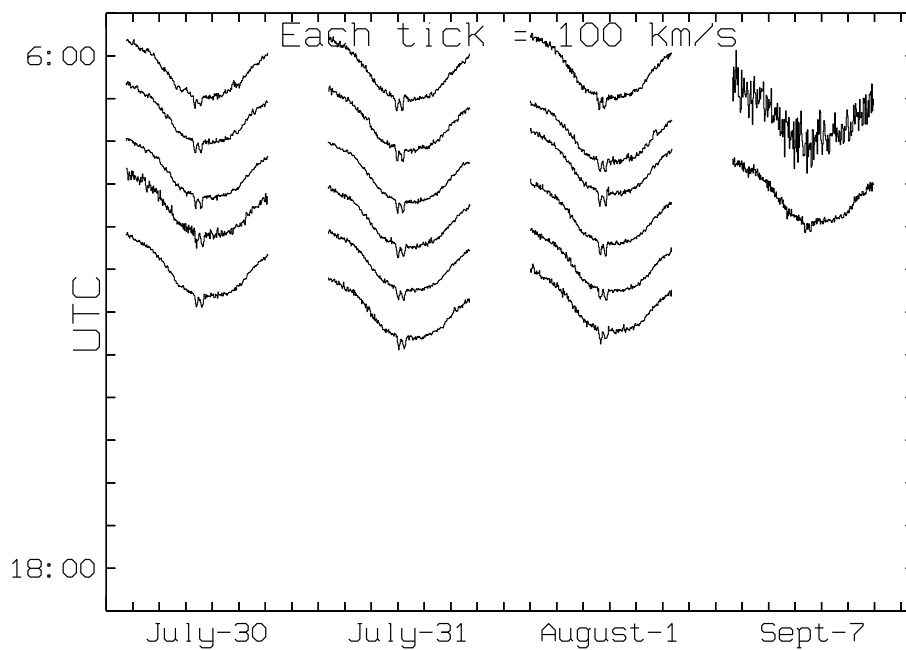


**Figure 6.59**: K line spectra of 68 Ophiuchus taken from MJUO in July, August and September.
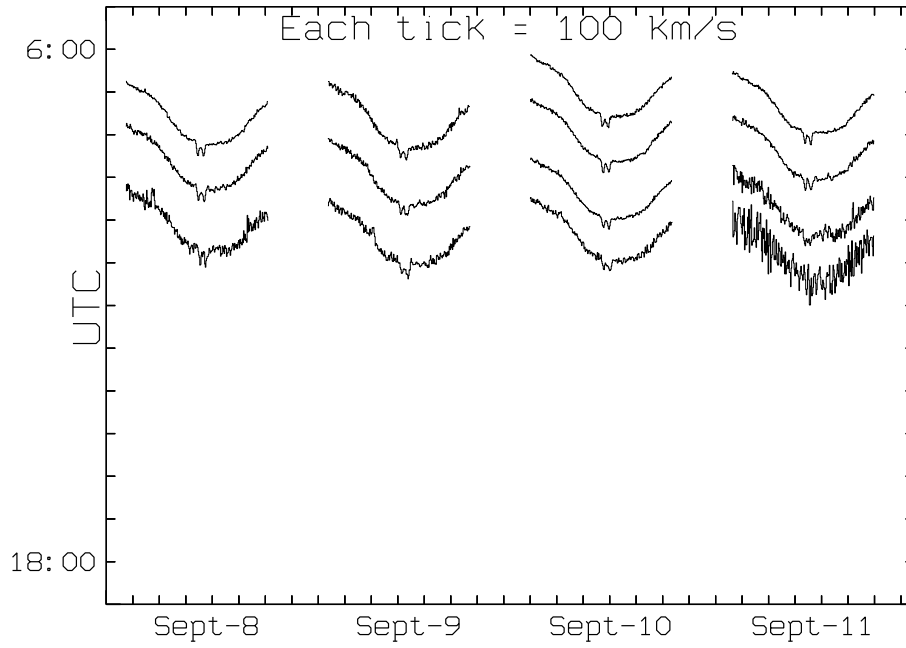
**Figure 6.60**: K line spectra of 68 Ophiuchus taken from MJUO in September.
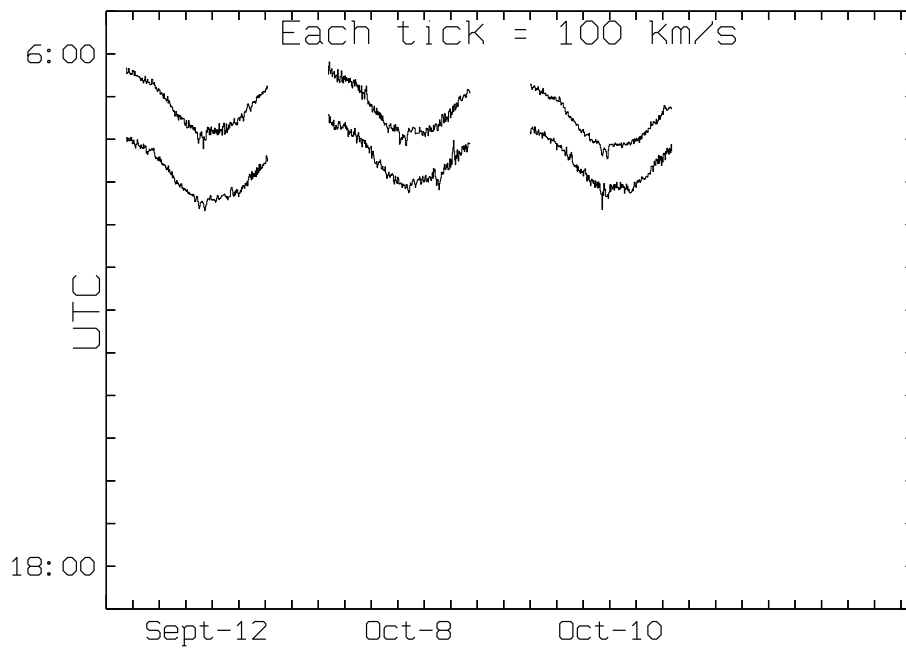


**Figure 6.61**: K line spectra of 68 Ophiuchus taken from MJUO in September and October.

# 6.3   The Alpha Piscis Australus H and K lines

The spectra of $\alpha$ PsA shows only the photospheric profile, but since the suspected dust disk is believed to be seen in the plane of the sky, it is unlikely any FEB in orbit around the star would cross the line of sight given this orientation. No variable absorption features are apparent in any of the spectra.
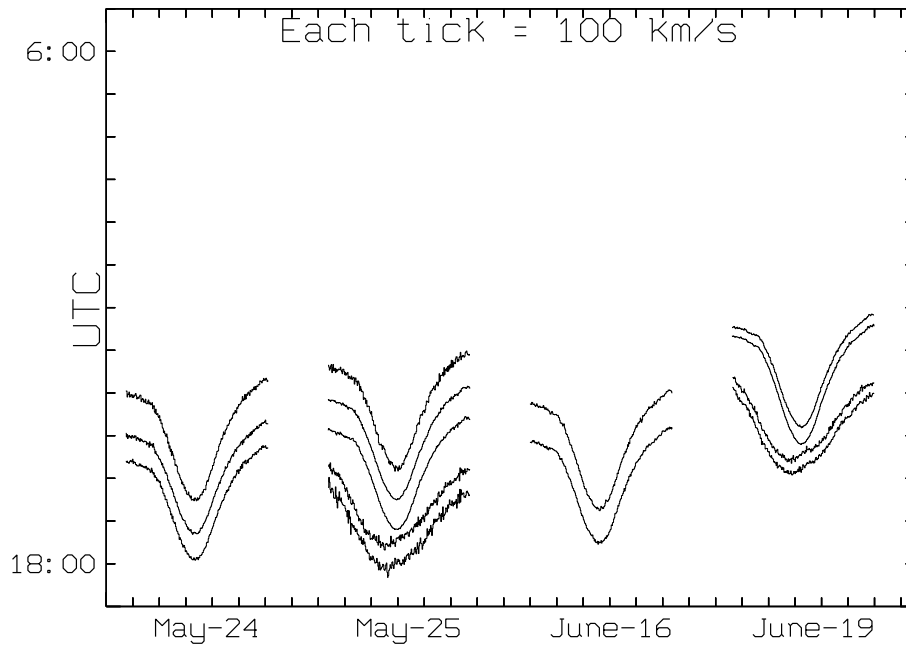


**Figure 6.62**: H & K line spectra of $\alpha$ Piscis Australus taken in May and June.
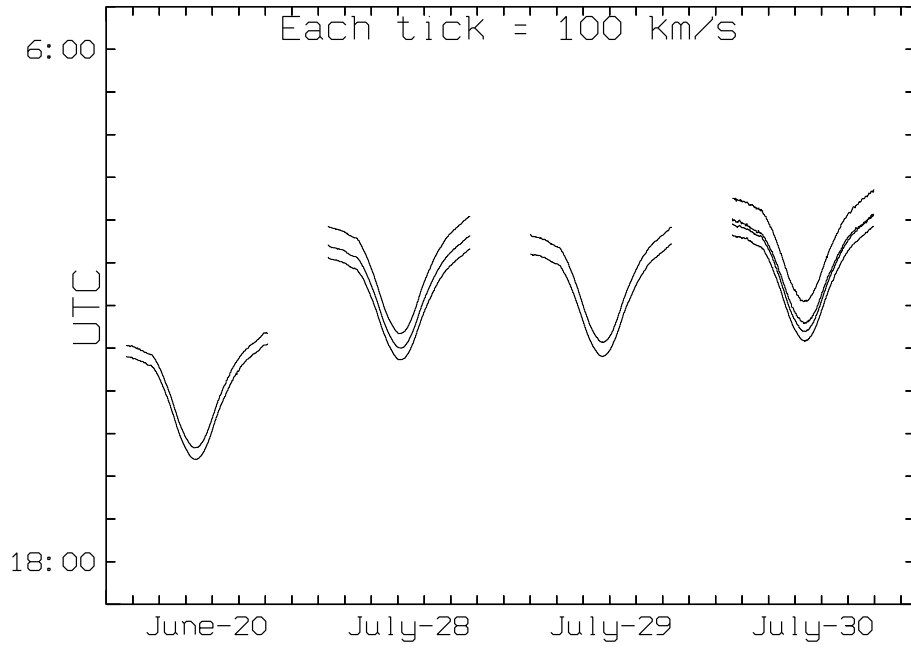
**Figure 6.63**: K line spectra of $\alpha$ Piscis Australus taken in June and July.
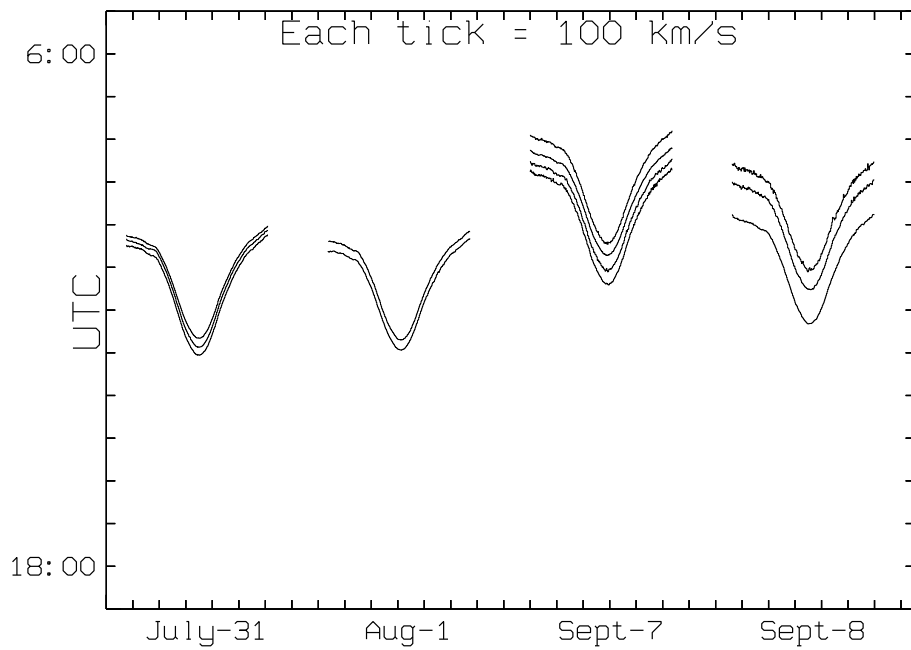


**Figure 6.64**: K line spectra of $\alpha$ Piscis Australus taken in July, August and September.
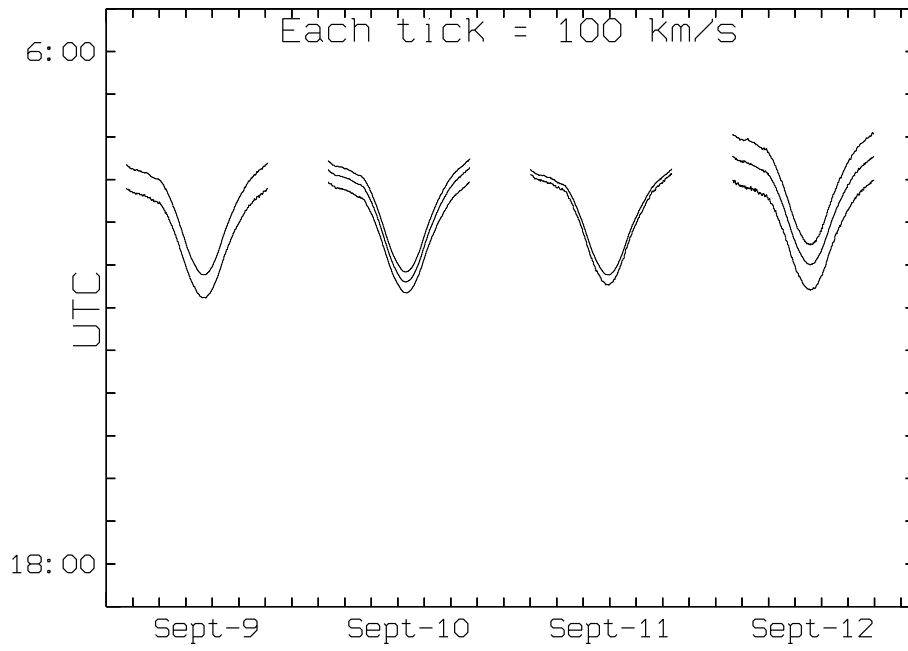
**Figure 6.65**: K line spectra of $\alpha$ Piscis Australus taken in September.
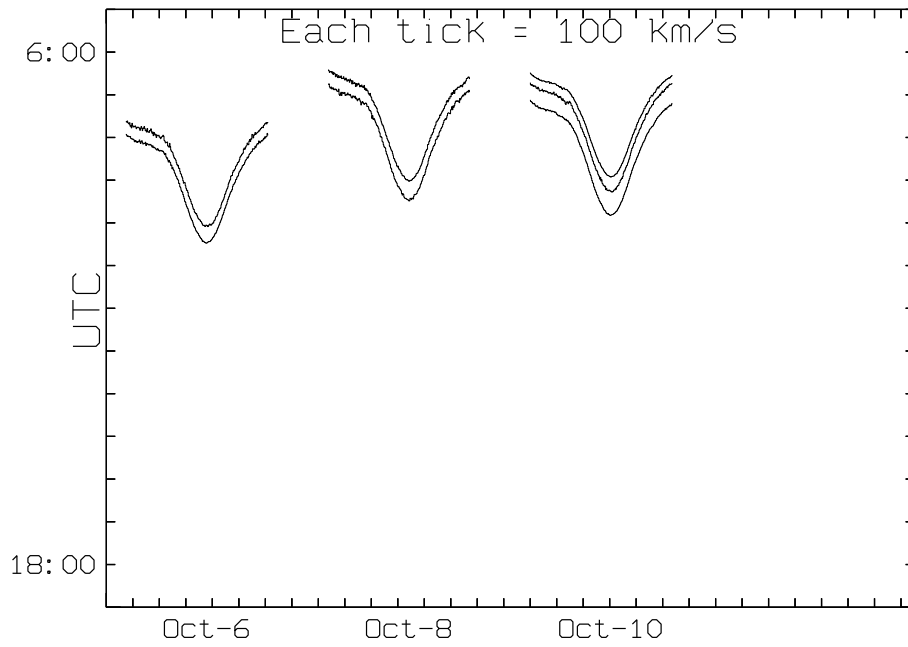


**Figure 6.66**: K line spectra of $\alpha$ Piscis Australus in October.

# Chapter 7

# Characterisation of $\beta$ Pictoris spectra

## 7.1 Normalising the spectra

Normalising the data to a common intensity scale is an important step along the path to extracting useful information.

Each of the Ca II H & K lines was plotted at the same wavelength scale and the flux level was scaled so that the plots could be overlayed for comparison. Then the CaII H & K line spectra were divided through by their respective reference spectra.

Each reference spectrum was made from spectra of each star taken at MJUO using the same equipment. The spectra selected had to be as free as possible of additional absorption features (if present), then the spectra were smoothed using the MIDAS FILTER/GAUSS command. The adopted H and K reference spectra are shown in Figs. 6.1-6.56. It was decided that the best way to normalise the spectra was to align the short-wavelength side of the circumstellar line of each observed spectrum with the corresponding feature in the reference spectrum, and then divide one by the other. The resulting division should then reveal the presence of absorption features by any departure from a horizontal straight line. Of course the circumstellar line is believed to be saturated, therefore the quality of the background subtraction during the reductions affects the line depth. Measurements near this line are expected to be more uncertain. The example of Figs. 7.1 and 7.2 illustrate the procedure. In Fig. 7.2 the observed spectrum of Fig. 7.1 has been aligned with and divided by the reference spectrum.

In the particular case of the Beta Pictoris reference spectra, the smoothed profile was made from spectra taken in previous years and were nearly completely free of additional absorption features. The reference spectra should only have the photospheric lines and the circumstellar feature present. Since observations of Beta Pictoris began at MJUO, there has never been a case where no additional features are present in good signal spectra. It was therefore necessary to adjust the smoothed spectrum after a few trials at normalising other spectra from different observing runs turned up some common absorption features, which were then removed. The normalised spectra are converted to a velocity scale centred on the circumstellar line (see Fig. 7.2). The MIDAS procedure which does the normalisation is found in Appendix B.4.
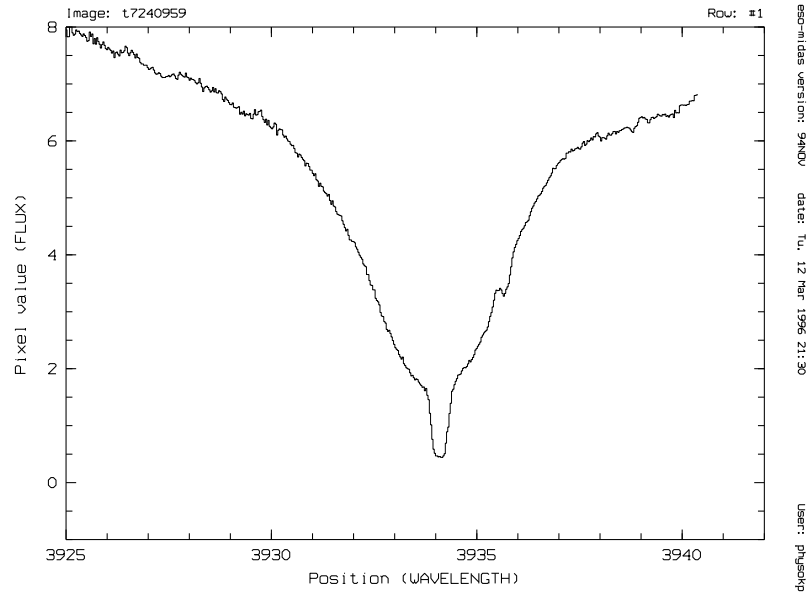
**Figure 7.1**: K line spectra taken on June-9-1995 showing the broadened circumstellar line and also a clear HVF.

## 7.2   Fitting the absorption features

With the normalised spectra, the existence of any absorption features can then be fitted with gaussians to best fit the absorption features attributed to the cometary bodies. The "continuum" is then fitted by either of a constant straight line, a line with a slope in wavelength or a quadratic in wavelength, whichever appears to fit the "continuum" best. The absorption features are fitted using the MIDAS non-linear fitting routines. The cursor was used to mark on the plot the approximate centre and depth of each feature, and also the FWHM. These initial values were then fed to the fitting routine which was used the following equation to compute each gaussian shaped feature:

$$GAUSS(x; a, b, c) = a \exp \left[ -\ln 2 \left( \frac{2(x - b)}{c} \right)^2 \right]$$

This process was repeated for each of the features in the plot. The Modified-Gauss-Newton method was used in the fitting. From the initial input from the cursor, the values of a,b and c were iterated many times to produce an optimum synthetic fit from which one can then extract velocity information about the cometary absorptions as well as their strengths and FWHMs (see Fig. 7.3). The MIDAS procedure which does the fitting is listed in Appendix B.5.
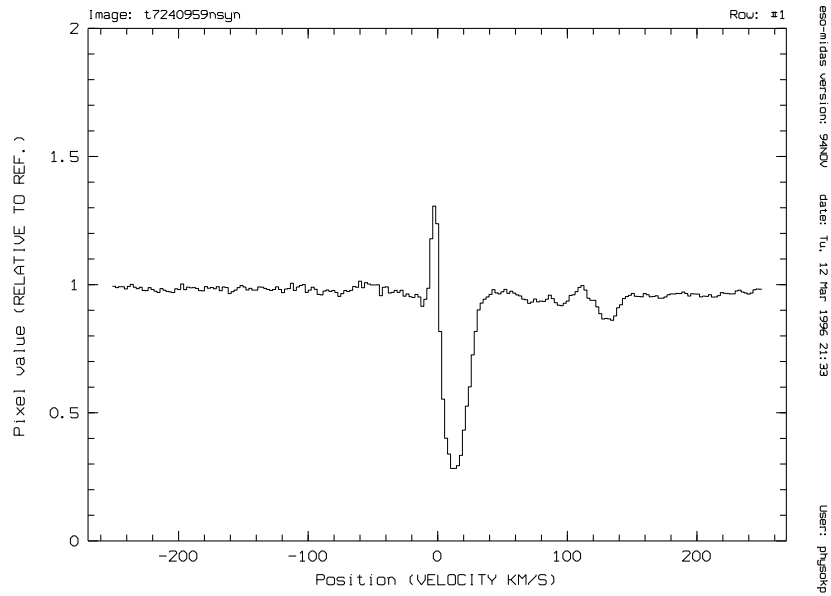
**Figure 7.2**: The normalised spectrum after being divided by the reference spectrum.
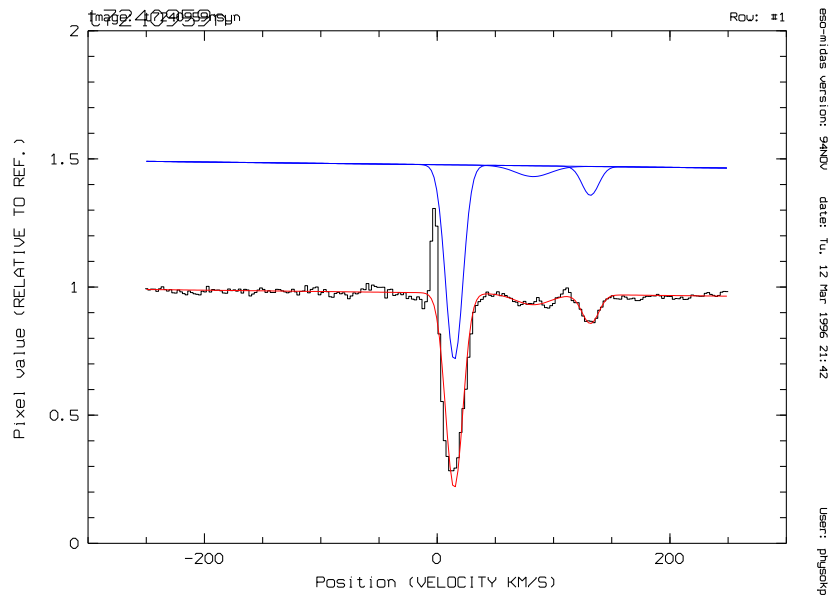


**Figure 7.3**: Plot showing the normalised spectrum and fitted gaussians to the variable absorption features. Note the well defined gaussian shaped absorption at $\sim150\text{kms}^{-1}$.

# Chapter 8

# Analysis

Presented here are the results of the spectroscopic observations taken of Beta Pictoris from MJUO during the 1992, 1993, 1994 international observing campaigns and the observations made in 1995. The data is presented as a series of plots (Figs. 8.1 - 8.56 showing the velocity, FWHM[1], depth and equivalent width. These data should be considered conjointly with the plots in chapter 6 figures 6.1 - 6.56. The symbols used for the absorption features identify what range of velocity they are in. There are a maximum of 3 velocity regions that can be plotted, usually the redshifted LVF region and then either the blueshifted and redshifted HVFs, or 2 ranges of HVFs in the red. Open symbols represent the data derived from the spectra taken of the Calcium K line and the filled symbols represent the data derived from the spectra taken of the Calcium H line. The same symbols are used for the same velocity range from day to day during the same observing run. The data on the variable absorption features seen in the spectra of $\beta$ Pictoris is also displayed in a table in Appendix C.

## 8.1   The 1992 observing campaign

139

Only observations of the Calcium K line were made in December 1992. The most remarkable feature of the observations (Figs. 8.1 - 8.10) is the presence of the long lived absorption feature at $\sim$20 kms$^{-1}$. In fact it is observed from December 8 to December 16, and even appears in a follow up observation on January 9 1993. It should be noted that the detection on the January 9 has been badly effected by a cosmic ray as can be seen in Fig. 6.10. Appearing from time to time are slightly higher redshifted features at $\sim$40 to 50 kms$^{-1}$ which appear out of the red wing of the $\sim$20 kms$^{-1}$ feature (see Figs 8.1, 8.3, 8.4, 8.7). This indicates that the infalling material is clumpy in structure, which supports the conclusions of Lagrange-Henri *et al.* 1995[46]. Even higher HVFs are observed which are generally broader with the centroid evolving in velocity (see Figs 8.5, 8.6, 8.9).

Also detected is the presence of 4 blueshifted absorption features (Figs 8.1, 8.4, 8.7, 8.8), not detected by Lagrange-Henri *et al.* 1996[46]. This is not surprising given the

---

[1]For some unknown reason, the lower error bars in the FWHM and Equivalent Width data plotted before 0$^h$ each Heliocentric Julian Day is misplotted at a very low value. This is clearly an error in the MIDAS 94NOV plot command overplot/error when a logarithmic scale is in use.

method of division by an unabsorbed stellar profile followed here, which allows for the detection of broad, shallow and some blended absorption features. All the blueshifted features were short lived, typically <3 hrs in duration, they appear and disappeared suddenly (<1 hr) and once present show little evolution in strength. 3 of the features appeared at low velocity while the other was a broad shallow absorption feature at high velocity (Fig 8.7), much as expected for the observation of the ion tail of an evaporating body close to the star.

The redshifted features at high velocity and the ones emerging from the $\sim20$ kms$^{-1}$ absorption feature appear and then disappear over timescales of about $2-8$ hours which correspond to the crossing times of orbiting bodies across the stellar disk. On the night of December 13 the feature seen at $\sim50$ kms$^{-1}$ shows evidence suggestive of the effect of stellar rotation on the evolution of an FEB feature's equivalent width. The decrease of equivalent width is slow, suggestive of an FEB crossing from the blueshifted side to the redshifted side of the stellar disk. However the rate of decline may be considerably different if errors are underestimated, and the apparent deceleration of the feature is unexpected. Could it be due to the FEB encountering some dense medium?

In calculating the number of events observed during an observation run and then giving a yearly estimate of infall, a number of problems need to be addressed. The timescale from which the estimate will be made from can have a great deal of impact on the result. Does one consider only the time observed and hence only count those features seen to appear? or the days on which observations are made and then count what appear to be individual features, regardless of them being already present and those new ones that subsequently appear. Of course if one looks at just the velocity a feature is seen to appear at, one could miss the signs of 2 or more features being present from examination of the equivalent width of the feature. With all these problems in mind it was decided that the estimate of the number of infalling bodies would be calculated from the bodies that appear in the velocity plots. Also the equivalent width of the features would be examined for strong evidence of additional bodies being present. The long lived features would only count as 1 body, despite the belief that they are due to more than 1, as there is no measurable evidence of additional features in this data. The time over which these features would be counted, is the days of observation since some of the features observed would appear during the day before observing began and disappeared after observing ended for the night. Hence the resulting estimate should give a lower bound to the number of infalling bodies that could be observed crossing the line of sight.

A count of the features observed gives 12 events detected over 8 days, both red and blueshifted plus the LVF at 20kms$^{-1}$. An estimate of the infalling rate gives >500 events observed per year!
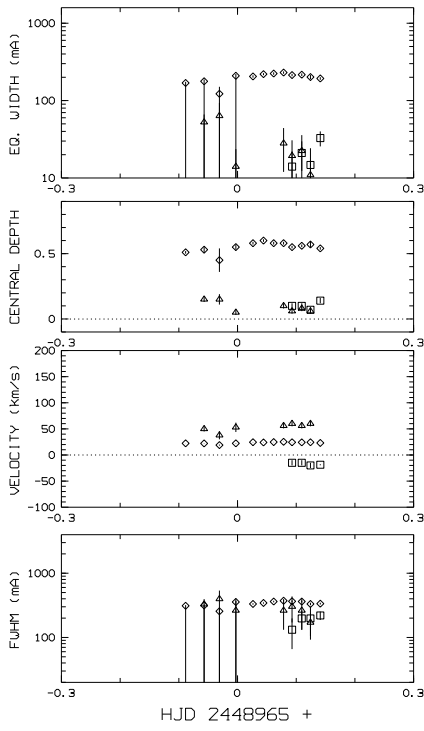
**Figure 8.1**: 8 December 1992
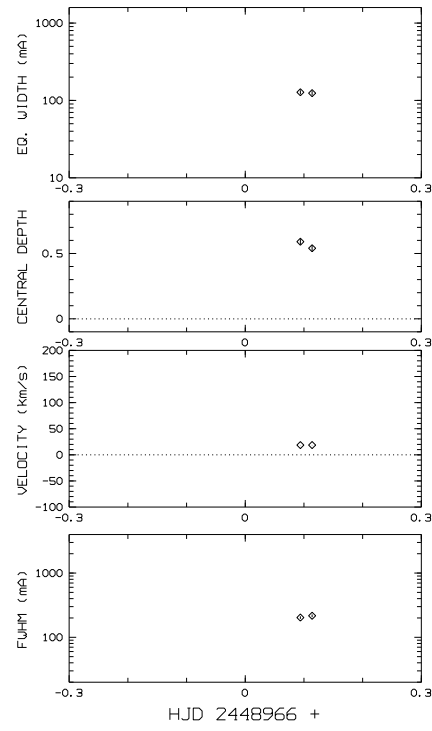


**Figure 8.2**: 9 December 1992
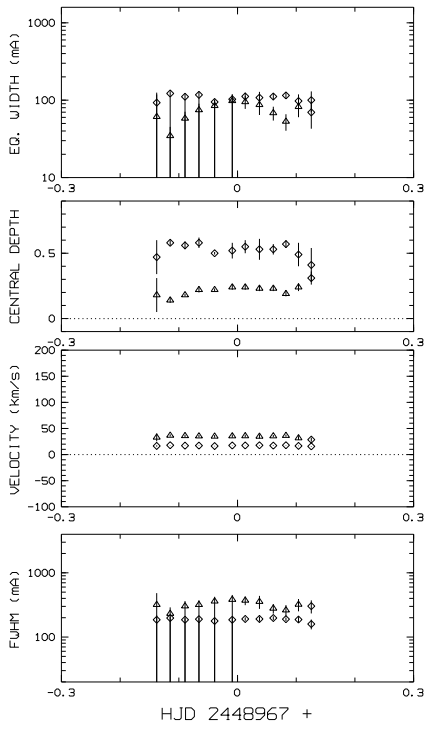


**Figure 8.3**: 10 December 1992
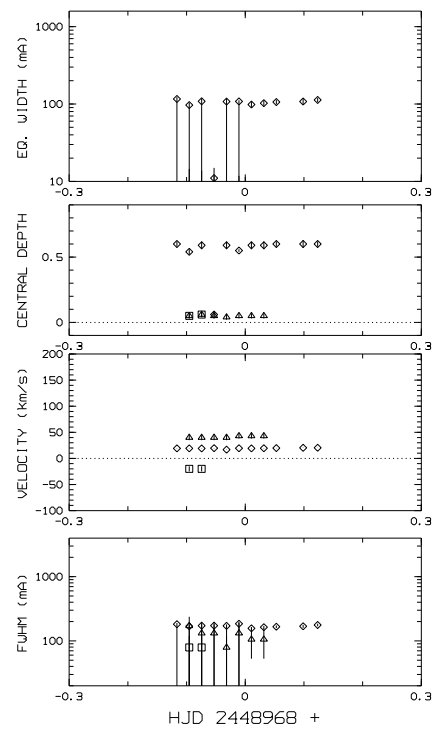


**Figure 8.4**: 11 December 1992
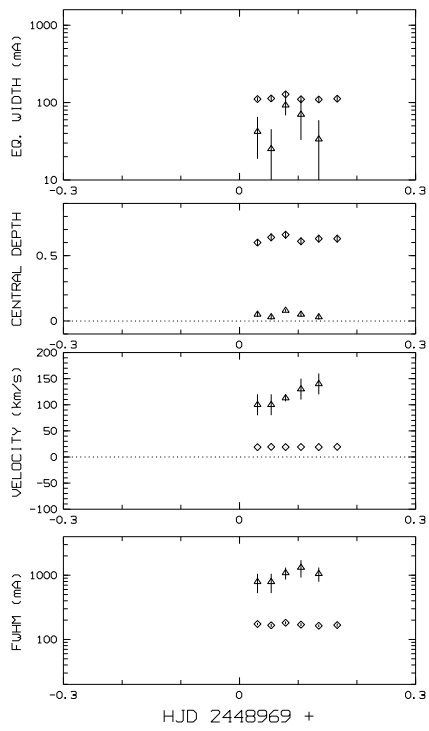
**Figure 8.5**: 12 December 1992
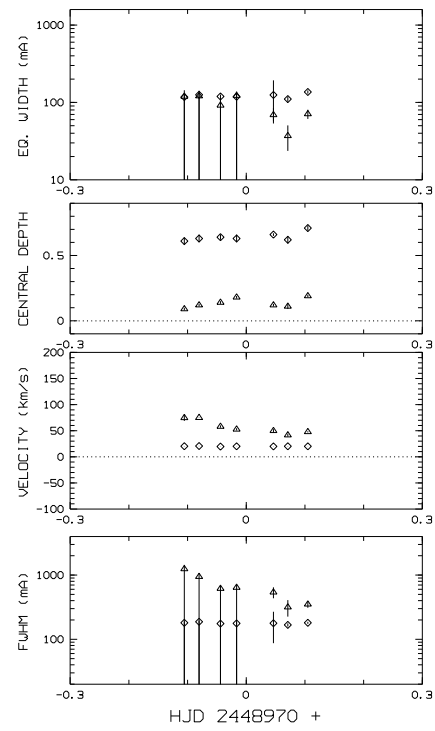


**Figure 8.6**: 13 December 1992
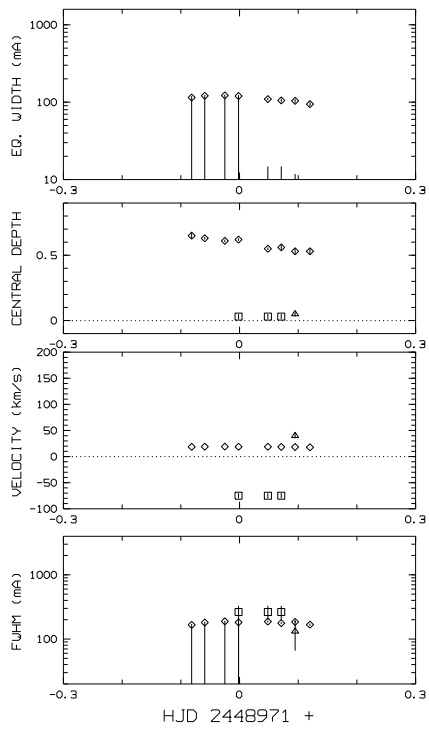


**Figure 8.7**: 14 December 1992
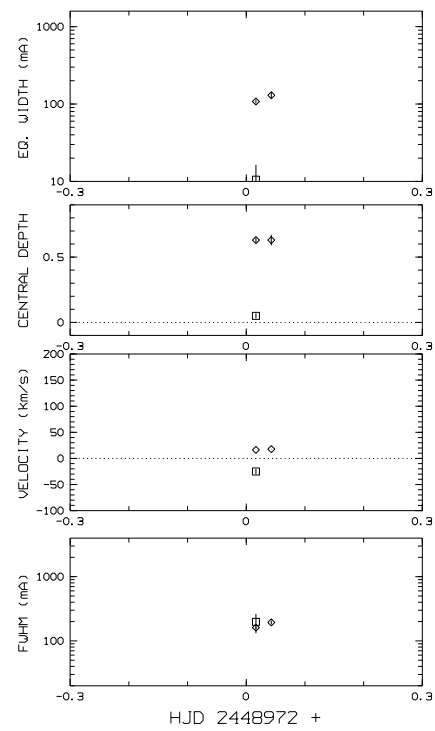


**Figure 8.8**: 15 December 1992
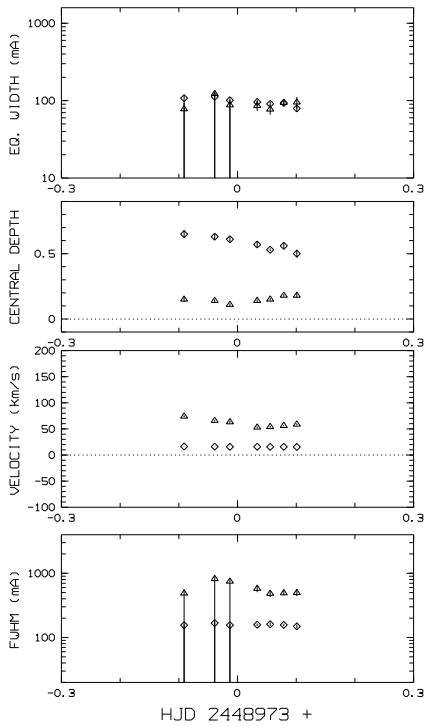
**Figure 8.9**: 16 December 1992
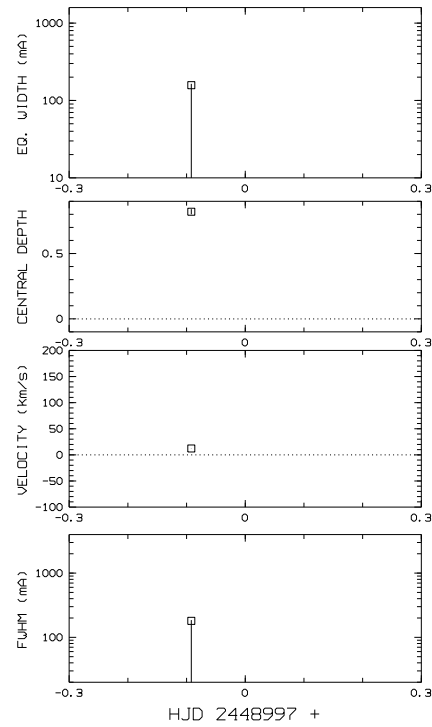


**Figure 8.10**: 9 January 1993

## 8.2   The 1993 observing campaign

Before the commencement of the 1993 campaign a few nights were used in April and October to optimise observing procedures and gain experience with altering the spectrograph set up so that observations of both the H and K lines could be made. On April 6 an absorption feature is seen in the wing of the circumstellar feature, also a broad feature is present blended with the other feature.

On October 24 features are seen at low redshift, one deep and distinct, and a shallower feature between it and the circumstellar line. Both however, are gone in the following night's observations (see Figs. 8.13 and 6.13), which show no discernible absorption features at all, except for the appearance of a broad HVF in the last H spectrum.

During the international observing campaign in November and December (Figs 8.14 - 8.18) a long lived shallow blueshifted feature is observed in the K line all week long, but only confirmed in the H on November 29. It is however clearly seen in some of the original spectra, most prominently on November 27 and 29 (see Figs. 6.14 and 6.16). The lack of detection in H may be entirely due to the difference in the oscillator strengths of H & K. At both ends of the run redshifted features appear in the spectra at low velocity predominately, also many broad features are seen, some even show suggestive evidence of evolution in equivalent width. On December 2 and 3 the evolution of equivalent width

in features at $\sim$40 kms$^{-1}$ is again suggestive of FEB passage from the blueshifted to redshifted sides of the stellar disk.

A count of the observed events indicates 10 seen over 8 days, giving the infalling rate at >450 per year, assuming, of course, that the sample is typical for the whole year.
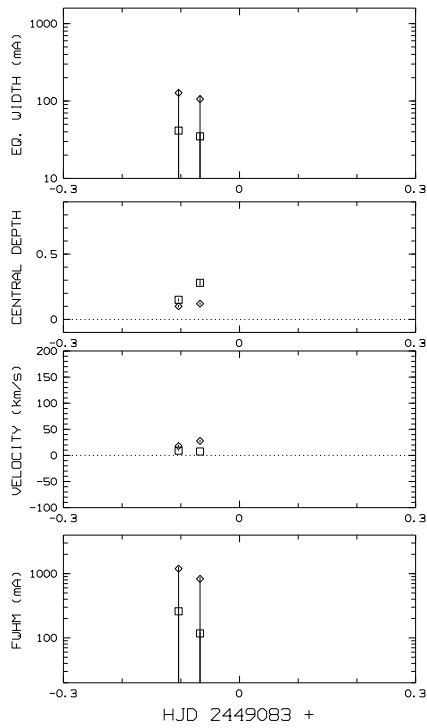


**Figure 8.11**: 6 April 1993                              **Figure 8.12**: 24 October 1993
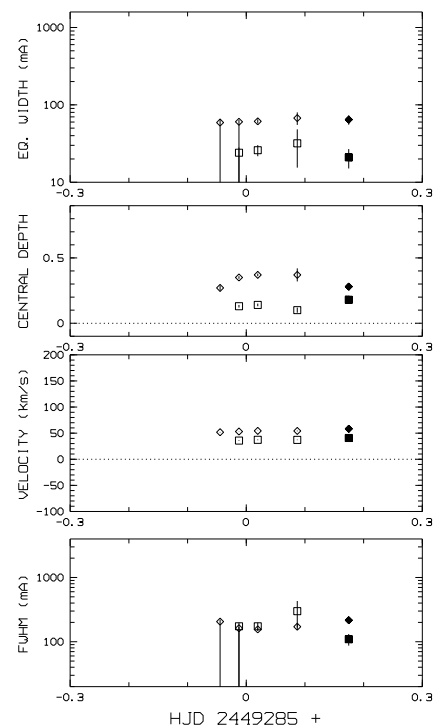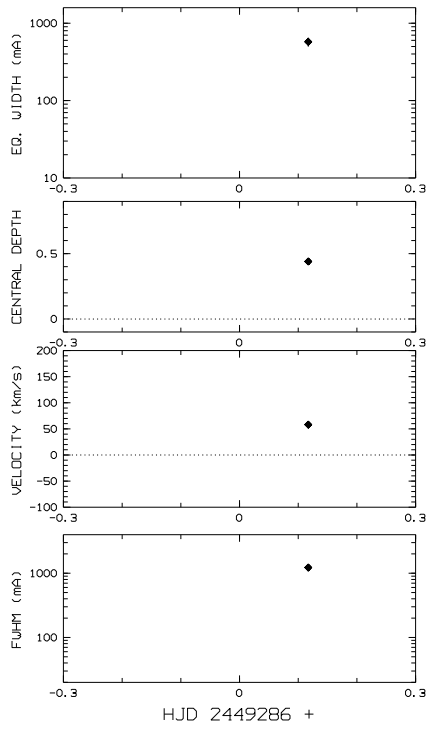
**Figure 8.13**: 25 October 1993
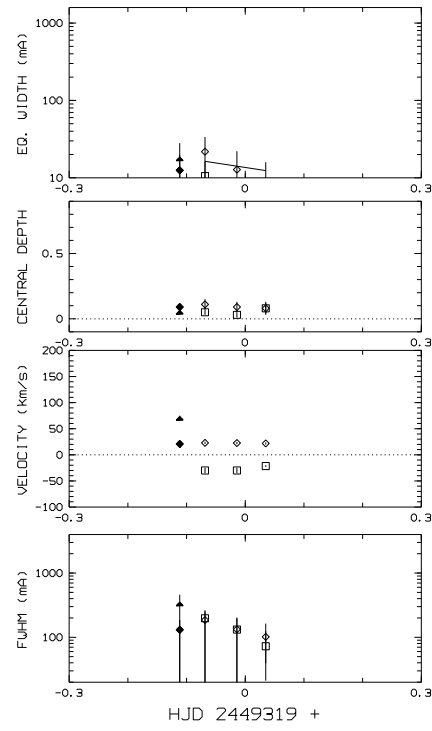


**Figure 8.14**: 27 November 1993
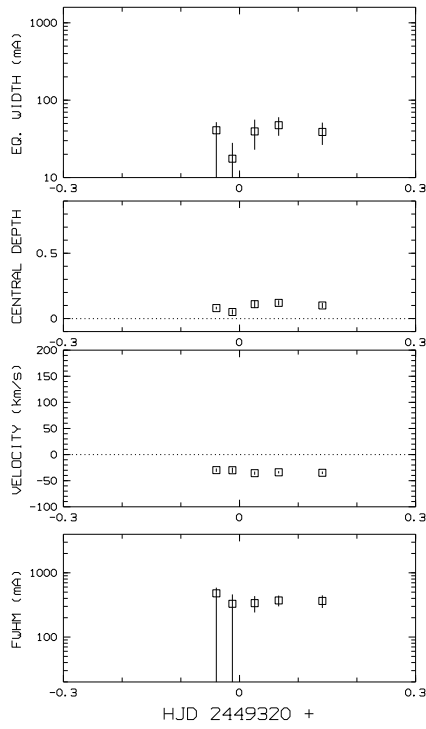


**Figure 8.15**: 28 November 1993
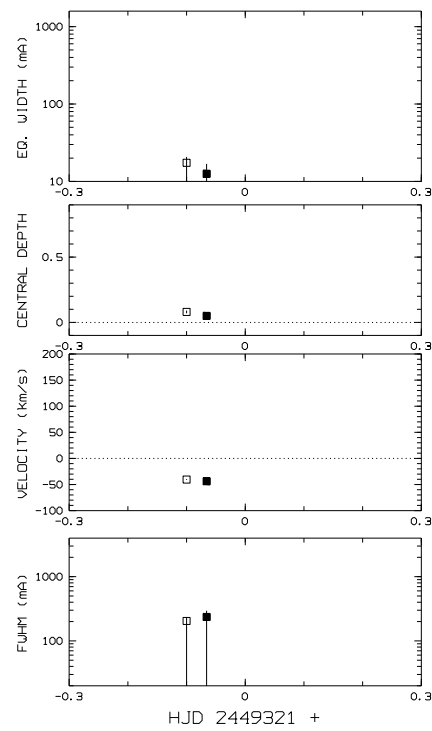


**Figure 8.16**: 29 November 1993
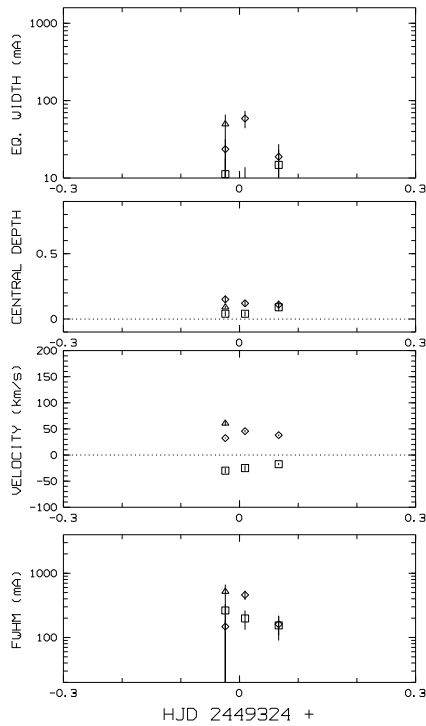
**Figure 8.17**: 2 December 1993
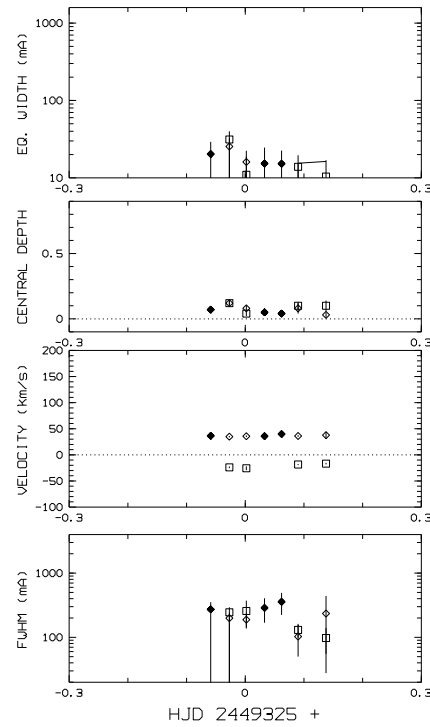


**Figure 8.18**: 3 December 1993

## 8.3   The 1994 observing campaign

The 1994 campaign reveals lots of varying features which come and go (Figs 8.19 - 8.25). On November 19 a broad LVF is seen at $25\mathrm{kms}^{-1}$ in both H and K, but has disappeared after only 1 1/2 hours of being first observed. From the 21 November a feature develops and is seen to start evolving, initially starting as a broad absorption in the red wing of the photospheric line at $\sim 60\mathrm{kms}^{-1}$. It then develops into a clear and unmistakable feature in the Ca II lines where it is seen in both H and K as a broad and deep feature on the 22 November. It is possible there is more than one FEB present and this maybe part of a shower of bodies. It then evolves into a broader feature on the 23 November and on the 24 November near the end of the night it is seen to separate into 2 features. From this and from the plots of equivalent width it is clear that this feature is evolving in a quite complicated fashion which suggests that more than one FEB is involved.

The circumstellar line is further broadened in its red wing indicating another feature superimposed, typical of the features seen at low velocity from bodies orbiting at quite large distances from the star ($\sim 1$ AU). In the few nights it is observed, it is seen to come and go, but is clearly seen from the 23 November. It appears to be remarkably stable and is not saturated (indicated by the difference in the equivalent width of the H and K lines). The long-term stability is reminiscent of the similar phenomenon observed in 1992.

For a brief period of time on 24 November a broad blueshifted feature is seen for about 1 hour which appears suddenly and disappears just as suddenly.

On the 26 November a LVF at $\sim 30 \mathrm{kms}^{-1}$ becomes broader as the night progresses and is still present the next night. It has clearly evolved over this time. Also on 26 November 2 broad HVFs are seen to come and go quickly, seen in one spectra and gone the next in spectra taken 1 hour apart.

Finally a count of events yields an infall rate of >520 events per year from the 10 events seen over the 7 days observed. This will be greater if the long-lived features are due to more than one body.
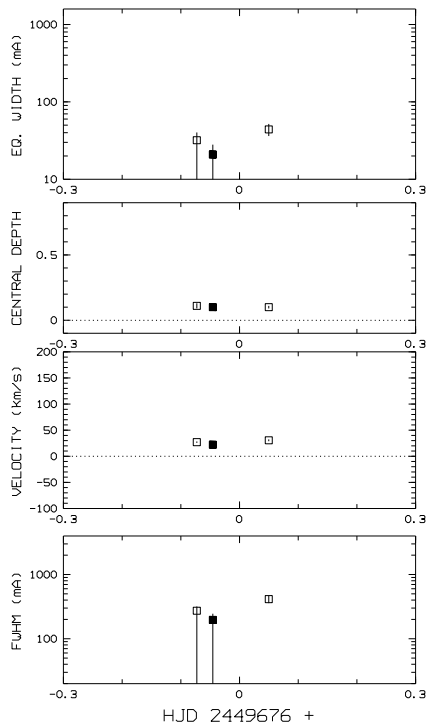


Figure 8.19: 19 November 1994
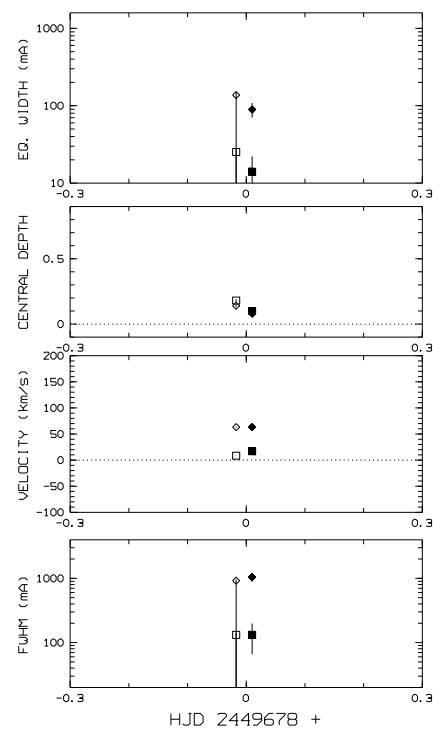
Figure 8.20: 21 November 1994
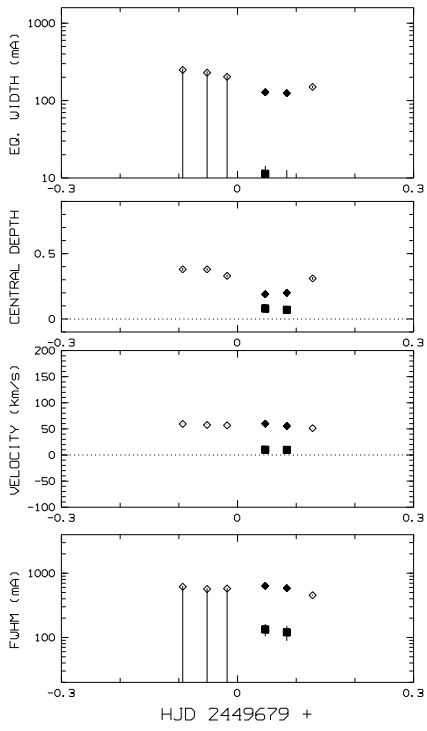
**Figure 8.21**: 22 November 1994
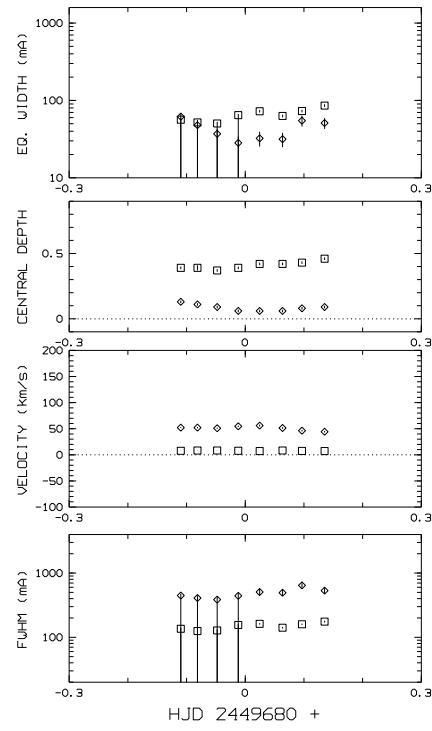


**Figure 8.22**: 23 November 1994
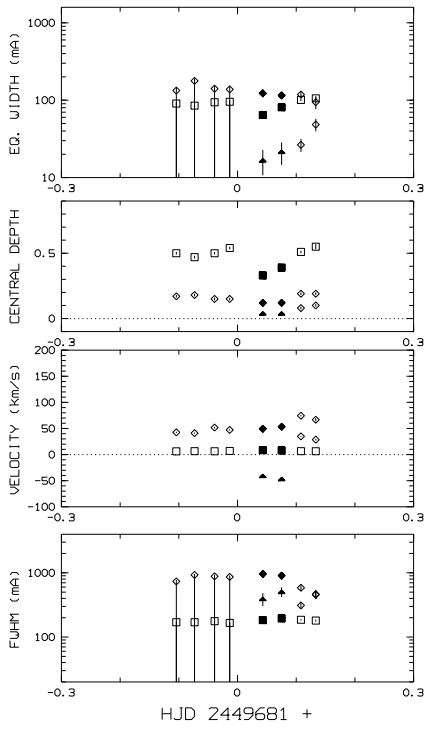


**Figure 8.23**: 24 November 1994
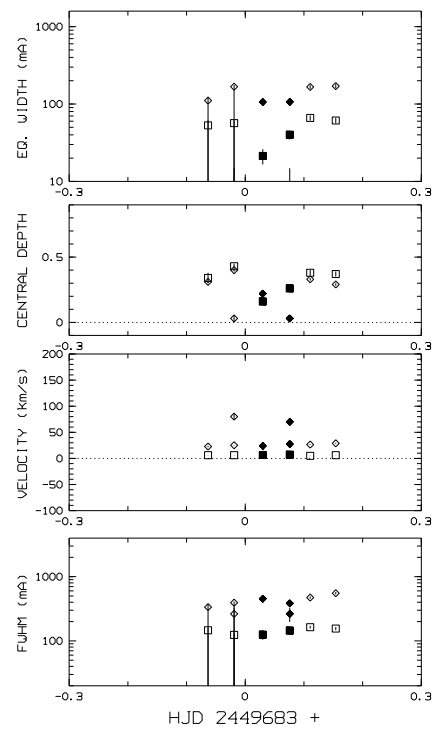


**Figure 8.24**: 26 November 1994
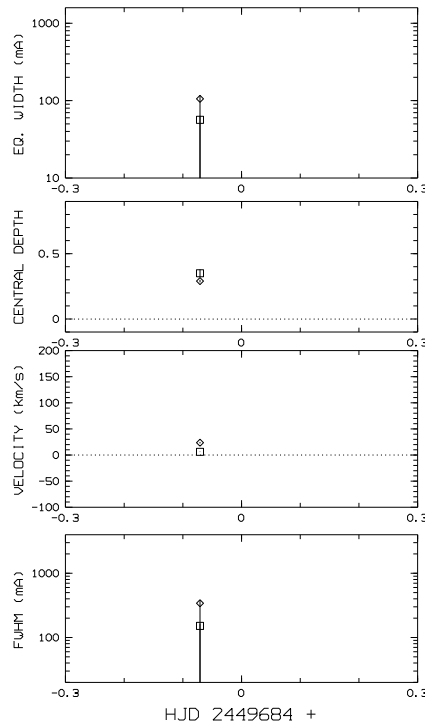
**Figure 8.25**: 27 November 1994

## 8.4   1995 observations Beta Pictoris

During this year the bulk of the data was collected on $\beta$ Pictoris in $\sim$1 week and $\sim$2 week runs. Initially there were 2 short observation runs to check instrumental settings, gain experience, and check for potential problems. The spectra are summarised in figures 8.26 - 8.56.

On 19 April $\beta$ Pictoris showed a number of features, a broad blueshifted feature at $\sim -80\text{kms}^{-1}$ and also some additional absorption in both wings of the circumstellar line. In the second initial observation run in May a LVF is seen at $\sim 15\text{kms}^{-1}$ on 24 May and is seen to grow in equivalent width as it gets broader. On the following night a feature is seen initially at $20\text{kms}^{-1}$ which then splits into 2 components in both H and K. Examination of the equivalent widths show it is entirely possible that this feature is a continuation of the previous night's feature. Also seen on 25 May is a clear blueshifted feature at $\sim -40\text{kms}^{-1}$ which clearly changes in equivalent width.

From 9 June a deep absorption feature is present at $\sim 10\text{kms}^{-1}$ which exhibits little change throughout the run to 20 June. Of particular note is a feature observed on June 9 at $\sim 130\text{kms}^{-1}$ as a deep and, given its high velocity, unexpectedly narrow absorption feature. It appears in only one spectra (K) giving it a timescale of less than hour as it is not observed in either of the spectra taken before or after (in H). There can be no doubt

as to its reality. Examination of the CCD image shows an absorption line right across the width of the spectrum. Such a feature is difficult to explain as its velocity indicates it is very close to the star (rough calculations estimate it to be less than 1 stellar radius from the surface of the star), but it may be explained by the FEB scenario explanation for LVFs with the axis of the parabolic orbit at low inclination to the line of sight (see Beust *et al.* 1991[9]). At the same time a broad HVF typical of a FEB close to the star is present during the time of observation at $80 \mathrm{kms}^{-1}$, which clearly changes in equivalent width.

The 11 June spectra reveal further blueshifted activity in the one high signal spectrum. In the last and particularly noisy spectrum a possible broad feature at $30 \mathrm{kms}^{-1}$ appears. On 19 June a broad and distinctive feature has appeared at $\sim 35 \mathrm{kms}^{-1}$ which is still visible the next night. It has weakened somewhat by the beginning of the night of 20 June, during which it changes only slightly in equivalent width. This is the inverse of the behaviour of the other relatively stable feature present at $10 \mathrm{kms}^{-1}$. A broad HVF is seen at $\sim 80 \mathrm{kms}^{-1}$ in the first half of the night of 20 June, but is gone in the later half when observations of $\beta$ Pictoris resume. The plot of equivalent width reveals it clearly evolves while it was observed with a slower fall than rise suggestive of an FEB crossing the stellar disk from blueshifted to redshifted side.

In late July a feature at $10 \mathrm{kms}^{-1}$ is still observed from the 27 July and though not as strong, it may be a continuation of the previous run's feature at that velocity. Also the feature observed at $40 \mathrm{kms}^{-1}$ is reminiscent of the previous run, but clearly varies in equivalent width. July 28 is filled with activity; in addition to the previously mentioned features a broad HVF at $\sim 70 \mathrm{kms}^{-1}$ is seen which seems to also change velocity. A HVF at $140 \mathrm{kms}^{-1}$ is briefly seen in one spectrum but unlike that on 9 June is broad. A blueshifted feature at $\sim -40 \mathrm{kms}^{-1}$ is seen to clearly change in equivalent width. Interestingly enough it is observed in H twice before it is seen in K. During the night of 29 July the feature at $\sim 40 \mathrm{kms}^{-1}$ persists. A blue feature appears and rapidly strengthens towards dawn.

On 30 July the $10 \mathrm{kms}^{-1}$ feature is unchanged, the $40 \mathrm{kms}^{-1}$ feature shows some interesting differences in H and K in that the H absorption starts considerably weaker than the K ones, but strengthens towards dawn, see Fig. 8.37. A HVF is seen at $\sim 140 \mathrm{kms}^{-1}$ which is broad and changes in equivalent width only slightly. At $\sim -15 \mathrm{kms}^{-1}$ a broad and difficult to detect feature is seen intermittently in some spectra, but does double in equivalent width. The feature at $40 \mathrm{kms}^{-1}$ becomes more distinctive on 31 July. A further broad HVF at $\sim 75 \mathrm{kms}^{-1}$ appears. Another blueshifted feature at $-30 \mathrm{kms}^{-1}$ is seen changing in strength.

The final night of the run (Fig. 8.39) reveals the feature at $40 \mathrm{kms}^{-1}$ as shallower than the previous night. Further blueshifted activity is also present. The blue features are clearly changing and the broad HVF at $-80 \mathrm{kms}^{-1}$ is only visible for $\sim$ half an hour.

Again on 7 September a feature is seen at $10 \mathrm{kms}^{-1}$ which is only a little weaker than the

previous run. Is this the same feature seen in June and July? If so, the FEB scenario will have great difficulty explaining such a very long-lived phenomenon, but the existence of such a long-lived low velocity absorption might hold clues to the origin of the circumstellar feature, the persistence of which is also problematic. Further blueshifted activity is seen in a changing feature at $-30\mathrm{kms}^{-1}$. The feature at $10\mathrm{kms}^{-1}$ is still present until 11 September but has disappeared two nights later. There is continuing activity on the blue side of the circumstellar line which varies significantly in equivalent width, but is constant in velocity. It remains a clearly seen feature throughout the observation run in September till the 13th when it quite suddenly changes in equivalent width and then disappears. On 8 September the features at $10\mathrm{kms}^{-1}$ and in the blue persists from the previous night, but several HVFs are seen in the red. They are seen to appear and strengthen, and then the feature at $70\mathrm{kms}^{-1}$ disappears. The HVFs appear in the H spectra first and vary rapidly. On 9 September a feature is easily seen at $\sim80\mathrm{kms}^{-1}$ which is broad and slowly changes in equivalent width during the night. Another one at $140\mathrm{kms}^{-1}$ appears briefly, changes rapidly in equivalent width and then disappears all in just over 2 hours. Both HVFs indicate in their equivalent width that they are crossing from the blueshifted to the redshifted sides of the stellar disk with different crossing times. On 10 September some new HVFs are observed. One feature is seen changing velocity from 90 to $60\mathrm{kms}^{-1}$ and staying there for the rest of the night. Upon examination of the equivalent width it is clear 2 bodies make up this feature, the original seen to change velocity and the second one that remains at a steady velocity. A further HVF appears at $130\mathrm{kms}^{-1}$ in the last spectrum of the night. The feature at $10\mathrm{kms}^{-1}$ remains unchanged in equivalent width during the night while the blueshifted features show some variation. On 11 September there are the blueshifted and $10\mathrm{kms}^{-1}$ features and a broad LVF at $\sim25\mathrm{kms}^{-1}$ which appears and a single HVF at $70\mathrm{kms}^{-1}$ in one H spectrum. On 13 September the $10\mathrm{kms}^{-1}$ feature is gone and the blueshifted feature is seen to disappear. The only other activity is the broad feature at $\sim50\mathrm{kms}^{-1}$.

In October another feature is seen at $15\mathrm{kms}^{-1}$ which is quite strong and changes little in equivalent width on October 6. Further blue activity is seen in the form of a broad absorption feature which is stronger in H than in K. Another broad HVF at $\sim90\mathrm{kms}^{-1}$ is seen to slowly change in equivalent width during the night (>6 hours). Further broad absorption is seen in K at lower velocity late in the night. The second night of observations (October 8) reveals little change with the $15\mathrm{kms}^{-1}$ still present and a broad feature at $40\mathrm{kms}^{-1}$ which can only be seen in the high signal spectra. The final night of observations (October 10) shows the $15\mathrm{kms}^{-1}$ feature to be getting weaker as the night progresses, while in contrast the blueshifted feature strongly evolves and is even stronger in H than it is in K. For a brief period of time broad HVFs are seen (<2 hours) at 90 and $130\mathrm{kms}^{-1}$.

November was last time data was collected, and as before it shows a wide range of activity. During the entire run an additional absorption is found in the wing of the

circumstellar line at $\sim 15 \text{kms}^{-1}$ and slowly evolves over the run from a difficult to detect feature to a prominent absorption. On 6 November it is seen to split into 2 features, one broader than the other. The broader feature is missing when observations begin on the night of the 7 November, but the remaining line is still present. On the 9 November it has become a clear feature in both Calcium spectra and slowly changes in depth though the rest of the run. During the run features appear and disappear, mostly they are broad and can be easily seen in the spectra. Some of the HVFs are difficult to detect due to being so broad and their typically short timescales of about a few hours at most. A number of blueshifted features are seen, all of which are broad and appear in H more than K.

In general the features all follow general trends which can be in most cases quite well explained by the FEB scenario. The differences in distance to the star, position over the stellar disk and the inclination of the line of sight all fit well between observation and theory.

Some 59 separate features were identified over the 31 nights of observation, which yields an estimated infall rate of >700 events per year. If the long-lived features are made up of many bodies falling at the correct angles, the actual infall numbers could of course be much higher.
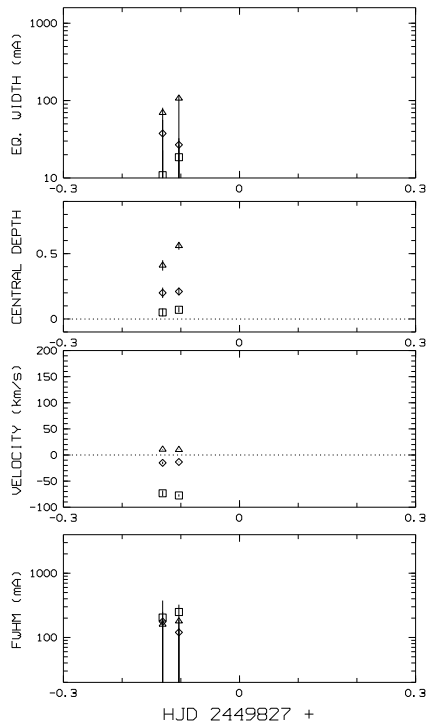


**Figure 8.26**: 19 April 1995
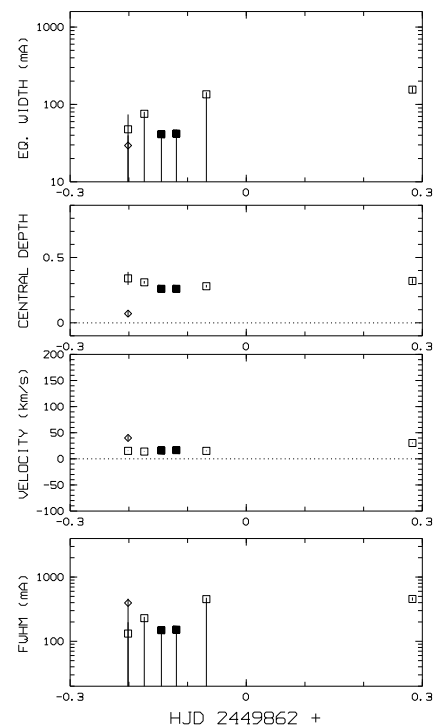


**Figure 8.27**: 24 May 1995
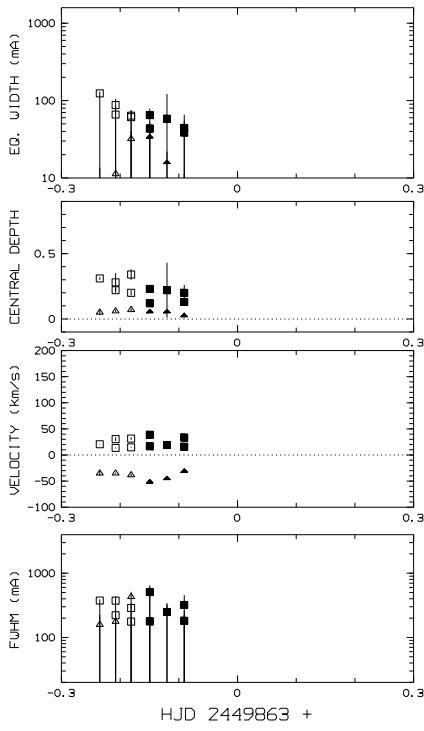
**Figure 8.28**: 25 May 1995
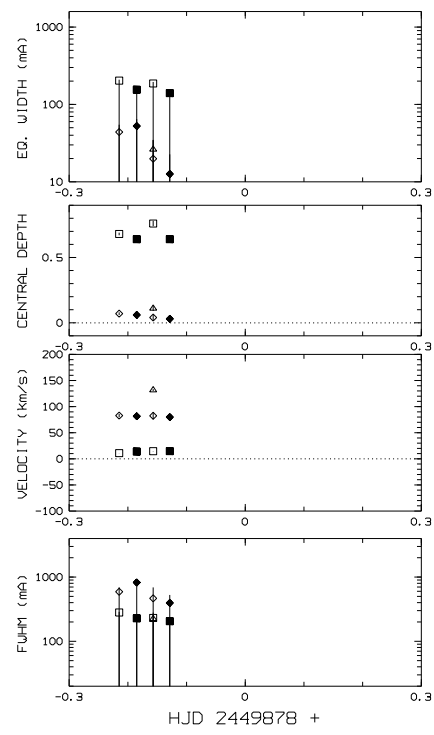


**Figure 8.29**: 9 June 1995
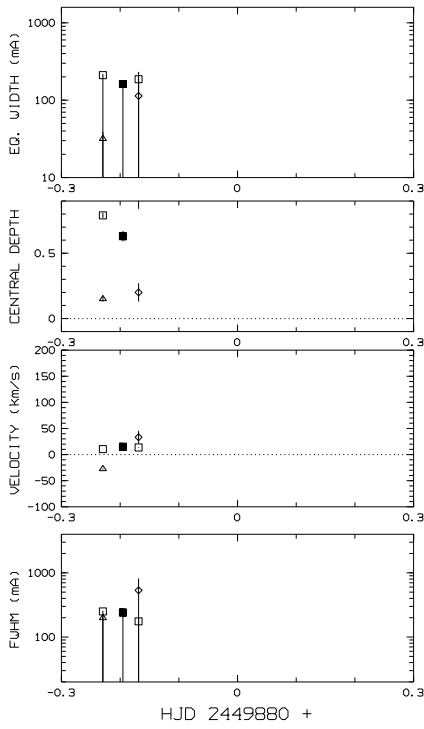


**Figure 8.30**: 11 June 1995
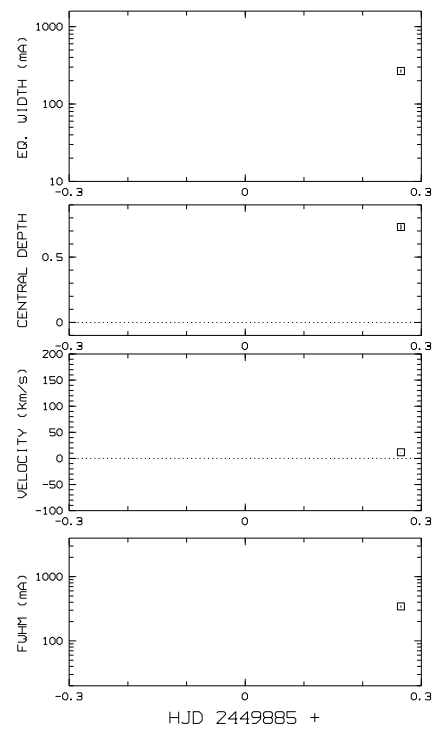


**Figure 8.31**: 16 June 1995
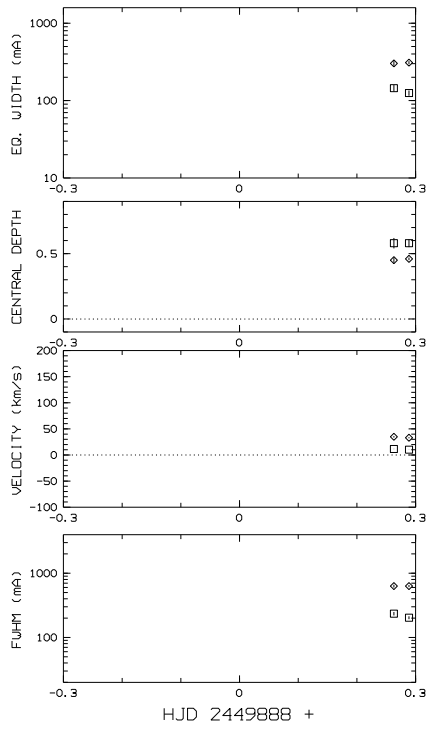
**Figure 8.32**: 19 June 1995
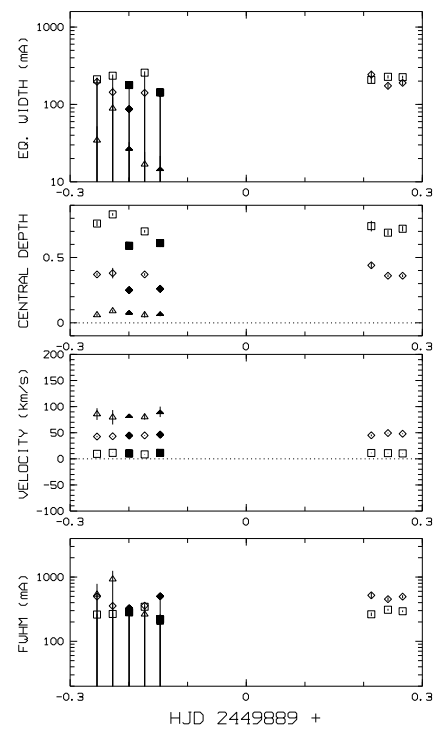


**Figure 8.33**: 20 June 1995
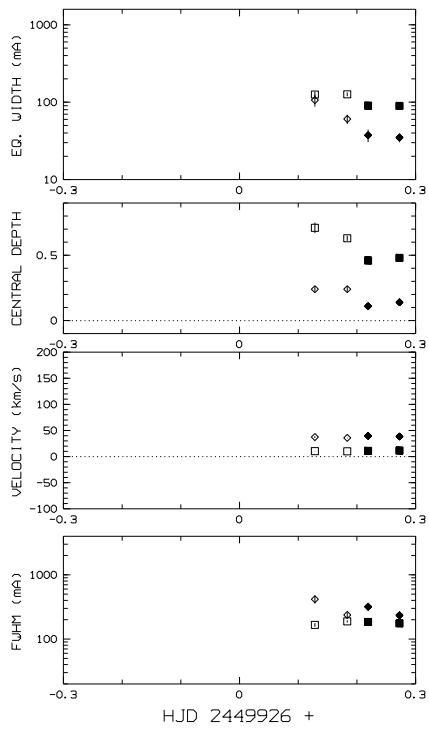


**Figure 8.34**: 27 July 1995
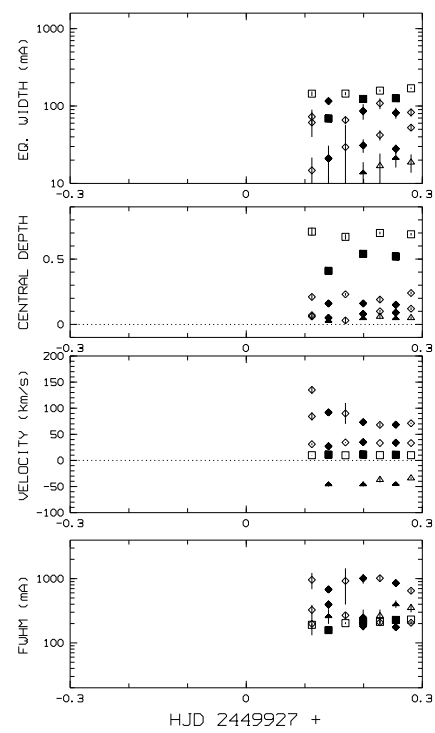


**Figure 8.35**: 28 July 1995
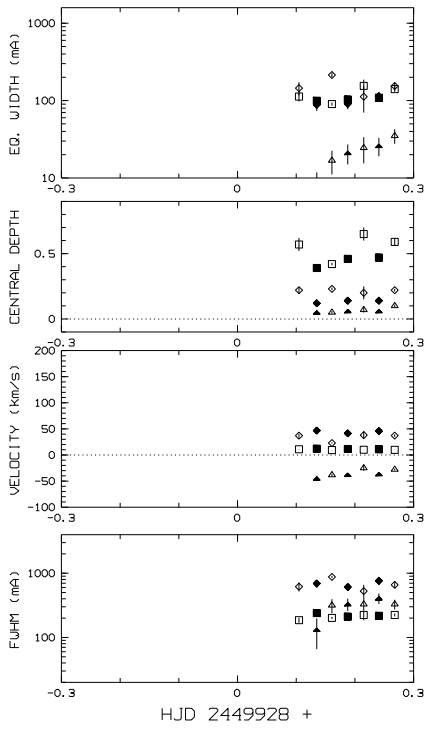
**Figure 8.36**: 29 July 1995
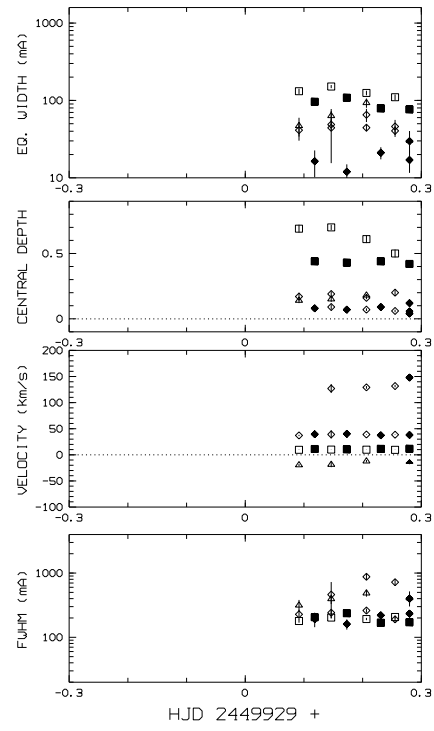


**Figure 8.37**: 30 July 1995
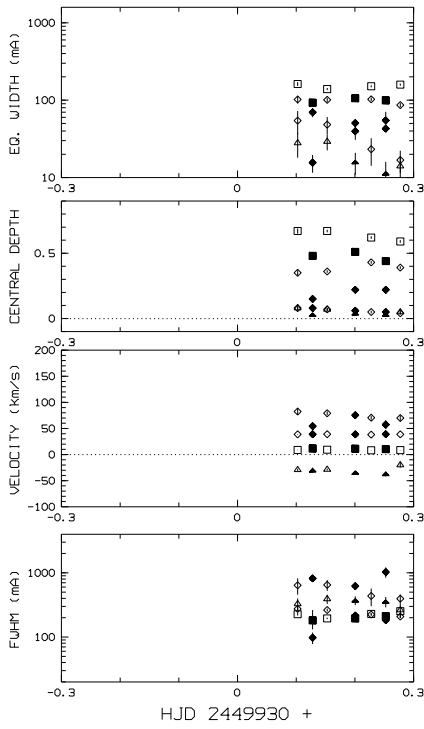


**Figure 8.38**: 31 July 1995
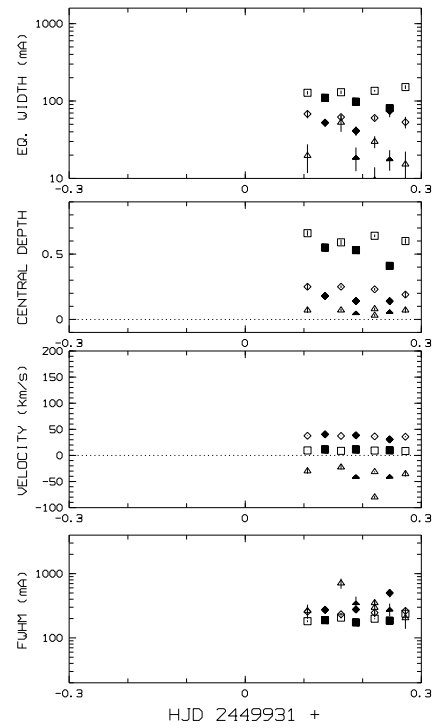


**Figure 8.39**: 1 August 1995
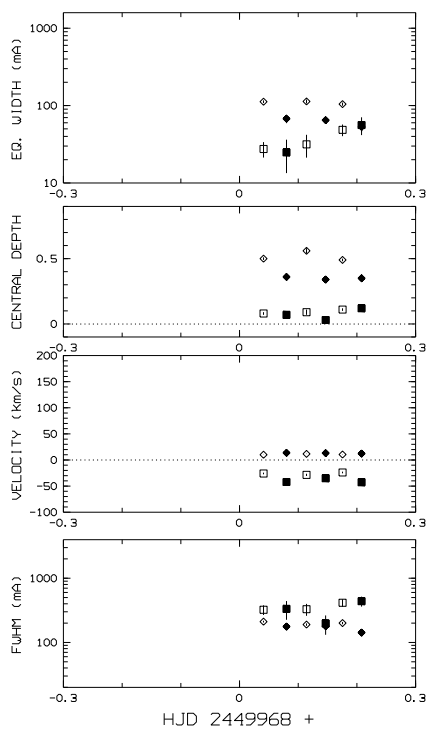
**Figure 8.40**: 7 September 1995
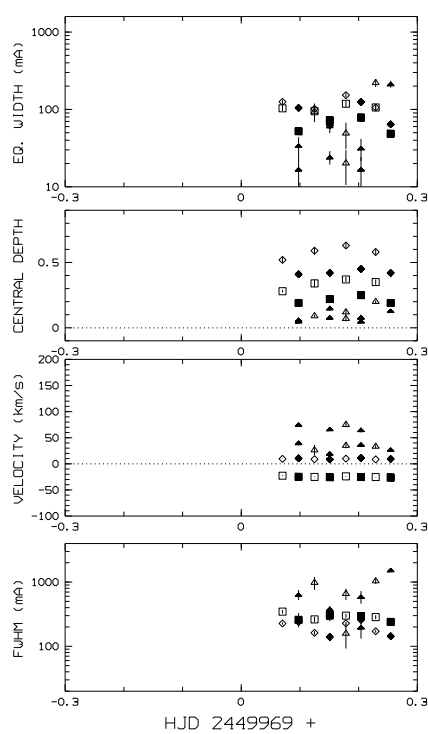


**Figure 8.41**: 8 September 1995
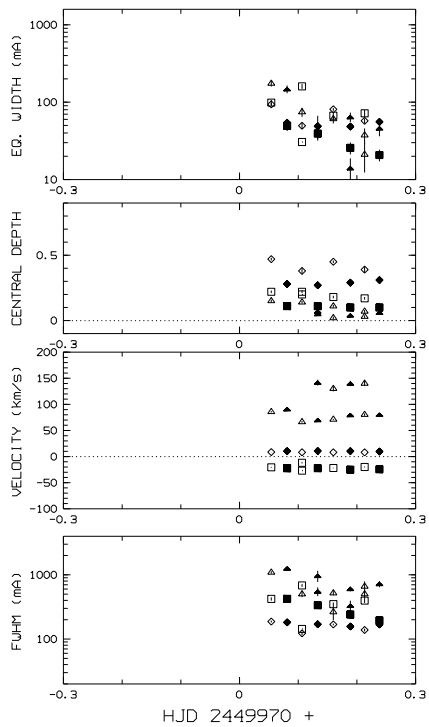


**Figure 8.42**: 9 September 1995
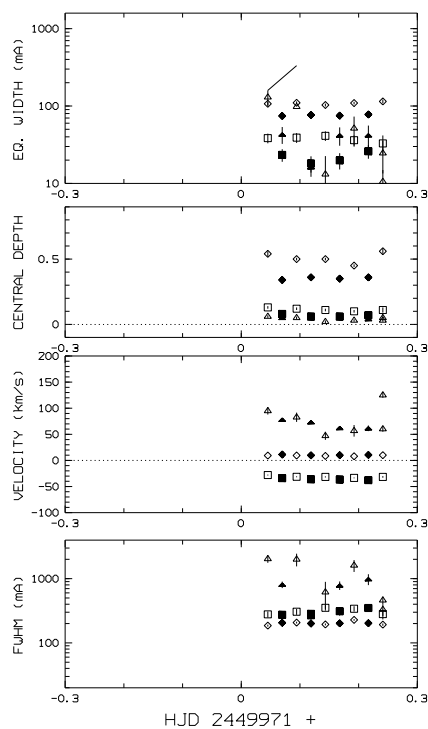


**Figure 8.43**: 10 September 1995
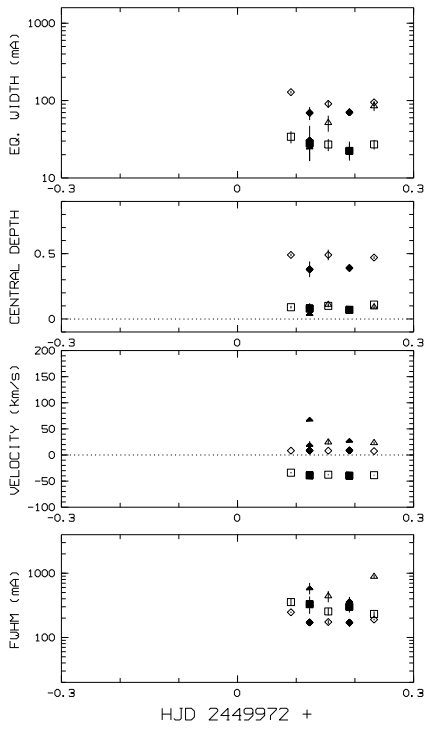
**Figure 8.44**: 11 September 1995
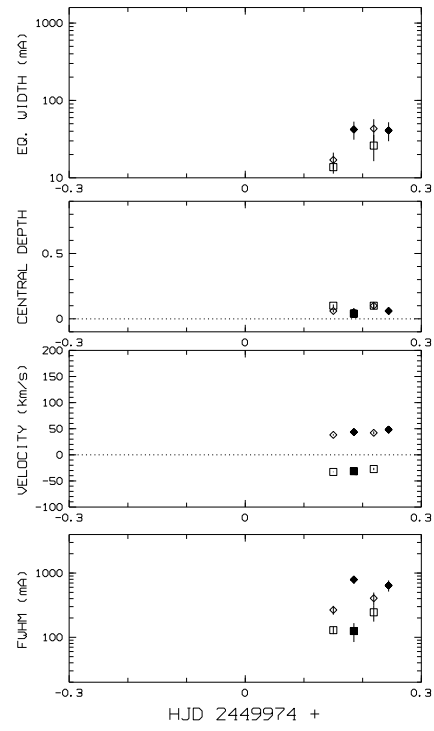


**Figure 8.45**: 13 September 1995
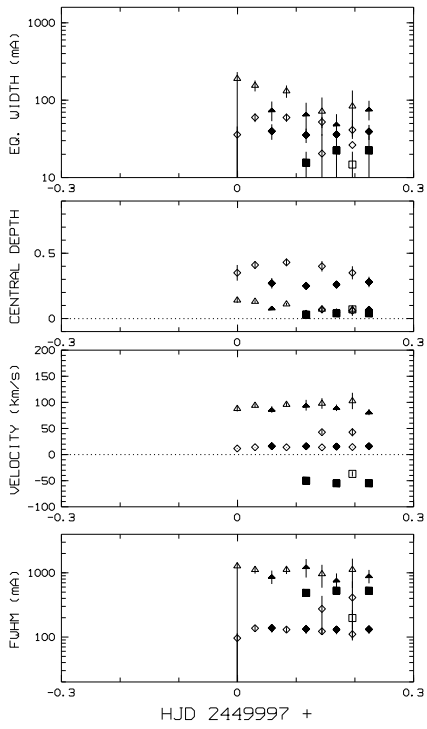


**Figure 8.46**: 6 October 1995
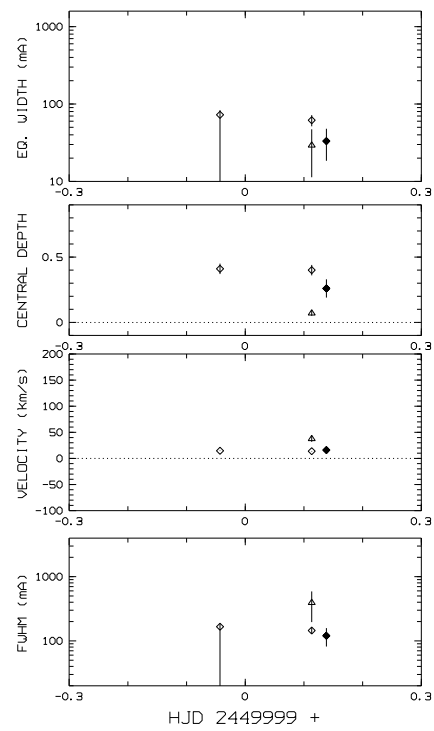


**Figure 8.47**: 8 October 1995
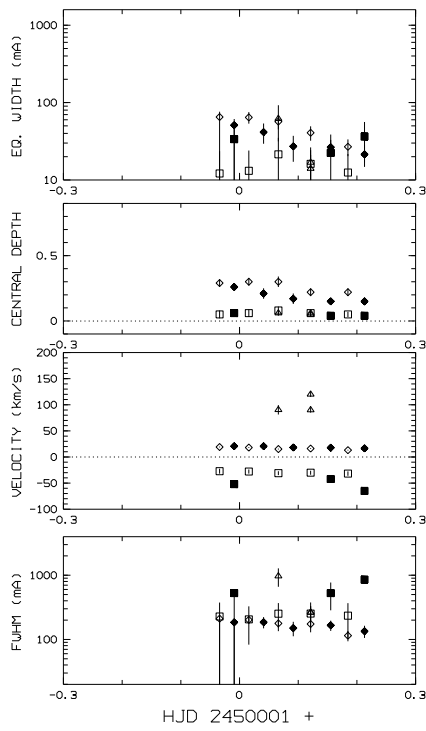
**Figure 8.48**: 10 October 1995
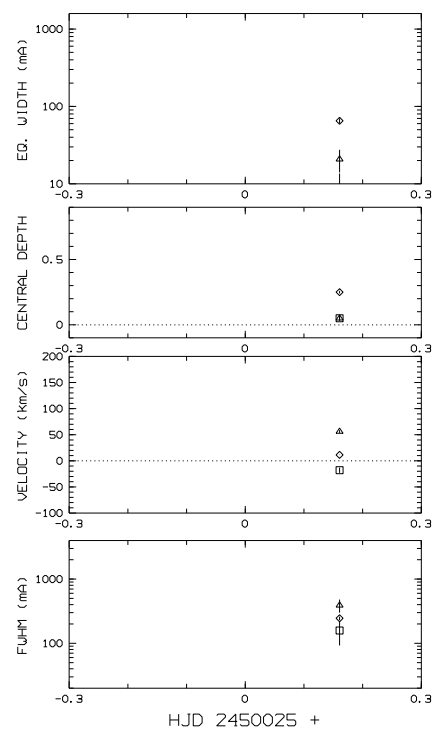


**Figure 8.49**: 3 November 1995
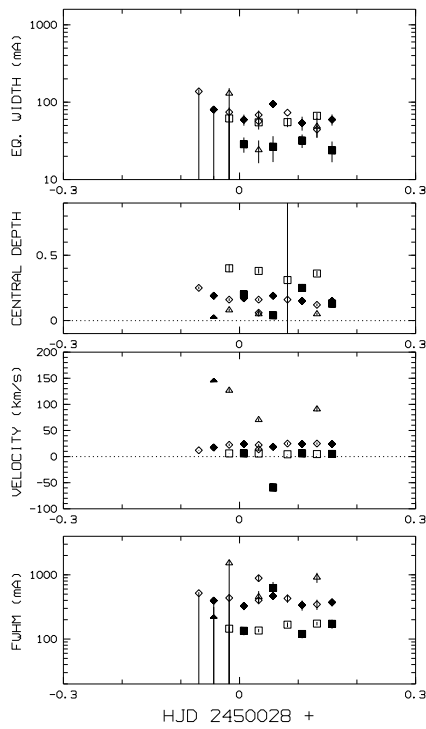


**Figure 8.50**: 6 November 1995
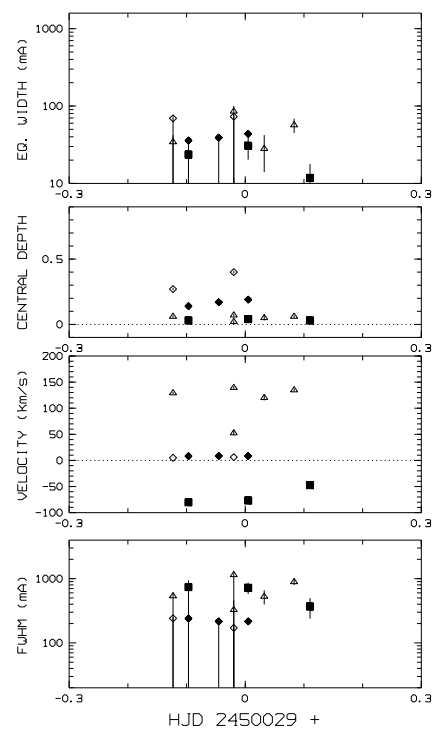


**Figure 8.51**: 7 November 1995
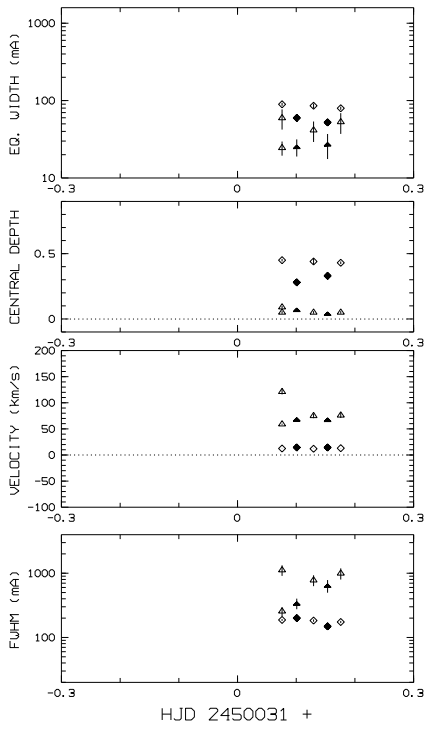
**Figure 8.52**: 9 November 1995
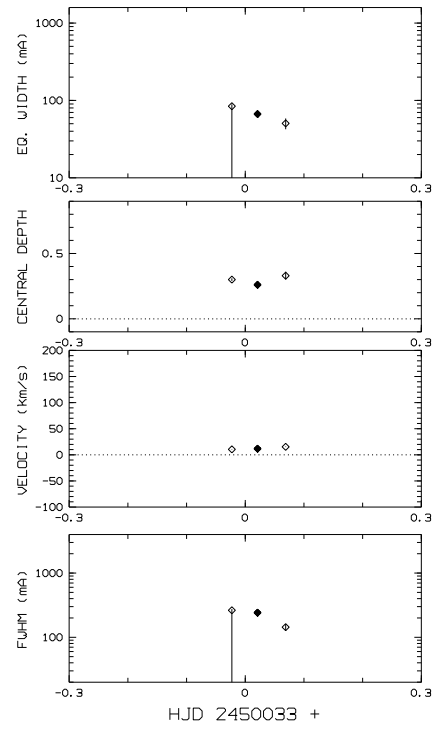


**Figure 8.53**: 11 November 1995
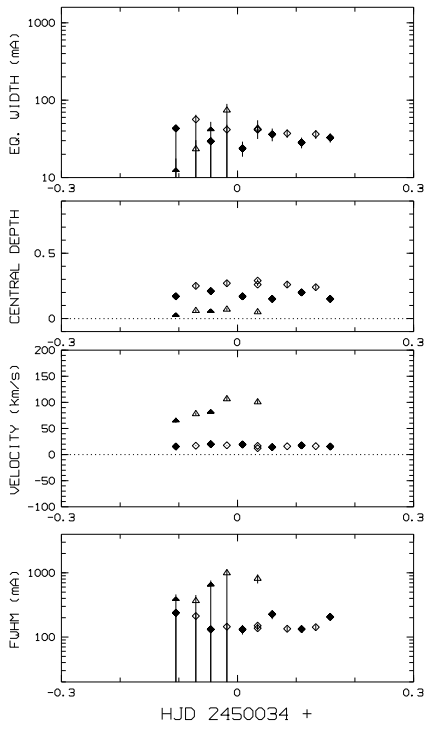


**Figure 8.54**: 12 November 1995
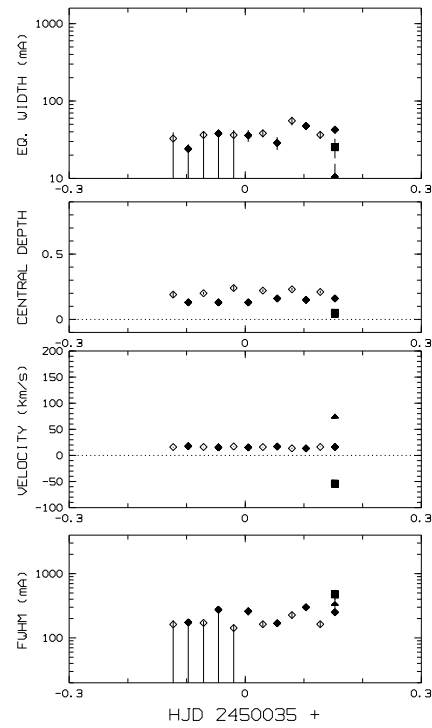


**Figure 8.55**: 13 November 1995
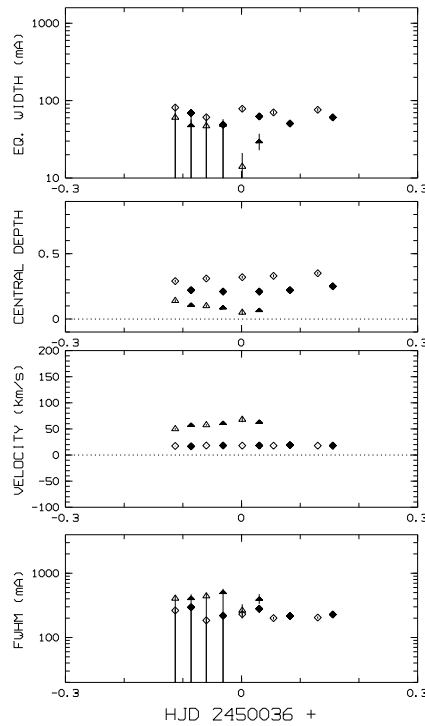
**Figure 8.56**: 14 November 1995

## 8.5    Summary of observational results

Of the 3 general types of absorption features found in the Calcium II H & K lines (see Sec. 3.2), the results of the observations from MJUO agree with there being 3 general types of features:

- a circumstellar feature at the radial velocity of the star.

- LVFs which tend to feature deep and narrow absorption lines which can last from hours to months. Also broad and shallow features appear which last for shorter timescales.

- HVFs which vary rapidly in timescales of hours and are almost invariably broad and shallow.

These descriptions certainly describe the redshifted features adequately, however the blueshifted features tend to be broad and shallow with short timescales. Occasionally however the blueshifted features while broad and shallow appear unchanged over many days before disappearing as suddenly as they appeared. It also should be noted that the circumstellar feature has exhibited variations in its FWHM either due to LVFs at $<8$ kms$^{-1}$ or changes in the circumstellar feature itself. However measurements of this variation fall outside the scope of this thesis.

Now the requirements for testing the FEB scenario will be addressed from the points raised in section 3.2.

The occurrence of the variable absorption features depends on the distance they can be found in around the star. The deepest and narrower lines are found at low velocity, $\sim 8$ to $20\mathrm{kms}^{-1}$ (see Fig. 8.58 and 8.59) and have FWHM from $\sim$100-350mÅ. In their 1996 paper analysing the 1992 data only, Lagrange-Henri *et al.* found a strong correlation between velocity and FWHM (see Fig. 8.57) and this is confirmed by our method of parameterising absorptions (see Fig. 8.58). The larger data set presented here shows the correlation is weaker than that found by Lagrange-Henri *et al.* In the blueshifted absorptions a strong correlation between velocity and FWHM is found. However this result should be treated with caution in case the experience of the redshifted correlation turning out to be weaker as more data is added proves also to be the case for the blueshifted absorptions.
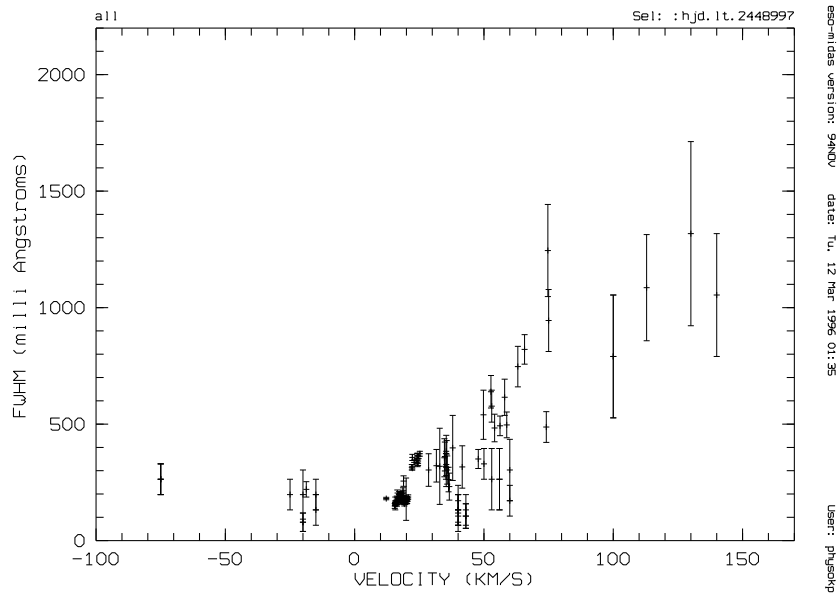


**Figure 8.57**: Plot of the MJUO data for 1992 showing the strong correlation in FWHM vs velocity as found in Lagrange-Henri *et al.* 1992. More data is present in this plot than Lagrange-Henri *et al.* found.

The deep absorption features in general are very long lived and the shallower absorption features tend in general to last for approximately the crossing time of an FEB across the stellar disk. A quick count of the features finds about 1/8 of all features seen are the deep features which typically last many days at least. However of all the features seen about 1/4 last long enough that more than 1 FEB must be responsible for its presence. From this data some conclusions can be made:

- The deep features, which are believed to be due to groups, account for only half the group events observed. Since these LVFs are supposed to occur at large distances
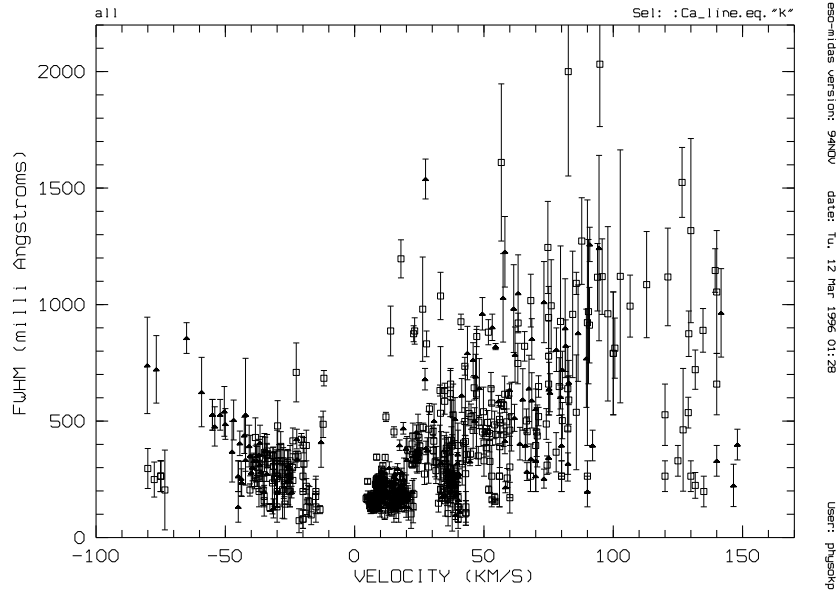
**Figure 8.58**: Plot of the MJUO data for all years showing the much weaker correlation in FWHM vs velocity.

from the star, one expects to see group events for FEBs closer to the star less often at higher velocities or blueshifted.

- The single events will tend to be the shallower features which appear most often and account for all the HVFs over $\sim 60 \text{kms}^{-1}$. This is not entirely surprising since as FEBs pass closer to the star, their crossing times get shorter and any other body in an orbit with a similar inclination to the line of sight has a smaller probability of occurring during the crossing time of another body.

Examining the plot of the depths of the absorption features against their velocity, it becomes clearly apparent that the deepest lines are found only at low velocities between redshifts of $\sim 8\text{-}20 \text{kms}^{-1}$. This corresponds to clouds of ions orbiting the star at large distances which can also cover large fractions of the stellar disk. A second set of features have depths about half as deep as the lower velocities lines which feature a definite cutoff at $\sim 60 \text{kms}^{-1}$. This may imply a limit in the inclinations of the parabolic orbits of FEBs appearing in Ca II spectra. Shallow and broad feature are found at most velocities and tend to represent individual FEBs. The blueshifted features show a similar cutoff in the depths of the features at $\sim -30 \text{kms}^{-1}$ (see Fig. 8.59).

The equivalent widths of the lines for a given velocity are all below $\sim 300 \text{m\AA}$ with the H line features generally smaller than K except at blueshifted velocities (see Fig. 8.60). This result implies that the blueshifted features occur under very special circumstances since the oscillator strength of the Calcium K line is twice the oscillator strength of the
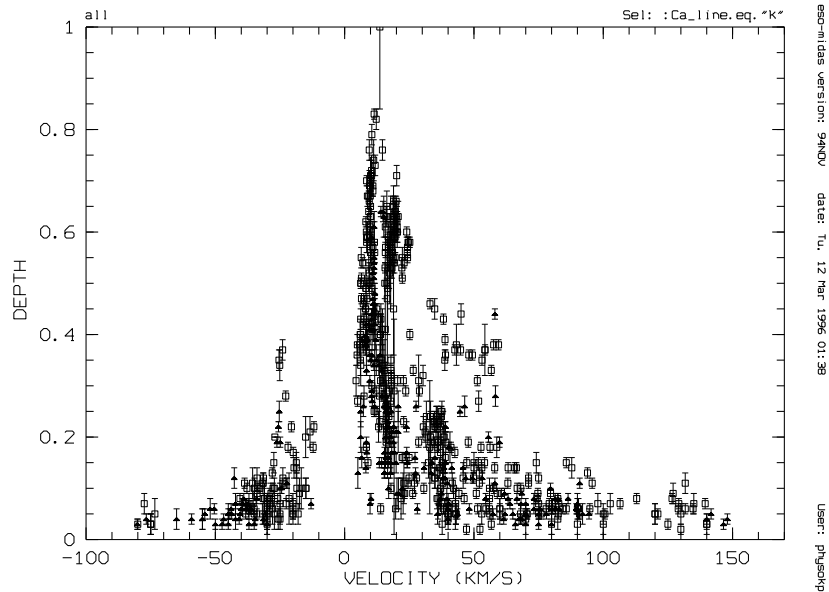
**Figure 8.59**: Plot of the depths of the absorption features observed vs their velocities over all observations.

H line.

In their 1992 paper Lagrange-Henri *et al.* showed that the depths of the Calcium lines taken simultaneously, or nearly so, can provide information on the size of the absorbing cloud of ions as a fraction of the stellar disk (see Fig 2.6). The plot of the line ratios for normal Ca II should have a value of pK/pH = 2 and for saturated lines pK/pH = 1, where p is the depth of the line. The line ratios in the FEB scenario sometimes have pK/pH is less than 1 when the Ca II cloud masks the part of the stellar disk rotating away from the observer. As can be seen in Fig. 8.61 (cf. Fig. 2.6, the deep lines can cover significant fractions of the stellar disk, 80% in some cases. The HVFs have much smaller depths and the amount of disk covered is also small ($\sim$10-50%). The blueshifted features only give lower limits on how much of the stellar disk they cover since none of those features have appeared to be saturated, hence they at least cover 10-40% of the stellar disk.

The timescales over which the observed variations in the spectroscopic lines vary over relate quite strongly to the velocity with respect to the star of the absorption feature. The lower the velocity the longer the timescale, especially if the absorption features are deep, and the higher the velocity the shorter the timescale of variation. The redshifted deep LVFs have been observed to last for weeks at a time and indeed one even appears to last several months, during which time they show little if any variation in their equivalent widths. As the velocity increases the timescales come down slowly till they reach the crossing time for an FEB across the stars disk of $\sim$12 hours at $\sim$60 kms$^{-1}$. Above that velocity the timescales for the FEBs are less than the maximum crossing time and typically
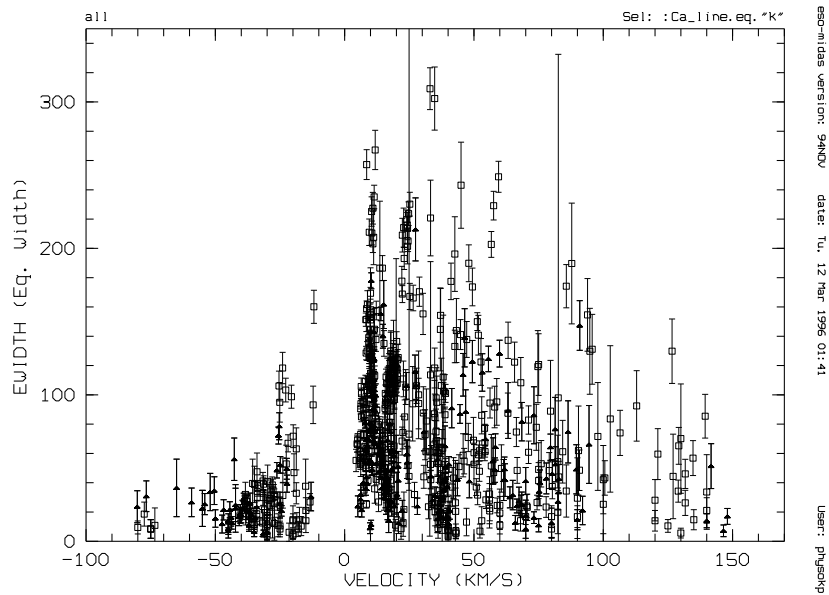
**Figure 8.60**: Plot of the equivalent widths in mÅof the absorption features observed vs their velocities over all observations.
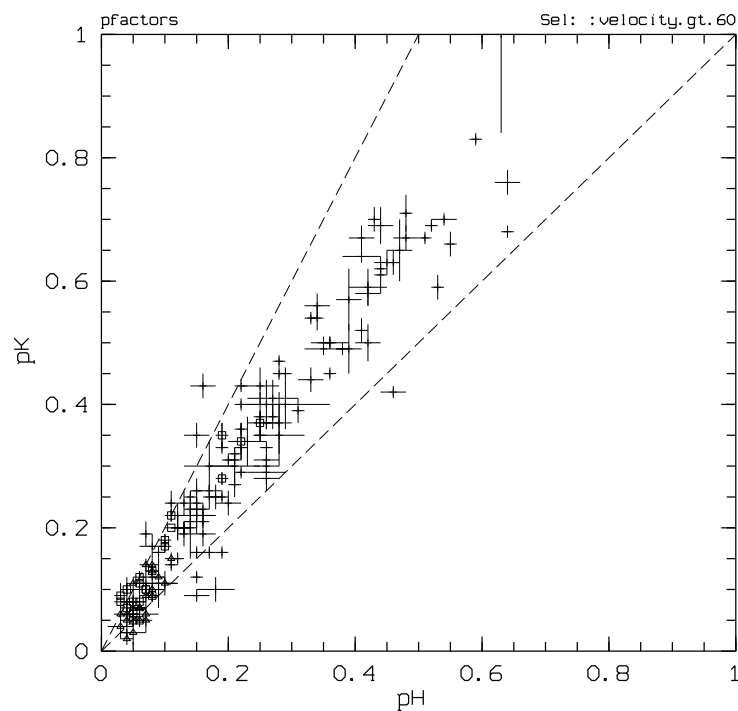


**Figure 8.61**: Plot of filling factors for quasi-simultaneous observations in H & K. Squares represent blueshifted features, crosses LVFs from $\sim$8-60kms$^{-1}$, and triangles for HVFs above 60kms$^{-1}$.

only appear for a few hours at most. Many absorptions have been seen in single spectra only indicating they cross the line of sight in the exposure time of the spectra ($\sim$1/2 hour) or slightly longer.

The blueshifted absorption features at low velocity also last quite long times, a few days at least, but most of the observed features lasted only short times typical of the crossing times of bodies in orbit around the star through the line of sight.

Despite the retraction of the observation of a dust disk around $\alpha$ Piscis Australus, as an IRAS point source it may have dust distributed at larger distances from the star and also may be viewed face on rather than edge on. The spectra taken during 1995 only show the photospheric lines with no additional absorption features.

Observations of 68 Ophiuchus in H and K failed to detect any absorption features except for the 2 lines believed to be due to interstellar clouds. While 2 additional features were observed in 2 spectra they turned out to be due to dust on the window in front of the detector.

## 8.6 Conclusion

This thesis contains spectroscopic observations of the stars $\beta$ Pictoris, $\alpha$ Piscis Australus and 68 Ophiuchus taken from December 1992 till November 1995 at the conclusion of observations for this thesis. From these spectra useful data has been obtained from the equipment at MJUO which have yielded new results from the prolonged time coverage these observations cover.

The method used here for the detection of absorption features produces the same results as Lagrange-Henri *et al.* in their paper on the 1992 observing campaign on $\beta$ Pictoris as well as detecting many more features that their method is insensitive to. More shallow absorption features are seen in this data as well as the detection of a number of blueshifted absorption features.

The predictions of the FEB scenario seem to explain many of the observations of the variable features seen in the resonance lines of Calcium II at H and K. The timescale of variations of the HVFs do agree well, since all the HVFs vary in less than the crossing time of $\sim$10 hours. The HVFs are generally broader and shallower than lower velocity features and appear more often in K than in H. There is evidence of the variation predicted by Beust and Lissauer of the equivalent widths of the H and K lines as an FEB crosses from one side of the stellar disk to the other due to doppler shift in the stars light from each side. The LVFs are found in greater numbers and are easier to detect than the HVFs, also the LVFs are the domain of the deep absorption lines. The features observed are both made up of single events and groups of bodies causing the observed variations. The numbers of each type of features observed were as expected however, some interesting features seem to defy explanation.

The long-lived events which almost always appear as deep absorption features are still problematical in that there is no adequate explanation as to how these lines can appear unchanging, for at least one case, months at a time. However a solution to this problem could help explain the circumstellar feature persistence.

There are many other puzzles yet to be solved from these observations on the timescales of features and the constant nature of the equivalent widths.

The observations of the Calcium lines found no variable absorption features in the spectra of either 68 Ophiuchus or $\alpha$ Piscis Australus. While they remain good candidates for further observations of the gas disk and infra red excess respectively, the presence of variable absorption features seems unlikely to be observed.

# Chapter 9

# Future work

Future work on studying the $\beta$ Pictoris system and other similar systems should include improvements in three domains: observations, reductions and analysis.

Improvements to the spectroscopic observation technique, especially for long term programmes should include observations of Canopus ($\alpha$ Carina). Canopus appears to have a very stable line profile and so it can be used correct for any changes in the setup of the échelle spectrograph causing changes in the shape of the profile of the photospheric lines in the programme stars. Canopus is conveniently situated only $\sim 5°$ from $\beta$ Pictoris.

A new 1024×1024 pixel CCD is on order for use at MJUO which has in addition to its larger size has a far higher quantum efficiency ($\sim 80\%$ over all wavelengths) than the current CCD system. Combined with the focal reducer which is being designed truly simultaneous observations of both the calcium H and K lines will become possible. In addition, the simultaneous observations and greater quantum efficiency will allow for better temporal characterisation of the variable absorption features and higher signal-to-noise ratios in the observed spectra. It will then be possible observationally to search for further and more convincing confirmation of the results of the result of Beust and Lissauer that the H line can sometimes be stronger than the K line, as is predicted by the FEB scenario.

Simultaneous observations will mean that it is no longer necessary to change the spectrograph settings during the night. This will improve smooth-fielding, and also make it easier to establish an independent wavelength scale. This observational improvement should result in improved reductions. The stability of the observing set up should insure that the background subtraction, important for accurate determination of the depth of the circumstellar feature, is done consistently.

The independent established wavelength scale will eliminate the need to align observed and reference spectra on the short-wavelength side of the circumstellar feature, which is a procedure which hides any low-velocity, blueshifted features. The uncertain matching of the circumstellar depths splits any broad, zero-velocity features into narrow features, one blueshifted and one redshifted. This uncertainty should be eliminated by better background subtraction and the improved wavelength scale.

In the interim some improvements can be made to the current reference spectra used for division of the observed spectra for extraction of absorption feature parameters. Primarily the region around the circumstellar feature needs some attention, given that the often low

signal levels can cause tiny differences to become problematic in the normalised spectra when fitting the gaussians to the features. Also it may be possible to make measurements of the circumstellar line with improvements to the division procedure by fitting a parabola to the currently used K line reference spectrum and another quadratic to the region of the circumstellar line in the H line reference spectrum. Since in the division by the reference spectrum of the observed spectra the circumstellar line does exhibits some variation it may be possible to measure this quantitatively and perhaps even characterise these changes.

The fitting of the gaussians to the absorption features, using the Modified-Gauss-Newton method, can be improved with better parameters for the fitting routine to use in the matching of the synthetic fit with the data. The modifications needed at this stage are merely refinements on a process that works quite well.

Obviously detailed modelling, outside the scope of this thesis, would lead to further refinements of the FEB scenario and its predictions.

# Chapter 10

# Acknowledgements

# References

[1] D. Aitkin, T. Moore, P. Roche, C. Smith, and C. Wright. *M.N.R.A.S*, 265:L41–L43, 1993.

[2] C. Allen. *Astrophysical Quantities.* Athlone Press, U. of London, 1973.

[3] P. Artymowicz, C. Burrows, and F. Paresce. *Ap.J.*, 337:494–513, 1989.

[4] H. Aumann, F. Gillett, C. Beichman, T. de Jong, J. Houck, F. Low, G. Neugebauer, R. Walker, and P. Wesselius. *Ap.J. Lett.*, 278:L23, 1984.

[5] D. Backman, F. Gillett, and F. Witteborn. *Ap.J.*, 385:670–679, 1992.

[6] H. Beust, A.M. Lagrange-Henri, A. Vidal-Madjar, and R. Ferlet. *A&A*, 223:304–312, 1989.

[7] H. Beust, A.M. Lagrange-Henri, A. Vidal-Madjar, and R. Ferlet. *A&A*, 236:202–216, 1990.

[8] H. Beust and M. Tagger. *Icarus*, 106:42–58, 1993.

[9] H. Beust, A. Vidal-Madjar, and R. Ferlet. *A&A*, 247:505–515, 1991.

[10] H. Beust, A. Vidal-Madjar, R. Ferlet, and A.M. Lagrange-Henri. *Ap. Space Sci.*, 212:147–157, 1994.

[11] H. Beust, A. Vidal-Madjar, A.M. Lagrange-Henri, and R. Ferlet. *A&A*, 241:488–492, 1991.

[12] A. Boss. Low-mass star and planet formation. *PASP*, 101(643):767–786, 1989.

[13] F. Bruhweiler, Y. Kondo, and C. Grady. *Ap.J.*, 371:L27–L31, 1991.

[14] K. Cheng, F. Bruhweiler, Y. Kondo, and C. Grady. *Ap.J.*, 396:L83–L86, 1992.

[15] R. Chini, E. Krugel, B. Shustov, A. Tutukov, and E. Kreysa. *A&A*, 252:220–228, 1991.

[16] E. Churchwell. In C.J. Lada and N.D. Kykafis, editors, *The physics of star formation and early stellar evolution*, volume 342 of *NATO ASI series C:Mathematical and physical sciences*, page 61. NATO advanced study institute, 1991.

[17] A. Crawford, J. Spyromilio, M. Barlow, F. Diego, and A. Lagrange. *M.N.R.A.S.*, 266:L65–L68, 1994.

[18] D. Crawford, J. Barnes, and J. Golson. *A.J.*, 75:624, 1970.

[19] M. Deleuil, C. Gry, A. Lagrange-Henri, A. Vidal-Madjar, H. Beust, R. Ferlet, H. Moos, T. Livengood, D. Ziskin, P. Feldman, and M. McGrath. *A&A*, 267:187–193, 1993.

[20] A. Lecavelier des Etangs, M. Deleuil, A. Vidal-Madjar, R. Ferlet, C. Nitschelm, B. Nicolet, and A. Lagrange-Henri. *A&A*, 299:557–562, 1995.

[21] A. Lecavelier des Etangs, G. Perrin, R. Ferlet, A. Vidal-Madjar, F. Colas, C. Builand F. Sevre, J. Arlot, A. Lagrange-Henri, J. Lecacheux, M. Deleuil, and C. Gry. *A&A*, 274:877–882, 1993.

[22]  T. Encrenaz, J. Bibring, and M. Blanc.  chapter 3. The Formation of the Solar System.  A&A Library. Springer-Verlag Berlin Heidelberg, 1990.

[23]  C. Turon et al. *Hipparcos Input Catalogue.* ESA Publications Division, 1992.

[24]  R. Ferlet, L. Hobbs, and A. Vidal-Madjar. *A&A*, 185:267–270, 1987.

[25]  R. Ferlet, A. Lagrange-Henri, H. Beust, R. Vitry, J. Zimmerman, M. Martin, S. Char, M. Belmahdi, J. Clavier, P. Coupiac, B. Foing, F. Sevre, and A. Vidal-Madjar. *A&A*, 267:137–144, 1993.

[26]  F. Gillett.  In F.P. Israel, editor, *Light on Dark Matter*, volume 124, page 61. Reidel, Dordrecht, 1986.

[27]  I. Glass. *MNASSA*, 33:53, 1974.

[28]  T. Gledhill, S. Scarrott, and R. Wolstencroft. *M.N.R.A.S.*, 252:50–54, 1991.

[29]  E. Green, P. Demarque, and C. King. *The Revised Yale Isochrones and Luminosity Functions.* Yale U. Obs., New Haven, 1987.

[30]  Beust H. and Lissauer J. *A&A*, 282:804–810, 1994.

[31]  B. Hauck and M. Mermilliod. *Astr. Ap. Suppl.*, 40:1, 1980.

[32]  J. Hearnshaw. *Proc. ASA*, 3(2):102–103, 1977.

[33]  G. Herbig.  In L. Danly H. Weaver, editor, *The Formation and Evolution of Planetary Systems*, page 296. Cambridge U. Press, Cambridge, 1989.

[34]  L. Hobbs. *Ap.J.*, 308:854–858, 1986.

[35]  L. Hobbs, A. Lagrange-Henri, R. Ferlet, A. Vidal-Madjar, and D. Welty. *Ap.J.*, 334:L41–L44, 1988.

[36]  L. Hobbs, A. Vidal-Madjar, R. Ferletand C. Albert, and C. Gry. *Ap.J.*, 293:L29–L33, June 1 1985.

[37]  D. Hoffleit and C. Jaschek. *The Bright Star Catalogue.* Yale U. Obs., 4th edition, 1982.

[38]  P. Kalas and D. Jewitt. *A.J.*, 110(2):794, 1995.

[39]  R. Knacke, S. Fajardo-acosta, C. Telesco, J. Hackwell, D. Lynch, and R. Russell. *Ap.J.*, 418:440–450, November 20 1993.

[40]  Y. Kondo and F. Bruhweiler. *Ap.J.*, 291:L1–L5, April 1 1985.

[41]  P. Lagage and E. Pantin. *Nature*, 369:628–630, June 23 1994.

[42]  A. Lagrange, R. Ferlet, and A. Vidal-Madjar. *A&A*, 173:289–292, 1987.

[43]  A. Lagrange-Henri, H. Beust, R. Ferlet, and A. Vidal-Madjar. *A&A*, 215:L5–L8, 1989.

[44]  A. Lagrange-Henri, R. Ferlet, A. Vidal-Madjar, H. Beust, C. Gry, and R. Lallement. *Astron. Astrophys. suppl. ser.*, 85:1089–1100, 1990.

[45]  A. Lagrange-Henri, E. Gosset, H. Beust, R. Ferlet, and A. Vidal-Madjar. *A&A*, 264:637–653, 1992.

[46] A. Lagrange-Henri, F. Plazy, H. Beust, D. Mouillet, M. Deleuil, R. Ferlet, J. Spyromilio, A. Vidal-Madjar, W. Tobin, J. Hearnshaw, M. Clark, and K. Thomas. 1996.

[47] A. Lagrange-Henri, A. Vidal-Madjar, and R. Ferlet. *A&A*, 190:275–282, 1988.

[48] C. Lance. *Ap. J. Suppl.*, 68:463, 1988.

[49] H. Levison, M. Duncan, and G. Wetherill. *Nature*, 372:441–444, December 1 1994.

[50] T. Mouschovias. In Lada C.J. and Kykafis N.D., editors, *The physics of star formation and early stellar evolution*, volume 342 of *NATO ASI series C:Mathematical and physical sciences*, page 61. NATO advanced study institute, 1991.

[51] G. Nankivell and N. Rumsey. In J.B. Hearnshaw and P.L. Cottrell, editors, *Instrumentation and research programs for small telescopes*, number 118 in Symposium, page p.101. IAU, D. Reidel publishing company, 1986.

[52] B. Palmer and R. Engleman. *Atlas of the Thorium Spectrum*. Los Alamos National Laboratory, 1983.

[53] F. Paresce. *A&A*, 247:L25–L27, 1991.

[54] F. Paresce and C.Burrows. *Ap.J. Lett.*, 319:L23, 1987.

[55] Photometrics Limited. *Photometrics 3000 users manuel for Forth programming system.*

[56] K. Pollard. *The nature of low mass supergiants: RV Tauri and R Coronae Borealis variables*. PhD thesis, Dept. Physics & Astronomy, University of Canterbury, 1994.

[57] F. Ruferner. *Catalogue of Stars Measured in the Geneva Observatory Photometric System*. Obs. de Geneve, 1988.

[58] M. Savoldini and G. Galletta. *A&A*, 285:467–468, 1994.

[59] T. Schmidt-Kaler. *Landolt-Bornstein*, 2b:1, 1982.

[60] A. Slettebak. *Ap.J.*, 197:137, 1975.

[61] A. Slettebak and K. Carpenter. *Ap.J. Suppl.*, 53:869, 1983.

[62] B. Smith, J. Fountain, and R. Terrille. *A&A*, 261:499–502, 1992. Research Note.

[63] B. Smith and R. Terrile. *Science*, 226:421, 1984.

[64] B. Smith and R. Terrile. *BAAS*, 19(829), 1987.

[65] A. Stern, M. Festou, and D. Weintraub. A map of a collionally evolving dust disk around fomalhaut. *Nature*, 369:766, 30 June 1994.

[66] S. Stern. Iauc 5732. IAU circular, 1993.

[67] B. Stromgren. *Ann. Rev. Astr. Ap.*, 4:433, 1966.

[68] C. Telesco, E. Becklin, R. Wolstencroft, and R. Desher. *Nature*, 335:51–53, September 1 1988.

[69] C. Telesco and R. Knacke. *Ap.J.*, 372:L29–L31, 1991.

[70] W. Tobin. Description of the system. Performance note, 1990.

[71] W. Tobin. Forth acquisition software. Performance note, 1991.

[72] A. Uesugi and I. Fukuda. *Revised Catalogue of Stellar Rotational Velocities*. Dept. of Astronomy, Kyoto U., 1982.

[73] A. Vidal-Madjar and et al. Iauc 5795. IAU circular, 1993.

[74] A. Vidal-Madjar, L. Hobbs, R. Ferlet, C. Gry, and C. Albert. *A&A*, 167:325–332, 1986.

[75] A. Vidal-Madjar, A. Lagrange-Henri, P. Feldman, H. Beust, J. Lissauer, M. Deleuil, R. Ferlet, C. Gry, L. Hobbs, M. McGrath, J. McPhate, and H. Moos. *A&A*, 290:245–258, 1994.

[76] H. Walker and R. Wolstencroft. *P.A.S.P.*, pages 1509–1521, December 1988.

[77] L. Waters and et al. Circumstellar gas and dust in 68 ophiuchi (a0ive). *A&A*, 299:173–178, 1995.

[78] P. Weissman. *Space Science Review*, 41:299, 1985.

[79] S. Wolff. The a-stars: Problems and perspectives. Technical report, NASA, 1983.

[80] R. Wooley, E. Epps, J. Penston, and S. Pocock. *R. Obs. Ann.*, 5, 1970.

# Appendix A

# Reducing MJUO CCD Echelle Spectra Using ESO-MIDAS

This manual has been updated to be applicable to any and all spectra taken with the MJUO CCD and being reduced with ESO-MIDAS 94NOV on "cantua".

To access Midas type **inmidas [unit # ] -p**
This will put you into Midas using a unit number that no-one else should be using. If you are using a WYSE terminal the unit number is replaced with 2 letters from XX ... to ... ZZ. Once this is done you can then load the spectra from your disk space and convert them from FITS format to the MIDAS binary data format.

The process starts with the spectra in FITS format on the computer disk.

## A.1   Creating Images of the Correct Format for *MIDAS*

**MIDAS⟩ intape/fits [numbers of images to be processed] [*MIDAS* files prefix] [FITS files prefix]**
Convert the spectral images in FITS format into the idiosyncratic *MIDAS* format.
Example: "MIDAS⟩ intape/fits 1-38 T001 T001_" will convert files 1 to 38 originally from Tape T001 and save them as T0010001.BDF, T0010002.BDF, ..., T0010038.BDF.
**Note**, all spacing in commands are important to MIDAS
 **MIDAS⟩ create/icat [name for catalogue] [*MIDAS* files prefix]\*.BDF**

Create an ASCII file listing the image files for subsequent operations.
Example: "MIDAS⟩ create/icat T001 T001\*.BDF"
will create a catalogue named T001.CAT listing all files named in the form T001\*.BDF.
 **MIDAS⟩ set/context echelle**

Make échelle-specific commands available for the following operations.
 **MIDAS⟩ rotate/echelle [catalogue name] [prefix for rotated files] flip XY**

Transform all of the images listed in the catalogue into the layout required by *MIDAS* – orders increasing from top to bottom and wavelength increasing from left to right as the images are displayed on the screen.
Example: "MIDAS⟩ rotate/echelle T001 T001 flip XY" will transform all of the files listed in the catalogue T001, retaining the same file names.

The "flip" option is used because *MIDAS* does not seem to be able to rotate 270° in one operation.

**Note** that the capital "XY" must be used to rotate all the files - a small "xy" causes funny things to happen with MIDAS. Also note that this operation creates new files named [*MI-DAS* file prefix]001.BDF... with sequential numbering independent of the numbers of the original files. If the files listed in the catalogue are not sequentially numbered beginning with 1, then it will be necessary either to keep track *manually* of the correspondences between the original and the transformed files or to rename the transformed files to correspond with the original files. If the names are the same, then UNIX is unable to transform the images, so a change in file name is required.

## A.2 Initializing for the *MIDAS* Session

**MIDAS⟩ create/graphics**
Make a window for displaying plots.
  **MIDAS⟩ create/display 0 576,384**

Make a window numbered "0" the right size for displaying the rotated images.
  **MIDAS⟩ load/lut pastel**

This will put any image into false colour and will show up all orders and cosmic rays more clearly for identification. Other palettes (ie. "look up tables") include: rainbow, backgr, color, heat, light, random, random1 ... 4, staircase, and stairs-8.
  **MIDAS⟩ init/echelle [previous session name]**

Set the échelle reduction parameters to those saved from a previous session, if available.

## A.3 Locating the Echelle Orders in the Images

This entire section is used only for the first reduction of a set of images made with a given set-up of the telescope and instruments. Once the orders have been found, usually from a smooth-field image, the same order table can be used for all stellar images obtained with that set-up. But, if the *tilt* of the orders changes, then the order-finding must be repeated. Normally the tilt only changes if the CCD cryostat has been removed from the spectrograph and then replaced, and in that case the observer should have obtained a new smooth-field image to define the new positions of the orders.
  **MIDAS⟩ set/echelle DEFMTD=std DEFPOL=2,2**

The DEFMTD's available are **std**, **com** when the width of the orders are larger than the interorder spacing. There is also the method **hough** when these above methods fail to work in the search/order command. (See Hough/echelle in "Other Useful Commands" at end). The DEFPOL fits a polynomial of degree X,Y where X = the polynomial for fitting

along the orders and Y = the polynomial for fitting across the orders. A 2-dimensional polynomial of degree 2,2 will normally be used to approximate the positions of the orders. This may need to be changed to degree 2,1 if there is difficulty in finding any orders ( eg. only 3 orders detected or present.).

**MIDAS⟩ show/echelle**

This shows what the echelle reduction parameters are. It is useful to check that the parameters have been changed.

```
***************  Echelle Parameters  ******************


Instrument   :  INSTR   = +++
Dispersers   :  GRATING = +++  CROSS = +++
Detector     :  CCD = +++   CCDBIN = 1.0,1.0
Image size   :  IMSIZE = 576,384 -  SCAN = 1,384
Orders       :  3 orders, from 1 to 3
Wavel. range :  3857.74341 - 4007.92017   wavel. units


--- 1. Order definition ----
    DEFMTD = hough  DEFPOL = 2,2
    ORDREF = ksmooth
      NBORDI = 3  WIDTHI = 0  THRESI = 0.0
      See also keyword  SCAN
--- 2. Background ---
    BKGMTD = poly   BKGVISU = YES
      BKGSTEP = 10  BKGPOL = 4,3
--- 3. Filtering ---
    MEDFILT  = 3.0,3.0,3.0
    CRFILT   = 15,41,3
    CCDFILT  = 7.1,4.3,5.0
--- 4. Extraction ---
    EXTMTD = linear   SLIT = 20.0   OFFSET = 0.02
    NSKY = 2  POSSKY = AUTO
    SKYWIND(1-2) = 0.0,0.0
    SKYWIND(3-4) = 0.0,0.0
--- 5. Lines searching ---
    SEAMTD = GAUSSIAN   WIDTH2 = 5.0  THRES2 = 400.0
--- 6. Wavelength calibration ---
```

```
    WLCMTD=guess  WLCOPT=1D  GUESS=cakl  WLCVISU=YES
    WLC = t8640025 LINCAT = thorlon
    DC  = 3          TOL = 0.25. See also CCDBIN
    WLCLOOP = 1.0, 0.2, 10.0
    WLCNITER = 3,20
--- 7. Rebin ---
    REBMTD = NO  SAMPLE = 0.03
--- 8. Flat Field correction ---
    FFOPT = yes
       FLAT = +++
       CORRECT = knormal   BLAZE  = blaze
--- 9. Response Correction ---
    RESPOPT = no
--- 10. Merging ---
    MGOPT = YES
       MRGMTD = NOAPPEND  MRGORD = 1,8
```

**MIDAS⟩ load/image [smooth-field image]**

Display the image in which the orders are to be located. The smooth-field image is used in preference to a stellar spectrum because of the intensity of the orders, the absence of absorption lines, the low background noise, and the width of the orders from the fully illuminated slit.

**MIDAS⟩ plot/col [smooth-field image] 288 1,384**

Plot a vertical section across the orders (the pixels and orders are numbered from bottom to top) to give an indication of the FWHM of the orders and the ADU threshold required to separate the orders from the background.

**MIDAS⟩ search/order [smooth-field image] [WIDTH1],[threshold],5**

This low-level command is used to ensure that the line width and ADU threshold are right. All orders should be found, with the full 59 sampling positions in each. Note that when the programme fails to locate orders and suggests that the threshold should be reduced, it is often more productive to leave the threshold high and *increase* the WIDTH1 parameter instead. This will also tell you what the parameters are, to locate the orders. The orders, when found, are numbered from the bottom of the display window. Note the "Y CENTRE" value of the order which you wish to use to determine the offset of the stellar spectra (see the next section) – it may be necessary to alter the parameters in the *select.prg* file to display that order properly in the graphics window.

**MIDAS⟩ set/echelle WIDTH1=[suitable width] THRES1=[suitable threshold] SLOPE=5**

Set the échelle parameters which are found to work. The "slope" parameter is wrong on

the face of it (the orders have a negative slope typically of about $-1{:}44$), but *MIDAS* cannot cope with a negative parameter here and "5" works. This step is actually unnecessary – it is easier simply to specify the parameters when giving the next command – but setting the parameters now means that that they can be saved for future sessions.

**MIDAS⟩ define/echelle [Smooth-field file]**

Locate the orders and record all the sampling positions in a table called "ORDER".

## A.4   Setting the Offset of the Orders in The Stellar Spectrum

Because the image of the star may not be in the exact centre of the slit, which will cause the observed orders to be offset with respect to the centres of the smooth-field orders, an offset measurement is required to tell the software exactly where to measure the recorded stellar spectrum.

**MIDAS⟩ set/graphic XAXIS=auto YAXIS=auto**

**MIDAS⟩ @@ select [Stellar spectral image]**

The program SELECT.PRG which must be present in the currently designated MID-WORK directory plots a cross-section of one of the orders of the stellar spectrum, and enables it to be analyzed using the mouse cursor. If you are using *MIDAS* for the first time you will have to get a copy of the program SELECT.PRG for your MIDWORK directory. The program first shows a vertical cross section of the CCD image, then a section of that image is used to obtain the offset correction. Select the pixel positions which include the order to be examined and sufficient background around that order. The parameters to be found are the centre of the order, the full width and the full width half maximum. A Gaussian is fitted to the intensity across the order by marking the background around the order with the mouse (position the cross cursor and click the left button). This operation can be repeated as many times as is desired. Mouse cursor operations in *MIDAS* are terminated by clicking the right button of the mouse and holding it down until the cursor is replaced by a skull and crossbones. The centre and the FWHM as displayed in the command window must be recorded *manually*, as well as the FW from the graphics display.

**MIDAS⟩ read/table ORDER**

Display the current table of order positions. Note the "Y-FITTED" value at X=288 in the same order that was displayed in the graphics window (check the Y-FITTED values in the table against the x-axis in the plot window if unsure). The orders are numbered from bottom to top as displayed in the image window. The Y-FITTED value in the table does not change, and once it has been recorded once, this step can be omitted.

**MIDAS⟩ set/echelle SLIT=[FW] MEDFILT=3,3,3 OFFSET=[calculated offset]**

Calculate the offset of the orders in the stellar spectrum from those of the order table as (Offset) = (Centre found using @@ select) - (Y-FITTED valued noted from order table). The value is positive if the stellar orders are positioned higher than the smooth-field orders; negative if they are lower. The parameter SLIT defines the width of the order that will be examined in the reduction step.

The MEDFILT parameters govern the filtering between the orders. At each pixel along the rows, the program takes the median value of all pixels in an extended box ±[first parameter] pixels width and ±[second parameter] pixels in height, then reduces to the median any pixel value which is more than [third parameter] times the standard deviation greater than the median. This median filtering is applied to the entire frame to give the same background level and eliminate all the cosmic rays present in the background by using the 7x7 box set by the MEDFILT parameters. If a large number of the cosmic rays are larger than this box, then the parameters must be set after the image is inspected by the image zoom.

## A.5   Calibrating the Echelle Spectrum for Wavelength

**MIDAS⟩ set/echelle EXTMTD=linear WIDTH2=5 THRES2=100**
Set further parameters for locating the emission lines in the thorium-arc spectrum. The "optimal" method of extraction still results in Fortran errors. The WIDTH2 parameter is the "thickness" of the lines along the order and it is the *MIDAS* default value. The ADU threshold of 100 is right for "200 th" images. Since these parameters are unlikely to change, it should be possible to omit this step once the echelle has been initialized. It is also a good idea to plot one of the orders of the thorium-arc spectrum to see where the background is for THRES2.

**MIDAS⟩ plot/row [thorium-arc image] [y-position] 1,576**

**MIDAS⟩ extract/echelle [thorium-arc image] [name for extracted image]**

Create a 1-dimensional image of all the orders present in the CCD spectrum.
Example: "extract/echelle T0010003 ARC" stores the 1-dimensional image in the file ARC.BDF.

**MIDAS⟩ search/echelle [name of extracted image]**

Locate the emission lines in the thorium-arc image and indicate in the display window which ones have been found. It might be necessary to change parameters (probably THRES2) if good lines are missed or spurious lines are found.

**MIDAS⟩ set/graphic XAXIS=auto YAXIS=auto**

At this point it is necessary to select the method to be used to fit a list of line wavelengths to the thorium-arc image. An interactive method must be used if the echelle cannot be initialized with a lines table from a previous reduction which has been saved

using "save/echelle". An automatic method can be used if the echelle can be initialized with a previously saved lines table. Line tables can be found in the "phys147/Midas/calib/data/inst/caspec/" directory called "lincat**.tbl", these tables will probably need to have more lines added to them. See the section on Tables at the end.

To select the interactive method, set the following parameters:

**MIDAS⟩ set/echelle WLCMTD=angle LINCAT= [name of wavelengths table]**

It is also a good idea to have a printed copy of the thorium-arc spectrum with lines already identified on them.

To select the automatic method, set the following parameters:

**MIDAS⟩ set/echelle WLCMTD=guess GUESS=[previous session name] LIN-CAT= [name of wavelengths table]**

**MIDAS⟩ ident/echelle [thorium-arc image]**

This starts the program for identifying lines in the spectral image.

If the interactive method has been selected, a mouse cursor will be enabled to allow lines of known wavelength to be selected. At least four lines must be selected, one from each order should do. A line is selected by positioning the box cursor over it and clicking the left-hand button. The box can be resized by using the arrow keys on the keyboard once the image display is selected. The command window should be checked after each line to make sure that it has been successfully located. In due course the command window will ask for the order number of the first selected line, and then the wavelengths of the selected lines. It will then fit a polynomial to the lines which will be recorded in a table. It should report a fitting rate better than 50%. If the automatic method has been selected, the operator must simply wait for the fitting to run its course. If the fitting success rate is less than 50% even though a good number of lines were found, the interactive method must be used instead. Possibly the tolerance may need to be adjusted if it is set to tight then good lines may be missed out.

**MIDAS⟩ plot/ident [extracted image] [order]**

Plots on the graphic window the lines that have been identified in the wavelength calibration for each order. Example: "plot/ident arc 1" plots the identified lines in the first order on the image.

## A.6   Filtering the Stellar Spectrum

**MIDAS⟩ clear/channel overlay**

Clear the overlaid emission line markers from the image display.

**MIDAS⟩ load/image [stellar spectral image]**

Display the stellar spectrum which is to be filtered.

**MIDAS⟩ set/echelle CRFILT=15,41,3 CCDFILT=7.1,4.3,5**

Set the remaining echelle filtering parameters. Since these parameters are unlikely to change, it should be possible to omit this step once the echelle has been initialized. If a significant part of the orders is being chopped off then the CRFILT will need to be changed especially if the order is near the top or bottom of the image. i.e. CRFILT=15,37,3

The CCDFILT parameters are always the same as they refer to the CCD detector being used. The CRFILT parameters remove any cosmic rays in the orders only.

Note the very ends of all the orders (a few pixels at each end) are removed at this stage.

**MIDAS⟩ @s echkaren [stellar spectral image] [name for filtered image]**

Filter the stellar spectrum. The length of time taken by the "expanding frame" step will depend on the MEDFILT parameters, set earlier. This also produces an image recording the difference between the filtered and unfiltered images called [stellar spectral image]cr. This can then be reduced to record the position of any cosmic rays that were in the orders. When there are only a few orders recorded on the CCD image, the polynomial used to fit the background will sometimes need to be changed. The default value is BKGPOL=3,4 and would be changed to something like 2,2.

**MIDAS⟩ load/image [filtered stellar spectral image]**

Display the filtered image and check for cosmic ray removal. Inspect in detail with "plot/row" and "plot/column" if necessary.

It may also be useful to keep a record of the position of any cosmic rays removed from the orders, by taking a difference frame and then extract the orders like any spectrum. See the "Other Useful Commands" section.

## A.7   Preparing the Scaled Smooth-field Image

The operations in this section are performed only once for each night's observations on a given set of spectrograph settings. They generate a smooth-field image with signal levels close to unity in the orders which can then be used in the reduction of all of the stellar spectra from that night on those settings. If, for any reason, the positions of the orders have to be redefined, then this section, too, should be repeated.

**MIDAS⟩ plot/col [smooth-field image] 288 1,384**

Plot the intensities of the orders in the smooth-field spectrum.

**MIDAS⟩ compute/image [name for scaled smooth-field image] = [smooth-field image]/[typical intensity of smooth-field orders]**

Normalize the smooth-field image. A divisor of 10,000 is suitable for the usual 100 lisse image.

## A.8   Reduction of the Stellar Spectrum

MIDAS⟩ set/echelle FFOPT=yes CORRECT=[normalized smooth-field image] RESPOPT=no SAMPLE=0.03 MRGMTD=noappend MRGORD=1,8

Set parameters for smooth-fielding and reduction to four files each containing one 1-dimensional order.  If there is no smooth-field image, set FFOPT=NO. The SAMPLE step should be set to whatever value has been used before on the star of interest. If this is a first time reduction for a particular spectrum then a value around 0.03 should be adequate.  Since these parameters are unlikely to change, it should be possible to omit this step once the echelle has been initialized.

  MIDAS⟩ reduce/echelle [filtered stellar spectral image] [prefix for reduced spectra]

Reduce the filtered stellar spectrum.  The reduced spectral orders are saved in separate files named [first 4 characters of prefix]0001... 0002... 0003... 0004,... containing the orders from the CCD image. Be very careful if using the tape name as a prefix!

  MIDAS⟩ set/graphic XAXIS=auto YAXIS=auto

  MIDAS⟩ plot/row [reduced spectrum of interest]

Plot the reduced spectrum.

Example: "plot/row RED0003" plots the reduced order 3 for examination of the line(s) of the spectrum.


   Below are some example steps in the further reduction of your spectra.  The actual process will depend on what one wishs to extract from the reduced spectra.

MIDAS⟩ normalize/spectrum [reduced order] [fit file]

This allows the user to both normalize the spectrum and give a flat continuum by using a cursor on the graphic window to plot the points which the user indicates to be the continuum and then fits a spline to those points. A minimum of four points are required. The fitted curve is then saved to a file.

Example: "MIDAS⟩ normalize/spectrum RED0003 fit"

MIDAS⟩ compute/image [normalized spectrum] = [reduced spectrum of interest]/[fit file]

Computes normalized spectrum from reduced spectrum and the fitted curve for the continuum.

Example: "MIDAS⟩ compute/image NOR0003 = RED0003/fit"

Then plot the resulting image.

  MIDAS⟩ plot/row [reduced spectrum of interest]

  MIDAS⟩ copy/graphics physps5

Print the displayed plot on the 5th floor printer.

**MIDAS⟩ reduce/echelle [thorium spectral image] [prefix for reduced spectra]**

Reduce thorium-arc spectrum to wavelength for recording.

**MIDAS⟩ plot/row [reduced thorium spectrum of interest]**

**MIDAS⟩ overplot/ident line :wavec :ident**

This is used to record the wavelength calibration of the Thorium lines used from the line catalogue. These are plotted over the lines found in the spectrum.

**MIDAS⟩ copy/graphics physps5**

## A.9  Saving the Session

Much setting of the échelle parameters, and a tedious session of interactive line calibration, can be eliminated by initializing the parameters from a previously saved session. To do this, of course, a previous session must have been saved. If the parameters have all been correctly set, the saving need only ever be done once for all observations in a given wavelength region (in effect, for each smooth-field file). If this is the first successful session for this wavelength region on the échelle, the following steps will save the parameters for future sessions in the region.

**MIDAS⟩ set/echelle WLCMTD=GUESS GUESS=[name of this session]**

Ensure that future line identifications will use the automatic, not the interactive, method.

**MIDAS⟩ save/echelle [session name]**

From now on, it should not be necessary to set any parameters except WIDTH1 and THRES1 (only if there is variation in the strength of the smooth-field orders from image to image), OFFSET (always), and SLIT and MEDFILT (if there is substantial variation in the strength of the stellar orders from image to image — values of about 10 and 12 will do for most images). All other parameters should in most cases be able to be used as saved from this session and set by init/echelle.

## A.10  Saving data as FITS format files

Once all the spectra has been reduced it would be likely that the data will be saved in the FITS format. This enables the data to looked at in any package for further analysis. It also allows for transfer of files between implementation of MIDAS on different computers, each of which has its own particular .bdf format.

**MIDAS⟩ outtape/fits [file].BDF [file].FITS**

This converts the files from the *MIDAS* format to the FITS format. The data can now be saved to diskette or tape.

## A.11    Creating MIDAS Tables

This section covers the creation of tables that will be used in *MIDAS* and some editting for those unfamilar with the EDIT/TABLE command.

  **MIDAS⟩ assign/print file [output file]**

This will output any table as an ASCII file which can then be edited by any editor of your choice

Example: "MIDAS⟩ assign/print file thar.dat"

  **MIDAS⟩ print/table [table]**

This prints out the table to the file you have specified.

Example: "MIDAS⟩ print/table lincat16"

Once the table has been edited, it must then be converted into the *MIDAS* format.

  **MIDAS⟩ create/table [table name] [number of columns] [number of rows]**

**[ASCII data file]**

This will create a table in the *MIDAS* format Example: "MIDAS⟩ create/table lincatokp 1 2078 thar.dat"

**MIDAS⟩ name/column [table name] #[column to be named] :[name of column] "[unit]" [format]**

This names the column so that *MIDAS* recognizes what the column refers to.

Example: "MIDAS⟩ name/table lincatokp #1 :wave "angstroms" f8.3"

## A.12    Other Useful Commands

Below are some *MIDAS* commands that may be useful for checking the filtering of the images that have been processed, to check that there has been no signal removed or where cosmic ray removal might affect the data.

  **MIDAS⟩ compute/image diff = [image]-[filtered image]**

Takes the difference between the filtered and unfiltered images, and puts the result in a file "diff"

  **MIDAS⟩ stat/image diff**

Shows the statistics of the image diff **MIDAS⟩ load/image diff cuts=[min],[max]**

Loads the image diff and shows the flux between the minimum and maximum values taken from the statistics of the image "diff"

Example: "MIDAS⟩ load/image diff cuts=-50,100" for an image that has min = -49, max = 2000 from the statistics.

**MIDAS⟩ show/echelle**

This shows what the echelle reduction parameters are.

**HOUGH TRANSFORM**

**MIDAS⟩ hough/echelle [image] [section of image to be scanned] 10,50 [# orders] HHV**

In the case where the search/order command fails to give a result for one or all orders, it may be better to use these commands. Example: "MIDAS⟩ hough/echelle image 1,384 10,50 3 HHV"

**MIDAS⟩ define/hough [image] [number of orders] 0 DENSE 0**

Same as the define/echelle command, but for the HOUGH TRANSFORM.

# Appendix B

# MIDAS command language programs

Presented here are the MIDAS command language programs that were used extensively throughout the reduction process of the obtained spectra.

## B.1 Select.prg

```
!+++++++++++++++++++++++++++++++++++++++++++++++++++++++++++++++++++++++++
!
! SELECT.PRG  allows selection of slit width and offset by plotting
! the image and cross-section. The procedure then calculates the
! position of the actual order using CENTER/MOMENT.
! The offset is calculated as: (fitted - defined) center position,
! where fitted = center/moment and defined = define/echelle methods
!
! usage: @@ select inframe
!
!+++++++++++++++++++++++++++++++++++++++++++++++++++++++++++++++++++++++++
!

DEFINE/PARAMETER P1 ? I " Input image frame: "

!WRITE/OUT "Loading image..."
!LOAD/IMAGE {P1}

!WRITE/OUT "Overlaying defined orders..."
!LOAD/ECHELLE

! modified OKP 28 Mar 95
 WRITE/OUT "Plotting image cross section..."
 AVERAGE/COL DUM = {P1} @283,@292 AVERAGE
 SET/GRAPH PMODE=1
 SET/GRAPH XAXIS=1,384
 PLOT/ROW DUM
```

```
 WRITE/OUT "Input pixel number's around order "
 WRITE/OUT "for cross section analysis..."

 DEFINE/PARAMETER P2 ? I " Pixel to left of Order: "
 DEFINE/PARAMETER P3 ? I " Pixel to right of Order: "
!

WRITE/OUT "Plotting order cross section..."
AVERAGE/COL DUM = {P1} @283,@292 AVERAGE
SET/GRAPH PMODE=1
SET/GRAPH XAXIS={P2},{P3}
PLOT/ROW DUM

WRITE/OUT "Indicate order position with cursor (LMB)"
CENTER/GAUSS GCURSOR

SET/GRAPH XAXIS=AUTO
```

## B.2 Echorlon.prg

```
!
! @@ echorlon.prg
!
! Program for reducing echelle spectra using ESO-MIDAS.
! WRITTEN BY ORLON PETTERSON APRIL 1995.
!
! This program follows the procedure layed out in the user guide
! for Reducing MJUO Echelle Spectra on CCD Using ESO-MIDAS.
!
! An initial reduction which which has already calibrated the
! thorium reference spectrum must be available and most of the
! other parameters already set.
!
! Parameters used are the images used for reduction, and also any
! values determined from those images.
!
!
```

```
WRITE/OUT " "
WRITE/OUT "This program will reduce spectra from images taken with"
WRITE/OUT "the MJUO CCD provided that data from a previous reduction"
WRITE/OUT "is available as a reference"

create/graphic
create/display 0 576,384

!
! This section will define the orders in another smooth-field image
! if data is for a different nights observations
!
! Uses program echorder.prg to define orders
!
WRITE/KEYWORD orders/C/1/1 " " ALL
WRITE/OUT " "
WRITE/OUT "Do you need to define the orders of the spectrum? y/n"
INQUIRE/KEYWORD orders
IF orders .EQ. "y" then
@@ echorder
ENDIF
!

clear/channel overlay
set/graph xaxis=auto yaxis=auto

!
! Asks for names of the images
!
WRITE/OUT " "
WRITE/OUT "Spectral image name: "
DEFINE/PARAMETER P1 ?
WRITE/OUT " "
WRITE/OUT "Thorium image name: "
DEFINE/PARAMETER P2 ?
WRITE/OUT " "
!
```

```
!
! This section finds where the centres of the orders are.
! Using the program select.prg
!
load/lut pastel
load/image {P1}
WRITE/OUT " "
WRITE/OUT "RECORD THE CENTRE AND THE FULL-WIDTH OF THE ORDER"
set/graph xaxis=auto yaxis=auto
WRITE/OUT " "
@@ select {P1}
WRITE/OUT " "
READ/TABLE order
WRITE/OUT " "
WRITE/OUT "Full-width: "
DEFINE/PARAMETER P3 ? NUM
WRITE/OUT " "
WRITE/OUT "Offset from smooth field: "
DEFINE/PARAMETER P4 ? NUM
WRITE/OUT " "
WRITE/OUT "Centre of order: "
DEFINE/PARAMETER P5 ? NUM
set/echelle slit={P3} offset={P4}
!

!
! This section then calibrates the spectrum with respect to the
! corresponding thorium spectrum for wavelength calibration.
!
! If calibration is inadaquate it then exits.
!
set/graph xaxis=auto yaxis=auto
plot/row {P2} {P5} 1,576
set/graph xaxis=auto yaxis=auto
extract/echelle {P2} {P2}z
search/echelle {P2}z
ident/echelle {P2}
WRITE/KEYWORD zaphod/C/1/1 " " ALL
WRITE/OUT "Is the wavelength calibration adaquate? y/n"
```

```
INQUIRE/KEYWORD zaphod
IF zaphod .EQ. "n" then
return/exit
endif
!copy/graph physps5
!


!
! This short section filters the spectral image using echkaren.prg
! and then loads the filtered spectrum at the end.
!
clear/channel overlay
load/image {P1}
@s echkaren {P1} {P1}f
load/image {P1}f
!
! Better to be able to see it always
!
!WRITE/KEYWORD ford/C/1/1 " " ALL
!WRITE/OUT "Do you wish to see the image containing the removed cosmic
            rays? y/n"
!INQUIRE/KEYWORD ford
!IF ford .EQ. "y" then
create/display 1 576,384
assign/display d,1
load/image {P1}cr
assign/display d,0
!ENDIF
!


!
! This section reduces the spectral image to one-dimensional spectra
! for recording as individual FITS files.
!
WRITE/OUT " "
WRITE/OUT "Enter 2 digit image number for reduced spectra:"
DEFINE/PARAMETER P6 ?
WRITE/OUT " "
WRITE/OUT "Enter 2 digit image number for reduced thorium spectra:"
```

```
DEFINE/PARAMETER P7 ?
reduce/echelle {P1}f {P6}rs
reduce/echelle {P1}cr {P6}cr
reduce/echelle {P2} {P7}th
set/graph xaxis=auto yaxis=auto
!
WRITE/OUT " "
WRITE/OUT "Reduced spectra are contained in files {P6}rs00xx and also"
WRITE/OUT "the position of cosnic rays in {P6}cr00xx which should now"
WRITE/OUT "be inspected.  Also reduced thorium lines in files {P7}th00xx"
```

## B.3   Echorder.prg

```
!
! This MIDAS program defines the orders in the smooth field image
!
! Written by Orlon Petterson April 1995
!

set/graph xaxis=auto yaxis=auto
clear/channel overlay
load/lut pastel
WRITE/OUT " "
WRITE/OUT "Enter name of smooth - field:"
DEFINE/PARAMETER P2 ? IMA
load/image {P2}

    DEFINE/LOCAL QZ/I/1/1 60
    DEFINE/LOCAL QY/I/1/1 900

WRITE/OUT " "
WRITE/OUT "Select method for defining orders of echelle spectrum"
WRITE/OUT "std, com, or hough methods."
DEFINE/PARAMETER P1 ? C
BRANCH P1(1:2) st,co,ho std,com,hough
!
WRITE/OUT "Invalid option - please try again"
```

```
RETURN
!


!
hough:
  set/echelle defmtd=hough
  plot/col {P2} 288 1,384
  WRITE/OUT " "
  WRITE/OUT "Number of orders to be found:"
  DEFINE/PARAMETER P3 ? NUM
  hough/echelle {P2} 1,384 10,50 {P2} HHV
  define/hough {P2} {P3} 0 DENSE 0
  goto end
!


!
std:
  set/echelle defmtd=std
  plot/col {P2} 288 1,384

  check1:
  WRITE/KEYWORD Q1/C/1/1 " " ALL
  WRITE/OUT " "
  WRITE/OUT "Are the FWHM and Threshold set to appropriate values?"
  WRITE/OUT "Default = no"
  INQUIRE/KEYWORD Q1
  IF AUX_MODE(7) .EQ. 0 Q1 = "n"

  IF Q1 .EQ. "n" then

    WRITE/OUT " "
    WRITE/OUT "Enter FWHM:"
    INQUIRE/KEYWORD QZ
    WRITE/OUT " "
    WRITE/OUT "Enter threshold:"
    INQUIRE/KEYWORD QY
    search/order {P2} {QZ},{QY},5
    goto check1
  ENDIF
```

```
set/echelle width1={Q2} thres1={Q3} slope=5
define/echelle {P2}
goto end
!

!
com:
  set/echelle defmtd=com
  plot/col {P2} 288 1,384

  check2:
  WRITE/KEYWORD Q1/C/1/1 " " ALL
  WRITE/OUT " "
  WRITE/OUT "Are the FWHM and Threshold set to appropriate values?"
  WRITE/OUT "Default = no"
  INQUIRE/KEYWORD Q1
  IF AUX_MODE(7) .EQ. 0 Q1 = "n"

  IF Q1 .EQ. "n" then

    WRITE/OUT " "
    WRITE/OUT "Enter FWHM:"
    INQUIRE/KEYWORD QZ
    WRITE/OUT " "
    WRITE/OUT "Enter threshold:"
    INQUIRE/KEYWORD QY
    search/order {P2} {QZ},{QY},5
    goto check2
  ENDIF
set/echelle width1={Q2} thres1={Q3} slope=5
define/echelle {P2}
goto end
!

!
end:
WRITE/OUT " "
WRITE/OUT "Orders are now defined and stored in table order"
WRITE/OUT " "
```

```
!


!
! This section will normalize the smooth-field image
!
WRITE/OUT "Now you need to normalize the smooth-field image"
WRITE/KEYWORD value/C/1/1 " "
WRITE/KEYWORD pref/C/1/1 " "
plot/col {P2} 288 1,384
WRITE/OUT "Enter prefix letter for normalised smooth-field"
INQUIRE/KEYWORD pref
WRITE/OUT "Enter value of typical intensity of orders"
INQUIRE/KEYWORD value
compute/image {pref}normal = {P2}/{value}
set/echelle correct={pref}normal
!
```

## B.4   knorm.prg

The only differences in the H line and K line versions of this program are in wavelength
scale and reference spectrum.

```
!
! MIDAS procedure knorm
!
!  Use  @@ knorm [P1]
!     where P1 = file name of spectrum to be shifted to href.bdf START and
!                STEP and divided by href.bdf
!
! 1995 Oct 17
!
define/parameter P1 ? I "Enter image:"

set/graph xaxis=3933,3935 bin=ON yaxis=0,100 colour=1

define/local temp/r/1/1 0.
define/local temp2/r/1/1 0.
define/local pixelno/i/1/1 0
define/local pixvalh/r/1/1 0.
define/local pixvalp1/r/1/1 0.
```

```
define/local shift/r/1/1 0.

compute/keyword pixelno = M$EXIST("kref.bdf")
if pixelno .EQ. 0 then
$ cp /astro/physokp/midwork/kref.bdf  .
endif

copy/dk kref START temp


pixelno = ((3923.5-{temp})/0.03)
create/image tmp
copy/id kref tmp imdata/r/1/600

copy/dk tmp imdata/r/{pixelno}/1 pixvalk

temp2 = {pixvalk}/2.
set/graph yaxis=-1,{temp2}
plot/row kref

copy/dk {P1} START temp

pixelno = ((3923.5-{temp})/0.03)
create/image tmp
copy/id {P1} tmp imdata/r/1/600

copy/dk tmp imdata/r/{pixelno}/1 pixvalp1

compute/image temp = {P1}*{pixvalk}/{pixvalp1}
set/graph  colour=3
over/row temp

inquire/keyword shift "Shift in pixels (+ to right) for {P1}?:"

temp = {temp} + 0.03*{shift}
copy/kd temp temp START

set/graph colour=2
over/row temp
```

```
rebin/linear temp temp2 kref

compute/image {p1}n = temp2/kref

set/graph xaxis=3930,3938 yaxis=0,2,.5,.1 colour=1

inquire/keyword temp2 "Hit return to continue:"

plot/row {P1}n
label/graph "{P1}n" 3930,2.05 0 1.3 1
label/graph "pixel shift:" 3936.7,1.8 0 0.7 2
set/format f5.2
label/graph "{shift}" 3936.8,1.8 0 0.7 1
set/graph colour=2
over/line  1 3933.8384,0 3933.8384,2
set/graph colour=3
over/line 1 3930,1 3938,1
set/graph colour=1
over/row {P1}n
```

## B.5   orlonkfit.prg

The differences in this program and the one for the H spectra, is in the wavelength values.

```
!
! Procedure orlon.prg
!   Conjointly fits multiple gaussians to an absorption-line spectrum.
!   Initial values for gaussians set using graphics cursor
!
! Use:
!   @@ orlon [P1]
!       where [P1] = name of image file containing spectrum presumed
!                     normalised to unity.
!
! 1995 October 20
!
define/parameter P1 ? I "Enter normalized spectrum file:"
```

```
define/local question/i/1/1 0
define/local N/i/1/1 0
define/local M/i/1/1 0
define/local length/i/1/1 0
define/local indx/i/1/1 0
define/local indx2/i/1/1 0
define/local A/r/1/1 0.
define/local B/r/1/1 0.
define/local C/r/1/1 0.


compute/image tmp = {P1}


compute/key indx = M$EXISTD("tmp","coords")
read/key indx
if {indx} .eq. 1 then
delete/descr tmp coords
endif


compute/key indx = M$EXISTK("xvals")
read/key indx
if {indx} .eq. 1 then
delete/keyword xvals
endif


set/format F20.12
copy/dk tmp START A
compute/keyword A = ({A}-3968.72)*75.54


copy/kd A tmp START


copy/dk tmp STEP A
compute/keyword A = {A}*75.54


copy/kd A tmp STEP


extract/image {P1}syn = tmp[-250.:250.]


write/descriptor {P1}syn CUNIT/C/1/16  "RELATIVE TO REF."
write/descriptor {P1}syn CUNIT/C/17/16 "VELOCITY KM/S    "
```

```
set/graph yaxis=0,2 xaxis=-300,300 ltype=1 stype=0 colour=1 bin=ON
plot/row {P1}syn
label/graph "{P1}"  -300,2.05  0 1.5 1


set/graph bin=OFF


!create/table orlon_fit   31 24
!reate/column orlon_fit :FUNCTIONS   " "  A60  C*60
!reate/column orlon_fit :PARAMETERS  " "  A60  C*60


write/keyword IN_A/c/1/60 " " ALL
write/keyword OUT_A/C/1/60 " " ALL
IN_A = "orlon"


INPUTI = 0


RUN APP_EXE:fittable


inquire/keyword question "What order of polynomial for continuum? 0, 1 or 2?:"


if {question} .eq. 0 then


orlon_fit,:FUNCTIONS,@1 = "POLY(X;A)"
orlon_fit,:PARAMETERS,@1 = "A=1."


endif


if {question} .eq. 1 then


orlon_fit,:FUNCTIONS,@1 = "POLY(X;A,B)"
orlon_fit,:PARAMETERS,@1 = "A=1.  B=0."


endif



if {question} .eq. 2 then


orlon_fit,:FUNCTIONS,@1 = "POLY(X;A,B,C)"
```

```
orlon_fit,:PARAMETERS,@1 = "A=1.  B=0.  C=0."

endif

! Now get parameters from which initial values of gaussian fits can be
! estimated

write/out "Mark position of absorption features using cursor"
write/out " "
write/out "First mark centre of line, then FWHM, left then right"
write/out " "

get/gcurs coords,des

show/descr {P1}syn coords

read/descriptor {P1}syn coords

copy/dk {P1}syn coords xvals


read/key xvals

set/format i2
compute/key length = {outputi(3)}/7
read/key length
compute/key N = (({length}/3)*3)

if  {N}  .NE. {length} then
    write/out "No of points selected not a multiple of 3"
    return
endif

! length gaussians are to be fitted

compute/keyword length = {length}/3

DO N = 1 {length} 1
```

```
! read/key N
compute/key M = {N}+1

compute/key indx = ({N}-1)*21+9
read/key indx
compute/key A = {xvals({indx})}-1.
compute/key indx = ({N}-1)*21+8
compute/key B = {xvals({indx})}
compute/key indx = ({N}-1)*21+15
compute/key indx2 = ({N}-1)*21+1
set/format f10.4
compute/key C = 0.5*({xvals({indx})}-{xvals({indx2})})

orlon_fit,:FUNCTIONS,@{M} = "GAUSS(X;A{M},B{M},C{M})"
orlon_fit,:PARAMETERS,@{M} = "A{M}={A}  B{M}={B}  C{M}={C}"

ENDDO

 read/table orlon_fit
! read/descr orlon_fit.tbl *

write/key outputi/i/1/1 0
compute/keyword IN_A = "orlon"
compute/keyword OUT_A = "orlon_fit"
RUN APP_EXE:tablefit

set/fit method=MGN

fit/image 20,0.0001,0.2 {P1}syn orlon

compute/fit temp
set/graph colour=2
over/row temp

set/graph colour=4

DO N = 1 {length} 1

compute/key M = {N}+1
```

```
select/fun orlon 1,{M}
compute/fit fit{N} = orlon
over fit{N} ? ? 0.5

ENDDO

set/graph default

! then do
!       assign/print physps5
!       print/fit orlon
!       copy/graph physps5
!
```

# Appendix C

# Data extracted from spectra

Contained below is the complete table of data on the variable features seen in each spectrum taken at MJUO. The columns are: Heliocentric Julian Day, Depth of the feature, error in depth, velocity of feature with respect to the circumstellar line, error in velocity, which calcium line, resolution determined from thorium spectra (where available), FWHM of the feature, error in FWHM, equivalent width of the feature, error in equivalent width, and the comments column (e = by eye estimate, uncertain = uncertain measurement, cr = affected by cosmic ray).

Table C.1: **Table of of results of analysis of $\beta$ Pic Ca II spectra.** The table below contains all the data on the observed variable features in the Ca II lines.

| HJD | Depth | error | Velocity | error | Ca line | Resolution | FWHM | error | Eq. width | error | Comments |
|---|---|---|---|---|---|---|---|---|---|---|---|
| 2448964.9116 | 0.51 | 0.01 | 22.3 | 0.2 | k | * | +310.9 | +7.91 | +168.800 | +5.769 | |
| 2448964.9431 | 0.53 | 0.02 | 22.1 | 0.4 | k | * | +314.9 | +11.86 | +177.650 | +10.081 | |
| 2448964.9431 | 0.15 | 0.02 | 50.0 | 5.0 | k | * | +329.4 | +65.88 | +52.592 | +13.457 | e |
| 2448964.9692 | 0.45 | 0.09 | 18.9 | 1.0 | k | * | +255.6 | +22.40 | +122.435 | +28.459 | |
| 2448964.9692 | 0.15 | 0.04 | 37.9 | 7.9 | k | * | +397.9 | 139.66 | +63.531 | +29.811 | |
| 2448964.9971 | 0.55 | 0.02 | 22.3 | 0.4 | k | * | +357.0 | +13.18 | +209.037 | +11.528 | |
| 2448964.9971 | 0.05 | 0.02 | 53.0 | 9.0 | k | * | +263.5 | 131.75 | +14.025 | +9.559 | e |
| 2448965.0263 | 0.58 | 0.01 | 24.5 | 0.3 | k | * | +332.0 | +9.22 | +204.984 | +7.134 | |
| 2448965.0442 | 0.60 | 0.01 | 24.0 | 0.3 | k | * | +343.9 | +7.91 | +219.625 | +6.638 | |

**Table C.1 cont.:**Table of results of anaylsis of $\beta$ Pic Ca II spectra

| HJD | Depth | error | Velocity | error | Ca line | Resolution | FWHM | error | Eq. width | error | Comments |
|---|---|---|---|---|---|---|---|---|---|---|---|
| 2448965.0616 | 0.58 | 0.01 | 24.7 | 0.3 | k | * | +362.3 | +10.54 | +223.692 | +8.052 | |
| 2448965.0785 | 0.58 | 0.01 | 25.2 | 0.3 | k | * | +372.9 | +10.54 | +230.200 | +8.114 | |
| 2448965.0785 | 0.10 | 0.02 | 56.0 | 5.0 | k | * | +263.5 | 131.75 | +28.049 | +16.079 | e |
| 2448965.0929 | 0.55 | 0.01 | 24.3 | 0.3 | k | * | +365.0 | +10.54 | +213.665 | +7.762 | |
| 2448965.0929 | 0.06 | 0.02 | 60.0 | 5.0 | k | * | +303.0 | 131.75 | +19.354 | +11.287 | e |
| 2448965.0929 | 0.10 | 0.02 | -15.0 | 5.0 | k | * | +131.8 | +65.88 | +14.025 | +8.040 | e |
| 2448965.1094 | 0.56 | 0.01 | 24.2 | 0.3 | k | * | +362.3 | +11.86 | +215.979 | +8.571 | |
| 2448965.1094 | 0.10 | 0.02 | -15.0 | 5.0 | k | * | +197.6 | +65.88 | +21.037 | +8.705 | e |
| 2448965.1094 | 0.08 | 0.02 | 56.0 | 5.0 | k | * | +263.5 | 131.75 | +22.439 | +13.353 | e |
| 2448965.1242 | 0.57 | 0.02 | 24.3 | 0.4 | k | * | +332.0 | +14.49 | +201.449 | +12.010 | |
| 2448965.1242 | 0.07 | 0.02 | -20.0 | 5.0 | k | * | +197.6 | 105.40 | +14.726 | +9.484 | e |
| 2448965.1242 | 0.06 | 0.02 | 60.0 | 5.0 | k | * | +171.3 | +65.88 | +10.939 | +5.927 | e |
| 2448965.1410 | 0.54 | 0.01 | 23.0 | 0.3 | k | * | +336.0 | +10.54 | +193.119 | +7.489 | |
| 2448965.1410 | 0.14 | 0.02 | -18.7 | 1.0 | k | * | +220.0 | +32.94 | +32.790 | +7.223 | |
| 2448966.0939 | 0.59 | 0.02 | 18.6 | 0.2 | k | * | +202.9 | +9.22 | +127.427 | +7.692 | |
| 2448966.1139 | 0.54 | 0.02 | 18.7 | 0.3 | k | * | +216.1 | +10.54 | +124.202 | +8.098 | |
| 2448966.8623 | 0.47 | 0.13 | 16.5 | 1.2 | k | * | +185.8 | +31.62 | +92.941 | +32.132 | |
| 2448966.8623 | 0.18 | 0.13 | 32.9 | 7.6 | k | * | +318.8 | 163.37 | +61.091 | +57.587 | |
| 2448966.8853 | 0.58 | 0.02 | 17.9 | 0.4 | k | * | +197.6 | +10.54 | +122.014 | +8.249 | |
| 2448966.8853 | 0.14 | 0.02 | 36.6 | 2.1 | k | * | +231.9 | +57.97 | +34.557 | +10.592 | |
| 2448966.9105 | 0.56 | 0.03 | 17.1 | 0.4 | k | * | +185.8 | +10.54 | +110.738 | +9.199 | |
| 2448966.9105 | 0.18 | 0.01 | 35.8 | 2.3 | k | * | +303.0 | +60.61 | +58.062 | +12.829 | |
| 2448966.9343 | 0.58 | 0.04 | 17.2 | 0.4 | k | * | +189.7 | +10.54 | +117.133 | +11.042 | |

**Table C.1 cont.:**Table of results of anaylsis of $\beta$ Pic Ca II spectra

| HJD | Depth | error | Velocity | error | Ca line | Resolution | FWHM | error | Eq. width | error | Comments |
|---|---|---|---|---|---|---|---|---|---|---|---|
| 2448966.9343 | 0.22 | 0.02 | 35.3 | 2.3 | k | * | +318.8 | +55.34 | +74.667 | +15.572 | |
| 2448966.9610 | 0.50 | 0.01 | 16.3 | 0.4 | k | * | +177.9 | +13.18 | +94.666 | +7.732 | |
| 2448966.9610 | 0.22 | 0.01 | 34.9 | 2.5 | k | * | +361.0 | +61.92 | +84.540 | +15.970 | |
| 2448966.9910 | 0.52 | 0.06 | 17.4 | 0.4 | k | * | +185.8 | +15.81 | +102.828 | +15.694 | |
| 2448966.9910 | 0.24 | 0.02 | 35.4 | 3.1 | k | * | +383.4 | +68.51 | +97.948 | +20.558 | |
| 2448967.0131 | 0.55 | 0.05 | 17.5 | 0.3 | k | * | +191.0 | +11.86 | +111.846 | +13.106 | |
| 2448967.0131 | 0.24 | 0.02 | 35.6 | 2.6 | k | * | +371.5 | +57.97 | +94.918 | +17.873 | |
| 2448967.0373 | 0.53 | 0.08 | 17.8 | 0.5 | k | * | +191.0 | +17.13 | +107.779 | +20.142 | |
| 2448967.0373 | 0.23 | 0.02 | 34.7 | 4.0 | k | * | +355.7 | +81.69 | +87.093 | +22.764 | |
| 2448967.0609 | 0.53 | 0.04 | 17.2 | 0.6 | k | * | +197.6 | +13.18 | +111.496 | +11.952 | |
| 2448967.0609 | 0.23 | 0.02 | 35.4 | 2.0 | k | * | +279.3 | +47.43 | +68.384 | +13.888 | |
| 2448967.0825 | 0.57 | 0.03 | 17.9 | 0.5 | k | * | +189.7 | +11.86 | +115.114 | +10.012 | |
| 2448967.0825 | 0.19 | 0.02 | 36.3 | 2.0 | k | * | +262.2 | +52.70 | +53.027 | +12.808 | |
| 2448967.1039 | 0.49 | 0.09 | 16.6 | 0.6 | k | * | +187.1 | +17.13 | +97.583 | +21.318 | |
| 2448967.1039 | 0.24 | 0.03 | 31.6 | 3.7 | k | * | +321.5 | +69.83 | +82.128 | +21.910 | |
| 2448967.1256 | 0.41 | 0.13 | 15.7 | 0.6 | k | * | +159.4 | +27.67 | +69.576 | +26.771 | |
| 2448967.1256 | 0.31 | 0.05 | 28.6 | 3.9 | k | * | +303.0 | +69.83 | +99.995 | +29.940 | |
| 2448967.8836 | 0.60 | 0.02 | 19.2 | 0.3 | k | * | +181.8 | +7.91 | +116.124 | +6.772 | |
| 2448967.9046 | 0.54 | 0.02 | 19.2 | 0.3 | k | * | +168.6 | +9.22 | +96.938 | +6.816 | |
| 2448967.9046 | 0.05 | 0.02 | 40.0 | 5.0 | k | * | +171.3 | +65.88 | +9.116 | +5.385 | e |
| 2448967.9046 | 0.05 | 0.02 | -20.0 | 5.0 | k | * | +79.1 | +39.53 | +4.207 | +2.868 | e |
| 2448967.9257 | 0.59 | 0.03 | 19.1 | 0.3 | k | * | +172.6 | +9.22 | +108.396 | +8.511 | |
| 2448967.9257 | 0.06 | 0.02 | -20.0 | 5.0 | k | * | +79.1 | +39.53 | +5.049 | +3.230 | e |

**Table C.1 cont.:**Table of results of anaylsis of $\beta$ Pic Ca II spectra

| HJD | Depth | error | Velocity | error | Ca line | Resolution | FWHM | error | Eq. width | error | Comments |
|---|---|---|---|---|---|---|---|---|---|---|---|
| 2448967.9257 | 0.06 | 0.02 | 40.0 | 5.0 | k | * | +131.8 | +65.88 | +8.415 | +5.383 | e |
| 2448967.9469 | 0.06 | 0.02 | 19.7 | 0.3 | k | * | +172.6 | +7.91 | +11.023 | +3.948 | |
| 2448967.9469 | 0.05 | 0.02 | 40.0 | 5.0 | k | * | +131.8 | +65.88 | +7.012 | +4.780 | e |
| 2448967.9681 | 0.59 | 0.03 | 16.8 | 0.3 | k | * | +171.3 | +9.22 | +107.569 | +8.480 | |
| 2448967.9681 | 0.04 | 0.02 | 40.0 | 5.0 | k | * | +79.1 | +39.53 | +3.366 | +2.534 | e |
| 2448967.9893 | 0.55 | 0.01 | 19.5 | 0.2 | k | * | +184.5 | +5.27 | +107.989 | +3.893 | |
| 2448967.9893 | 0.05 | 0.02 | 43.0 | 5.0 | k | * | +131.8 | +65.88 | +7.012 | +4.780 | e |
| 2448968.0105 | 0.59 | 0.03 | 19.2 | 0.2 | k | * | +156.8 | +7.91 | +98.467 | +7.506 | |
| 2448968.0105 | 0.05 | 0.02 | 43.0 | 5.0 | k | * | +105.4 | +52.70 | +5.610 | +3.824 | e |
| 2448968.0317 | 0.59 | 0.03 | 19.5 | 0.3 | k | * | +163.4 | +7.91 | +102.604 | +7.666 | |
| 2448968.0317 | 0.05 | 0.02 | 43.0 | 5.0 | k | * | +105.4 | +52.70 | +5.610 | +3.824 | e |
| 2448968.0529 | 0.60 | 0.02 | 19.8 | 0.3 | k | * | +166.0 | +7.91 | +106.026 | +6.560 | |
| 2448968.0986 | 0.60 | 0.03 | 20.3 | 0.3 | k | * | +168.6 | +9.22 | +107.709 | +8.496 | |
| 2448968.1233 | 0.60 | 0.02 | 20.4 | 0.2 | k | * | +176.5 | +7.91 | +112.758 | +6.700 | |
| 2448969.0306 | 0.60 | 0.02 | 18.8 | 0.2 | k | * | +173.9 | +6.59 | +111.075 | +5.966 | |
| 2448969.0306 | 0.05 | 0.02 | 100.0 | 20.0 | k | * | +790.5 | 263.50 | +42.074 | +23.320 | e |
| 2448969.0539 | 0.64 | 0.03 | 19.4 | 0.3 | k | * | +166.0 | +9.22 | +113.094 | +8.751 | |
| 2448969.0539 | 0.03 | 0.02 | 100.0 | 20.0 | k | * | +790.5 | 263.50 | +25.244 | +20.030 | e |
| 2448969.0785 | 0.66 | 0.03 | 18.9 | 0.3 | k | * | +181.8 | +9.22 | +127.736 | +9.261 | |
| 2448969.0785 | 0.08 | 0.01 | 112.9 | 6.3 | k | * | 1085.6 | 227.93 | +92.450 | +24.047 | |
| 2448969.1047 | 0.61 | 0.03 | 19.1 | 0.3 | k | * | +170.0 | +9.22 | +110.360 | +8.603 | |
| 2448969.1047 | 0.05 | 0.02 | 130.0 | 20.0 | k | * | 1317.5 | 395.26 | +70.123 | +37.323 | e |
| 2448969.1350 | 0.63 | 0.03 | 19.0 | 0.2 | k | * | +163.4 | +7.91 | +109.560 | +7.918 | |

**Table C.1 cont.:**Table of results of anaylsis of $\beta$ Pic Ca II spectra

| HJD | Depth | error | Velocity | error | Ca line | Resolution | FWHM | error | Eq. width | error | Comments |
|---|---|---|---|---|---|---|---|---|---|---|---|
| 2448969.1350 | 0.03 | 0.02 | 140.0 | 20.0 | k | * | 1054.0 | 263.50 | +33.659 | +25.511 | e |
| 2448969.1664 | 0.63 | 0.03 | 19.4 | 0.3 | k | * | +167.3 | +9.22 | +112.211 | +8.701 | |
| 2448969.8945 | 0.61 | 0.03 | 20.3 | 0.3 | k | * | +180.5 | +9.22 | +117.204 | +8.848 | |
| 2448969.8945 | 0.09 | 0.01 | 74.7 | 5.9 | k | * | 1245.1 | 197.63 | +119.279 | +24.602 | uncertain |
| 2448969.9196 | 0.63 | 0.03 | 20.7 | 0.3 | k | * | +187.1 | +9.22 | +125.464 | +9.154 | |
| 2448969.9196 | 0.12 | 0.01 | 75.0 | 0.4 | k | * | +944.7 | 133.07 | +120.668 | +21.023 | uncertain |
| 2448969.9561 | 0.64 | 0.02 | 19.6 | 0.2 | k | * | +175.2 | +7.91 | +119.377 | +6.974 | |
| 2448969.9561 | 0.14 | 0.01 | 58.0 | 2.2 | k | * | +615.3 | +77.73 | +91.693 | +14.166 | |
| 2448969.9835 | 0.63 | 0.03 | 20.1 | 0.2 | k | * | +176.5 | +9.22 | +118.396 | +8.909 | |
| 2448969.9835 | 0.18 | 0.01 | 52.7 | 2.1 | k | * | +639.0 | +69.83 | +122.435 | +15.977 | |
| 2448970.0463 | 0.66 | 0.01 | 19.9 | 0.2 | k | * | +177.9 | +90.91 | +124.959 | +68.017 | |
| 2448970.0463 | 0.12 | 0.01 | 49.8 | 3.2 | k | * | +540.2 | 105.40 | +69.001 | +15.584 | |
| 2448970.0708 | 0.62 | 0.03 | 20.2 | 0.3 | k | * | +167.3 | +9.22 | +110.430 | +8.622 | |
| 2448970.0708 | 0.11 | 0.02 | 41.6 | 2.9 | k | * | +316.2 | +90.91 | +37.025 | +13.407 | cr hit |
| 2448970.1049 | 0.71 | 0.02 | 20.1 | 0.2 | k | * | +180.5 | +6.59 | +136.417 | +6.695 | |
| 2448970.1049 | 0.19 | 0.01 | 47.8 | 1.2 | k | * | +350.5 | +40.84 | +70.880 | +9.648 | |
| 2448970.9185 | 0.65 | 0.02 | 18.7 | 0.2 | k | * | +166.0 | +5.27 | +114.861 | +5.406 | |
| 2448970.9408 | 0.63 | 0.01 | 18.9 | 0.1 | k | * | +180.5 | +3.95 | +121.046 | +3.485 | |
| 2448970.9750 | 0.61 | 0.01 | 19.1 | 0.1 | k | * | +188.4 | +3.95 | +122.337 | +3.467 | |
| 2448970.9983 | 0.62 | 0.01 | 18.8 | 0.1 | k | * | +181.8 | +3.95 | +119.994 | +3.458 | |
| 2448970.9983 | 0.03 | 0.02 | -75.0 | 5.0 | k | * | +263.5 | +65.88 | +8.415 | +6.378 | e |
| 2448971.0483 | 0.55 | 0.01 | 18.8 | 0.2 | k | * | +187.1 | +5.27 | +109.532 | +3.909 | |
| 2448971.0483 | 0.03 | 0.02 | -75.0 | 5.0 | k | * | +263.5 | +65.88 | +8.415 | +6.378 | e |

**Table C.1 cont.:** Table of results of anaylsis of $\beta$ Pic Ca II spectra

| HJD | Depth | error | Velocity | error | Ca line | Resolution | FWHM | error | Eq. width | error | Comments |
|---|---|---|---|---|---|---|---|---|---|---|---|
| 2448971.0711 | 0.56 | 0.02 | 18.5 | 0.2 | k | * | +176.5 | +6.59 | +105.241 | +5.786 | |
| 2448971.0711 | 0.03 | 0.02 | -75.0 | 5.0 | k | * | +263.5 | +65.88 | +8.415 | +6.378 | e |
| 2448971.0947 | 0.53 | 0.02 | 18.3 | 0.2 | k | * | +184.5 | +6.59 | +104.063 | +5.755 | |
| 2448971.0947 | 0.05 | 0.02 | 40.0 | 5.0 | k | * | +131.8 | +65.88 | +7.012 | +4.780 | e |
| 2448971.1200 | 0.53 | 0.02 | 17.7 | 0.2 | k | * | +167.3 | +6.59 | +94.400 | +5.480 | |
| 2448972.0165 | 0.63 | 0.02 | 16.3 | 0.2 | k | * | +160.7 | +6.59 | +107.793 | +5.949 | |
| 2448972.0165 | 0.05 | 0.02 | -25.0 | 5.0 | k | * | +197.6 | +65.88 | +10.518 | +5.830 | e |
| 2448972.0427 | 0.63 | 0.04 | 17.8 | 0.4 | k | * | +193.7 | +13.18 | +129.882 | +12.865 | |
| 2448972.9090 | 0.65 | 0.03 | 16.3 | 0.3 | k | * | +155.5 | +7.91 | +107.569 | +7.863 | |
| 2448972.9090 | 0.15 | 0.02 | 74.1 | 2.1 | k | * | +487.5 | +65.88 | +77.837 | +15.730 | |
| 2448972.9611 | 0.63 | 0.02 | 16.0 | 0.2 | k | * | +167.3 | +5.27 | +112.211 | +5.342 | |
| 2448972.9611 | 0.14 | 0.01 | 65.7 | 1.7 | k | * | +820.8 | +63.24 | +122.323 | +13.680 | |
| 2448972.9870 | 0.61 | 0.02 | 15.7 | 0.2 | k | * | +155.5 | +6.59 | +100.949 | +5.757 | |
| 2448972.9870 | 0.11 | 0.01 | 63.1 | 2.4 | k | * | +747.0 | +86.96 | +87.471 | +13.752 | |
| 2448973.0335 | 0.57 | 0.02 | 15.8 | 0.2 | k | * | +158.1 | +6.59 | +95.928 | +5.562 | |
| 2448973.0335 | 0.14 | 0.01 | 53.0 | 1.9 | k | * | +577.1 | +68.51 | +85.999 | +12.684 | |
| 2448973.0556 | 0.53 | 0.01 | 15.6 | 0.3 | k | * | +160.7 | +9.22 | +90.683 | +5.831 | |
| 2448973.0556 | 0.15 | 0.01 | 54.1 | 1.7 | k | * | +483.5 | +59.29 | +77.205 | +11.470 | |
| 2448973.0788 | 0.56 | 0.02 | 15.7 | 0.2 | k | * | +156.8 | +6.59 | +93.460 | +5.486 | |
| 2448973.0788 | 0.18 | 0.01 | 56.2 | 1.2 | k | * | +492.8 | +42.16 | +94.414 | +10.253 | |
| 2448973.1010 | 0.50 | 0.03 | 15.5 | 0.3 | k | * | +148.9 | +10.54 | +79.239 | +7.828 | |
| 2448973.1010 | 0.18 | 0.02 | 58.8 | 1.7 | k | * | +496.7 | +55.34 | +95.171 | +15.940 | |
| 2448996.9081 | 0.82 | 0.02 | 12.2 | 0.2 | k | * | +180.5 | +5.27 | +157.552 | +6.381 | |

**Table C.1 cont.:**Table of results of anaylsis of $\beta$ Pic Ca II spectra

| HJD | Depth | error | Velocity | error | Ca line | Resolution | FWHM | error | Eq. width | error | Comments |
|---|---|---|---|---|---|---|---|---|---|---|---|
| 2449082.8962 | 0.15 | 0.01 | 9.0 | 0.6 | k | * | +259.6 | +2.64 | +41.443 | +2.975 | |
| 2449082.8962 | 0.10 | 0.01 | 17.9 | 2.1 | k | * | 1196.3 | +81.69 | +127.343 | +16.414 | |
| 2449082.9327 | 0.28 | 0.02 | 7.5 | 0.3 | k | * | +117.3 | +9.22 | +34.949 | +3.953 | |
| 2449082.9327 | 0.12 | 0.01 | 27.8 | 2.0 | k | * | +831.4 | +55.34 | +106.194 | +12.056 | |
| 2449284.9554 | 0.27 | 0.02 | 51.8 | 0.5 | k | * | +205.5 | +15.81 | +59.072 | +6.715 | |
| 2449284.9876 | 0.35 | 0.01 | 53.1 | 0.3 | k | * | +162.1 | +7.91 | +60.376 | +3.633 | |
| 2449284.9876 | 0.13 | 0.01 | 35.8 | 0.7 | k | * | +173.9 | +23.72 | +24.066 | +4.011 | |
| 2449285.0196 | 0.37 | 0.01 | 54.3 | 0.3 | k | * | +155.5 | +7.91 | +61.231 | +3.753 | |
| 2449285.0196 | 0.14 | 0.01 | 37.2 | 0.7 | k | * | +173.9 | +23.72 | +25.917 | +4.247 | |
| 2449285.0869 | 0.37 | 0.05 | 54.2 | 0.7 | k | * | +171.3 | +18.45 | +67.458 | +12.409 | |
| 2449285.0869 | 0.10 | 0.02 | 37.1 | 0.5 | k | * | +299.1 | 131.75 | +31.836 | +16.396 | |
| 2449285.1746 | 0.28 | 0.02 | 58.3 | 0.7 | h | * | +216.1 | +23.72 | +64.401 | +8.977 | |
| 2449285.1746 | 0.18 | 0.03 | 40.7 | 0.7 | h | * | +109.4 | +22.40 | +20.953 | +5.890 | |
| 2449285.9054 | * | * | * | * | k | * | * | * | * | * | |
| 2449285.9364 | * | * | * | * | h | * | * | * | * | * | |
| 2449285.9597 | * | * | * | * | k | * | * | * | * | * | |
| 2449285.9879 | * | * | * | * | h | * | * | * | * | * | |
| 2449286.0109 | * | * | * | * | k | * | * | * | * | * | |
| 2449286.0412 | * | * | * | * | h | * | * | * | * | * | |
| 2449286.0655 | * | * | * | * | h | * | * | * | * | * | |
| 2449286.0946 | * | * | * | * | k | * | * | * | * | * | |
| 2449286.1171 | 0.44 | 0.01 | 58.1 | 4.2 | h | * | 1226.6 | 151.52 | +574.504 | +76.810 | |
| 2449318.8883 | 0.09 | 0.03 | 20.8 | 1.8 | h | * | +130.4 | +55.34 | +12.496 | +7.177 | |

| HJD | Depth | error | Velocity | error | Ca line | Resolution | FWHM | error | Eq. width | error | Comments |
|---|---|---|---|---|---|---|---|---|---|---|---|
| 2449318.8883 | 0.05 | 0.02 | 70.0 | 5.0 | h | * | +329.4 | 131.75 | +17.531 | +10.557 | e |
| 2449318.9314 | 0.11 | 0.04 | 22.9 | 2.1 | k | * | +185.8 | +67.19 | +21.752 | +11.876 | |
| 2449318.9314 | 0.05 | 0.02 | -30.0 | 5.0 | k | * | +197.6 | +65.88 | +10.518 | +5.830 | e |
| 2449318.9858 | 0.09 | 0.04 | 22.6 | 2.2 | k | * | +133.1 | +69.83 | +12.748 | +9.332 | |
| 2449318.9858 | 0.03 | 0.02 | -30.0 | 5.0 | k | * | +131.8 | +65.88 | +4.207 | +3.732 | e |
| 2449319.0349 | 0.08 | 0.04 | 21.8 | 2.0 | k | * | +101.4 | +61.92 | +8.639 | +7.256 | |
| 2449319.0349 | 0.08 | 0.05 | -21.5 | 1.7 | k | * | +72.5 | +51.38 | +6.171 | +6.209 | |
| 2449319.1565 | * | * | * | * | k | * | * | * | * | * | |
| 2449319.9605 | 0.08 | 0.01 | -29.8 | 3.3 | k | * | +479.6 | 108.04 | +40.840 | +11.200 | |
| 2449319.9878 | 0.05 | 0.02 | -30.0 | 5.0 | k | * | +329.4 | 131.75 | +17.531 | +10.557 | e |
| 2449320.0258 | 0.11 | 0.03 | -35.6 | 3.0 | k | * | +337.3 | +96.18 | +39.493 | +16.588 | |
| 2449320.0667 | 0.12 | 0.02 | -33.9 | 2.2 | k | * | +371.5 | +71.15 | +47.459 | +12.825 | |
| 2449320.1037 | * | * | * | * | h | * | * | * | * | * | |
| 2449320.1411 | 0.10 | 0.02 | -34.9 | 2.5 | k | * | +365.0 | +81.69 | +38.848 | +12.413 | |
| 2449320.9000 | 0.08 | 0.01 | -40.5 | 0.8 | k | * | +204.2 | +26.35 | +17.391 | +3.326 | |
| 2449320.9341 | 0.05 | 0.01 | -43.7 | 1.9 | h | * | +235.8 | +59.29 | +12.552 | +4.292 | |
| 2449323.9758 | 0.15 | 0.03 | 32.4 | 1.0 | k | * | +147.6 | +38.21 | +23.561 | +8.206 | |
| 2449323.9758 | 0.09 | 0.01 | 60.6 | 4.3 | k | * | +519.1 | 147.56 | +49.731 | +16.157 | |
| 2449323.9758 | 0.04 | 0.02 | -30.0 | 5.0 | k | * | +263.5 | +65.88 | +11.220 | +6.677 | e |
| 2449324.0094 | 0.12 | 0.02 | 45.8 | 2.3 | k | * | +459.8 | +76.42 | +58.735 | +14.716 | |
| 2449324.0094 | 0.04 | 0.02 | -25.0 | 5.0 | k | * | +197.6 | +65.88 | +8.415 | +5.383 | e |
| 2449324.0667 | 0.11 | 0.03 | 38.0 | 1.7 | k | * | +160.7 | +52.70 | +18.821 | +8.544 | |
| 2449324.0667 | 0.09 | 0.03 | -17.5 | 2.1 | k | * | +154.2 | +64.56 | +14.768 | +8.415 | |

**Table C.1 cont.:**Table of results of anaylsis of $\beta$ Pic Ca II spectra

| HJD | Depth | error | Velocity | error | Ca line | Resolution | FWHM | error | Eq. width | error | Comments |
|---|---|---|---|---|---|---|---|---|---|---|---|
| 2449324.9411 | 0.07 | 0.02 | 36.4 | 2.5 | h | * | +272.7 | +80.37 | +20.322 | +8.879 | |
| 2449324.9729 | 0.12 | 0.02 | 34.8 | 1.3 | k | * | +198.9 | +42.16 | +25.413 | +7.293 | |
| 2449324.9729 | 0.12 | 0.02 | -23.9 | 1.5 | k | * | +245.1 | +48.75 | +31.303 | +8.648 | |
| 2449325.0018 | 0.04 | 0.02 | -25.7 | 3.7 | k | * | +256.9 | 115.94 | +10.939 | +7.843 | |
| 2449325.0018 | 0.08 | 0.02 | 35.7 | 1.6 | k | * | +188.4 | +51.38 | +16.044 | +6.319 | |
| 2449325.0328 | 0.05 | 0.02 | 35.9 | 3.8 | h | * | +287.2 | 118.58 | +15.287 | +9.354 | |
| 2449325.0618 | 0.04 | 0.01 | 39.9 | 4.2 | h | * | +357.0 | 134.39 | +15.203 | +7.312 | |
| 2449325.0900 | 0.08 | 0.04 | 36.1 | 1.7 | k | * | +102.8 | +52.70 | +8.751 | +6.672 | |
| 2449325.0900 | 0.10 | 0.03 | -18.5 | 1.0 | k | * | +130.4 | +31.62 | +13.884 | +5.701 | |
| 2449325.1376 | 0.03 | 0.02 | 37.7 | 6.6 | k | * | +234.5 | 206.85 | +7.489 | +8.814 | |
| 2449325.1376 | 0.10 | 0.04 | -16.8 | 1.4 | k | * | +97.5 | +42.16 | +10.378 | +6.508 | |
| 2449675.9272 | 0.11 | 0.02 | 27.0 | 1.4 | k | 0.107 | +272.7 | +44.80 | +31.934 | +8.329 | |
| 2449675.9545 | 0.10 | 0.02 | 22.3 | 1.5 | h | 0.114 | +196.3 | +48.75 | +20.897 | +7.093 | |
| 2449676.0498 | 0.10 | 0.01 | 30.6 | 1.7 | k | 0.109 | +413.7 | +55.34 | +44.037 | +7.829 | |
| 2449676.0805 | * | * | * | * | h | * | * | * | * | * | |
| 2449677.9828 | 0.18 | 0.01 | 8.4 | 0.3 | k | 0.107 | +131.8 | +10.54 | +25.244 | +2.617 | |
| 2449677.9828 | 0.14 | 0.01 | 63.2 | 1.1 | k | 0.107 | +920.9 | +42.16 | +137.245 | +12.395 | |
| 2449678.0100 | 0.08 | 0.01 | 63.2 | 4.4 | h | 0.113 | 1048.7 | 164.69 | +89.309 | +19.081 | |
| 2449678.0100 | 0.10 | 0.02 | 17.0 | 5.0 | h | 0.113 | +131.8 | +65.88 | +14.025 | +8.040 | |
| 2449678.9067 | 0.38 | 0.01 | 59.5 | 0.5 | k | 0.108 | +615.3 | +18.45 | +248.881 | +10.568 | |
| 2449678.9481 | 0.38 | 0.01 | 57.6 | 0.5 | k | 0.106 | +566.5 | +17.13 | +229.162 | +9.778 | |
| 2449678.9822 | 0.33 | 0.01 | 56.7 | 0.5 | k | 0.106 | +577.1 | +15.81 | +202.712 | +8.815 | |
| 2449679.0473 | 0.19 | 0.01 | 59.9 | 0.8 | h | 0.111 | +633.7 | +26.35 | +128.171 | +9.151 | |

**Table C.1 cont.:**Table of results of anaylsis of $\beta$ Pic Ca II spectra

| HJD | Depth | error | Velocity | error | Ca line | Resolution | FWHM | error | Eq. width | error | Comments |
|---|---|---|---|---|---|---|---|---|---|---|---|
| 2449679.0473 | 0.08 | 0.01 | 10.2 | 0.9 | h | 0.111 | +133.1 | +28.99 | +11.332 | +3.029 | |
| 2449679.1279 | 0.31 | 0.01 | 51.3 | 0.3 | k | 0.110 | +454.5 | +9.22 | +149.993 | +6.085 | |
| 2449679.0839 | 0.20 | 0.01 | 55.6 | 0.7 | h | 0.111 | +585.0 | +25.03 | +124.538 | +8.725 | |
| 2449679.0839 | 0.07 | 0.02 | 9.8 | 1.0 | h | 0.111 | +119.9 | +31.62 | +8.934 | +3.698 | |
| 2449679.8902 | 0.39 | 0.01 | 7.7 | 0.2 | k | 0.108 | +135.7 | +5.27 | +56.337 | +2.791 | |
| 2449679.8902 | 0.13 | 0.01 | 52.1 | 0.9 | k | 0.108 | +446.6 | +30.30 | +61.806 | +6.748 | |
| 2449679.9186 | 0.39 | 0.02 | 8.2 | 0.2 | k | 0.109 | +125.2 | +6.59 | +51.961 | +4.065 | |
| 2449679.9186 | 0.11 | 0.01 | 52.1 | 1.2 | k | 0.109 | +408.4 | +40.84 | +47.824 | +6.880 | |
| 2449679.9521 | 0.37 | 0.01 | 8.3 | 0.2 | k | 0.109 | +127.8 | +5.27 | +50.334 | +2.642 | |
| 2449679.9521 | 0.09 | 0.01 | 50.9 | 1.1 | k | 0.109 | +386.0 | +36.89 | +36.983 | +5.770 | |
| 2449679.9881 | 0.39 | 0.01 | 7.8 | 0.1 | k | 0.107 | +155.5 | +3.95 | +64.541 | +2.481 | |
| 2449679.9881 | 0.06 | 0.01 | 54.6 | 1.4 | k | 0.107 | +442.7 | +44.80 | +28.274 | +5.868 | |
| 2449680.0245 | 0.42 | 0.01 | 7.2 | 0.1 | k | 0.108 | +162.1 | +3.95 | +72.451 | +2.629 | |
| 2449680.0245 | 0.06 | 0.01 | 56.0 | 1.8 | k | 0.108 | +507.2 | +59.29 | +32.397 | +7.020 | |
| 2449680.0635 | 0.42 | 0.01 | 8.3 | 0.1 | k | 0.108 | +141.0 | +3.95 | +63.027 | +2.468 | |
| 2449680.0635 | 0.06 | 0.01 | 51.4 | 1.5 | k | 0.108 | +494.1 | +51.38 | +31.555 | +6.599 | |
| 2449680.0966 | 0.43 | 0.01 | 7.5 | 0.1 | k | 0.109 | +159.4 | +3.95 | +72.970 | +2.640 | |
| 2449680.0966 | 0.08 | 0.01 | 46.2 | 1.4 | k | 0.109 | +643.0 | +52.70 | +54.752 | +8.712 | |
| 2449680.1351 | 0.46 | 0.01 | 7.2 | 0.2 | k | 0.107 | +175.2 | +5.27 | +85.802 | +3.389 | |
| 2449680.1351 | 0.09 | 0.01 | 44.2 | 1.5 | k | 0.107 | +532.3 | +52.70 | +50.993 | +8.079 | |
| 2449680.8957 | 0.50 | 0.01 | 6.2 | 0.1 | k | 0.108 | +170.0 | +5.27 | +90.459 | +3.553 | |
| 2449680.8957 | 0.17 | 0.01 | 42.6 | 1.2 | k | 0.108 | +735.2 | +38.21 | +133.037 | +11.116 | |
| 2449680.9268 | 0.47 | 0.01 | 6.5 | 0.1 | k | 0.107 | +170.0 | +5.27 | +85.031 | +3.404 | |

**Table C.1 cont.:**Table of results of anaylsis of $\beta$ Pic Ca II spectra

| HJD | Depth | error | Velocity | error | Ca line | Resolution | FWHM | error | Eq. width | error | Comments |
|---|---|---|---|---|---|---|---|---|---|---|---|
| 2449680.9268 | 0.18 | 0.01 | 41.1 | 1.1 | k | 0.107 | +926.2 | +32.94 | +177.467 | +12.461 | |
| 2449680.9609 | 0.50 | 0.01 | 6.3 | 0.2 | k | 0.107 | +176.5 | +5.27 | +93.965 | +3.594 | |
| 2449680.9609 | 0.15 | 0.01 | 51.7 | 1.5 | k | 0.107 | +881.4 | +54.02 | +140.737 | +13.567 | |
| 2449680.9867 | 0.54 | 0.01 | 7.0 | 0.1 | k | 0.108 | +166.0 | +3.95 | +95.423 | +3.064 | |
| 2449680.9867 | 0.15 | 0.01 | 47.2 | 1.3 | k | 0.108 | +863.0 | +43.48 | +137.792 | +12.257 | |
| 2449681.0430 | 0.33 | 0.01 | 8.5 | 0.2 | h | 0.110 | +183.1 | +9.22 | +64.331 | +4.025 | |
| 2449681.0430 | 0.12 | 0.01 | 49.4 | 2.1 | h | 0.110 | +960.5 | +69.83 | +122.687 | +14.443 | |
| 2449681.0430 | 0.04 | 0.01 | -40.8 | 2.8 | h | 0.110 | +392.6 | +89.59 | +16.717 | +6.023 | |
| 2449681.0751 | 0.39 | 0.01 | 7.9 | 0.2 | h | 0.110 | +195.0 | +6.59 | +80.950 | +3.655 | |
| 2449681.0751 | 0.12 | 0.01 | 53.2 | 1.6 | h | 0.110 | +902.5 | +56.65 | +115.282 | +12.803 | |
| 2449681.0751 | 0.04 | 0.01 | -46.8 | 2.7 | h | 0.110 | +504.6 | +85.64 | +21.486 | +6.911 | |
| 2449681.1080 | 0.51 | 0.01 | 6.5 | 0.1 | k | 0.108 | +185.8 | +5.27 | +100.851 | +3.702 | |
| 2449681.1080 | 0.19 | 0.01 | 34.8 | 1.0 | k | 0.108 | +585.0 | +55.34 | +118.312 | +13.633 | |
| 2449681.1080 | 0.08 | 0.01 | 74.4 | 1.4 | k | 0.108 | +310.9 | +39.53 | +26.478 | +5.025 | |
| 2449681.1333 | 0.55 | 0.02 | 6.4 | 0.1 | k | 0.108 | +180.5 | +6.59 | +105.675 | +5.796 | |
| 2449681.1333 | 0.19 | 0.01 | 28.6 | 1.5 | k | 0.108 | +465.1 | +76.42 | +94.063 | +17.275 | |
| 2449681.1333 | 0.10 | 0.01 | 66.7 | 3.1 | k | 0.108 | +454.5 | +63.24 | +48.385 | +8.825 | |
| 2449682.9366 | 0.34 | 0.04 | 6.2 | 0.3 | k | 0.104 | +146.2 | +14.49 | +52.929 | +8.667 | |
| 2449682.9366 | 0.31 | 0.01 | 22.7 | 1.3 | k | 0.104 | +336.0 | +32.94 | +110.864 | +12.180 | |
| 2449682.9810 | 0.43 | 0.02 | 6.2 | 0.2 | k | 0.104 | +123.8 | +7.91 | +56.687 | +4.766 | |
| 2449682.9810 | 0.40 | 0.01 | 25.2 | 0.6 | k | 0.104 | +392.6 | +17.13 | +167.173 | +8.948 | |
| 2449682.9810 | 0.03 | 0.02 | 80.0 | 5.0 | k | 0.104 | +263.5 | +65.88 | +8.415 | +6.378 | e |
| 2449683.0298 | 0.22 | 0.01 | 23.9 | 1.2 | h | 0.108 | +453.2 | +30.30 | +106.138 | +9.135 | |

**Table C.1 cont.:**Table of results of anaylsis of $\beta$ Pic Ca II spectra

| HJD | Depth | error | Velocity | error | Ca line | Resolution | FWHM | error | Eq. width | error | Comments |
|---|---|---|---|---|---|---|---|---|---|---|---|
| 2449683.0298 | 0.16 | 0.02 | 6.6 | 0.5 | h | 0.108 | +125.2 | +21.08 | +21.317 | +4.759 | |
| 2449683.0758 | 0.26 | 0.02 | 7.2 | 0.4 | h | 0.108 | +144.9 | +14.49 | +40.110 | +5.387 | |
| 2449683.0758 | 0.26 | 0.01 | 27.6 | 1.0 | h | 0.108 | +384.7 | +28.99 | +106.475 | +9.588 | |
| 2449683.0758 | 0.03 | 0.02 | 70.0 | 5.0 | h | 0.108 | +263.5 | +65.88 | +8.415 | +6.378 | e |
| 2449683.1106 | 0.38 | 0.02 | 4.9 | 0.2 | k | 0.105 | +163.4 | +7.91 | +66.084 | +5.029 | |
| 2449683.1106 | 0.33 | 0.01 | 26.5 | 0.7 | k | 0.105 | +473.0 | +18.45 | +166.149 | +8.735 | |
| 2449683.1542 | 0.37 | 0.02 | 6.2 | 0.2 | k | 0.106 | +155.5 | +9.22 | +61.231 | +5.231 | |
| 2449683.1542 | 0.29 | 0.01 | 28.9 | 0.9 | k | 0.106 | +552.0 | +23.72 | +170.413 | +9.993 | |
| 2449683.9292 | 0.35 | 0.03 | 6.1 | 0.4 | k | 0.104 | +151.5 | +13.18 | +56.449 | +7.337 | |
| 2449683.9292 | 0.29 | 0.01 | 23.6 | 1.3 | k | 0.104 | +341.2 | +34.26 | +105.339 | +11.902 | |
| 2449826.8690 | 0.41 | 0.04 | 10.6 | 0.6 | k | 0.103 | +159.4 | +18.45 | +69.576 | +11.209 | |
| 2449826.8690 | 0.20 | 0.04 | -15.1 | 2.3 | k | 0.103 | +176.5 | +73.78 | +37.586 | +18.537 | e |
| 2449826.8690 | 0.05 | 0.03 | -73.4 | 5.3 | k | 0.103 | +204.2 | 171.28 | +10.869 | +11.931 | |
| 2449826.8967 | 0.56 | 0.03 | 10.1 | 0.3 | k | 0.102 | +179.2 | +7.91 | +106.811 | +7.891 | |
| 2449826.8967 | 0.21 | 0.03 | -13.4 | 0.5 | k | 0.102 | +119.9 | +17.13 | +26.801 | +5.764 | |
| 2449826.8967 | 0.07 | 0.02 | -77.5 | 2.3 | k | 0.102 | +249.0 | +75.10 | +18.555 | +8.205 | |
| 2449861.7986 | 0.34 | 0.05 | 15.2 | 0.4 | k | 0.104 | +131.8 | +65.88 | +47.684 | +26.455 | e |
| 2449861.7986 | 0.07 | 0.02 | 40.0 | 5.0 | k | 0.104 | +395.3 | +65.88 | +29.452 | +10.370 | e |
| 2449861.8263 | 0.31 | 0.01 | 13.9 | 0.3 | k | 0.104 | +229.2 | +10.54 | +75.649 | +4.523 | |
| 2449861.8554 | 0.26 | 0.02 | 16.1 | 0.5 | h | 0.109 | +148.9 | +14.49 | +41.204 | +5.442 | |
| 2449861.8810 | 0.26 | 0.02 | 16.6 | 0.4 | h | 0.109 | +151.5 | +13.18 | +41.934 | +5.182 | |
| 2449861.9320 | 0.28 | 0.01 | 15.2 | 0.7 | k | 0.106 | +453.2 | +22.40 | +135.085 | +8.768 | |
| 2449862.2831 | 0.32 | 0.02 | 30.3 | 0.8 | k | 0.105 | +455.9 | +26.35 | +155.280 | +14.072 | |

**Table C.1 cont.:**Table of results of anaylsis of $\beta$ Pic Ca II spectra

| HJD | Depth | error | Velocity | error | Ca line | Resolution | FWHM | error | Eq. width | error | Comments |
|---|---|---|---|---|---|---|---|---|---|---|---|
| 2449862.7653 | 0.31 | 0.01 | 20.5 | 0.5 | k | 0.105 | +375.5 | +15.81 | +123.907 | +6.996 | |
| 2449862.7653 | 0.05 | 0.02 | -35.0 | 5.0 | k | 0.105 | +158.1 | +65.88 | +8.415 | +5.174 | e |
| 2449862.7923 | 0.28 | 0.07 | 13.5 | 0.8 | k | 0.105 | +221.3 | +23.72 | +65.972 | +19.101 | |
| 2449862.7923 | 0.22 | 0.02 | 30.4 | 3.6 | k | 0.105 | +374.2 | +63.24 | +87.626 | +17.901 | |
| 2449862.7923 | 0.06 | 0.01 | -35.0 | 1.2 | k | 0.105 | +176.5 | +36.89 | +11.276 | +3.208 | |
| 2449862.8187 | 0.34 | 0.04 | 14.7 | 0.7 | k | 0.106 | +176.5 | +17.13 | +63.896 | +10.372 | |
| 2449862.8187 | 0.20 | 0.02 | 31.4 | 2.3 | k | 0.106 | +287.2 | +55.34 | +61.147 | +14.129 | |
| 2449862.8187 | 0.07 | 0.01 | -38.4 | 2.5 | k | 0.106 | +429.5 | +84.32 | +32.004 | +8.272 | |
| 2449862.8505 | 0.23 | 0.03 | 16.7 | 0.5 | h | 0.109 | +177.9 | +23.72 | +43.546 | +8.646 | |
| 2449862.8505 | 0.12 | 0.01 | 38.8 | 3.5 | h | 0.109 | +508.6 | +92.23 | +64.962 | +13.801 | |
| 2449862.8505 | 0.06 | 0.01 | -50.4 | 3.0 | h | 0.109 | +541.5 | 106.72 | +34.585 | +9.502 | |
| 2449862.8798 | 0.22 | 0.21 | 19.1 | 8.0 | h | 0.109 | +249.0 | +92.23 | +58.314 | +63.558 | |
| 2449862.8798 | 0.06 | 0.01 | -43.9 | 2.3 | h | 0.109 | +253.0 | +73.78 | +16.156 | +5.777 | |
| 2449862.9092 | 0.20 | 0.06 | 15.8 | 1.6 | h | 0.109 | +181.8 | +43.48 | +38.708 | +15.808 | |
| 2449862.9092 | 0.13 | 0.02 | 33.4 | 5.6 | h | 0.109 | +320.2 | 134.39 | +44.304 | +21.084 | |
| 2449862.9092 | 0.03 | 0.02 | -30.0 | 5.0 | h | 0.109 | +197.6 | +65.88 | +6.311 | +5.007 | |
| 2449877.7852 | 0.68 | 0.01 | 10.9 | 0.2 | k | 0.105 | +280.6 | +6.59 | +203.132 | +5.990 | |
| 2449877.7852 | 0.07 | 0.01 | 82.8 | 3.2 | k | 0.105 | +590.3 | 104.08 | +43.981 | +10.625 | |
| 2449877.8151 | 0.64 | 0.01 | 14.0 | 0.2 | h | 0.111 | +227.9 | +5.27 | +155.280 | +4.613 | |
| 2449877.8151 | 0.06 | 0.01 | 81.6 | 0.3 | h | 0.111 | +823.5 | 110.67 | +52.592 | +11.987 | |
| 2449877.8431 | 0.76 | 0.02 | 14.6 | 0.3 | k | 0.103 | +230.6 | +7.91 | +186.527 | +8.582 | |
| 2449877.8431 | 0.11 | 0.02 | 131.7 | 1.8 | k | 0.103 | +224.0 | +55.34 | +26.226 | +8.564 | |
| 2449877.8431 | 0.04 | 0.02 | 82.4 | 6.8 | k | 0.103 | +466.4 | 223.98 | +19.859 | +14.655 | |

| HJD | Depth | error | Velocity | error | Ca line | Resolution | FWHM | error | Eq. width | error | Comments |
|---|---|---|---|---|---|---|---|---|---|---|---|
| 2449877.8714 | 0.64 | 0.02 | 14.8 | 0.3 | h | 0.110 | +205.5 | +9.22 | +140.022 | +8.150 | |
| 2449877.8714 | 0.03 | 0.02 | 80.0 | 5.0 | h | 0.110 | +395.3 | 131.75 | +12.622 | +10.015 | e |
| 2449879.7706 | 0.79 | 0.02 | 10.5 | 0.2 | k | 0.105 | +250.3 | +6.59 | +210.509 | +8.183 | |
| 2449879.7706 | 0.15 | 0.02 | -27.4 | 1.0 | k | 0.105 | +198.9 | +31.62 | +31.766 | +7.015 | |
| 2449879.8047 | 0.63 | 0.04 | 15.1 | 0.5 | h | 0.108 | +241.1 | +17.13 | +161.690 | +16.399 | |
| 2449879.8314 | 1.00 | 0.16 | 13.6 | 0.6 | k | 0.102 | +175.2 | +28.99 | +186.527 | +45.695 | |
| 2449879.8314 | 0.20 | 0.07 | 33.2 | 12.2 | k | 0.102 | +533.6 | 285.90 | +113.599 | +77.391 | |
| 2449885.2652 | 0.73 | 0.02 | 11.8 | 0.4 | k | 0.106 | +343.9 | +13.18 | +267.211 | +13.398 | |
| 2449888.2630 | 0.58 | 0.04 | 11.5 | 0.3 | k | 0.105 | +234.5 | +14.49 | +144.790 | +14.273 | |
| 2449888.2630 | 0.45 | 0.02 | 34.8 | 1.5 | k | 0.105 | +631.1 | +31.62 | +302.300 | +21.553 | |
| 2449888.2887 | 0.58 | 0.03 | 10.2 | 0.2 | k | 0.106 | +202.9 | +10.54 | +125.268 | +9.775 | |
| 2449888.2887 | 0.46 | 0.01 | 33.0 | 1.1 | k | 0.106 | +631.1 | +23.72 | +309.018 | +14.281 | |
| 2449888.7457 | 0.76 | 0.02 | 9.5 | 0.3 | k | 0.105 | +260.9 | +7.91 | +211.042 | +9.016 | |
| 2449888.7457 | 0.37 | 0.01 | 42.6 | 1.2 | k | 0.105 | +498.0 | +59.29 | +196.148 | +25.490 | |
| 2449888.7457 | 0.06 | 0.01 | 85.7 | 11.2 | k | 0.105 | +537.5 | 246.38 | +34.332 | +17.824 | |
| 2449888.7724 | 0.83 | 0.01 | 11.4 | 0.2 | k | 0.104 | +266.1 | +7.91 | +235.136 | +8.023 | |
| 2449888.7724 | 0.38 | 0.04 | 43.2 | 0.6 | k | 0.104 | +355.7 | +34.26 | +143.892 | +21.852 | |
| 2449888.7724 | 0.09 | 0.01 | 79.6 | 13.9 | k | 0.104 | +927.5 | 324.11 | +88.860 | +34.684 | |
| 2449888.8005 | 0.59 | 0.01 | 10.3 | 0.2 | h | 0.108 | +283.3 | +6.59 | +177.902 | +5.450 | |
| 2449888.8005 | 0.25 | 0.01 | 44.6 | 0.5 | h | 0.108 | +326.7 | +18.45 | +86.953 | +6.404 | |
| 2449888.8005 | 0.08 | 0.01 | 82.5 | 1.4 | h | 0.108 | +317.5 | +46.11 | +27.039 | +5.515 | |
| 2449888.8269 | 0.70 | 0.01 | 8.5 | 0.4 | k | 0.104 | +345.2 | +11.86 | +257.211 | +10.186 | |
| 2449888.8269 | 0.37 | 0.01 | 44.8 | 0.7 | k | 0.104 | +358.4 | +22.40 | +141.144 | +10.231 | |

**Table C.1 cont.:**Table of results of anaylsis of $\beta$ Pic Ca II spectra

| HJD | Depth | error | Velocity | error | Ca line | Resolution | FWHM | error | Eq. width | error | Comments |
|---|---|---|---|---|---|---|---|---|---|---|---|
| 2449888.8269 | 0.06 | 0.02 | 80.0 | 5.0 | k | 0.104 | +263.5 | +65.88 | +16.830 | +7.465 | e |
| 2449888.8533 | 0.61 | 0.03 | 11.4 | 0.4 | h | 0.108 | +220.0 | +13.18 | +142.869 | +11.785 | |
| 2449888.8533 | 0.26 | 0.02 | 46.4 | 1.6 | h | 0.108 | +502.0 | +55.34 | +138.928 | +19.879 | |
| 2449888.8533 | 0.07 | 0.02 | 90.0 | 10.0 | h | 0.108 | +197.6 | +65.88 | +14.726 | +6.882 | e |
| 2449889.2130 | 0.74 | 0.04 | 11.2 | 0.6 | k | 0.104 | +263.5 | +17.13 | +207.564 | +18.679 | |
| 2449889.2130 | 0.44 | 0.02 | 45.0 | 1.7 | k | 0.104 | +519.1 | +54.02 | +243.130 | +29.389 | |
| 2449889.2414 | 0.69 | 0.02 | 10.9 | 0.4 | k | 0.105 | +309.6 | +10.54 | +227.409 | +10.823 | |
| 2449889.2414 | 0.36 | 0.01 | 49.4 | 0.8 | k | 0.105 | +453.2 | +28.99 | +173.681 | +12.891 | |
| 2449889.2664 | 0.72 | 0.02 | 10.4 | 0.3 | k | 0.103 | +293.8 | +9.22 | +225.179 | +10.047 | |
| 2449889.2664 | 0.36 | 0.01 | 48.0 | 0.8 | k | 0.103 | +495.4 | +27.67 | +189.837 | +12.605 | |
| 2449926.1284 | 0.71 | 0.04 | 10.4 | 0.3 | k | 0.106 | +166.0 | +10.54 | +125.464 | +11.337 | |
| 2449926.1284 | 0.24 | 0.02 | 37.4 | 1.7 | k | 0.106 | +416.3 | +59.29 | +106.363 | +18.681 | |
| 2449926.1542 | * | * | * | * | k | 0.107 | * | * | * | * | |
| 2449926.1835 | 0.63 | 0.02 | 10.1 | 0.2 | k | 0.106 | +188.4 | +7.91 | +126.348 | +7.076 | |
| 2449926.1835 | 0.24 | 0.02 | 35.8 | 0.6 | k | 0.106 | +237.2 | +22.40 | +60.586 | +8.123 | |
| 2449926.2190 | 0.46 | 0.01 | 11.0 | 0.2 | h | 0.111 | +184.5 | +7.91 | +90.318 | +4.620 | |
| 2449926.2190 | 0.11 | 0.01 | 39.7 | 1.3 | h | 0.111 | +318.8 | +46.11 | +37.333 | +6.789 | |
| 2449926.2725 | 0.48 | 0.01 | 11.6 | 0.2 | h | 0.111 | +175.2 | +5.27 | +89.533 | +3.487 | |
| 2449926.2725 | 0.14 | 0.01 | 38.4 | 0.7 | h | 0.111 | +234.5 | +23.72 | +34.949 | +4.606 | |
| 2449927.1118 | 0.71 | 0.03 | 10.0 | 0.3 | k | 0.103 | +191.0 | +9.22 | +144.383 | +9.860 | |
| 2449927.1118 | 0.21 | 0.02 | 31.1 | 1.8 | k | 0.103 | +325.4 | +64.56 | +72.746 | +17.041 | |
| 2449927.1118 | 0.06 | 0.01 | 84.3 | 7.9 | k | 0.103 | +957.8 | 271.41 | +61.175 | +21.408 | |
| 2449927.1118 | 0.07 | 0.02 | 135.0 | 7.0 | k | 0.103 | +197.6 | +65.88 | +14.726 | +6.882 | e |

| HJD | Depth | error | Velocity | error | Ca line | Resolution | FWHM | error | Eq. width | error | Comments |
|---|---|---|---|---|---|---|---|---|---|---|---|
| 2449927.1401 | 0.41 | 0.02 | 11.1 | 0.3 | h | 0.110 | +158.1 | +9.22 | +69.001 | +5.585 | |
| 2449927.1401 | 0.16 | 0.01 | 27.2 | 1.9 | h | 0.110 | +679.8 | +46.11 | +115.787 | +11.368 | |
| 2449927.1401 | 0.05 | 0.02 | 92.0 | 5.0 | h | 0.110 | +395.3 | +65.88 | +21.037 | +9.704 | e |
| 2449927.1401 | 0.03 | 0.01 | -45.0 | 5.0 | h | 0.110 | +263.5 | +65.88 | +8.415 | +3.732 | e |
| 2449927.1690 | 0.67 | 0.02 | 9.9 | 0.2 | k | 0.106 | +202.9 | +6.59 | +144.706 | +6.794 | |
| 2449927.1690 | 0.23 | 0.01 | 34.4 | 0.8 | k | 0.106 | +268.8 | +26.35 | +65.803 | +7.512 | |
| 2449927.1690 | 0.03 | 0.02 | 90.0 | 20.0 | k | 0.106 | +922.3 | 527.01 | +29.452 | +27.528 | e |
| 2449927.1992 | 0.54 | 0.02 | 11.3 | 0.2 | h | 0.110 | +214.8 | +6.59 | +123.445 | +6.319 | |
| 2449927.1992 | 0.16 | 0.02 | 34.9 | 0.7 | h | 0.110 | +181.8 | +25.03 | +30.966 | +6.130 | |
| 2449927.1992 | 0.08 | 0.01 | 73.2 | 5.4 | h | 0.110 | 1010.5 | 173.91 | +86.055 | +19.485 | |
| 2449927.1992 | 0.05 | 0.01 | -45.0 | 5.0 | h | 0.110 | +263.5 | +65.88 | +14.025 | +4.780 | e |
| 2449927.2277 | 0.70 | 0.01 | 10.1 | 0.1 | k | 0.106 | +212.1 | +5.27 | +158.057 | +4.822 | |
| 2449927.2277 | 0.19 | 0.02 | 33.3 | 0.5 | k | 0.106 | +208.2 | +19.76 | +42.102 | +6.353 | |
| 2449927.2277 | 0.10 | 0.01 | 68.1 | 3.9 | k | 0.106 | 1017.1 | 113.31 | +108.270 | +17.253 | |
| 2449927.2277 | 0.06 | 0.02 | -37.0 | 5.0 | k | 0.106 | +263.5 | +65.88 | +16.830 | +7.465 | e |
| 2449927.2548 | 0.52 | 0.01 | 10.9 | 0.1 | h | 0.109 | +227.9 | +5.27 | +126.165 | +4.039 | |
| 2449927.2548 | 0.15 | 0.01 | 10.9 | 0.1 | h | 0.109 | +175.2 | +18.45 | +27.979 | +3.711 | |
| 2449927.2548 | 0.09 | 0.01 | 68.5 | 2.7 | h | 0.109 | +852.4 | +86.96 | +81.665 | +13.113 | |
| 2449927.2548 | 0.05 | 0.01 | -44.4 | 1.6 | h | 0.109 | +404.5 | +52.70 | +21.528 | +5.470 | |
| 2449927.2807 | 0.69 | 0.01 | 10.0 | 0.1 | k | 0.106 | +230.6 | +3.95 | +169.347 | +4.047 | |
| 2449927.2807 | 0.24 | 0.01 | 33.2 | 0.4 | k | 0.106 | +205.5 | +13.18 | +52.508 | +4.273 | |
| 2449927.2807 | 0.12 | 0.01 | 71.1 | 1.3 | k | 0.106 | +648.2 | +46.11 | +82.801 | +9.658 | |
| 2449927.2807 | 0.05 | 0.01 | -34.0 | 1.6 | k | 0.106 | +351.8 | +52.70 | +18.723 | +4.980 | |

**Table C.1 cont.:** Table of results of anaylsis of $\beta$ Pic Ca II spectra

| HJD | Depth | error | Velocity | error | Ca line | Resolution | FWHM | error | Eq. width | error | Comments |
|---|---|---|---|---|---|---|---|---|---|---|---|
| 2449928.1047 | 0.57 | 0.05 | 10.9 | 0.4 | k | 0.105 | +185.8 | +17.13 | +112.716 | +15.269 | |
| 2449928.1047 | 0.22 | 0.02 | 37.0 | 3.6 | k | 0.105 | +617.9 | +98.81 | +144.706 | +28.335 | |
| 2449928.1350 | 0.39 | 0.02 | 12.0 | 0.3 | h | 0.110 | +239.8 | +13.18 | +99.547 | +7.964 | |
| 2449928.1350 | 0.12 | 0.01 | 46.8 | 3.1 | h | 0.110 | +691.7 | +94.86 | +88.355 | +15.093 | |
| 2449928.1350 | 0.05 | 0.02 | -45.0 | 5.0 | h | 0.110 | +131.8 | +65.88 | +7.012 | +4.780 | e |
| 2449928.1608 | 0.42 | 0.01 | 9.4 | 0.2 | k | 0.105 | +201.6 | +7.91 | +90.122 | +4.401 | |
| 2449928.1608 | 0.23 | 0.01 | 22.8 | 1.3 | k | 0.105 | +874.8 | +34.26 | +214.184 | +13.341 | |
| 2449928.1608 | 0.05 | 0.01 | -38.3 | 2.4 | k | 0.105 | +316.2 | +77.73 | +16.830 | +5.678 | |
| 2449928.1878 | 0.46 | 0.02 | 11.5 | 0.2 | h | 0.110 | +210.8 | +10.54 | +103.221 | +7.281 | |
| 2449928.1878 | 0.14 | 0.01 | 41.4 | 2.5 | h | 0.110 | +610.0 | +72.46 | +90.907 | +13.414 | |
| 2449928.1878 | 0.06 | 0.01 | -37.9 | 2.2 | h | 0.110 | +329.4 | +71.15 | +21.037 | +6.110 | |
| 2449928.2150 | 0.65 | 0.05 | 10.0 | 0.2 | k | 0.105 | +224.0 | +39.53 | +154.972 | +31.757 | e |
| 2449928.2150 | 0.20 | 0.05 | 38.1 | 7.5 | k | 0.105 | +527.0 | 131.75 | +112.197 | +42.226 | e |
| 2449928.2150 | 0.07 | 0.02 | -25.0 | 5.0 | k | 0.105 | +329.4 | +65.88 | +24.543 | +9.112 | e |
| 2449928.2408 | 0.47 | 0.02 | 10.9 | 0.2 | h | 0.110 | +217.4 | +9.22 | +108.761 | +6.957 | |
| 2449928.2408 | 0.14 | 0.01 | 45.8 | 2.5 | h | 0.110 | +762.8 | +73.78 | +113.683 | +14.550 | |
| 2449928.2408 | 0.06 | 0.01 | -36.6 | 2.3 | h | 0.110 | +407.1 | +75.10 | +26.002 | +6.881 | |
| 2449928.2678 | 0.59 | 0.03 | 9.8 | 0.2 | k | 0.105 | +224.0 | +11.86 | +140.667 | +10.992 | |
| 2449928.2678 | 0.22 | 0.01 | 37.1 | 2.6 | k | 0.105 | +658.8 | +67.19 | +154.271 | +18.339 | |
| 2449928.2678 | 0.10 | 0.01 | -27.7 | 1.8 | k | 0.105 | +329.4 | +56.65 | +35.061 | +7.426 | e |
| 2449929.0915 | 0.69 | 0.03 | 9.6 | 0.3 | k | 0.105 | +179.2 | +10.54 | +131.607 | +10.248 | |
| 2449929.0915 | 0.17 | 0.03 | 37.1 | 1.2 | k | 0.105 | +227.9 | +40.84 | +41.246 | +11.042 | |
| 2449929.0915 | 0.14 | 0.02 | -19.6 | 1.9 | k | 0.105 | +314.9 | +67.19 | +46.926 | +12.828 | uncertain |

**Table C.1 cont.:**Table of results of anaylsis of $\beta$ Pic Ca II spectra

| HJD | Depth | error | Velocity | error | Ca line | Resolution | FWHM | error | Eq. width | error | Comments |
|---|---|---|---|---|---|---|---|---|---|---|---|
| 2449929.1183 | 0.44 | 0.02 | 11.2 | 0.3 | h | 0.111 | +205.5 | +9.22 | +96.265 | +6.545 | |
| 2449929.1183 | 0.08 | 0.02 | 39.5 | 1.5 | h | 0.111 | +192.4 | +48.75 | +16.381 | +6.207 | |
| 2449929.1464 | 0.70 | 0.02 | 10.0 | 0.2 | k | 0.105 | +202.9 | +6.59 | +151.185 | +6.960 | |
| 2449929.1464 | 0.19 | 0.02 | 39.1 | 7.9 | k | 0.105 | +241.1 | +26.35 | +48.764 | +7.877 | |
| 2449929.1464 | 0.09 | 0.02 | 127.0 | 8.6 | k | 0.105 | +462.5 | 263.50 | +44.304 | +28.844 | e |
| 2449929.1464 | 0.15 | 0.02 | -18.7 | 5.0 | k | 0.105 | +395.3 | +65.88 | +63.111 | +14.339 | e |
| 2449929.1730 | 0.43 | 0.01 | 10.5 | 0.2 | h | 0.111 | +237.2 | +6.59 | +108.550 | +4.186 | |
| 2449929.1730 | 0.07 | 0.01 | 40.2 | 0.9 | h | 0.111 | +160.7 | +28.99 | +11.977 | +2.933 | |
| 2449929.2064 | 0.61 | 0.03 | 9.8 | 0.2 | k | 0.104 | +192.4 | +7.91 | +124.903 | +8.521 | |
| 2449929.2064 | 0.16 | 0.01 | 38.9 | 0.6 | k | 0.104 | +260.9 | +19.76 | +44.430 | +4.645 | |
| 2449929.2064 | 0.07 | 0.01 | 129.2 | 2.6 | k | 0.104 | +874.8 | +97.50 | +65.186 | +12.573 | uncertain |
| 2449929.2064 | 0.18 | 0.01 | -12.2 | 2.2 | k | 0.104 | +486.2 | +56.65 | +93.151 | +12.801 | |
| 2449929.2309 | 0.44 | 0.01 | 11.4 | 0.2 | h | 0.110 | +168.6 | +6.59 | +78.987 | +3.800 | |
| 2449929.2309 | 0.09 | 0.01 | 37.4 | 0.8 | h | 0.110 | +220.0 | +27.67 | +21.079 | +3.765 | |
| 2449929.2552 | 0.50 | 0.03 | 9.5 | 0.2 | k | 0.105 | +206.9 | +10.54 | +110.093 | +9.225 | |
| 2449929.2552 | 0.20 | 0.02 | 38.5 | 0.5 | k | 0.105 | +189.7 | +22.40 | +40.391 | +6.652 | |
| 2449929.2552 | 0.06 | 0.01 | 131.7 | 2.3 | k | 0.105 | +720.7 | +84.32 | +46.029 | +9.978 | uncertain |
| 2449929.2798 | 0.42 | 0.02 | 11.6 | 0.2 | h | 0.110 | +171.3 | +6.59 | +76.574 | +4.990 | |
| 2449929.2798 | 0.12 | 0.01 | 38.1 | 0.5 | h | 0.110 | +233.2 | +17.13 | +29.788 | +3.522 | |
| 2449929.2798 | 0.07 | 0.01 | -13.0 | 5.0 | h | 0.110 | +409.7 | 108.04 | +30.532 | +9.746 | |
| 2449929.2798 | 0.04 | 0.01 | 148.0 | 2.0 | h | 0.110 | +399.2 | +65.88 | +16.998 | +5.420 | |
| 2449930.1024 | 0.67 | 0.02 | 8.8 | 0.3 | k | 0.105 | +226.6 | +10.54 | +161.619 | +9.508 | |
| 2449930.1024 | 0.35 | 0.02 | 38.7 | 0.7 | k | 0.105 | +274.0 | +25.03 | +102.099 | +11.710 | |

**Table C.1 cont.:**Table of results of anaylsis of $\beta$ Pic Ca II spectra

| HJD | Depth | error | Velocity | error | Ca line | Resolution | FWHM | error | Eq. width | error | Comments |
|---|---|---|---|---|---|---|---|---|---|---|---|
| 2449930.1024 | 0.08 | 0.01 | 82.4 | 5.2 | k | 0.105 | +639.0 | 181.82 | +54.415 | +18.002 | |
| 2449930.1024 | 0.08 | 0.02 | -29.2 | 2.2 | k | 0.105 | +328.1 | +71.15 | +27.937 | +9.842 | |
| 2449930.1279 | 0.48 | 0.02 | 11.7 | 0.2 | h | 0.111 | +181.8 | +10.54 | +92.899 | +7.060 | |
| 2449930.1279 | 0.15 | 0.02 | 39.0 | 0.5 | h | 0.111 | +97.5 | +19.76 | +15.567 | +4.021 | |
| 2449930.1279 | 0.08 | 0.01 | 54.5 | 5.0 | h | 0.111 | +819.5 | +13.18 | +69.786 | +9.362 | |
| 2449930.1279 | 0.03 | 0.01 | -30.0 | 5.0 | h | 0.111 | +197.6 | +65.88 | +6.311 | +3.167 | e |
| 2449930.1527 | 0.67 | 0.01 | 9.3 | 0.1 | k | 0.105 | +195.0 | +5.27 | +139.068 | +4.571 | |
| 2449930.1527 | 0.36 | 0.01 | 39.0 | 0.4 | k | 0.105 | +263.5 | +13.18 | +100.977 | +6.148 | |
| 2449930.1527 | 0.07 | 0.01 | 79.1 | 3.7 | k | 0.105 | +648.2 | 123.85 | +48.301 | +12.266 | |
| 2449930.1527 | 0.07 | 0.01 | -28.6 | 1.9 | k | 0.105 | +391.3 | +63.24 | +29.157 | +6.695 | |
| 2449930.2006 | 0.51 | 0.01 | 11.3 | 0.1 | h | 0.111 | +195.0 | +3.95 | +105.858 | +3.178 | |
| 2449930.2006 | 0.22 | 0.01 | 38.8 | 0.3 | h | 0.111 | +216.1 | +11.86 | +50.601 | +3.838 | |
| 2449930.2006 | 0.06 | 0.01 | 75.5 | 2.4 | h | 0.111 | +621.9 | +81.69 | +39.718 | +8.972 | |
| 2449930.2006 | 0.04 | 0.01 | -34.6 | 1.8 | h | 0.111 | +372.9 | +57.97 | +15.876 | +4.975 | |
| 2449930.2277 | 0.62 | 0.01 | 8.2 | 0.2 | k | 0.104 | +229.2 | +5.27 | +151.297 | +4.523 | |
| 2449930.2277 | 0.43 | 0.01 | 38.2 | 0.3 | k | 0.104 | +224.0 | +10.54 | +102.520 | +5.729 | |
| 2449930.2277 | 0.05 | 0.01 | 70.6 | 3.9 | k | 0.104 | +436.1 | 133.07 | +23.211 | +9.014 | |
| 2449930.2525 | 0.44 | 0.01 | 10.4 | 0.2 | h | 0.110 | +212.1 | +6.59 | +99.350 | +4.070 | |
| 2449930.2525 | 0.22 | 0.01 | 39.0 | 0.3 | h | 0.110 | +183.1 | +11.86 | +42.887 | +3.612 | |
| 2449930.2525 | 0.05 | 0.01 | 57.4 | 8.3 | h | 0.110 | 1029.0 | 189.72 | +54.766 | +15.858 | |
| 2449930.2525 | 0.03 | 0.01 | -37.0 | 5.0 | h | 0.110 | +355.7 | +65.88 | +11.360 | +4.611 | e |
| 2449930.2773 | 0.59 | 0.01 | 8.5 | 0.2 | k | 0.104 | +253.0 | +6.59 | +158.871 | +5.255 | |
| 2449930.2773 | 0.39 | 0.01 | 38.8 | 0.3 | k | 0.104 | +208.2 | +10.54 | +86.420 | +5.221 | |

| HJD | Depth | error | Velocity | error | Ca line | Resolution | FWHM | error | Eq. width | error | Comments |
|---|---|---|---|---|---|---|---|---|---|---|---|
| 2449930.2773 | 0.04 | 0.01 | 70.0 | 5.0 | k | 0.104 | +395.3 | +65.88 | +16.830 | +5.383 | e |
| 2449930.2773 | 0.05 | 0.01 | -20.0 | 5.0 | k | 0.104 | +263.5 | +65.88 | +14.025 | +4.780 | e |
| 2449931.1060 | 0.66 | 0.02 | 9.5 | 0.2 | k | 0.105 | +181.8 | +6.59 | +127.736 | +6.423 | |
| 2449931.1060 | 0.25 | 0.02 | 37.6 | 0.6 | k | 0.105 | +255.6 | +21.08 | +68.019 | +8.320 | |
| 2449931.1060 | 0.07 | 0.02 | -30.0 | 5.0 | k | 0.105 | +263.5 | +65.88 | +19.634 | +7.935 | e |
| 2449931.1359 | 0.55 | 0.01 | 11.4 | 0.2 | h | 0.110 | +188.4 | +5.27 | +110.303 | +3.917 | |
| 2449931.1359 | 0.18 | 0.01 | 40.3 | 0.6 | h | 0.110 | +274.0 | +21.08 | +52.508 | +5.304 | |
| 2449931.1631 | 0.59 | 0.02 | 8.7 | 0.1 | k | 0.104 | +206.9 | +6.59 | +129.910 | +6.432 | |
| 2449931.1631 | 0.25 | 0.01 | 37.3 | 0.4 | k | 0.104 | +233.2 | +11.86 | +62.059 | +4.274 | |
| 2449931.1631 | 0.07 | 0.01 | -22.6 | 4.3 | k | 0.104 | +708.8 | 126.48 | +52.817 | +12.851 | |
| 2449931.1886 | 0.53 | 0.01 | 11.4 | 0.2 | h | 0.110 | +173.9 | +6.59 | +98.116 | +4.420 | |
| 2449931.1886 | 0.14 | 0.01 | 38.4 | 0.9 | h | 0.110 | +276.7 | +30.30 | +41.232 | +5.739 | |
| 2449931.1886 | 0.05 | 0.01 | -40.4 | 2.7 | h | 0.110 | +351.8 | +86.96 | +18.723 | +6.337 | |
| 2449931.2204 | 0.64 | 0.01 | 9.3 | 0.1 | k | 0.107 | +198.9 | +3.95 | +135.534 | +3.647 | |
| 2449931.2204 | 0.23 | 0.01 | 36.4 | 0.4 | k | 0.107 | +246.4 | +11.86 | +60.320 | +4.165 | |
| 2449931.2204 | 0.08 | 0.01 | -31.5 | 1.2 | k | 0.107 | +350.5 | +38.21 | +29.844 | +5.269 | |
| 2449931.2204 | 0.03 | 0.01 | -80.0 | 2.7 | k | 0.107 | +296.4 | +85.64 | +9.467 | +4.445 | |
| 2449931.2460 | 0.41 | 0.03 | 9.8 | 0.2 | h | 0.110 | +185.8 | +13.18 | +81.076 | +8.795 | |
| 2449931.2460 | 0.14 | 0.01 | 30.7 | 3.1 | h | 0.110 | +500.7 | +72.46 | +74.611 | +12.819 | |
| 2449931.2460 | 0.06 | 0.01 | -40.0 | 2.0 | h | 0.110 | +279.3 | +61.92 | +17.839 | +5.267 | |
| 2449931.2728 | 0.60 | 0.02 | 8.4 | 0.3 | k | 0.105 | +237.2 | +9.22 | +151.466 | +8.258 | |
| 2449931.2728 | 0.19 | 0.02 | 35.8 | 1.0 | k | 0.105 | +263.5 | +31.62 | +53.293 | +9.056 | |
| 2449931.2728 | 0.07 | 0.02 | -35.4 | 5.0 | k | 0.105 | +204.2 | +65.88 | +15.217 | +6.980 | e |

**Table C.1 cont.:**Table of results of anaylsis of $\beta$ Pic Ca II spectra

| HJD | Depth | error | Velocity | error | Ca line | Resolution | FWHM | error | Eq. width | error | Comments |
|---|---|---|---|---|---|---|---|---|---|---|---|
| 2449968.0409 | 0.50 | 0.01 | 10.1 | 0.2 | k | 0.103 | +210.8 | +6.59 | +112.197 | +4.431 | |
| 2449968.0409 | 0.08 | 0.01 | -25.9 | 1.6 | k | 0.103 | +322.8 | +55.34 | +27.488 | +6.208 | |
| 2449968.0800 | 0.36 | 0.03 | 13.7 | 0.5 | h | 0.108 | +176.5 | +14.49 | +67.655 | +8.424 | |
| 2449968.0800 | 0.07 | 0.02 | -42.2 | 3.4 | h | 0.108 | +333.3 | 108.04 | +24.838 | +11.424 | |
| 2449968.1141 | 0.56 | 0.02 | 11.6 | 0.3 | k | 0.104 | +189.7 | +7.91 | +113.094 | +6.607 | |
| 2449968.1141 | 0.09 | 0.02 | -28.5 | 2.1 | k | 0.104 | +329.4 | +69.83 | +31.555 | +10.317 | |
| 2449968.1467 | 0.34 | 0.02 | 13.2 | 0.3 | h | 0.109 | +179.2 | +10.54 | +64.850 | +5.743 | |
| 2449968.1467 | 0.03 | 0.01 | -35.0 | 5.0 | h | 0.109 | +197.6 | +65.88 | +6.311 | +3.167 | e |
| 2449968.1755 | 0.49 | 0.01 | 10.5 | 0.3 | k | 0.103 | +200.3 | +7.91 | +104.455 | +4.941 | |
| 2449968.1755 | 0.11 | 0.01 | -23.9 | 1.6 | k | 0.103 | +415.0 | +55.34 | +48.595 | +8.348 | |
| 2449968.2079 | 0.35 | 0.03 | 12.2 | 0.4 | h | 0.108 | +142.3 | +13.18 | +53.013 | +7.120 | |
| 2449968.2079 | 0.12 | 0.02 | -42.7 | 2.3 | h | 0.108 | +438.7 | +77.73 | +56.042 | +14.511 | |
| 2449969.0703 | 0.52 | 0.02 | 9.5 | 0.3 | k | 0.105 | +226.6 | +9.22 | +125.436 | +7.477 | |
| 2449969.0703 | 0.28 | 0.01 | -22.8 | 0.7 | k | 0.105 | +346.5 | +22.40 | +103.277 | +8.119 | |
| 2449969.0976 | 0.41 | 0.01 | 10.6 | 0.3 | h | 0.108 | +239.8 | +10.54 | +104.652 | +5.600 | |
| 2449969.0976 | 0.06 | 0.02 | 40.0 | 5.0 | h | 0.108 | +263.5 | +65.88 | +16.830 | +7.465 | e |
| 2449969.0976 | 0.05 | 0.01 | 75.2 | 3.2 | h | 0.108 | +639.0 | 113.31 | +34.010 | +9.677 | |
| 2449969.0976 | 0.19 | 0.01 | -24.9 | 0.7 | h | 0.108 | +258.2 | +22.40 | +52.228 | +5.640 | |
| 2449969.1248 | 0.59 | 0.03 | 8.8 | 0.2 | k | 0.104 | +162.1 | +10.54 | +101.777 | +8.944 | |
| 2449969.1248 | 0.34 | 0.03 | -25.1 | 0.6 | k | 0.104 | +262.2 | +26.35 | +94.890 | +13.509 | |
| 2449969.1248 | 0.09 | 0.01 | 26.3 | 10.0 | k | 0.104 | +980.2 | 223.98 | +93.909 | +25.399 | |
| 2449969.1508 | 0.42 | 0.03 | 8.4 | 0.2 | h | 0.108 | +139.7 | +9.22 | +62.438 | +6.466 | |
| 2449969.1508 | 0.15 | 0.02 | 19.9 | 2.4 | h | 0.108 | +382.1 | +43.48 | +61.007 | +11.384 | |

**Table C.1 cont.:**Table of results of anaylsis of $\beta$ Pic Ca II spectra

| HJD | Depth | error | Velocity | error | Ca line | Resolution | FWHM | error | Eq. width | error | Comments |
|---|---|---|---|---|---|---|---|---|---|---|---|
| 2449969.1508 | 0.22 | 0.01 | -25.6 | 0.5 | h | 0.108 | +308.3 | +18.45 | +72.199 | +5.775 | |
| 2449969.1508 | 0.08 | 0.01 | 66.6 | 1.2 | h | 0.108 | +283.3 | +38.21 | +24.122 | +4.722 | |
| 2449969.1783 | 0.63 | 0.02 | 9.9 | 0.3 | k | 0.105 | +227.9 | +10.54 | +152.854 | +9.127 | |
| 2449969.1783 | 0.37 | 0.02 | -24.0 | 0.6 | k | 0.105 | +300.4 | +19.76 | +118.312 | +10.724 | |
| 2449969.1783 | 0.12 | 0.02 | 35.0 | 5.0 | k | 0.105 | +158.1 | +65.88 | +20.195 | +9.648 | e |
| 2449969.1783 | 0.07 | 0.02 | 75.0 | 5.0 | k | 0.105 | +658.8 | 131.75 | +49.086 | +18.223 | e |
| 2449969.2040 | 0.45 | 0.02 | 11.4 | 0.4 | h | 0.108 | +259.6 | +11.86 | +124.328 | +8.435 | |
| 2449969.2040 | 0.25 | 0.02 | -25.3 | 0.7 | h | 0.108 | +295.1 | +22.40 | +78.538 | +9.219 | |
| 2449969.2040 | 0.05 | 0.01 | 65.0 | 5.0 | h | 0.108 | +592.9 | 131.75 | +31.555 | +10.043 | e |
| 2449969.2040 | 0.08 | 0.02 | 37.0 | 5.0 | h | 0.108 | +197.6 | +65.88 | +16.830 | +7.465 | e |
| 2449969.2290 | 0.58 | 0.02 | 8.5 | 0.2 | k | 0.105 | +171.3 | +9.22 | +105.745 | +7.198 | |
| 2449969.2290 | 0.35 | 0.02 | -25.4 | 0.5 | k | 0.105 | +284.6 | +19.76 | +106.026 | +10.150 | |
| 2449969.2290 | 0.20 | 0.01 | 33.2 | 3.9 | k | 0.105 | 1036.9 | 101.45 | +220.747 | +25.819 | |
| 2449969.2545 | 0.42 | 0.02 | 9.3 | 0.2 | h | 0.108 | +143.6 | +6.59 | +64.205 | +4.519 | |
| 2449969.2545 | 0.19 | 0.01 | -26.2 | 0.6 | h | 0.108 | +239.8 | +21.08 | +48.497 | +5.290 | |
| 2449969.2545 | 0.13 | 0.01 | 27.4 | 3.2 | h | 0.108 | 1538.9 | +85.64 | +212.949 | +21.522 | |
| 2449970.0541 | 0.47 | 0.01 | 8.6 | 0.2 | k | 0.103 | +187.1 | +6.59 | +93.600 | +4.099 | |
| 2449970.0541 | 0.22 | 0.01 | -20.6 | 0.7 | k | 0.103 | +421.6 | +25.03 | +98.733 | +7.859 | |
| 2449970.0541 | 0.15 | 0.01 | 85.7 | 1.3 | k | 0.103 | 1090.9 | +47.43 | +174.186 | +14.758 | |
| 2449970.0811 | 0.28 | 0.01 | 10.4 | 0.3 | h | 0.108 | +181.8 | +10.54 | +54.191 | +3.928 | |
| 2449970.0811 | 0.11 | 0.01 | -22.4 | 1.2 | h | 0.108 | +422.9 | +42.16 | +49.521 | +7.112 | |
| 2449970.0811 | 0.11 | 0.01 | 90.9 | 2.0 | h | 0.108 | 1258.2 | +73.78 | +147.328 | +16.966 | |
| 2449970.1065 | 0.38 | 0.02 | 8.2 | 0.2 | k | 0.104 | +122.5 | +7.91 | +49.563 | +4.393 | |

**Table C.1 cont.:**Table of results of anaylsis of $\beta$ Pic Ca II spectra

| HJD | Depth | error | Velocity | error | Ca line | Resolution | FWHM | error | Eq. width | error | Comments |
|---|---|---|---|---|---|---|---|---|---|---|---|
| 2449970.1065 | 0.20 | 0.00 | -27.0 | 0.0 | k | 0.104 | +143.6 | +0.00 | +30.574 | +0.000 | |
| 2449970.1065 | 0.14 | 0.01 | 66.4 | 1.6 | k | 0.104 | +500.7 | +51.38 | +74.611 | +9.931 | |
| 2449970.1065 | 0.22 | 0.01 | -11.9 | 1.2 | k | 0.104 | +683.8 | +32.94 | +160.133 | +11.290 | |
| 2449970.1332 | 0.27 | 0.01 | 10.7 | 0.3 | h | 0.108 | +170.0 | +9.22 | +48.848 | +3.416 | |
| 2449970.1332 | 0.11 | 0.01 | -22.3 | 0.1 | h | 0.108 | +336.0 | +35.57 | +39.339 | +5.844 | |
| 2449970.1332 | 0.07 | 0.01 | 70.0 | 2.9 | h | 0.108 | +552.0 | +85.64 | +41.134 | +9.234 | |
| 2449970.1332 | 0.05 | 0.01 | 141.7 | 5.6 | h | 0.108 | +964.4 | 189.72 | +51.330 | +15.329 | |
| 2449970.1598 | 0.45 | 0.01 | 8.1 | 0.2 | k | 0.104 | +168.6 | +5.27 | +80.782 | +3.297 | |
| 2449970.1598 | 0.18 | 0.01 | -21.9 | 0.6 | k | 0.104 | +349.1 | +21.08 | +66.897 | +5.843 | |
| 2449970.1598 | 0.11 | 0.01 | 71.1 | 1.1 | k | 0.104 | +519.1 | +39.53 | +60.783 | +7.673 | |
| 2449970.1598 | 0.02 | 0.01 | 130.0 | 5.0 | k | 0.104 | +263.5 | +65.88 | +5.610 | +3.338 | e |
| 2449970.1888 | 0.29 | 0.01 | 10.5 | 0.3 | h | 0.107 | +156.8 | +9.22 | +48.399 | +3.513 | |
| 2449970.1888 | 0.10 | 0.01 | 79.6 | 1.6 | h | 0.107 | +603.4 | +51.38 | +64.233 | +8.981 | |
| 2449970.1888 | 0.10 | 0.01 | -25.0 | 1.0 | h | 0.107 | +241.1 | +31.62 | +25.665 | +4.506 | |
| 2449970.1888 | 0.04 | 0.01 | 140.0 | 5.0 | h | 0.107 | +329.4 | +65.88 | +14.025 | +4.780 | e |
| 2449970.2131 | 0.39 | 0.02 | 8.1 | 0.2 | k | 0.104 | +138.3 | +6.59 | +57.431 | +4.278 | |
| 2449970.2131 | 0.17 | 0.01 | -19.9 | 0.9 | k | 0.104 | +396.6 | +32.94 | +71.764 | +7.775 | |
| 2449970.2131 | 0.07 | 0.01 | 80.3 | 2.3 | k | 0.104 | +502.0 | +77.73 | +37.404 | +8.389 | |
| 2449970.2131 | 0.03 | 0.01 | 140.0 | 5.0 | k | 0.104 | +658.8 | 131.75 | +21.037 | +8.705 | e |
| 2449970.2384 | 0.31 | 0.01 | 9.7 | 0.2 | h | 0.107 | +168.6 | +7.91 | +55.650 | +3.371 | |
| 2449970.2384 | 0.10 | 0.01 | -24.4 | 0.8 | h | 0.107 | +195.0 | +25.03 | +20.756 | +3.596 | |
| 2449970.2384 | 0.06 | 0.01 | 80.3 | 2.4 | h | 0.107 | +720.7 | +79.05 | +46.029 | +9.776 | |
| 2449971.0452 | 0.54 | 0.02 | 9.3 | 0.2 | k | 0.104 | +185.8 | +6.59 | +106.783 | +5.829 | |

| HJD | Depth | error | Velocity | error | Ca line | Resolution | FWHM | error | Eq. width | error | Comments |
|---|---|---|---|---|---|---|---|---|---|---|---|
| 2449971.0452 | 0.13 | 0.01 | -28.0 | 0.9 | k | 0.104 | +278.0 | +30.30 | +38.469 | +5.463 | |
| 2449971.0452 | 0.06 | 0.01 | 94.8 | 6.9 | k | 0.104 | 2031.6 | 267.46 | +129.756 | +29.336 | |
| 2449971.0698 | 0.34 | 0.01 | 11.3 | 0.2 | h | 0.108 | +205.5 | +6.59 | +74.386 | +3.445 | |
| 2449971.0698 | 0.08 | 0.01 | -34.0 | 1.0 | h | 0.108 | +274.0 | +32.94 | +23.337 | +4.308 | |
| 2449971.0698 | 0.05 | 0.01 | 78.0 | 2.8 | h | 0.108 | +806.3 | +93.54 | +42.915 | +10.563 | |
| 2449971.0943 | 0.50 | 0.01 | 9.4 | 0.2 | k | 0.103 | +206.9 | +6.59 | +110.093 | +4.407 | |
| 2449971.0943 | 0.12 | 0.01 | -31.4 | 0.9 | k | 0.103 | +305.7 | +32.94 | +39.044 | +5.662 | |
| 2449971.0943 | 0.46 | 0.01 | 82.6 | 8.9 | k | 0.103 | 2000.0 | 447.96 | +979.310 | +234.590 | |
| 2449971.1188 | 0.36 | 0.01 | 9.7 | 0.2 | h | 0.108 | +200.3 | +5.27 | +76.743 | +3.126 | |
| 2449971.1188 | 0.06 | 0.01 | 73.2 | 1.3 | h | 0.108 | +253.0 | +40.84 | +16.156 | +3.991 | |
| 2449971.1188 | 0.06 | 0.01 | -36.2 | 1.3 | h | 0.108 | +283.3 | +42.16 | +18.092 | +4.303 | |
| 2449971.1433 | 0.50 | 0.01 | 8.6 | 0.2 | k | 0.105 | +193.7 | +6.59 | +103.081 | +4.330 | |
| 2449971.1433 | 0.11 | 0.01 | -31.6 | 1.1 | k | 0.105 | +351.8 | +34.26 | +41.190 | +5.841 | |
| 2449971.1433 | 0.02 | 0.01 | 47.1 | 7.8 | k | 0.105 | +616.6 | 276.68 | +13.127 | +9.388 | |
| 2449971.1677 | 0.35 | 0.01 | 10.1 | 0.2 | h | 0.108 | +201.6 | +7.91 | +75.102 | +3.879 | |
| 2449971.1677 | 0.06 | 0.01 | -36.6 | 1.5 | h | 0.108 | +310.9 | +46.11 | +19.859 | +4.716 | |
| 2449971.1677 | 0.05 | 0.01 | 62.0 | 3.3 | h | 0.108 | +785.2 | 118.58 | +41.793 | +11.149 | |
| 2449971.1922 | 0.45 | 0.01 | 8.0 | 0.2 | k | 0.103 | +227.9 | +6.59 | +109.181 | +4.237 | |
| 2449971.1922 | 0.10 | 0.01 | -33.5 | 0.8 | k | 0.103 | +339.9 | +32.94 | +36.183 | +5.363 | |
| 2449971.1922 | 0.03 | 0.01 | 56.7 | 11.1 | k | 0.103 | 1610.0 | 337.29 | +51.414 | +21.547 | |
| 2449971.2166 | 0.36 | 0.01 | 10.5 | 0.2 | h | 0.108 | +202.9 | +7.91 | +77.752 | +3.960 | |
| 2449971.2166 | 0.07 | 0.01 | -37.8 | 1.3 | h | 0.108 | +349.1 | +42.16 | +26.016 | +5.180 | |
| 2449971.2166 | 0.04 | 0.01 | 61.5 | 5.4 | h | 0.108 | +982.9 | 188.41 | +41.849 | +14.034 | |

**Table C.1 cont.:**Table of results of anaylsis of $\beta$ Pic Ca II spectra

| HJD | Depth | error | Velocity | error | Ca line | Resolution | FWHM | error | Eq. width | error | Comments |
|---|---|---|---|---|---|---|---|---|---|---|---|
| 2449971.2412 | 0.56 | 0.02 | 10.0 | 0.2 | k | 0.104 | +192.4 | +7.91 | +114.665 | +6.646 | |
| 2449971.2412 | 0.11 | 0.02 | -31.6 | 1.5 | k | 0.104 | +280.6 | +48.75 | +32.860 | +8.796 | |
| 2449971.2412 | 0.05 | 0.02 | 60.0 | 5.0 | k | 0.104 | +461.1 | +65.88 | +24.543 | +11.097 | e |
| 2449971.2412 | 0.03 | 0.01 | 125.0 | 5.0 | k | 0.104 | +329.4 | +65.88 | +10.518 | +4.353 | e |
| 2449972.0910 | 0.49 | 0.01 | 8.3 | 0.2 | k | 0.103 | +246.4 | +6.59 | +128.507 | +4.601 | |
| 2449972.0910 | 0.09 | 0.01 | -33.9 | 1.4 | k | 0.103 | +355.7 | +44.80 | +34.080 | +6.092 | |
| 2449972.1228 | 0.38 | 0.06 | 8.4 | 0.2 | h | 0.108 | +171.3 | +14.49 | +69.282 | +13.211 | |
| 2449972.1228 | 0.09 | 0.03 | 20.2 | 6.1 | h | 0.108 | +333.3 | 100.13 | +31.934 | +15.254 | |
| 2449972.1228 | 0.04 | 0.01 | 68.5 | 3.4 | h | 0.108 | +588.9 | 118.58 | +25.076 | +8.568 | |
| 2449972.1228 | 0.08 | 0.01 | -39.0 | 1.0 | h | 0.108 | +329.4 | +32.94 | +28.049 | +4.780 | |
| 2449972.1546 | 0.49 | 0.04 | 8.2 | 0.2 | k | 0.103 | +173.9 | +11.86 | +90.711 | +10.270 | |
| 2449972.1546 | 0.11 | 0.01 | 24.5 | 4.3 | k | 0.103 | +441.4 | +88.27 | +51.681 | +12.086 | |
| 2449972.1546 | 0.10 | 0.01 | -37.8 | 1.0 | k | 0.103 | +254.3 | +34.26 | +27.067 | +4.834 | |
| 2449972.1906 | 0.39 | 0.02 | 8.8 | 0.2 | h | 0.108 | +170.0 | +7.91 | +70.558 | +5.200 | |
| 2449972.1906 | 0.07 | 0.01 | -39.5 | 1.8 | h | 0.108 | +300.4 | +56.65 | +22.383 | +5.637 | |
| 2449972.1906 | 0.06 | 0.01 | 28.1 | 4.1 | h | 0.108 | +374.2 | +54.02 | +23.898 | +5.609 | |
| 2449972.2326 | 0.47 | 0.01 | 7.4 | 0.1 | k | 0.105 | +189.7 | +5.27 | +94.918 | +3.535 | |
| 2449972.2326 | 0.11 | 0.01 | -38.7 | 0.7 | k | 0.105 | +231.9 | +22.40 | +27.152 | +3.834 | |
| 2449972.2326 | 0.09 | 0.01 | 23.2 | 2.1 | k | 0.105 | +886.7 | +56.65 | +84.947 | +11.590 | |
| 2449974.1500 | 0.06 | 0.01 | 38.2 | 1.3 | k | 0.104 | +266.1 | +42.16 | +16.998 | +4.161 | |
| 2449974.1500 | 0.10 | 0.01 | -32.8 | 0.5 | k | 0.104 | +129.1 | +17.13 | +13.744 | +2.430 | |
| 2449974.1850 | 0.05 | 0.01 | 43.6 | 3.4 | h | 0.108 | +791.8 | 114.62 | +42.144 | +11.076 | |
| 2449974.1850 | 0.04 | 0.01 | -31.4 | 1.3 | h | 0.108 | +125.2 | +40.84 | +5.329 | +2.332 | |

**Table C.1 cont.:**Table of results of anaylsis of $\beta$ Pic Ca II spectra

| HJD | Depth | error | Velocity | error | Ca line | Resolution | FWHM | error | Eq. width | error | Comments |
|---|---|---|---|---|---|---|---|---|---|---|---|
| 2449974.2189 | 0.10 | 0.02 | 42.1 | 2.8 | k | 0.104 | +405.8 | +92.23 | +43.196 | +13.921 | |
| 2449974.2189 | 0.10 | 0.02 | -27.2 | 2.2 | k | 0.104 | +245.1 | +69.83 | +26.086 | +9.667 | |
| 2449974.2442 | 0.06 | 0.01 | 48.2 | 3.5 | h | 0.108 | +641.6 | 126.48 | +40.980 | +11.261 | |
| 2449996.9995 | 0.14 | 0.02 | 87.8 | 5.2 | k | 0.103 | 1272.7 | 185.77 | +189.669 | +41.236 | |
| 2449996.9995 | 0.35 | 0.06 | 11.6 | 0.6 | k | 0.103 | +96.2 | +18.45 | +35.833 | +9.812 | |
| 2449997.0298 | 0.41 | 0.03 | 14.1 | 0.4 | k | 0.102 | +137.0 | +13.18 | +59.801 | +7.692 | |
| 2449997.0298 | 0.13 | 0.01 | 93.9 | 3.9 | k | 0.102 | 1117.3 | 144.93 | +154.607 | +24.820 | |
| 2449997.0583 | 0.27 | 0.04 | 16.1 | 0.7 | h | 0.108 | +138.3 | +21.08 | +39.760 | +8.995 | |
| 2449997.0583 | 0.08 | 0.01 | 86.4 | 6.2 | h | 0.108 | +877.5 | 206.85 | +74.723 | +21.224 | |
| 2449997.0834 | 0.43 | 0.03 | 14.0 | 0.4 | k | 0.102 | +130.4 | +11.86 | +59.703 | +7.283 | |
| 2449997.0834 | 0.11 | 0.01 | 95.7 | 4.4 | k | 0.102 | 1119.9 | 162.06 | +131.130 | +23.855 | |
| 2449997.1169 | 0.25 | 0.03 | 15.9 | 0.6 | h | 0.108 | +133.1 | +21.08 | +35.412 | +7.492 | |
| 2449997.1169 | 0.05 | 0.01 | 94.5 | 10.3 | h | 0.108 | 1242.4 | 397.89 | +66.126 | +26.578 | |
| 2449997.1169 | 0.03 | 0.01 | -50.0 | 5.0 | h | 0.108 | +487.5 | +65.88 | +15.567 | +5.960 | e |
| 2449997.1438 | 0.40 | 0.04 | 13.8 | 0.5 | k | 0.103 | +122.5 | +14.49 | +52.172 | +8.602 | |
| 2449997.1438 | 0.07 | 0.03 | 42.9 | 4.5 | k | 0.103 | +274.0 | 163.37 | +20.420 | +15.960 | |
| 2449997.1438 | 0.07 | 0.02 | 97.9 | 10.1 | k | 0.103 | +960.5 | 374.18 | +71.568 | +36.806 | |
| 2449997.1686 | 0.26 | 0.03 | 15.3 | 0.6 | h | 0.107 | +130.4 | +19.76 | +36.099 | +7.318 | |
| 2449997.1686 | 0.06 | 0.01 | 89.6 | 6.2 | h | 0.107 | +769.4 | 210.80 | +49.142 | +16.776 | |
| 2449997.1686 | 0.04 | 0.02 | -55.0 | 5.0 | h | 0.107 | +527.0 | +65.88 | +22.439 | +12.311 | e |
| 2449997.1957 | 0.35 | 0.05 | 14.4 | 0.6 | k | 0.103 | +110.7 | +18.45 | +41.232 | +9.635 | |
| 2449997.1957 | 0.06 | 0.04 | 42.8 | 7.8 | k | 0.103 | +412.4 | 324.11 | +26.338 | +28.895 | |
| 2449997.1957 | 0.07 | 0.02 | 102.7 | 15.7 | k | 0.103 | 1121.2 | 542.82 | +83.545 | +49.994 | |

**Table C.1 cont.:**Table of results of anaylsis of $\beta$ Pic Ca II spectra

| HJD | Depth | error | Velocity | error | Ca line | Resolution | FWHM | error | Eq. width | error | Comments |
|---|---|---|---|---|---|---|---|---|---|---|---|
| 2449997.1957 | 0.07 | 0.02 | -37.0 | 5.0 | k | 0.103 | +197.6 | +65.88 | +14.726 | +6.882 | e |
| 2449997.2239 | 0.28 | 0.04 | 15.9 | 0.6 | h | 0.108 | +131.8 | +19.76 | +39.269 | +8.659 | |
| 2449997.2239 | 0.08 | 0.01 | 81.4 | 5.9 | h | 0.108 | +898.6 | 212.12 | +76.518 | +21.758 | |
| 2449997.2239 | 0.04 | 0.02 | -55.0 | 5.0 | h | 0.108 | +527.0 | +65.88 | +22.439 | +12.311 | e |
| 2449998.9570 | 0.41 | 0.04 | 14.6 | 0.5 | k | 0.103 | +166.0 | +17.13 | +72.451 | +10.951 | |
| 2449999.1132 | 0.40 | 0.04 | 13.8 | 0.5 | k | 0.102 | +144.9 | +17.13 | +61.708 | +10.169 | |
| 2449999.1132 | 0.07 | 0.02 | 37.5 | 5.8 | k | 0.102 | +392.6 | 196.31 | +29.255 | +17.934 | |
| 2449999.1382 | 0.26 | 0.07 | 16.0 | 1.2 | h | 0.106 | +119.9 | +38.21 | +33.182 | +14.736 | |
| 2450000.9660 | 0.29 | 0.03 | 19.1 | 0.8 | k | 0.104 | +210.8 | +26.35 | +65.074 | +11.240 | |
| 2450000.9660 | 0.05 | 0.03 | -27.2 | 4.7 | k | 0.104 | +227.9 | 147.56 | +12.131 | +11.399 | |
| 2450000.9909 | 0.26 | 0.03 | 20.7 | 0.9 | h | 0.108 | +184.5 | +27.67 | +51.050 | +10.284 | |
| 2450000.9909 | 0.06 | 0.02 | -52.0 | 5.0 | h | 0.108 | +527.0 | +65.88 | +33.659 | +12.756 | e |
| 2450001.0158 | 0.30 | 0.03 | 18.0 | 0.8 | k | 0.103 | +201.6 | +25.03 | +64.373 | +10.926 | |
| 2450001.0158 | 0.06 | 0.03 | -27.9 | 3.9 | k | 0.103 | +205.5 | 122.53 | +13.127 | +10.873 | |
| 2450001.0410 | 0.21 | 0.04 | 20.7 | 1.2 | h | 0.108 | +185.8 | +36.89 | +41.527 | +12.164 | |
| 2450001.0662 | 0.30 | 0.04 | 15.2 | 0.8 | k | 0.105 | +177.9 | +25.03 | +56.800 | +11.722 | |
| 2450001.0662 | 0.06 | 0.02 | 90.4 | 9.0 | k | 0.105 | +969.7 | 309.62 | +61.933 | +30.431 | |
| 2450001.0662 | 0.08 | 0.03 | -31.0 | 3.7 | k | 0.105 | +251.6 | 117.26 | +21.430 | +13.644 | |
| 2450001.0916 | 0.17 | 0.04 | 18.2 | 1.2 | h | 0.108 | +150.2 | +38.21 | +27.180 | +10.026 | |
| 2450001.1211 | 0.22 | 0.03 | 16.2 | 0.8 | k | 0.104 | +173.9 | +25.03 | +40.727 | +8.596 | |
| 2450001.1211 | 0.06 | 0.02 | -30.1 | 3.9 | k | 0.104 | +253.0 | 123.85 | +16.156 | +10.186 | |
| 2450001.1211 | 0.06 | 0.02 | 90.0 | 5.0 | k | 0.104 | +263.5 | +65.88 | +16.830 | +7.465 | e |
| 2450001.1211 | 0.05 | 0.02 | 120.0 | 5.0 | k | 0.104 | +263.5 | +65.88 | +14.025 | +7.042 | e |

**Table C.1 cont.:**Table of results of anaylsis of $\beta$ Pic Ca II spectra

| HJD | Depth | error | Velocity | error | Ca line | Resolution | FWHM | error | Eq. width | error | Comments |
|---|---|---|---|---|---|---|---|---|---|---|---|
| 2450001.1553 | 0.15 | 0.02 | 17.7 | 0.9 | h | 0.107 | +166.0 | +30.30 | +26.506 | +6.378 | |
| 2450001.1553 | 0.04 | 0.02 | -42.2 | 7.4 | h | 0.107 | +527.0 | 242.42 | +22.439 | +16.229 | e |
| 2450001.1847 | 0.22 | 0.03 | 13.1 | 0.7 | k | 0.105 | +114.6 | +21.08 | +26.843 | +6.542 | |
| 2450001.1847 | 0.05 | 0.02 | -31.8 | 4.2 | k | 0.105 | +234.5 | 133.07 | +12.482 | +9.224 | |
| 2450001.2129 | 0.15 | 0.03 | 16.6 | 0.9 | h | 0.107 | +134.4 | +28.99 | +21.458 | +6.719 | |
| 2450001.2129 | 0.04 | 0.02 | -65.0 | 5.0 | h | 0.107 | +856.4 | +65.88 | +36.464 | +19.636 | e |
| 2450025.1607 | 0.25 | 0.01 | 11.4 | 0.4 | k | * | +245.1 | +14.49 | +65.214 | +4.956 | |
| 2450025.1607 | 0.05 | 0.01 | 56.1 | 2.7 | k | * | +390.0 | +89.59 | +20.756 | +6.730 | |
| 2450025.1607 | 0.05 | 0.02 | -18.0 | 5.0 | k | * | +158.1 | +65.88 | +8.415 | +5.174 | e |
| 2450027.9306 | 0.25 | 0.01 | 12.1 | 0.6 | k | * | +517.8 | +19.76 | +137.792 | +8.110 | |
| 2450027.9561 | 0.19 | 0.01 | 17.4 | 0.7 | h | * | +396.6 | +22.40 | +80.207 | +6.591 | |
| 2450027.9561 | 0.03 | 0.01 | 146.5 | 2.8 | h | * | +224.0 | +90.91 | +7.153 | +3.999 | |
| 2450027.9824 | 0.40 | 0.03 | 6.0 | 0.2 | k | * | +144.9 | +11.86 | +61.708 | +7.291 | |
| 2450027.9824 | 0.16 | 0.01 | 22.5 | 2.3 | k | * | +436.1 | +55.34 | +74.274 | +11.183 | |
| 2450027.9824 | 0.08 | 0.01 | 126.6 | 4.1 | k | * | 1524.4 | 150.20 | +129.812 | +21.994 | |
| 2450028.0074 | 0.20 | 0.03 | 6.2 | 0.5 | h | * | +134.4 | +19.76 | +28.610 | +6.398 | |
| 2450028.0074 | 0.17 | 0.01 | 24.0 | 1.6 | h | * | +328.1 | +46.11 | +59.366 | +9.629 | |
| 2450028.0326 | 0.38 | 0.02 | 5.8 | 0.2 | k | * | +135.7 | +7.91 | +54.892 | +4.587 | |
| 2450028.0326 | 0.16 | 0.01 | 22.2 | 1.5 | k | * | +401.8 | +46.11 | +68.440 | +9.520 | |
| 2450028.0326 | 0.06 | 0.01 | 13.9 | 3.0 | k | * | +886.7 | 106.72 | +56.631 | +12.393 | |
| 2450028.0326 | 0.05 | 0.01 | 70.4 | 2.8 | k | * | +453.2 | 105.40 | +24.122 | +7.876 | |
| 2450028.0571 | 0.19 | 0.01 | 18.8 | 0.8 | h | * | +469.0 | +25.03 | +94.862 | +7.569 | |
| 2450028.0571 | 0.04 | 0.01 | -59.2 | 4.5 | h | * | +624.5 | 148.88 | +26.591 | +9.778 | |

**Table C.1 cont.:**Table of results of anaylsis of $\beta$ Pic Ca II spectra

| HJD | Depth | error | Velocity | error | Ca line | Resolution | FWHM | error | Eq. width | error | Comments |
|---|---|---|---|---|---|---|---|---|---|---|---|
| 2450028.0817 | 0.31 | 0.03 | 4.4 | 0.3 | k | * | +167.3 | +14.49 | +55.215 | +7.634 | |
| 2450028.0817 | 0.16 | 24.9 | 24.9 | 2.4 | k | * | +429.5 | +63.24 | +73.152 | 12118.62 | |
| 2450028.1066 | 0.25 | 0.03 | 6.2 | 0.4 | h | * | +119.9 | +17.13 | +31.906 | +6.337 | |
| 2450028.1066 | 0.15 | 0.01 | 24.2 | 1.9 | h | * | +337.3 | +60.61 | +53.854 | +10.987 | |
| 2450028.1319 | 0.36 | 0.02 | 4.8 | 0.3 | k | * | +173.9 | +10.54 | +66.645 | +5.833 | |
| 2450028.1319 | 0.12 | 0.01 | 24.9 | 2.0 | k | * | +346.5 | +63.24 | +44.262 | +9.453 | |
| 2450028.1319 | 0.05 | 0.01 | 90.8 | 4.3 | k | * | +911.7 | 162.06 | +48.525 | +13.821 | |
| 2450028.1576 | 0.13 | 0.03 | 5.1 | 0.8 | h | * | +172.6 | +27.67 | +23.884 | +7.144 | |
| 2450028.1576 | 0.15 | 0.01 | 24.2 | 2.0 | h | * | +372.9 | +51.38 | +59.534 | +9.702 | |
| 2450028.8769 | 0.27 | 0.01 | 5.0 | 0.3 | k | * | +241.1 | +10.54 | +69.296 | +4.226 | |
| 2450028.8769 | 0.06 | 0.01 | 129.0 | 2.0 | k | * | +536.2 | +65.88 | +34.248 | +7.548 | |
| 2450028.9033 | 0.14 | 0.01 | 8.2 | 0.6 | h | * | +239.8 | +21.08 | +35.735 | +4.309 | |
| 2450028.9033 | 0.03 | 0.01 | -80.2 | 0.6 | h | * | +739.1 | 206.85 | +23.603 | +10.936 | |
| 2450028.9548 | 0.17 | 0.01 | 8.6 | 0.6 | h | * | +216.1 | +18.45 | +39.101 | +4.315 | |
| 2450028.9804 | 0.40 | 0.01 | 6.2 | 0.2 | k | * | +171.3 | +5.27 | +72.928 | +3.078 | |
| 2450028.9804 | 0.07 | 0.01 | 139.4 | 2.6 | k | * | 1146.2 | +93.54 | +85.410 | +14.958 | |
| 2450028.9804 | 0.02 | 0.01 | 52.3 | 4.1 | k | * | +326.7 | 133.07 | +6.956 | +4.775 | |
| 2450029.0050 | 0.19 | 0.01 | 8.4 | 0.5 | h | * | +216.1 | +15.81 | +43.701 | +4.193 | |
| 2450029.0050 | 0.04 | 0.01 | -76.7 | 4.1 | h | * | +722.0 | 144.93 | +30.742 | +10.492 | |
| 2450029.0323 | 0.05 | 0.02 | 120.0 | 5.0 | k | * | +527.0 | 131.75 | +28.049 | +14.084 | e |
| 2450029.0579 | * | * | * | * | h | * | * | * | * | * | |
| 2450029.0832 | 0.06 | 0.01 | 134.7 | 2.6 | k | * | +889.3 | +93.54 | +56.800 | +11.916 | |
| 2450029.1103 | 0.03 | 0.01 | -47.4 | 4.1 | h | * | +368.9 | 130.43 | +11.781 | +6.094 | |

**Table C.1 cont.:** Table of results of anaylsis of $\beta$ Pic Ca II spectra

| HJD | Depth | error | Velocity | error | Ca line | Resolution | FWHM | error | Eq. width | error | Comments |
|---|---|---|---|---|---|---|---|---|---|---|---|
| 2450029.1370 | * | * | * | * | k | * | * | * | * | * | |
| 2450029.1619 | * | * | * | * | h | * | * | * | * | * | |
| 2450031.0759 | 0.45 | 0.01 | 12.4 | 0.2 | k | * | +187.1 | +6.59 | +89.617 | +3.972 | |
| 2450031.0759 | 0.09 | 0.01 | 59.0 | 1.1 | k | * | +255.6 | +40.84 | +24.487 | +5.073 | |
| 2450031.0759 | 0.05 | 0.01 | 121.1 | 5.1 | k | * | 1118.6 | 209.49 | +59.534 | +17.364 | |
| 2450031.1009 | 0.28 | 0.01 | 14.4 | 0.3 | h | * | +200.3 | +10.54 | +59.689 | +4.041 | |
| 2450031.1009 | 0.07 | 0.01 | 68.2 | 1.9 | h | * | +338.6 | +63.24 | +25.230 | +6.315 | |
| 2450031.1295 | 0.44 | 0.02 | 11.9 | 0.2 | k | * | +183.1 | +7.91 | +85.774 | +5.724 | |
| 2450031.1295 | 0.05 | 0.01 | 75.0 | 4.4 | k | * | +778.7 | 150.20 | +41.443 | +12.258 | |
| 2450031.1534 | 0.33 | 0.02 | 14.4 | 0.3 | h | * | +148.9 | +7.91 | +52.298 | +4.486 | |
| 2450031.1534 | 0.04 | 0.01 | 67.4 | 4.1 | h | * | +640.3 | 142.29 | +27.264 | +9.708 | |
| 2450031.1759 | 0.43 | 0.01 | 13.0 | 0.2 | k | * | +173.9 | +6.59 | +79.604 | +3.766 | |
| 2450031.1759 | 0.05 | 0.01 | 76.0 | 5.2 | k | * | +994.7 | 197.63 | +52.943 | +15.888 | |
| 2450032.9772 | 0.30 | 0.01 | 10.5 | 0.4 | k | * | +263.5 | +11.86 | +84.148 | +5.016 | |
| 2450033.0209 | 0.26 | 0.02 | 11.6 | 0.5 | h | * | +241.1 | +17.13 | +66.729 | +7.438 | |
| 2450033.0688 | 0.33 | 0.03 | 15.3 | 0.5 | k | * | +143.6 | +17.13 | +50.446 | +8.053 | |
| 2450033.8950 | 0.17 | 0.01 | 15.4 | 0.7 | h | * | +238.5 | +22.40 | +43.154 | +5.091 | |
| 2450033.8950 | 0.03 | 0.01 | 66.0 | 5.0 | h | * | +395.3 | +65.88 | +12.622 | +5.007 | |
| 2450033.9290 | 0.25 | 0.02 | 16.9 | 0.7 | k | * | +212.1 | +23.72 | +56.449 | +8.261 | |
| 2450033.9290 | 0.06 | 0.01 | 77.9 | 2.5 | k | * | +366.3 | +84.32 | +23.393 | +7.077 | |
| 2450033.9544 | 0.21 | 0.01 | 19.9 | 0.5 | h | * | +131.8 | +15.81 | +29.452 | +4.048 | |
| 2450033.9544 | 0.06 | 0.01 | 82.8 | 2.8 | h | * | +665.3 | +94.86 | +42.495 | +9.921 | |
| 2450033.9818 | 0.27 | 0.02 | 17.8 | 0.5 | k | * | +144.9 | +18.45 | +41.653 | +6.529 | |

**Table C.1 cont.:**Table of results of anaylsis of $\beta$ Pic Ca II spectra

| HJD | Depth | error | Velocity | error | Ca line | Resolution | FWHM | error | Eq. width | error | Comments |
|---|---|---|---|---|---|---|---|---|---|---|---|
| 2450033.9818 | 0.07 | 0.01 | 106.5 | 3.9 | k | * | +993.4 | 133.07 | +74.022 | +15.431 | |
| 2450034.0085 | 0.17 | 0.02 | 19.3 | 0.7 | h | * | +131.8 | +22.40 | +23.842 | +5.247 | |
| 2450034.0343 | 0.29 | 0.01 | 12.2 | 0.3 | k | * | +137.0 | +10.54 | +42.298 | +3.796 | |
| 2450034.0343 | 0.26 | 0.01 | 16.6 | 0.4 | k | * | +150.2 | +11.86 | +41.569 | +3.886 | |
| 2450034.0343 | 0.05 | 0.01 | 100.6 | 3.7 | k | * | +812.9 | 129.12 | +43.266 | +11.763 | |
| 2450034.0591 | 0.15 | 0.01 | 14.3 | 1.1 | h | * | +226.6 | +36.89 | +36.183 | +6.776 | |
| 2450034.0846 | 0.26 | 0.02 | 15.9 | 0.3 | k | * | +134.4 | +11.86 | +37.193 | +4.635 | |
| 2450034.1091 | 0.20 | 0.02 | 17.6 | 0.5 | h | * | +133.1 | +14.49 | +28.330 | +4.459 | |
| 2450034.1333 | 0.24 | 0.02 | 16.1 | 0.4 | k | * | +142.3 | +13.18 | +36.352 | +4.820 | |
| 2450034.1579 | 0.15 | 0.01 | 15.4 | 0.7 | h | * | +205.5 | +22.40 | +32.818 | +4.463 | |
| 2450034.8772 | 0.19 | 0.02 | 16.0 | 0.8 | k | * | +162.1 | +25.03 | +32.775 | +6.522 | |
| 2450034.9029 | 0.13 | 0.01 | 17.7 | 0.6 | h | * | +173.9 | +19.76 | +24.066 | +3.515 | |
| 2450034.9289 | 0.20 | 0.01 | 16.1 | 0.4 | k | * | +171.3 | +13.18 | +36.464 | +3.561 | |
| 2450034.9543 | 0.13 | 0.01 | 15.5 | 0.9 | h | * | +274.0 | +28.99 | +37.923 | +5.280 | |
| 2450034.9803 | 0.24 | 0.02 | 17.1 | 0.5 | k | * | +142.3 | +17.13 | +36.352 | +5.665 | |
| 2450035.0051 | 0.13 | 0.01 | 15.3 | 1.1 | h | * | +259.6 | +36.89 | +35.917 | +6.179 | |
| 2450035.0300 | 0.22 | 0.01 | 16.0 | 0.5 | k | * | +163.4 | +15.81 | +38.259 | +4.354 | |
| 2450035.0544 | 0.16 | 0.02 | 17.0 | 0.7 | h | * | +168.6 | +21.08 | +28.722 | +5.405 | |
| 2450035.0795 | 0.23 | 0.01 | 13.6 | 0.9 | k | * | +226.6 | +25.03 | +55.481 | +7.011 | |
| 2450035.1035 | 0.15 | 0.01 | 13.4 | 0.8 | h | * | +299.1 | +26.35 | +47.754 | +5.616 | |
| 2450035.1277 | 0.21 | 0.01 | 16.2 | 0.5 | k | * | +163.4 | +15.81 | +36.520 | +4.193 | |
| 2450035.1528 | 0.03 | 0.01 | 75.0 | 5.0 | h | * | +342.6 | +65.88 | +10.939 | +4.481 | |
| 2450035.1528 | 0.16 | 0.01 | 16.0 | 0.6 | h | * | +250.3 | +21.08 | +42.635 | +4.759 | |

| HJD | Depth | error | Velocity | error | Ca line | Resolution | FWHM | error | Eq. width | error | Comments |
|---|---|---|---|---|---|---|---|---|---|---|---|
| 2450035.1528 | 0.05 | 0.01 | -54.1 | 2.6 | h | * | +476.9 | +84.32 | +25.385 | +7.213 | |
| 2450035.8870 | 0.29 | 0.01 | 17.3 | 0.5 | k | * | +263.5 | +15.81 | +81.343 | +5.992 | |
| 2450035.8870 | 0.14 | 0.01 | 50.0 | 1.4 | k | * | +405.8 | +47.43 | +60.474 | +8.818 | |
| 2450035.9140 | 0.22 | 0.01 | 16.6 | 0.7 | h | * | +295.1 | +22.40 | +69.113 | +6.508 | |
| 2450035.9140 | 0.11 | 0.01 | 58.1 | 1.6 | h | * | +415.0 | +55.34 | +48.595 | +8.348 | |
| 2450035.9400 | 0.31 | 0.01 | 18.1 | 0.3 | k | * | +184.5 | +9.22 | +60.867 | +3.855 | |
| 2450035.9400 | 0.10 | 0.01 | 57.6 | 1.5 | k | * | +441.4 | +50.07 | +46.982 | +7.563 | |
| 2450035.9685 | 0.21 | 0.01 | 18.2 | 0.5 | h | * | +218.7 | +14.49 | +48.890 | +4.247 | |
| 2450035.9685 | 0.09 | 0.01 | 61.8 | 1.7 | h | * | +513.8 | +57.97 | +49.226 | +8.298 | |
| 2450036.0012 | 0.32 | 0.01 | 18.0 | 0.3 | k | * | +230.6 | +10.54 | +78.538 | +4.630 | |
| 2450036.0012 | 0.05 | 0.02 | 68.0 | 5.0 | k | * | +263.5 | +65.88 | +14.025 | +7.042 | |
| 2450036.0301 | 0.21 | 0.01 | 18.2 | 0.6 | h | * | +279.3 | +18.45 | +62.438 | +5.411 | |
| 2450036.0301 | 0.07 | 0.01 | 63.9 | 2.1 | h | * | +403.2 | +69.83 | +30.041 | +7.180 | |
| 2450036.0545 | 0.33 | 0.01 | 17.9 | 0.3 | k | * | +200.3 | +9.22 | +70.347 | +4.128 | |
| 2450036.0825 | 0.22 | 0.01 | 18.9 | 0.4 | h | * | +216.1 | +11.86 | +50.601 | +3.838 | |
| 2450036.1298 | 0.35 | 0.01 | 17.9 | 0.2 | k | * | +204.2 | +7.91 | +76.083 | +3.897 | |
| 2450036.1555 | 0.25 | 0.01 | 18.0 | 0.5 | h | * | +227.9 | +18.45 | +60.656 | +5.829 | |